

MASARYKOVA UNIVERZITA
PŘÍRODOVĚDECKÁ FAKULTA
ÚSTAV CHEMIE

Habilitační práce

BRNO 2015

JANA PAVLŮ



MASARYKOVA UNIVERZITA
PŘÍRODOVĚDECKÁ FAKULTA
ÚSTAV CHEMIE



Ab initio and semiempirical modelling of intermetallic phases

Habilitační práce

Jana Pavlů

Brno 2015

Bibliografický záznam

- Autor:** Mgr. Jana Pavlů, Ph.D.
Přírodovědecká fakulta, Masarykova univerzita
Ústav chemie
- Název práce:** Ab initio and semiempirical modelling of intermetallic phases
- Akademický rok:** 2015/2016
- Počet stran:** 43+95
- Klíčová slova:** ab-initio výpočty; semiempirické modelování metodou CALPHAD; stabilita fází; termodynamické vlastnosti; magnetické vlastnosti; intermetalické fáze; sigma fáze; Lavesovy fáze

Bibliographic entry

Author: Mgr. Jana Pavlů, Ph.D.
Faculty of Science, Masaryk University
Department of Chemistry

Title of Thesis: Ab initio and semiempirical modelling of intermetallic phases

Academic Year: 2015/2016

Number of Pages: 43+95

Keywords: ab-initio calculations; semiempirical modelling by CALPHAD method; phase stability; thermodynamic properties; magnetic properties; intermetallic phases; sigma phase; Laves phases

Abstract

This work summarises the results obtained during the study of physical and chemical properties (crystallographic structure, magnetism, lattice stability, Gibbs energy, enthalpy) of solid state phases. In particular, the intermetallic structures with practical impact were investigated, among them sigma phases found in superaustenitic steels and influencing mechanical properties of alloys; Laves phases in systems considered as possible hyperconducting or hydrogen-storage materials, etc. For such phases, the detailed description providing information about their behaviour in complex systems under various conditions such as composition and temperature is desired. This description is not only a collection of data but it also includes thermodynamic polynomials applicable for predictions of phase equilibria in high-order systems.

In this survey, different methods had to be applied depending on the scale of studied issue. To study the relations between electronic structure and crystallographic, magnetic and energetic properties, the DFT calculations based on Kohn-Sham equations were used. These calculations are working on nano-scale level. Nevertheless, sometimes such a detailed attitude was not necessary. In these cases, the macro-scale modelling is more effective as it provides the complex description of complicated systems. One of the macro-scale methods is the semiempirical CALPHAD (Computer Coupling of Phase Diagrams and Thermochemistry) approach assessing the data from both experiments and theoretical sources and providing the thermodynamic properties and phase diagrams.

The results obtained were published in several scientific papers which are listed in the *List of author's publications* where the specification of author's contribution is provided.

In principle, the ab initio modelling should start from characterisation and study of properties of known structures and than it can proceed to hypothetical structures or experimentally inaccessible phases. This two steps usually go together especially in case where the ab initio results are intended to be employed in the subsequent thermodynamic modelling and phase diagram calculations. The publications [VI, XIII] deal with experimentally well defined intermetallic phases such as PdBi, PdBi₂, FePd, FePd₃, FePt, FePt₃ and provide comparison of the experimentally found energies of formation with theoretical ones. This type of publications, where one type of variable is studied by various approaches, provide valuable data. In case of disagreement between results from different methods, the weak aspects of approaches can be revealed and improved. In addition to the energies of formation, the information about the crystallographic arrangement and possible magnetic ordering [XIII] are provided.

On the same principle, the studies of Fe-based C14 Laves phases [XVI] and sigma phases in Cr-Fe and Cr-Co [X] and Ni-Fe [VII] systems are based. In addition, they also include characterisation of structural configurations that are experimentally inaccessible. In case of sigma phase study [X], the detailed overview of magnetic behaviour and its

influence on lattice stability is provided over the whole composition region.

Not only pure ab initio calculations can be challenging but also their combinations with thermodynamic CALPHAD modelling can bring interesting results. The interplay of these methods was for the first time applied on the sigma phase in Cr-Fe [I] and Co-Cr [II] binary system. The implementation of the ab initio results into the thermodynamic description of the sigma phase using the two-sublattice model enabled us to perform the phase diagram calculations using the parameters having the physical meaning. This approach can be of course used for many intermetallic phases [IV, IX, XI] and high-order systems [III]. This procedure is now widely used in the CALPHAD community.

As the thermodynamic modelling is very efficient tool for phase equilibria predictions, its combination with ab initio calculations pushes its applicability to less and less experimentally explored regions. One of them is the modelling at low temperatures, where phase transformations also occur and interesting physical (superconductivity) phenomena take place. The extension of the ordinary used SGTE (Scientific Group Thermodata Europe) unary data to 0 K temperatures was developed [XIV] and its application to the intermetallic phases was demonstrated [XVII].

Acknowledgement

My work presented in this thesis could not be realised without the help of prof. Jan Vřešťál (MU Brno, diploma supervisor, Ph.D. supervisor) and prof. Mojmír Šob (MU Brno, group leader), who are acknowledged for long term cooperation, many encouraging scientific discussions and for a critical reading of this thesis. I would like also to thank my family, namely my parents Ludmila and Ladislav Houserovi, for outstanding support.

Declaration

I hereby confirm that I have written the habilitation thesis independently, that I have not used other sources than the ones mentioned and that I have not submitted the habilitation thesis elsewhere.

Brno 10th September 2015

.....
Jana Pavlů

Contents

Introduction	1
1 Structures studied	4
2 Ab initio calculations	6
2.1 Theory and methodology	6
2.1.1 DFT (Density Functional Theory)	7
2.1.2 Exchange-correlation potentials	8
2.1.3 Calculations for periodic solids	9
2.1.4 Methodology of performed calculations	10
2.2 Results and discussion	14
2.2.1 Crystal structure	14
2.2.2 Energies of formation	17
2.2.3 Magnetic properties	18
2.2.4 Mechanical properties	20
3 CALPHAD modelling	21
3.1 Theory and methodology	21
3.1.1 Sigma phase modelling	23
3.1.2 Modelling at low temperatures	24
3.2 Results and discussion	26
3.2.1 Binary systems	26
3.2.2 Ternary systems	28
3.2.3 Thermodynamic modelling at low temperatures	28
Conclusions and main results	31
4.1 Ab initio calculations	31
4.2 CALPHAD modelling	32
List of author's publications and the specification of author's contribution	35
Bibliography	39
Appendix I	44
Appendix II	52

Appendix III	62
Appendix IV	66
Appendix VI	73
Appendix VII	77
Appendix IX	83
Appendix X	89
Appendix XI	98
Appendix XIII	105
Appendix XIV	112
Appendix XVI	124
Appendix XVII	131

Introduction

There is no doubt that materials and their development are essential for the evolution of the society we live in. During the last century, the achievements in electronic science, computer technology etc. have opened up enormous possibilities for progress in materials science leading to research and development of more sophisticated materials.

Most, if not all, of properties of solids can be described by theoretical approaches working on different scale. It is only the question of priority which method is used whether nano-scale *ab initio* (first-principles) electronic structure calculations or CALPHAD (Computer Coupling of Phase Diagrams and Thermochemistry) modelling, which works on macroscopic level, or even some other approaches. Anyway, both of the above mentioned methods can significantly contribute to understanding and prediction of the physical and chemical properties of materials. At present, the possibilities are almost unlimited and the problem of choice of suitable method to study particular problem makes high demands on author's experience.

In principle, all properties of material are directly related to the behaviour of electrons that constitute inter-atomic bonds in solids. The bridge to the macroscopic properties such as e.g. total energy, crystallographic arrangement, magnetic ordering, mechanical properties etc. is constituted by the rules of quantum mechanics implemented to **ab initio (first-principles) approaches** [1–4]. The theory of electronic structure is not only helpful in understanding and interpreting experiments, but it also becomes a predictive tool in the physics and chemistry of condensed matter. The advantage of methods based on electronic structure calculations consists in their physical transparency and independence on experimental data and fitting parameters as input values. On the other hand, some price for this independence has to be paid in the form of high computational demands on software, hardware and time. For application of *ab initio* approach in the research, fast development of computing facilities, numeric methods and their increasing accessibility (via networks and workstations) in recent decades has been crucial. As an illustration of the detailed *ab initio* study of physical and chemical properties of intermetallic phases, the paper [X] can be mentioned here. In this work, the comprehensive study of magnetism of sigma phases in Fe-Cr and Co-Cr binary system and its influence on phase stability is presented.

In spite of the fruitfulness of the *ab initio* methods, some disadvantages related to them should be mentioned here. The first one is that these approaches require many approximations (e.g. adiabatic (Born-Oppenheimer) approximation, approximations of functional of exchange-correlation energy etc.) which result in lowering the accuracy of calculation. The other disadvantage is that the *ab initio* calculations are performed for 0 K temperature which disables their direct usage for phase equilibria studies at higher

temperature.

In this case, the material science turns towards a macro-scale method omitting the role of electrons - **the CALPHAD approach** [5]. This widely used semiempirical method is based on the laws of thermodynamics and uses the Gibbs energies of phases as building stones for description of system. From this reason, the knowledge of the Gibbs energy dependence on composition and temperature for all structures occurring in the system (stable and even metastable) is crucial. Unfortunately, this information is for metastable phases experimentally inaccessible. Nevertheless, the lack of proper data can be bridged by ab initio calculations of lattice stability [6]. In the field of phase equilibria calculations, the main advantage of the ab initio methods is the ability to deal with systems far from equilibrium or with metastable or hypothetical states providing their total energies of formation with respect to the reference states at $T = 0$ K [IX, XVII, 7, 8], consequently applied in the CALPHAD modelling. Such approach can put the thermodynamic data describing the metastable states on the sound physical basis.

One of the first applications of this combined approach was presented in our work [I] in 2002 and we have continued with further studies of complex phases such as sigma and Laves phase etc. [III, IV, IX, XVII]. This approach is now being used by many research groups [7–10] as the combination of both above mentioned different-scale methods becomes very useful tool for description of multi-component systems with complex intermetallic phases where experiments seldom provide satisfactory set of thermodynamic or phase data.

In some cases, not only the question of thermodynamic stability should be treated in phase modelling but also the mechanical stability becomes crucial. This topic can be studied via the analysis of the elastic constants [XVII, 11] or, more completely, via the phonon spectra [XVII, 12].

From the point of basic science, the CALPHAD method is currently being developed by extending the theoretical background into the fields which have not been covered yet. In [XIV], a method for the extension of SGTE (Scientific Group Thermodata Europe) Gibbs energy expressions for pure elements [13] to zero Kelvin temperature was presented. It is based on the Einstein formula for the temperature dependence of heat capacity extended to provide the temperature dependence of the Gibbs energies below the limiting temperature of validity of SGTE unary data. The application of this method to low temperature modelling of intermetallic phases was presented in [XVII].

At present, the knowledge of phase diagrams (or their sections) and relevant thermodynamic properties is crucial in a design of modern materials. However, to obtain the full understanding of material behaviour and to make reliable predictions, it is crucial to combine the theoretical methods on one side and experiments on the other because the quality of theoretical predictions of course increases when more information about the system is available.

The **metallic systems studied in this thesis** were chosen not only because of scientific reasons looking for understanding of physical and chemical background of material behaviour but also according to their applicability in material engineering. The stress was laid on the systems found in supraustenitic steels containing the sigma phase (Cr-Fe [I, X], Co-Cr [II, X], Cr-Fe-Ni [III], Co-Mo [IV], Fe-Mo [IV], Cr-Fe-W [VII]) and binary systems with Laves phases (Cr-Zr [IX], Cr-Hf [XI], Cr-Ti [XI], V-Zr [XVII]) which have become candidates for some functional as well as structural applications, e.g. hydrogen

storage materials [14], superconductors [15], and materials with a high strength up to high temperatures [16]. The list of systems and phases studied is not complete here. Further examples can be found in *List of author's publications*.

Chapter 1

Structures studied

As this thesis concerns the intermetallic phases, the characterisation of those which form the nub of this work is provided here.

Sigma phase was first observed by Bain [17] in Cr–Fe system in 1923 and, at present, about 50 binary transition-metal systems exhibiting this phase are known [18], e.g. Fe–Mo, Co–Mo or Fe–V. The sigma phase has the space group No. 136 ($P42/mnm$) and its repeat cell contains thirty atoms accommodated in five crystallographically inequivalent sublattices ($2a$, $4f$, $8i$, $8i'$ and $8j$) [19–21], see Figure 1.1. If these sublattices are occupied by studied constituents in various succession, 32 different configurations are formed.

The sigma phase is very crucial in material science and technology because its properties are very disadvantageous. It is brittle and therefore it can cause a strong degradation of material (crack nucleation sites). It develops in heat affected zones of welded super-austenitic stainless steels [22] and it was concluded that it is formed after longer ageing times in the temperature range of 500–1100 °C. It is also known that high concentrations of Cr and Mo promote precipitation of this phase. From the thermodynamic point of view, the sigma phase is very stable.

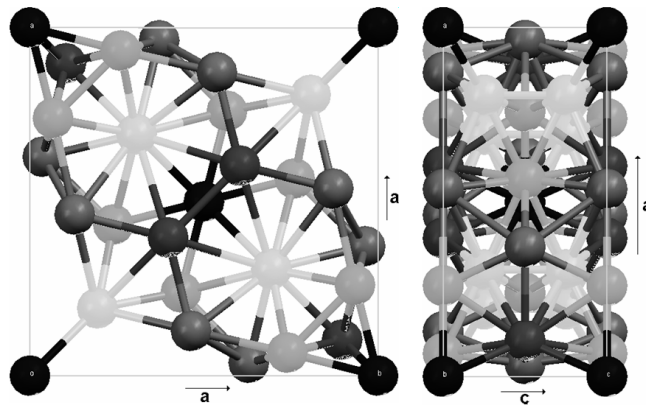


Figure 1.1: The structure of the sigma phase [XIX]. The brightness of atoms in sublattices is increasing in the order of positions $2a$, $4f$, $8i$, $8i'$ and $8j$.

Laves phases can be found in metallic systems in three polytypes: cubic C15 (prototype MgCu_2 , space group 227, $Fd\bar{3}m$), hexagonal C14 (prototype MgZn_2 , space group 194, $P63/mmc$) and hexagonal C36 (prototype MgNi_2 , space group 194 $P63/mmc$). All three

structures are shown in Figure 1.2. In this thesis, our attention was mainly drawn to the C14 and C15 Laves phases.

Laves phases have a significant influence on mechanical properties of modern high-Cr steels. They precipitate mostly on ferrite subgrain boundaries and on prior austenite grain boundaries. It has been found that the presence of silicon in the steels accelerates the precipitation of Laves phase and that the phase itself than contains significant amount of Si [23].

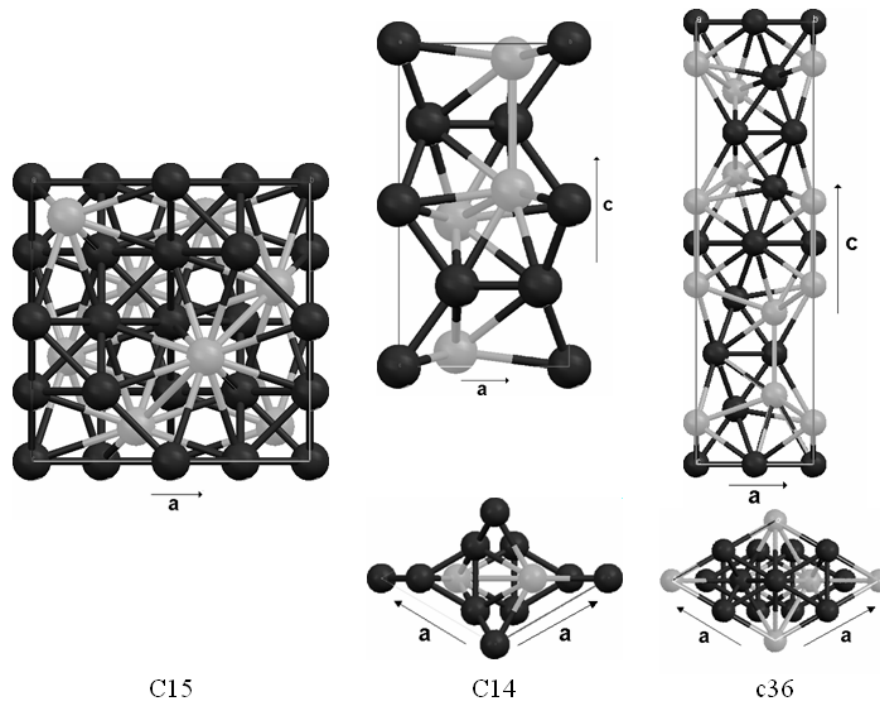


Figure 1.2: The structures of Laves phases [XIX]. Bright and dark spheres correspond to the A and B atoms in the general formula A_2B .

Chapter 2

Ab initio calculations

This part of thesis addresses problems concerning the properties of particular phase such as equilibrium structure parameters (lattice parameters, angles, atomic positions), magnetic ordering, total energies and mechanical properties. In the case of experimentally accessible phases, the above mentioned values can be compared with experimental data and can form a strong background for methods using these data as input values. The mutual interactions between phases can be also investigated for example by means of lattice stabilities, grain boundary energies, etc., however, these values are usually obtained from the post-processing of ab initio results than from multi-phase ab initio calculations. Accordingly, a range of DFT (Density Functional Theory) quantum chemistry approaches is employed from the LMTO-ASA (Linear Muffin-Tin Orbitals method within the Atomic Sphere Approximation) method, FLAPW (Full-potential - Linear Augmented Plane Wave) method to pseudopotential approach within the LDA (Local Density Approximation) and GGA (Generalised Gradient Approximation) employed for the exchange-correlation term.

2.1 Theory and methodology

The properties of material depend on the electronic structure which is described by the wave functions calculated from the Schrödinger equation

$$H_{e,\{\mathbf{R}_\alpha\}}\Psi = E\Psi, \quad (2.1)$$

where $\{\mathbf{R}_\alpha\}$ are positions of atomic nuclei, Ψ is wave function, E energy and Hamiltonian H is defined as

$$H_{e,\{\mathbf{R}_\alpha\}} = -\sum_i \nabla_i^2 + \sum_i V_{e,\{\mathbf{R}_\alpha\}}(\mathbf{r}_i) + \sum_{i,j,i \neq j} \frac{1}{|\mathbf{r}_i - \mathbf{r}_j|}. \quad (2.2)$$

Here, \mathbf{r}_i and \mathbf{r}_j are positions of electrons. The first term in Equation (2.2) stands for the kinetic energy of electrons, the second one is the potential acting on the electron i coming from surrounding nuclei and the last term describes the interaction between two electrons. The $V_{e,\{\mathbf{R}_\alpha\}}(\mathbf{r}_i)$ potential is defined as

$$V_{e,\{\mathbf{R}_\alpha\}}(\mathbf{r}_i) = -2 \sum_\alpha \frac{Z_\alpha}{|\mathbf{r} - \mathbf{R}_\alpha|}, \quad (2.3)$$

where Z_α are the proton numbers of studied elements. To evaluate the total energy, the Rydberg atomic units with $\hbar = 1$, $2m_e = 1$ and $Ke^2 = 2$ are often used, where $\hbar = h/2\pi$, h stands for the Planck constant, m_e and e are the electron mass and charge, respectively, and K is Coulomb law constant ($K = 1/(4\pi\epsilon_0)$, where ϵ_0 is permittivity of vacuum).

As there are approximately 10^{23} interacting particles in one mole of a real solid, it is impossible to solve the Schrödinger equation for such a huge number of objects. From this reason various approximations has to be employed resulting in lowering the accuracy of results.

2.1.1 DFT (Density Functional Theory)

Ab initio results commented in this thesis are based on the DFT [1–4], which simplifies the many-particle problem. It is based on two theorems published in 1964 by Hohenberg and Kohn [24] showing the elegant reduction of many-electron problem.

The first theorem (existence theorem) introduces the density of electrons $\rho(\mathbf{r})$ whose a non-degenerate ground state defines fully the Hamiltonian of the whole system (by means of determination of external potential). From this Hamiltonian, it is possible to determine all the basic properties of the studied material (e.g. lattice constants, total energy, etc.). Thus, all the characteristics of the system in the ground state may be treated as functionals of one function - electron density $\rho(\mathbf{r})$. The existence theorem induces a huge decrease in number of degrees of freedom as the electron density is a function of sole three variables.

According to **the second theorem (variational principle)**, the total energy of a system of electrons $E[\rho]$ reaches its minimum for electron density of the ground state. On the base of DFT, the electron density is being changed until the minimum of total energy is obtained, regardless to the number of particles in the system.

Based on these theorems, it can be stated that the equilibrium ground-state electron density corresponds to the minimum of total energy and vice versa. Furthermore, the formulation of the above mentioned theorems yielded the introduction of the Kohn-Sham equations [25]

$$H_s \psi_i(\mathbf{r}) = \epsilon_i \psi_i(\mathbf{r}) = [-\nabla^2 + V_{eff}(\mathbf{r})] \psi_i(\mathbf{r}), \quad (2.4)$$

which are again a single-particle equations. These equations describe the behaviour of an electron moving in the field evoked by the other electrons and nuclei. H_s is one-electron Kohn-Sham Hamiltonian. ψ_i are one-electron wave functions that are solutions of Kohn-Sham equation. ϵ_i are eigenenergies of one-electron states and V_{eff} is the effective potential which is, in general, nonlocal. V_{eff} defined as

$$V_{eff}(\mathbf{r}) = V_{ext}(\mathbf{r}) + V_H(\mathbf{r}) + V_{xc}(\mathbf{r}) \quad (2.5)$$

can be constructed on the basis of electron density and includes important effects of exchange and correlation. The particular potentials - external $V_{ext}(\mathbf{r})$, Hartree $V_H(\mathbf{r})$ and exchange-correlation $V_{xc}(\mathbf{r})$ potential are characterised as follows:

- External potential describes the effect of nuclei and external fields on electron.

- Hartree potential

$$V_H(\mathbf{r}) = \int \frac{2\rho(\mathbf{r}')}{|\mathbf{r}-\mathbf{r}'|} d^3r' \quad (2.6)$$

corresponds to the classical repulsion of electron with other electrons.

- Exchange-correlation potential

$$V_{xc}(\mathbf{r}) = \frac{\delta E_{xc}[\rho]}{\delta \rho(\mathbf{r})} \quad (2.7)$$

is functional of so-called exchange-correlation energy E_{xc} and its exact form is not known, because its determination is equivalent to the solution of many-electron problem. It contains the non-classical part of the electron-electron interaction and the difference between the kinetic energy of interacting and non-interacting electron system [1]. For this term various approximations has to be used.

The one-particle density $\rho(\mathbf{r})$ used in previous equations is defined as the sum over the occupied one-electron energy states of N -electron system

$$\rho(\mathbf{r}) = \sum_{i=1}^N |\psi_i(\mathbf{r})|^2 . \quad (2.8)$$

The total energy of the system may be calculated according to following formula

$$E = \sum_{i=1}^N \varepsilon_i + \int \int \frac{\rho(\mathbf{r})\rho(\mathbf{r}')}{|\mathbf{r}-\mathbf{r}'|} d^3r d^3r' - \int V_{xc}(\mathbf{r}) \rho(\mathbf{r}) d^3r + E_{xc}[\rho] . \quad (2.9)$$

2.1.2 Exchange-correlation potentials

The most often used methods for determination of exchange-correlation energy are LDA (Local Density Approximation), LSDA (Local Spin Density Approximation) and GGA (Generalised Gradient Approximation).

The LDA defines the exchange-correlation energy $E_{xc}[\rho]$ as

$$E_{xc}[\rho] = \int \rho(\mathbf{r}) \varepsilon_{xc}[\rho(\mathbf{r})] d^3r , \quad (2.10)$$

where $\varepsilon_{xc}[\rho(\mathbf{r})]$ is the exchange-correlation energy per particle in a homogeneous system of density ρ .

Similarly, the exchange-correlation energy in **LSDA** is

$$E_{xc}[\rho \downarrow, \rho \uparrow] = \int \rho(\mathbf{r}) \varepsilon_{xc}[\rho \downarrow(\mathbf{r}), \rho \uparrow(\mathbf{r})] d^3r . \quad (2.11)$$

The most frequently employed approximations are due to Hedin and Lundqvist [26], von Barth and Hedin [27], Janak [28], Ceperley and Alder [29] as parametrised by Perdew and Zunger [30], Vosko, Wilk and Nusair [31] and Perdew and Wang [32]. As here defined ε_{xc} corresponds to a homogeneous electron gas, the application of L(S)DA is limited to the systems with slowly varying electron density. In the case of strong gradients, e.g. due to

the directional bonding, these approximations are less successful. For example, they fail in reproduction of the ground state of iron.

From this reason, it was necessary to include the magnitude of gradient of the electron density into the exchange-correlation energy evaluation. This was done by **the GGA** where the term $\varepsilon_{xc}[\rho(\mathbf{r})]$ in Equation (2.10) is substituted by the term $\varepsilon_{xc}[\rho(\mathbf{r}), \nabla\rho(\mathbf{r})]$.

2.1.3 Calculations for periodic solids

Equations (2.4), (2.5) and (2.8) are solved self-consistently until the electron density $\rho(\mathbf{r})$ and potential $V_{eff}(\mathbf{r})$ correspond to each other within certain limits. This process is significantly simplified by the idea of periodicity of crystal structure, which is characterised by the translation vector \mathbf{T} in crystal lattice. In the periodic systems, the effective potential has to obey the periodicity condition $V_{eff}(\mathbf{r} + \mathbf{T}) = V_{eff}(\mathbf{r})$. This condition results in **the Bloch theorem**, according to which the solution of Equation (2.4) can be expressed as

$$\psi_{\mathbf{k}}(\mathbf{r}) = e^{i\mathbf{k}\cdot\mathbf{r}} u_{\mathbf{k}}(\mathbf{r}) . \quad (2.12)$$

Here, \mathbf{k} is the reciprocal lattice vector and $u_{\mathbf{k}}$ is a periodic function with the same period as the crystal lattice. Based on this assumptions, it is sufficient to find the wave function $\psi_{\mathbf{k}}(\mathbf{r})$ in the primitive cell and the region of \mathbf{k} -vectors is constrained to a primitive cell in the reciprocal space, i.e. to the first Brillouin zone [33, 34].

If we suppose that the electron interaction between the atoms in the solid is quite weak (i.e. the electrons are mainly localised in the vicinity of atoms) then the wave functions may be written as a linear combination of orbitals localised at the positions of nuclei. When solving the Kohn-Sham equation (2.4), the one-electron wave functions are expanded into a series

$$\psi_{n\mathbf{k}}(\mathbf{r}) = \sum_i c_{i,n\mathbf{k}} \chi_{i\mathbf{k}}(\mathbf{r}) . \quad (2.13)$$

The index n is a counting index (band index), $c_{i,n\mathbf{k}}$ are expansion coefficients and $\chi_{i\mathbf{k}}(\mathbf{r})$ are the basis functions (orbitals) that satisfy the Bloch condition - Equation (2.12). For expansion coefficients $c_{i,n\mathbf{k}}$ we obtain

$$\sum_j [H_{ij} - \varepsilon_{n\mathbf{k}} O_{ij}] c_{i,n\mathbf{k}} = 0 , \quad (2.14)$$

where

$$H_{ij} = \langle \chi_{i\mathbf{k}} | H_s | \chi_{j\mathbf{k}} \rangle = \int_{\Omega} \chi_{i\mathbf{k}}(\mathbf{r}) \chi_{j\mathbf{k}}^*(\mathbf{r}) d^3\mathbf{r} \quad (2.15)$$

are matrix elements of Hamiltonian and

$$O_{ij} = \langle \chi_{i\mathbf{k}} | \chi_{j\mathbf{k}} \rangle = \int_{\Omega} \chi_{i\mathbf{k}}(\mathbf{r}) \chi_{j\mathbf{k}}^*(\mathbf{r}) d^3\mathbf{r} \quad (2.16)$$

are overlap integrals with the volume of the unit cell Ω . The energies $\varepsilon_{n\mathbf{k}}$ are determined by the secular equation

$$\det [H_{ij} - \epsilon_{nk} O_{ij}] = 0 . \quad (2.17)$$

The Bloch theorem enables us to calculate the electronic wave functions and corresponding electron energies by effective block-diagonalisation of the Hamiltonian matrix, with each block (corresponding to a particular k) having a manageable size.

The methods used for the electronic structure calculations differ in the type of basis functions χ_i which has to be chosen carefully with respect to the problem solved. We can use the plane waves or their modifications (Plane Wave - PW, Orthogonalised Plane Wave – OPW, Augmented Plane Wave - APW); Linear Combination of Atomic (LCAO), Gaussian (LCGO) and Augmented Slater-Type (LASTO) Orbitals; Augmented Spherical Waves (ASW), Muffin-Tin Orbitals (MTO), Linear Muffin-Tin Orbitals (LMTO), etc. The Green function of Kohn-Sham equation is used in Korringa-Kohn-Rostoker (KKR) method, alternatively called Green Function (GF) method. The detailed information about basis functions can be found in many publications [35–37] . The pseudopotential approach [38] is also widely used. This method modifies the potential close to the nucleus (i.e. in the region of electron shell with the lowest energy) to narrow down the basis set.

2.1.4 Methodology of performed calculations

The primary reason for the execution of *ab initio* calculations was to provide the input data for the CALPHAD modelling - so called lattice stabilities. The lattice stabilities are the energies of formation of particular phase which has to be calculated with respect to exactly defined reference states. In the articles listed in *List of author's publications*, the reference states are structures of the pure constituents that are stable at a temperature T of 298 K and pressure p of 1 bar, such as FM (ferromagnetic) hcp (hexagonal close packed) Co, FM bcc (body centered cubic) Fe, AFM (antiferromagnetic) bcc Cr, NM (non-magnetic) bcc Mo, etc. These phases are denoted SER (Standard Element Reference) states in this thesis. From this reason, not only intermetallic phases but also SER structures had to be included in the *ab initio* calculations.

At the beginning of any study, the suitable method has to be chosen. In the case of study of phases with the same symmetry, **the LMTO-ASA** method [4, 39, 40] implemented in the code by Krier et al. [41] can be used. This code was employed for calculations of various sigma phase configurations in: Cr–Fe and Cr–Co binary system [X], Fe–Ni binary system [III]; and for structure relaxations of sigma phases of pure elements, e.g. Cr, Fe, Co and Mo [I, II, IV, X]. Here, the exchange-correlation energy was evaluated within the GGA [42]. The *s-p-d* basis with the *f* states incorporated by the down-folding procedure and with the combined-correction term included [39, 41] was used. This is apparently the best performance the LMTO-ASA method may provide. For all computational methods the optimum technical parameters had to be found to get the required precision of total energy of phase. In case of LMTO-ASA, these parameters were: the number of k -points in the whole Brillouin zone and the sphere radii, which define the size of non-overlapping Muffin-Tin spheres with the spherically symmetric potential. Outside the spheres, the potential was constant. The partitioning of the unit cell into atomic spheres is shown in Figure 2.1.

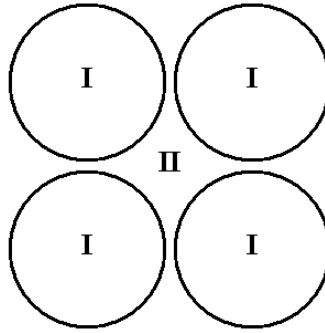


Figure 2.1: Partitioning of the unit cell into atomic spheres (I) and interstitial region (II).

Nevertheless, the LMTO-ASA method does not provide reliable structural energy differences for structures of different symmetry, although the total energy differences calculated by this method for the same crystallographic structures are considered to be quite reliable [43–45]. To calculate the energy differences between the structures of different symmetry, the FLAPW and pseudopotential methods were employed.

The FLAPW method [38] implemented in the WIEN97 / WIEN2k code [46] / [47] was used in all works related to the sigma phases [I-IV,VII,X] employing the GGA [42] for the exchange-correlation term. This method is considered to be one of the most reliable methods. At the beginning of FLAPW calculations, the optimisations of technical parameters (the RMT (Radius Muffin-Tin) parameter and number of k-points) were performed. The optimum values are provided in relevant publications.

The last ab initio approach employed in this thesis is **the pseudopotential method** [38] incorporated in the VASP (Vienna Ab initio Simulation Package) [48, 49] and combined with the PAW–PBE (Projector Augmented Wave–Perdew–Burke–Ernzerhof) pseudopotential [50–52] (i.e. the GGA was employed for the exchange-correlation energy). This method was employed in the study of magnetism of sigma phases in Fe–Cr and Co–Cr binary system [X]; and in the investigations of Laves phases in the following systems: V–Zr [XVII], Cr–Zr [IX], Cr–Hf and Cr–Ti both [XI] and in Fe-based systems [XVI]. Furthermore, the studies of the intermetallics PdBi, PdBi₂ [VI] and NiTi, FePd, FePd₃, FePt, FePt₃ [XIII] used this method. The optimised technical parameters for this approach are: the cut-off energy restricting the number of plane waves in the basis set and the number of k-points.

Except for the above mentioned optimised technical parameters, there are further parameters employed in the discussed calculations which influenced the obtained results. Their detailed descriptions are provided in user guides / manuals of particular codes.

As the properties of phases studied are directly related to their crystal structure, **the optimisation of crystallographic arrangement** with respect to total energy had to be performed. In case of LMTO and FLAPW approaches, this optimisation was rather demanding. It was performed by alternating minimisation of total energy as a function of lattice parameter a (unit cell volume V) at a constant c/a ratio and minimisation of total energy as a function of the c/a ratio at the constant parameter a_{min} (V_{min}) from the previous optimisation. These two steps were repeated until the change of total energy was small enough (lower than 0.1 mRy/atom). In this way, the equilibrium energies of studied

phases were found. In comparison with LMTO and FLAPW codes used, the structure optimisation by VASP is more comfortable as this code automatically calculates the forces and the stress tensor, which are used to search directions to the equilibrium positions of atoms. Using the structure optimisation, the equilibrium structure parameters (lattice constants, angles, atomic positions) corresponding to the minimum energy were obtained.

To find the equilibrium crystal structure and energy of phases studied, their **magnetic arrangement** had to be also taken into account as it significantly influences the stability of particular phases as it had been found in the case of iron [53]. When the spin polarised calculations are performed [X, XIII], the detailed information about the magnetic moments of individual atoms is obtained, which is usually not accessible by experimental methods.

After the evaluation of equilibrium total energies, **the molar total energies of formation** ΔE_{fm} can be calculated. The expression for ΔE_{fm} between two phases of pure constituent is very simple

$$\Delta E_{fm}^{ph} = E_m^{ph} - E_m^{SER}, \quad (2.18)$$

where E_m^{SER} (E_m^{ph}) stands for the molar total energy per atom of SER state (studied phase).

The molar energy of formation of the intermetallic phase (*int*) is calculated with respect to the weighted average of the total energies of SER states of pure constituents as

$$\Delta E_{fm}^{int} = E_m^{int} - [xE_m^{SER1} + (1-x)E_m^{SER2}]. \quad (2.19)$$

Here, the subscripts 1 and 2 following the name of structure denote different pure constituents and x is the molar fraction of constituent 1.

It is also possible to combine the results of two ab initio methods for the evaluation of the energy of formation of intermetallics. This approach was used for analysis of energetics of various configurations of sigma phases [X]. In this case, it is necessary to use the following equation

$$\begin{aligned} \Delta E_{fm}^{\sigma} &= \Delta E_{fm}^{(i)} + \Delta E_{fm}^{(ii)} = \\ &= \{E_m^{\sigma} - [xE_m^{\sigma1} + (1-x)E_m^{\sigma2}]\}_{\text{LMTO or FLAPW or pseudopotential}} + \\ &\quad + \{xE_m^{\sigma1} + (1-x)E_m^{\sigma2} - [xE_m^{SER1} + (1-x)E_m^{SER2}]\}_{\text{FLAPW or pseudopotential}}. \end{aligned} \quad (2.20)$$

The ΔE_{fm}^{σ} in Equation (2.20) consists of two parts: (i) the energy difference of alloy sigma phase with respect to weighted average of total energies of pure constituents in the sigma phase structure, both calculated by means of the LMTO, FLAPW or pseudopotential method (the LMTO method may be used here as the systems considered have the same type of structure), and (ii) the energy difference of weighted average of total energies of pure constituents in the sigma phase and SER states, both calculated by means of the FLAPW or pseudopotential method (here a more reliable, but also more time consuming method had to be used as the structures involved have different types of symmetry). Both energy differences (i) and (ii) may be considered as quite reliable, as the total energies used for their determination were obtained by the same method on equal footing.

The mechanical stability can be also evaluated when the mechanical properties (bulk moduli [XIV] and elastic constants [XVII]) are calculated from the total energy depen-

dencies on structure deformation. For example, when the dependencies of total energy on volume are expressed in polynomial form of the third order ($y = ax^3 + bx^2 + cx + d$), the bulk modulus (B) can be calculated from its second derivative as

$$B = V_{min}(6aV_{min} + 2b) . \quad (2.21)$$

To judge the mechanical stability, the elastic constant has to be calculated and the elastic stability criteria has to be fulfilled. For cubic phase, the elastic stability criteria are as follows: $C_{11} > 0$; $C_{44} > 0$; $C_{11} > |C_{12}|$; and $(C_{11} + 2C_{12}) > 0$, where C_{11} , C_{12} and C_{44} are elastic constants.

The mechanical stability can be also evaluated on the base of phonon spectra [XVII] where no negative branches can occur.

2.2 Results and discussion

As mentioned in section 2.1.4 *Methodology of performed calculations*, the results obtained during the *ab initio* studies are rather complex as they form a logically integrated set of data related to studied system. However, for greater clarity, they are divided into particular sections in this thesis. The results obtained are demonstrated on chosen exemplary systems: Cr-Fe [I,X] for sigma phases and V-Zr [XVII] for Laves phases. The citations of analogous results are provided and if it is needed the details on studies of further phases are provided [VI, XIII].

2.2.1 Crystal structure I-IV,VI,VII,IX-XI,XIII,XIV,XVI,XVII

The equilibrium crystallographic data were obtained for all phases commented in this work and were listed in tables in corresponding publications. In the case of **SER states**, the results are summarised in Table 2.1.

The results correspond very well to experimental findings and the deviations from experimental volume $\Delta\%_{exp}$ ranges from -5.12 % for NM bcc V to 5.02 % for NM fcc Pd. However, the deviation for most structures is within $\pm 3\%$, which is generally acceptable

Structure	Method	a (nm)	c/a	V_{at} (nm ³ .10 ³)	Ref.	a (nm)	c/a	V_{at} (nm ³ .10 ³)	Ref.	$\Delta\%_{exp}$
FM hcp Co	FLAPW	0.2446	1.6025	10.1496	[II]	0.2506	1.6237	11.0650	[18]	-8.27
	FLAPW	0.2498	1.6194	10.9342	[IV, X]					-1.18
	PP	0.2492	1.6190	10.8435	[X]					-2.00
AFM bcc Cr	FLAPW	0.2866	1	11.7743	[I, II, X]	0.2879	1	11.9281	[54]	-1.29
	PP	0.2855	1	11.6327	[IX-XI,XVI]	0.2879	1	11.9281	[54]	-2.48
FM bcc Fe	FLAPW	0.2865	1	11.7603	[I, IV, X]	0.2858	1	11.6669	[54]	0.80
						0.2866	1	11.7709	[55]	-0.09
	PP	0.2836	1	11.4025	[X, XIII, XVI]	0.2858	1	11.6669	[54]	-2.27
					0.2866	1	11.7709	[55]	-3.13	
NM hcp Hf	PP	0.3195	1.5786	22.2901	[XI]	0.3230	1.5851	23.1300	[18]	-3.63
NM bcc Mo	FLAPW	0.3160	1	15.7762	[IV]	0.3145	1	15.5553	[18]	1.42
	PP	0.3149	1	15.6174	[XVI]					0.40
FM fcc Ni	PP	0.3523	1	10.9287	[XIII]	0.3520	1	10.9036	[56]	0.23
NM fcc Pd	PP	0.3954	1	15.4543	[XIII]	0.3890	1	14.7160	[18]	5.02
NM fcc Pt	PP	0.3977	1	15.7280	[XIII]	0.3923	1	15.0937	[18]	4.20
NM diam. Si	PP	0.5469	1	20.4501	[XVI]	0.5431	1	20.0227	[18]	2.13
NM hcp Ti	PP	0.2924	1.5818	17.1210	[XI, XIII]	0.2950	1.5866	17.6442	[18]	-2.97
NM bcc Ta	PP	0.3309	1	18.1159	[XVI]	0.3302	1	17.9996	[18]	0.65
NM bcc V	PP	0.2978	1	13.2092	[XVII]	0.3031	1	13.9215	[18]	-5.12
NM bcc W	PP	0.3171	1	15.9360	[XVI]	0.3165	1	15.8492	[18]	0.55
NM hcp Zr	PP	0.3236	1.5977	23.4332	[IX, XVII]	0.3232	1.5930	23.2838	[54]	0.64

Table 2.1: Structural properties of SER states. a and c are the lattice parameters, V_{at} is the volume per atom and $\Delta\%_{exp}$ is the deviation of *ab initio* results from experimental data in % of experimental value, PP stands for pseudopotential. The high deviation of $\Delta\%_{exp} = -8.27$ in the third row is caused by old set of calculation parameters for FM hcp Co.

error. The example of FLAPW calculation of energy dependence on volume for FM bcc Fe and AFM bcc Cr is shown in Figure 2.2.

Similar investigation was done for hypothetical **sigma phases of pure constituents Fe and Cr** [I]. In Figure 2.3(a), there are depicted two energy dependencies on volume calculated by LMTO and FLAPW method. In Figure 2.3(b) [I], the curves of energy dependence on volume calculated by FLAPW approach for both Fe and Cr are shown.

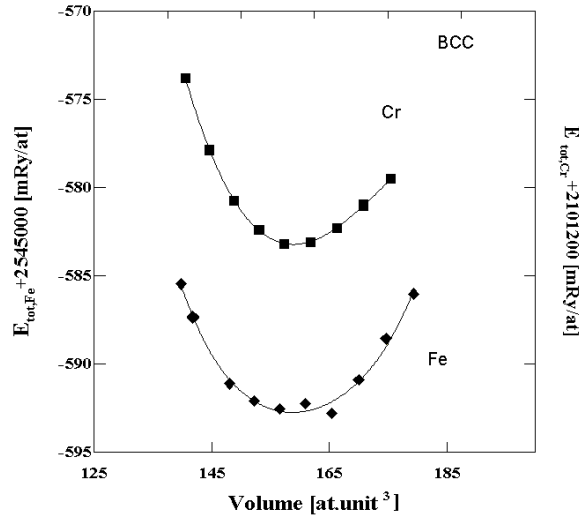
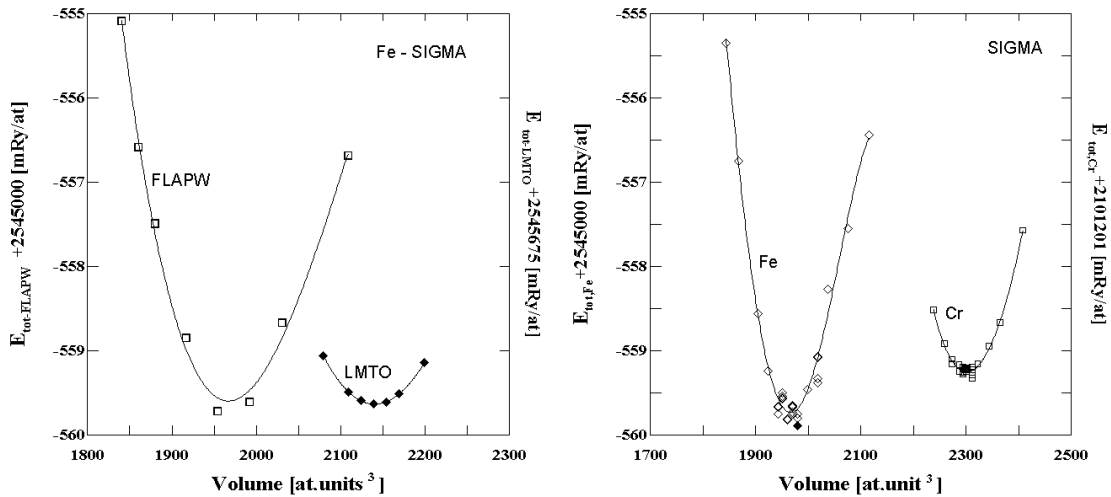


Figure 2.2: Volume dependence of total energy of AFM bcc Cr (■) and FM bcc Fe (◆) calculated by FLAPW method [I]. The volume corresponds to two-atom unit cell.



(a) Pure Fe, FLAPW (□) and LMTO (◆) optimisation. (b) Final FLAPW optimisation for pure Cr (□) and Fe (◆) sigma phase at constant c/a ratio; $c/a_{Fe} = 0.5174$, $c/a_{Cr} = 0.5237$ [I]. Full symbols represent the crossing points with previous optimisation of total energy vs. c/a ratio.

Figure 2.3: Volume dependence of total energy of sigma phases (30 atoms).

In the case of complex phases, not only lattice parameters but also the atomic positions were optimised. The easiest way how to perform such an optimisation is to employ the pseudopotential VASP code with its automatic relaxation. The equilibrium atomic positions of sigma phases of pure constituents [X] are listed in Table 2.2, columns 6-8. The internal parameters describing the atomic positions in chosen experimentally studied sigma phases are given in the same table in columns 3-5. The equilibrium data given in Table 2.2 reveal only very small scatter and the fully relaxed parameters describing the positions of atoms correspond well to those determined experimentally for alloy sigma phases.

The equilibrium lattice parameters of **Co**, **Cr** and **Fe sigma phases** calculated by LMTO, FLAPW and pseudopotential approaches are summarised in Table 2.3 [X]. In this case, LMTO method results in the highest values of the lattice parameter a and atomic volume V_{at} , the medium values are provided by the VASP code and finally the lowest numbers are obtained from the WIEN97 calculations. The scatter of the values is reasonably small, in units of percent. From this point of view, the all methods used can be considered as equivalent. Analogously the structural parameters of binary sigma phases can be obtained [X].

Subl.	Param.	Cr-Fe ^a	Cr-Co ^b	Co-Mo ^c	Co	Cr	Fe
		Ref. [19]	Ref. [20]	Ref. [21]		[X]	
4f	x	0.3986	0.3984	0.3973	0.4019	0.3982	0.4030
8i	x	0.4635	0.4627	0.4635	0.4613	0.4671	0.4572
	y	0.1312	0.1291	0.1283	0.1332	0.1285	0.1315
8i'	x	0.7399	0.7404	0.7450	0.7346	0.7434	0.7366
	y	0.0661	0.0654	0.0670	0.0669	0.0594	0.0660
8j	x	0.1827	0.1826	0.1820	0.1812	0.1877	0.1821
	z	0.2520	0.2500	0.2500	0.2507	0.2553	0.2503

Table 2.2: Experimental (columns 3-5) and by VASP calculated (columns 6-8) equilibrium values of internal structure parameters of NM sigma phases [X]. ^a $x_{Cr} = 0.495$, $T = 923$ K; ^b $x_{Cr} = 0.564$ and ^c $x_{Co} = 0.4$, $T = 1673$ K. The symbols x_{Cr} and x_{Co} represent the molar fraction of Cr and Co, respectively. The exact atomic positions can be calculated from these parameters using simple relations corresponding to the given sublattice and particular space group.

Elem.	LMTO			WIEN97			VASP		
	a (au)	c/a	V_{at} (au ³)	a (au)	c/a	V_{at} (au ³)	a (au)	c/a	V_{at} (au ³)
Co	16.1116	0.5161	71.9496	15.8602	0.5197	69.1126	15.9252	0.5289	71.2044
Cr	16.6677	0.5216	80.5088	16.3792	0.5237	76.7078	16.5267	0.5214	78.4528
Fe	16.0465	0.5180	71.3427	15.5987	0.5174	65.4592	15.9325	0.5210	70.2374

Table 2.3: Equilibrium lattice parameters and atomic volumes of NM sigma phase of pure constituents calculated by LMTO, WIEN97 and VASP codes [X].

The **V-Zr system** [XVII] was chosen as an example for modelling of Laves phases. The dependence of structural parameters on composition can be demonstrated for example on C14 Laves phase, see Figure 2.4, where the occupation of the $6h$ and $4f$ sublattice is changing.

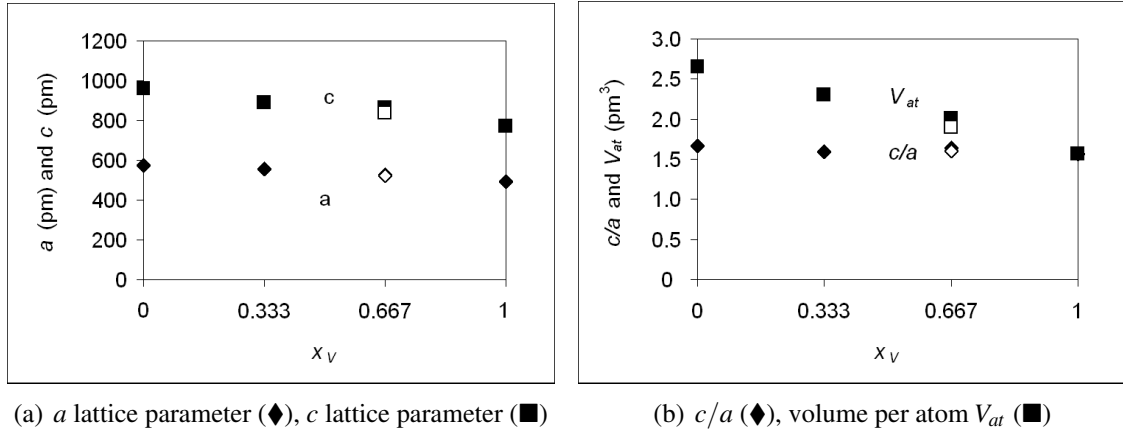


Figure 2.4: Composition dependence of structural parameters of C14 Laves phase in V-Zr system [XVII]. The open symbols correspond to experimental values [18].

It was found that the volume per atom V_{at} decreases with increasing molar fraction of vanadium. Similarly, the composition dependencies of structural parameters were studied in **Cr-Zr** [IX], **Cr-Hf** and **Cr-Ti** [XI] and **Fe-X** ($X = \text{Si, Cr, Mo, W, Ta}$) [XVI] system. In all the above mentioned systems, the dependence of volume on composition is linear. There are some deviations from linear dependencies of lattice parameters on composition in case of Cr_6X_6 and Cr_2X_{10} configurations in systems where $X = \text{Hf, Ti}$. Their values of a are higher and values of c are lower than the values from linear approximation. These deviations compensate in volume calculation.

2.2.2 Energies of formation I-IV,VI,VII,IX-XI,XIII,XIV,XVI,XVII

The energies of formation of studied structures (even of hypothetical phases consisting of pure constituents or phases with occupation of sublattices which has not been observed experimentally) can be evaluated according to the Equation (2.18), (2.19) or (2.20). The values obtained for **intermetallic phases** were compared with experimental data if available (Table 2.4). Sometimes, the ab initio methods can successfully reproduce the experimental values as it was found in case of Fe_2Ta C14 Laves phase, NiTi, FePt and FePt₃. But there are phases, for which the agreement is worse, e.g. Fe_2W , Cr_2Hf and FePd₃. This disagreement between theory and experiments is caused by different temperatures at which the experiments (room temperature or higher) and calculations (0 K) are performed.

In case of **sigma phase** [X], it was found that some atoms preferentially occupy certain sublattices which significantly influences the stability of particular configurations of this phase. Fe and Co (in binary systems with Cr) prefer the δ_i sublattice and Cr the δ_i and δ_j sublattices. The same findings concerning the site preferences in Cr-Fe system were reported by Korzhavyi [36] and were confirmed by experimental results [20].

Phase	$\Delta E_{f,abinitio}^{int}$ (kJ/mol of atoms)	Ref.	$\Delta H_{f,experiment}^{int}$ (kJ/mol of atoms)	Ref.
Fe ₂ Ta - C14 Laves phase	-18.61	[XVI]	-19.27	[57]
Fe ₂ W - C14 Laves phase	0.68	[XVI]	-7.61±3.14	[58]
Cr ₂ Hf - C15 Laves phase	-10.38	[XI]	-4.8±4.3	[59]
NiTi	-33.1	[XIII]	-32.7±1.0	[XIII]
FePt	-23.1	[XIII]	-23.0±1.9	[XIII]
FePt ₃	-19.2	[XIII]	-20.7 ± 2.3	[XIII]
FePd ₃	-10.0	[XIII]	-16.0 ± 2.7	[XIII]
Fe-Cr - sigma phase				
$x_{Cr} = 0.4$, NM	10.23	[X]	7.7 ^a	[60]
$x_{Cr} = 0.4$, FM	6.89	[X]		
$x_{Cr} = 0.533$, NM	8.01	[X]	6.5 ^b	[61]
$x_{Cr} = 0.533$, FM	7.90	[X]		
Cr-Co - sigma phase				
$x_{Cr} = 0.533$, NM	11.50	[X]	9.37 ^c	[62]
$x_{Cr} = 0.533$, FM	9.98	[X]		
$x_{Cr} = 0.6$, NM	9.40	[X]	(-2.9;5.1) ^d	[61]
$x_{Cr} = 0.6$, FM	9.04	[X]	(2.64;6.77) ^e	[63]

Table 2.4: Ab initio calculated energies of formation and experimental enthalpies of formation of intermetallic phases.

^a $x_{Cr} = 0.45$, ^b $x_{Cr} = 0.45$, ^c $x_{Cr} = 0.6$, ^d $x_{Cr} = 0.45 - 0.63$ and ^e $x_{Cr} = 0.57 - 0.61$.

2.2.3 Magnetic properties X,XIII

Some elements such as Cr, Fe, Co and Ni have tendencies to magnetic ordering in pure state, which was confirmed by experiments. In this case, their magnetic arrangement has to be reproduced by ab initio calculations. The overview of magnetic properties of studied elements in **SER states** is given in Table 2.5.

When intermetallic phases contain elements listed above, there is a high probability that the magnetism will play an important role in their behaviour. Sometimes, it is confirmed by experiment but sometimes the magnetic ordering is important only at very low temperatures which has to be taken into account when performing ab initio calculations at 0 K. The detailed study of magnetic properties for all 32 configurations of **sigma phases** in **Fe-Cr** and **Co-Cr** binary system was performed [X].

It turns out, for example, that elemental iron in the sigma phase structure exhibits different magnetic moments at different sublattices. At the *4f*, *8i* and *8j* sublattices, the local magnetic moment of Fe atoms equals to 2.29 $\mu_B/atom$, 2.00 $\mu_B/atom$ and 1.87 $\mu_B/atom$, respectively, the highest magnetic moment being at the sublattice *4f* possessing the highest coordination number. Magnetic moments of iron in *8i'* and *2a* sublattices with the lowest coordination numbers are substantially lower: 1.22 $\mu_B/atom$ and 1.10 $\mu_B/atom$. In case of elemental Co, the magnetic moment decreases from 1.70 $\mu_B/atom$, 1.67 $\mu_B/atom$, 1.59 $\mu_B/atom$ to 1.54 $\mu_B/atom$ which corresponds to the sublattices *4f*,

Structure	Method	μ (μ_B)	Ref.	μ_{exp} (μ_B)	Ref.	B_{teor} (GPa)	Ref.	B_{exp} [64] (GPa)
FM hcp Co	FLAPW	1.74	*	1.72	[56]	225.08	*	191.4
	PP	1.56	*			210.94	*	
AFM bcc Cr	FLAPW	1.07	*	0.59	[54]	193.32	*	190.1
	PP	1.08	*			186	[XVI]	
FM bcc Fe	FLAPW	2.28	*	2.22	[56]	167.79	*	168.3
	PP	2.18	[XIII]	2.12	[54]	194	[XVI]	
NM hcp Hf	PP					112.68	*	109
NM bcc Mo	FLAPW					264.09	*	272.5
	PP					271	[XVI]	
FM fcc Ni	PP	0.6	[XIII]	0.61	[56]	196.97	*	186
NM fcc Pd	PP					223.54	*	180.8
NM fcc Pt	PP					249.33	*	278.3
NM diam. Si	PP					90	[XVI]	98.8
NM hcp Ti	PP					117.46	*	105.1
NM bcc Ta	PP					201	[XVI]	200
NM bcc V	PP					188.5	[XVII]	161.9
NM bcc W	PP					315	[XVI]	323.2
NM hcp Zr	PP					97.6	[XVII]	83.3

Table 2.5: Magnetic and mechanical properties of SER states. μ is the magnetic moment, B bulk modulus and PP stands for pseudopotential. * this work.

(δi , δj), $\delta i'$ and $2a$, respectively. Again, the atomic magnetic moment decreases with decreasing coordination number. On the other hand, the sigma phase of elemental Cr is nonmagnetic because the magnetic moments found are very close to zero. However, it does not mean at all that the chromium atoms are nonmagnetic through the whole composition region. Their magnetic moment calculated by VASP reaches even $-1.21 \mu_B/atom$ ($-1.29 \mu_B/atom$) in CrCoCoCoCo (CrFeFeFeFe) configuration. In binary sigma phases we can see that the atomic magnetic moments of all three constituents (i.e. Fe, Co, Cr) mostly decrease with increasing molar fraction of chromium. Similarly as in elemental Fe and Co, the highest values of magnetic moments are found at the $4f$ sublattice with the highest coordination number. In Cr–Fe system, the Cr atoms exhibit very often antiferromagnetic behaviour with respect to Fe atoms, i.e. they have the opposite orientation of magnetic moments. This fact is fully manifested at δi , $\delta i'$ and δj sublattices with some exceptions for higher chromium concentrations. The antiparallel arrangement of magnetic moments is also found at the $2a$ and $4f$ sublattices, again with some exceptions. In sporadic cases the antiferromagnetic arrangement occurs at Fe atoms in the sublattice $2a$ for FeCrFeCrFe configuration and in $\delta i'$ for FeFeCrFeCr and CrCrCrFeCr. In Cr–Co system Cr atoms also exhibit antiferromagnetic behaviour with respect to Co atoms. However, with increasing molar fraction of Cr atoms, we observe increasing amount of Cr atoms that behave in the ferromagnetic way with respect to Co atoms. In contrast to the Cr–Fe system the occurrence of this arrangement is not fully connected with particular sublattices, but it is

most frequent at the $2a$ and $4f$ sublattices.

Similarly, the magnetism had to be included in study of **NiTi**, **FePd**, **FePd₃**, **FePt** and **FePt₃** phases [XIII]. The FePd, FePd₃, FePt and FePt₃ structures are ferromagnetic whereas the NiTi intermetallics in both the cubic and the monoclinic arrangement are nonmagnetic. The comparison of found and experimental magnetic moments (Table 4C in [XIII]) in FM bcc Fe, FM fcc Ni, FM FePd, FM FePd₃ and FM FePt provides an excellent agreement. In the case of FePt₃, the AFM arrangement of the structures is reported [65]. Nevertheless, the magnetic moments found in the literature agree very well with the calculated ones.

2.2.4 Mechanical properties ^{XVI,XVII}

The values of bulk moduli of **SER states** were presented in [XVI, XVII] and are listed in Table 2.5. It shows that the deviations from experiments are higher than those found for structure parameters but they are usually within ± 20 GPa, which is acceptable. This limit was exceeded for FM hcp Co, FM bcc Fe, NM fcc Pd, NM fcc Pt and NM bcc V.

To judge the mechanical stability of phase, the elastic constants has to be calculated. This was done for cubic **C15 V₂Zr Laves phase** where three elastic constants $C_{11} = 162.33$ GPa, $C_{44} = 6.60$ GPa and $C_{12} = 136.62$ GPa were evaluated (Table 4 in [XVII]). This phase was declared to be mechanically stable as the elastic stability criteria: $C_{11} > 0$; $C_{44} > 0$; $C_{11} > |C_{12}|$; and $(C_{11} + 2C_{12}) > 0$ were fulfilled. Additionally the stability of C15 V₂Zr Laves phase was confirmed by phonon spectra calculations [XVII].

Chapter 3

CALPHAD modelling

Nowadays, more sophisticated and complex materials with excellent properties are required in material engineering and technologies. These advanced materials often consist of more than 10 elements and many of them are used in extreme conditions. Nevertheless, the tendency to reach thermodynamic equilibrium, either stable or metastable, after long-term exploitation, is characteristic for most of such materials. Some alloying elements can significantly improve desired properties, but they can also introduce some unexpected features (e.g. precipitation of unwanted or new phases, brittleness, degradation processes, etc.) in long term run that can outweigh their positive influence [66]. In all such cases the deep knowledge of relevant phase diagrams (or their sections) and thermodynamic properties is crucial for prediction of structural and material development towards the equilibrium or metastable state.

The powerful combination of *ab initio* electronic structure calculations, semiempirical thermodynamic approach using the CALPHAD method [5, 67] and carefully selected experimental investigations is employed to model phase diagrams of complex materials and to construct a consistent thermodynamic database for these systems [I-IV, VII, IX, XI, XVII]. Furthermore, the extension of the thermodynamic modelling down to 0 K temperature is presented [XIV, XVII].

3.1 Theory and methodology

The CALPHAD method [5, 67] is based on the modelling of the Gibbs energies of all phases possibly existing in the system, followed by the minimisation of total Gibbs energy of the system. The Gibbs energies of relevant phases are obtained by assessing pre-defined polynomials to the experimental phase equilibrium data (the positions of phase boundaries, compositions of phases in equilibrium, etc.) and known thermodynamic quantities (e.g. heat capacities, activities). It means that CALPHAD method is dependent on certain amount of robust experimental or *ab initio* data for simpler systems, especially for binary and ternary ones.

The molar Gibbs energy of the whole system is defined as the sum of molar Gibbs energies of all included phases G^f , multiplied by their molar fraction x^f

$$G^{tot} = \sum_f x^f G^f, \quad (3.1)$$

where

$$G^f = \sum_i y_i {}^0G_i^f + G^{id} + G^E + G^{mag} + G^{pres}. \quad (3.2)$$

The molar Gibbs energy of phase G^f contains the sum of molar Gibbs energies of pure constituents i in the phase f multiplied by their lattice fractions ($\sum y_i {}^0G_i^f$), the terms describing ideal (G^{id}) and nonideal (G^E) mixing and, when needed, some special terms such as magnetic (G^{mag}) or pressure (G^{pres}) contributions. For a binary system (A-B), the terms describing the mixing may be evaluated by relatively simple formulas

$$G^{id} = RT (y_A \ln y_A + y_B \ln y_B) \quad (3.3)$$

and

$$G^E = y_A y_B \left(L^0(T) + L^1(T) (y_A y_B) + L^2(T) (y_A - y_B)^2 + \dots \right), \quad (3.4)$$

where L^0 , L^1 and L^2 are the expansion coefficients of the Redlich-Kister polynomial [68], T is temperature and R is the universal gas constant. The temperature dependence of L -parameters is given by an equation of the following type

$$L^{0 \text{ or } 1 \text{ or } 2 \dots} = a + bT + c T \ln T. \quad (3.5)$$

In the CALPHAD modelling, various models for ${}^0G_i^f$ can be used [67]. Here, more details are provided on a sublattice model as this approach was used for intermetallic phases studied in papers commented in this thesis. In general, the number of sublattices in sublattice model can change according to the crystallography of phase and the needs of modelling but, for simplification, the presented description is limited to two sublattices.

In the two-sublattice model, the Gibbs energy of the reference state is

$$G^{ref.f} = y_A^1 y_A^2 {}^0G_{A:A}^f + y_B^1 y_A^2 {}^0G_{B:A}^f + y_A^1 y_B^2 {}^0G_{A:B}^f + y_B^1 y_B^2 {}^0G_{B:B}^f \quad (3.6)$$

with y_A^1 , y_B^1 , y_A^2 and y_B^2 being lattice fractions of components A and B in sublattices 1 and 2. The Gibbs energies of end-members (${}^0G_{A:A}^f$, ${}^0G_{B:A}^f$, ${}^0G_{A:B}^f$, ${}^0G_{B:B}^f$) can be temperature dependent according to equation of the same type as Equation (3.5). Here, a , b and c are constants determined from experiments or from optimisation of the thermodynamic parameters.

In case of intermetallic phases such as Laves or sigma phase, only some of the Gibbs energies of four end-members in Equation (3.6) can be experimentally determined namely, the ${}^0G_{A:B}$. The quantities ${}^0G_{A:A}$ and ${}^0G_{B:B}$ characterise, formally, the Gibbs energies of pure constituents in the sigma or Laves phase structures, which may be given some reasonable positive value. In the presented papers [I, II, IV, IX, XI, XVII], the arbitrariness in choosing the values of the Gibbs energy of these formal end-members is overcome by determining their total energies with the help of ab initio calculations. The Gibbs energies of the end-members are then expressed by the following two equations

$${}^0G^{int} = G^{SER} + \Delta^0G^{int-SER} \quad (3.7)$$

and

$$\Delta^0G^{int-SER} = {}^0G^{int} - {}^0G^{SER} = \Delta^0H^{int-SER} - T {}^0S^{int-SER}, \quad (3.8)$$

where H is enthalpy, S is entropy and *int* stands for intermetallic phase. The difference in enthalpies $\Delta^0H^{int-SER}$ is obtained as

$$\Delta^0H^{int-SER} = \Delta^0E^{int-SER} + \int \Delta C_p^{int-SER} dT \quad (3.9)$$

and vibrational contribution to the entropy can be expressed by

$$\Delta^0S^{int-SER} = \int \left(\Delta C_p^{int-SER} / T \right) dT, \quad (3.10)$$

where C_p is the heat capacity at constant pressure.

At $T = 0$ K and at the equilibrium volume, $\Delta^0H^{int-SER} = \Delta^0E^{int-SER}$, i.e. the difference in enthalpies is equal to the total energy difference between the intermetallic phase and the SER state, which was calculated ab initio in the presented papers. These ab initio values may be successfully employed in the phase diagram calculations, as it is shown below.

Employing the equations provided in this section, the sets of thermodynamic parameters describing the behaviour of Gibbs energy with respect to temperature and composition were obtained [I, II, IV, IX, XI, XVII] and the corresponding phase diagrams were calculated.

3.1.1 Sigma phase modelling I-IV,VII

The Gibbs energy of sigma phase can be in principle described by Equation (3.6) extended to five sublattices, which corresponds to the number of crystallographic sublattices. However, the number of parameters used in such model would be too large and their values would be experimentally inaccessible. Therefore, the situation in sigma phase modelling required some simplifications.

At the beginning, the Gibbs energy of bcc phase was used in the sublattice model instead of the Gibbs energy of sigma phase. Later on, the estimations were done using extrapolation of experimental data [69]. Now, the model of a substitutional structure $(B)_8(A)_4(A,B)_{18}$ or $(B)_{10}(A)_4(A,B)_{16}$ is often applied. Such modelling is performed using the assumption that the atoms are ordered in two or more sublattices [70–72]. The problem here consists in the dilemma into which sublattice each element goes and, further, how to reduce the number of five sublattices in order to restrict the number of model parameters. The solution was proposed in [71], however, it was not possible to describe the Gibbs energy of sigma phase close to the regions of pure elements as it is obvious from the formula $(B)_{10}(A)_4(A,B)_{16}$.

Using the knowledge, that the sigma phase does not behave like rigid stoichiometric phase, which means that the sublattices in sigma phase are not exclusively occupied by one kind of atoms (mixing is possible), we have proposed a new physical (1 1) two-sublattice model [I]. In this solid solution model (analogous to model of fcc or bcc [5]), the label (1 1) means that the solution phase contains two sublattices, each of them having one lattice site

(only one atom can be placed here). In this thermodynamic description the five sublattices found in the X-ray experiments are reduced to two. This reduction gives us the possibility to describe the sigma phase in the whole composition region which is demonstrated for Cr-Fe system [I] in the following equation

$$G_{Cr,Fe}^{sigma} = y_{Fe} {}^0G_{Fe}^{sigma} + y_{Cr} {}^0G_{Cr}^{sigma} + G_{Cr,Fe}^{id,sigma} + G_{Cr,Fe}^{E,sigma}, \quad (3.11)$$

where 0G is given by Equations (3.7) and (3.8). Similarly, the (1 1) two-sublattice model was also used in the thermodynamic modelling of sigma phases in Cr-Co [III] and both Co-Mo and Fe-Mo [IV] binary systems, and Fe-Ni-Cr [III] and Cr-Fe-W [VII] ternary systems.

3.1.2 Modelling at low temperatures ^{XIV,XVII}

To describe the phase equilibria at low temperatures (i.e. below the temperature limit T_{lim} used for the SGTE Gibbs energy expressions for pure elements [13]), it is necessary to find polynomials which

- obey the thermodynamic laws at low temperatures and
- have the same function value and the value of the first derivative at T_{lim} as the corresponding SGTE Gibbs energy expressions [13].

Furthermore, the values of SGTE polynomials of Gibbs energy above T_{lim} should be left unchanged, because they are based on experiments and are widely used.

In Ref. [XIV], the SGTE polynomials are extended below T_{lim} using the Einstein formula for the temperature dependence of the heat capacity. In this first step, magnetic and pressure contributions to the Gibbs energy and the temperature and concentration dependence of the Einstein (T_E) and Debye (T_D) temperature are not considered.

According to [73], the heat capacity of pure nonmagnetic elements at low temperatures can be represented by equation

$$C_{p,low} = 3AR \left(\frac{T_E}{T} \right)^2 + aT + bT^2 + cT^3, \quad (3.12)$$

where T is the temperature in K and $A = \frac{e^{T_E/T}}{(e^{T_E/T} - 1)^2}$. The first term in Equation (3.12) represents the contribution of the harmonic lattice vibrations. The second term consists of contributions from electronic excitations and low-order anharmonic corrections (dilatational and explicitly anharmonic) and the parameter a can be related to a non-thermodynamic information, e.g., electron density of states at Fermi level. The third term corresponds to the high-order anharmonic lattice vibrations and it is seldom that one can find experimental information to validate the parameter b . Parameter c is added for smooth continuation of C_p through the T_{lim} .

The low temperature Gibbs energy related to the SER states is evaluated as [73]

$$G_{low}(T) = E_0 + \frac{3}{2}RT_E + 3RT \ln \left(1 - e^{-T_E/T} \right) - \frac{a}{2}T^2 - \frac{b}{20}T^5 - \frac{c}{6}T^3, \quad (3.13)$$

where E_0 is the total energy of a nonmagnetic structure of an element at 0 K relative to the SER state and the second term is the energy of zero-point lattice vibrations [74, 75].

The condition for smooth connecting of the extended $G_{low}(T)$ function to the $G(T)$ in SGTE data [13] at contact temperature T_{lim} , (usually, but not always 298.15 K) means that function values and values of first derivative of both functions have to be equal at T_{lim} . Similarly, the condition for a smooth connection of heat capacity function below ($C_{p,low}(T)$) and above ($C_p(T)$) T_{lim} has to be fulfilled. Based on these four conditions, four equations for $G_{low}(T_{lim})$, $\frac{dG_{low}}{dT}(T_{lim})$, $C_{p,low}(T_{lim})$ and $\frac{dC_{p,low}}{dT}(T_{lim})$ including E_0 , a , b and c parameter were obtained and solved. On the left side of these equations, there are expressions for low-temperature polynomials based on Equations (3.12) and (3.13) for T_{lim} . Here, the Einstein temperature is related to the Debye temperature T_D as $T_E \cong 0.77T_D$ [75]. On the right side of equations, there are expressions for the same variables (at T_{lim}), however, expressed from polynomials valid above T_{lim} and provided in [13]. More details on this approach and values of E_0 , a , b and c parameters for particular elements are provided in [XIV].

3.2 Results and discussion

3.2.1 Binary systems I,II,IV,IX,XI,XVII

The modelling of **sigma phase** is represented here by the **Cr-Fe** binary system [I]. The Gibbs energies and enthalpies for phases found in this system [I] are shown in Figure 3.1. Here, the differences between the results obtained using the old three-sublattice [72] and new (1 1) two-sublattice [76] model for description of sigma phase is shown. It is obvious that the values based on the (1 1) two-sublattice model run through the whole composition region, which is convenient in modelling of more-components systems.

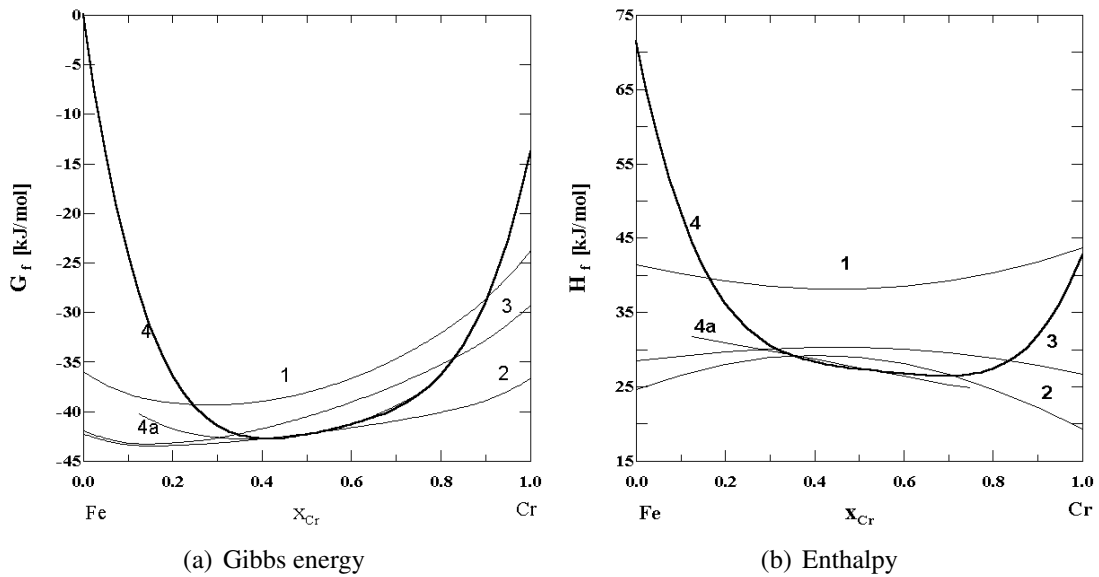


Figure 3.1: Concentration dependence of Gibbs energy (1000 K) and enthalpy in Cr–Fe system [I]. (1) liquid, (2) bcc phase, (3) fcc phase, (4) sigma phase (new two-sublattice model), (4a) sigma phase (three-sublattice model).

The phase diagram calculated using the new (1 1) two-sublattice model [76] (Figure 3.2) yields better agreement with experimental data than that obtained by means of an older three-sublattice model [72].

The thermodynamic modelling of sigma phases based on the same theoretical approach as described for Cr-Fe binary system [I] was performed in **Cr-Co** [II] and both **Co-Mo** and **Fe-Mo** [IV] binary systems. The results of modelling in ternary systems are described in Section 3.2.2 *Ternary systems*.

In case of **Laves phases**, mostly, the two-sublattice model $(A,B)_2(A,B)$ with four end-members was employed [IX, XI, XVII] and **Cr-Zr** binary system [IX] was chosen as an example. The Gibbs energy of all three Laves phases (C14, C15 and C36) in Cr-Zr system was modelled with the help of ab initio calculated total energy differences, presented in Table 3 in Ref. [IX]. The C14 and C36 Laves phases were also modelled by three-sublattice model $(A,B)_4(A,B)_6A_2$ employing the total energy differences for the Cr_6Zr_6 and Cr_2Zr_{10} configuration.

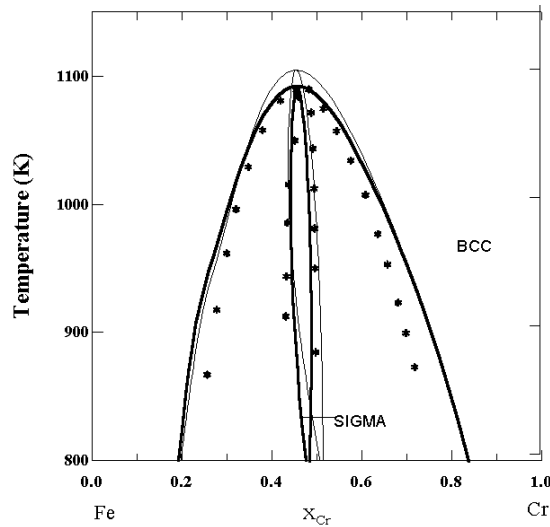


Figure 3.2: Phase diagrams of Cr–Fe system [I]. Thick line: calculated by the new two-sublattice model (for data see Table 4 in Ref. [I]), thin line: calculated by three-sublattice model (data from [72]), stars: experimental data [77].

In both cases, the Gibbs energy is obtained from Equations (3.7) and (3.8) where the entropy term, containing also the vibration contribution to the enthalpy, is adjusted to the experimental data. The L -parameters describing the excess Gibbs energy G^E of non-ideal mixing in Equation (3.4) are obtained in the same way. The thermodynamic parameters for all other phases (liquid, hcp, bcc, fcc) are based on unary data from [13]. The calculated phase diagram is presented in Figure 3.3, where the equilibria with all three Laves phases are denoted. It was shown that ab initio calculated structural energy differences fit well the two-sublattice model of C15 and three-sublattice model of C14 and

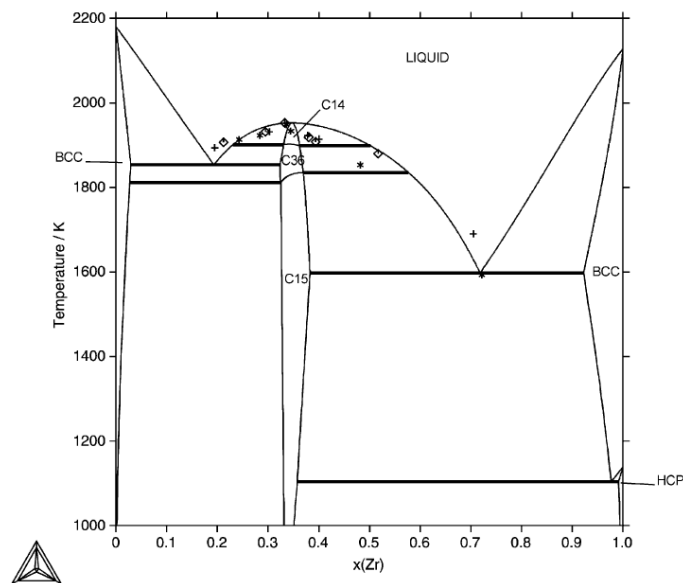


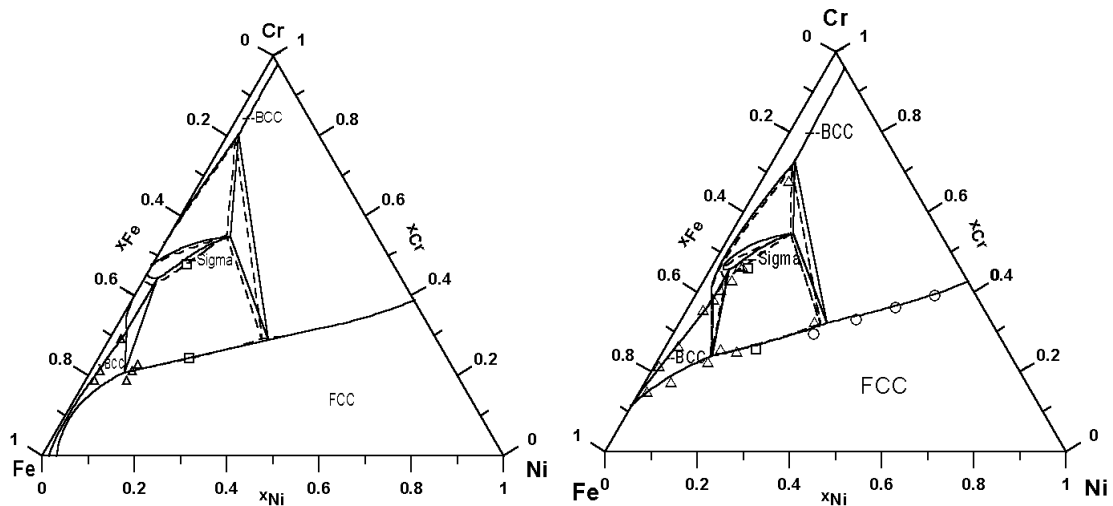
Figure 3.3: Phase diagram of Cr–Zr system with experimental data [IX].

C36 Laves phases. Moreover, a substantially smaller number of adjustable parameters was necessary for thermodynamic description of Laves phases than in previous attempts in literature. By analogy, the thermodynamic modelling and phase equilibria calculations with Laves phases were performed in **Cr-Hf** [XI] and **Cr-Ti** [XI] system.

3.2.2 Ternary systems III,VII

As mentioned in Section 3.2.1 *Binary systems*, the modelling of sigma phases using the (1 1) two-sublattice model had been performed in several binary systems and it was extended to more-components systems, i.e. to ternary system **Fe-Ni-Cr** [III] and **Cr-Fe-W** [VII].

The calculated phase diagrams of Cr-Fe-Ni system at various temperatures are presented in Figure 3.4 and it was found that the (1 1) two-sublattice model of the sigma phase can be also used for a reasonable description of phase equilibria with sigma phase in the Fe-Cr-W system, although the sigma phase is not stable in two binary subsystems, i.e. in Fe-W and Cr-W.



(a) $T = 1073$ K; experimental data: triangles for bcc/fcc [79], squares for fcc/sigma [80].

(b) $T = 1173$ K; experimental data: triangles for bcc/fcc [81], squares for fcc/sigma [80], circles for fcc [82].

Figure 3.4: Calculated phase diagram of Fe-Ni-Cr system [III]. Full lines: the two-sublattice model of sigma phase, dashed lines: the three-sublattice model [72] using data from [78].

3.2.3 Thermodynamic modelling at low temperatures XIV,XVII

The temperature dependencies of G and C_p for **pure elements** at low temperatures were modelled and the results for chosen elements are demonstrated, in Figure 3.5. These figures show that the knowledge of the Debye (Einstein) temperature makes it possible to obtain a realistic extension of Gibbs energy function as the temperature falls towards 0 K.

The thermodynamic modelling at low temperatures presented for pure elements [XIV] can be also applied to complicated **intermetallic phases** such as C15 Laves phase in **V-Zr**

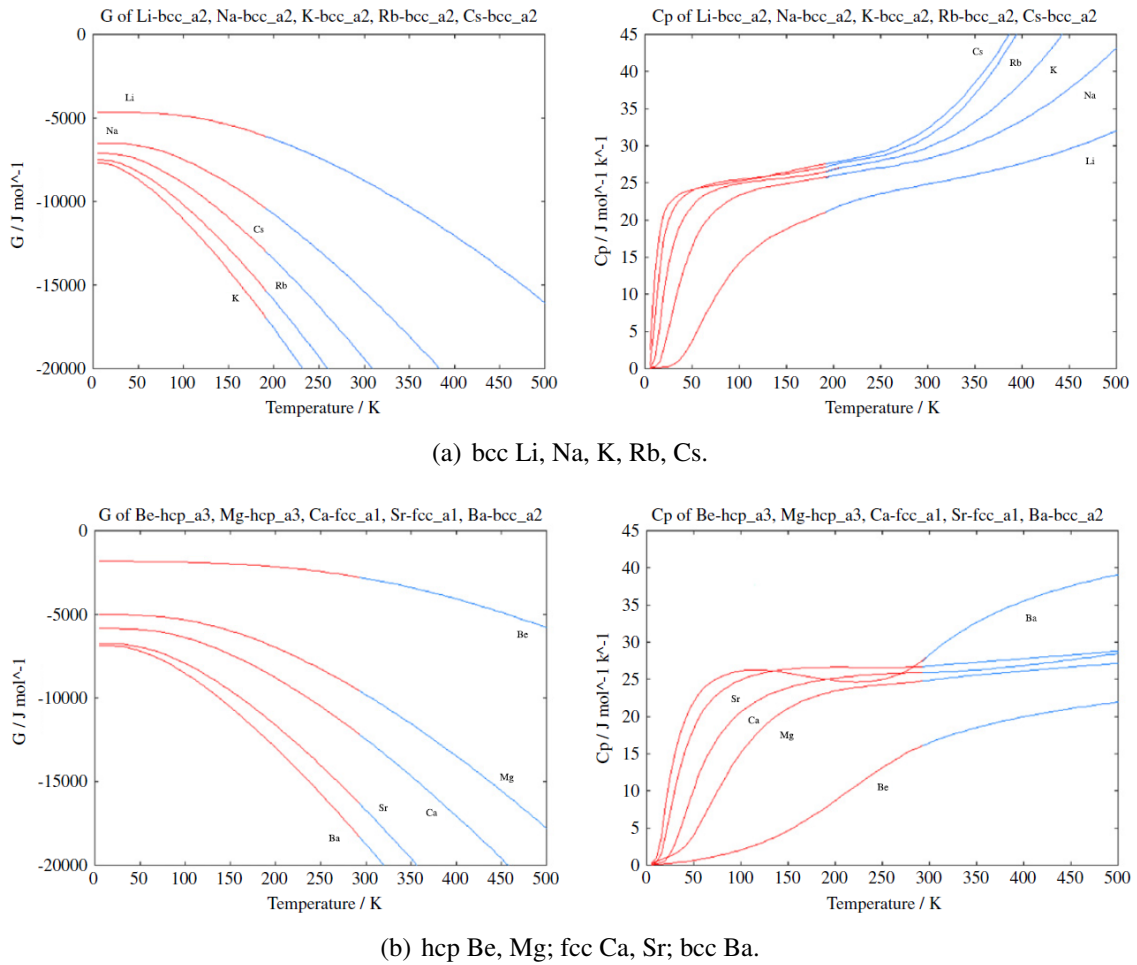


Figure 3.5: Temperature dependence of Gibbs energy and heat capacity for extended and SGTE functions [XIV].

system [XVII]. In this system the thermodynamic data above room temperature were taken from literature [10] and improved for C15 Laves phase and a hcp phase. The new extension of expression of Gibbs energy of C15 Laves phase and rhombohedral phase to zero Kelvin compatible with Gibbs energy expressions above 298.15 K [10] and based on respective values of Debye temperatures [83–85] was provided.

The phase diagram including the phase equilibria at low temperatures is presented in Figure 3.6. The shape of corresponding molar Gibbs energy $G(T)$ functions for V_2Zr C15 Laves phase and for V_2Zr rhombohedral phase in the temperature region 0–400 K is designed in Figure 3.7.

The work [XVII] shows that the methodology of calculation of unary data [XIV] at temperatures below 298.15 K is transferable to more complicated structures.

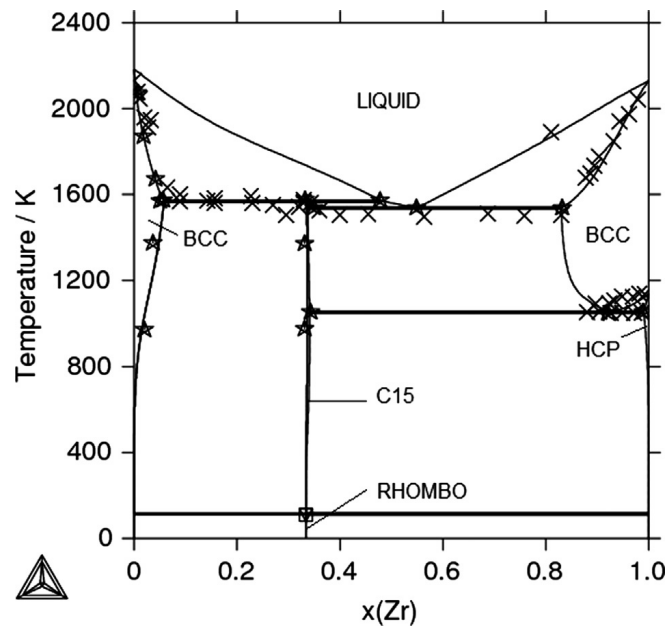


Figure 3.6: Phase diagram of V–Zr binary system [XVII] compared with experimental data: stars [86], crosses [87], square [88] and triangle [89].

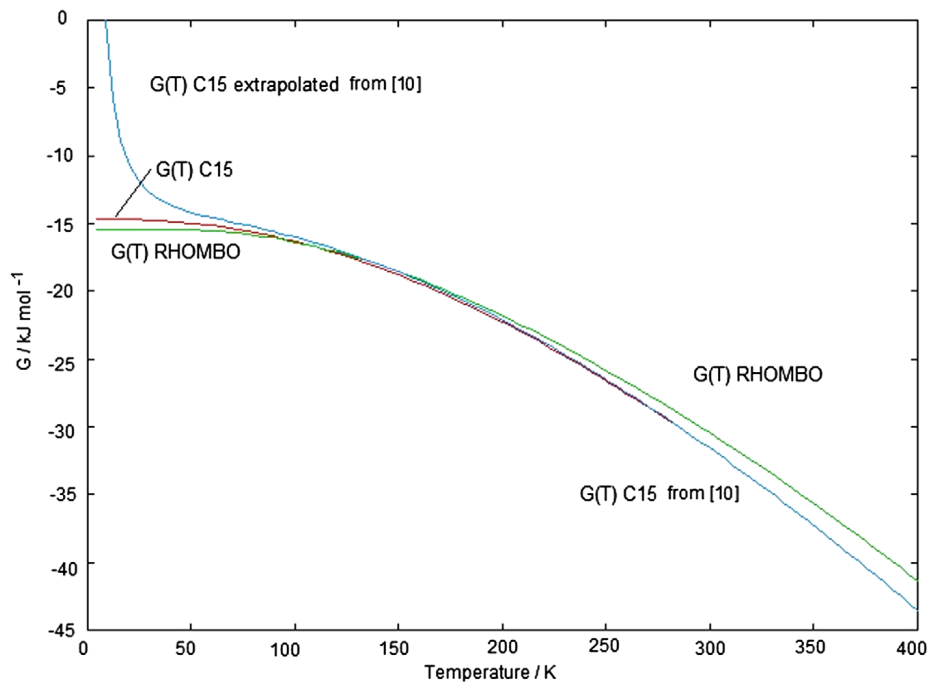


Figure 3.7: Temperature dependence of the molar Gibbs energy of V_2Zr C15 Laves phase and of V_2Zr rhombohedral phase [XVII]. Blue curve represents the Gibbs energy of the V_2Zr C15 Laves phase according to [10] including its extrapolation below 298.15 K, the red / green curve show the extension of the Gibbs energy [XIV] of the V_2Zr C15 Laves phase / V_2Zr rhombohedral phase based on our new model to zero Kelvin temperature.

Conclusions and main results

In this thesis, the results of ab initio electronic structure calculations and the CALPHAD modelling were summarised. It was shown that the combination of both approaches provides a better physical insight into the construction of phase diagrams [I-IV,VII,IX-XI,XVII]. The advantage of implementation of ab initio calculated lattice stabilities into CALPHAD modelling is especially crucial when the system studied contains complex phases such as sigma and Laves phases. The above mentioned theoretical methods are very important in both basic materials science and practical applications in industrial laboratories to plan effectively their experimental program from the point of view of economy and time.

4.1 Ab initio calculations

Our first-principles calculations provide the basic information about the properties of metallic phases. They validate the efficiency of methods applied when the experimental data are available for comparison. On the other hand, they also provide new experimentally inaccessible data, e.g. magnetic moments of particular atoms [X, XIII], preferential occupation of sublattices by particular elements in complex phases [III, VII, X], and energies of formation of metastable phases [I-IV,VII,IX-XI,XVII]. The ab initio data obtained may be considered as the first step to determination of both thermodynamic and mechanical stability of various intermetallic phases influencing the properties of materials.

Detailed conclusions about ab initio calculations

The structural, magnetic and mechanical properties of **SER states** of pure constituents were over-viewed and compared with experimental data [I,II,IV,VIII-XI,XIII,XVI,XVII] providing good agreement. The calculated total energies were subsequently used to evaluate the lattice stabilities of intermetallic phases.

The detailed ab initio study was accomplished for **sigma phases** in **Cr-Fe** and **Cr-Co** binary system [X] using the LMTO-ASA, FLAPW and pseudopotential method. The energies of formation and magnetic ordering were discussed and compared with experimental data. The inclusion of magnetic ordering stabilises the sigma phase in these systems and results in the shift of stability region towards the configurations with a higher concentration of iron or cobalt. We predicted that Cr-Fe and Cr-Co sigma phases are magnetically ordered at 0 K, which corresponds to experimental findings. Our study reveals that the largest part of magnetisation is carried by the iron or cobalt atoms and that the chromium

atoms do not contribute to this effect very much although they induce a decrease of the total magnetic moment by their AFM behaviour in some sublattices. The magnetic moments depend on the kind and position of the atom. The influence of the sublattice on the magnetic moment is the same for both Fe and Co atoms and their magnetic moments decrease from the sublattices $4f$, $8i$, $8j$, $8i'$ to $2a$. The magnetic moment of Cr in the sigma phase structure is close to zero. However, it increases with the increasing number of Fe or Co atoms in the structure. Combining the LMTO-ASA and FLAPW method, the concentration dependence of the energy of formation of **sigma phase** in **Fe-Ni** [III], **Ni-Cr** [III], **Cr-W** [VII] and **Fe-W** [VII] systems was calculated and compared with the Gibbs energies of various phases in Fe-Ni and Ni-Cr system and with Gibbs energy of sigma phase in Cr-W and Fe-W system. Energies of formation of the sigma phase in Fe-Ni, Fe-W and Cr-W binary systems are mainly positive and they are in agreement with supposed metastability in mentioned systems.

With the help of ab initio electronic structure calculations, the relations between the electronic structure, size of the atoms and the thermodynamic as well as structural properties of **C14 Laves phases** in **Fe-X** ($X = \text{Si, Cr, Mo, W, Ta}$) binary systems were understood [XVI]. It was found that the structure parameters and energies of formations strongly depend on the molar fraction of iron and that the calculated equilibrium parameters correspond very well to the experimental values. Our calculations reveal that the C14 Laves phase is unstable at zero temperature in both Fe-Mo and Fe-W system which is in contradiction with experiments. However, the absolute value of the total energy of formation is very low. We suppose that the instability at higher temperatures is suppressed by the entropy effects. The Fe_2Ta C14 Laves phase is stable at low temperatures. In **Cr-Zr** [IX], **Cr-Hf** [XI], **Cr-Ti** [XI] and **V-Zr** [XVII] system, the ab initio calculated structural parameters and energies of formation of Laves phases correspond reasonably well to both experimental data where available and to previous theoretical results.

The total energies of formation and magnetism were also studied in **NiTi**, **FePd**, **FePd₃**, **FePt** and **FePt₃** [XIII]. The ab initio calculated values were compared with the experimental enthalpies of formation and with values calculated using the semi-empirical model of Miedema and co-workers [90]. It was shown that the energies of formation corresponding to the equilibrium arrangement can significantly contribute to the analysis of the energetics of intermetallic phases in spite of the fact that they are calculated at 0 K. Ab initio calculated energies of formation of **PdBi** and **PdBi₂** intermetallics were successfully used as a basis for a thermodynamic assessment of the phase diagram of the Bi-Pd system [VI].

Except for the lattice stabilities, the so called **mechanical stabilities** can be obtained from ab initio calculations of elastic constants and phonon spectra. This was demonstrated in case of V_2Zr C15 Laves phase [XVII].

4.2 CALPHAD modelling

We were among the first groups in the world applying the combination of CALPHAD method and ab initio techniques in phase diagram modelling of systems with complex intermetallic phases [I,II]. We implemented this approach into the new (1 1) two-sublattice model for sigma phase [I-IV,VII] defining the Gibbs energy of this phase in the whole

composition region which is crucial for predictions of phase equilibria in multicomponent systems. The extensive thermodynamic modelling of phase equilibria with Laves phases was successfully accomplished [IX, XI, XVII]. Recently, we suggested a method for the extension of SGTE data for pure elements to zero Kelvin temperature [XIV]. This approach was extended to intermetallic phases [XVII] which is important for modelling of phase equilibria in multicomponent systems in materials under extreme conditions.

Detailed conclusions about CALPHAD modelling

A new approach to calculation of phase equilibria with **sigma phase** using the ab initio calculated total energies of formation of sigma phase of pure constituents was proposed [I,II]. The procedure was successfully tested on four binary systems: **Cr-Fe** [I], **Cr-Co** [II], **Co-Mo** [IV] and **Fe-Mo** [IV]; and it was extended to two ternary systems: **Cr-Fe-Ni** [III] and **Cr-Fe-W** [VII]. The calculated phase equilibria involving the sigma phase agree well with the experimental data. In Cr-Fe [I] and Cr-Co [II] binary system, the phase diagrams constructed using the new (1 1) two-sublattice model [I] yielded better agreement with experimental data than diagrams obtained by means of an older three-sublattice model [72]. It was found that the (1 1) two-sublattice model of the sigma phase can be also used for a reasonable description of phase equilibria in the Fe-Cr-W system [VII], although the sigma phase is not stable in two binary subsystems, i.e. in Fe-W and Cr-W systems. The approach based on combination of ab initio and CALPHAD modelling provides a reasonable physical interpretation of the individual terms in the mathematical expression for the Gibbs energy difference between the sigma phase and SER state of the pure constituents. The proposed procedure enables us to predict the stability region of sigma phase in metallic materials.

The ab initio calculated energies of formation also form a solid base for the thermodynamic modelling and phase diagram calculations in systems containing **Laves phases**. The total energy differences fit well the two-sublattice model of C15 and three-sublattice model of C14 and C36 Laves phase in **Cr-Zr** [IX], **Cr-Hf** [XI] and **Cr-Ti** [XI] systems. The ab initio analysis of relative stability of Laves phase structures confirms the sequence of decreasing stability C15-C36-C14 and it can be fully utilised in the thermodynamic modelling of those phases except for Cr-Hf system, which lacks phase equilibrium data for C36 structure. Phase diagrams in the above mentioned binary systems were calculated and compared with experimental data.

The extension of the SGTE data to low temperatures was proposed [XIV]. This extension is based on the knowledge of the Debye (Einstein) temperature and the Einstein function, which can be used to evaluate the heat capacity, Gibbs energy and their first derivatives with respect to temperature. The extension method maintains the SGTE unary data above the limiting temperature T_{lim} and forces the low temperature extension to have the same function value and the value of the first derivative at T_{lim} as the corresponding SGTE polynomial has. The temperature dependencies of Gibbs energies and heat capacities of pure elements were presented and some problems were pointed out [XIV]. It was shown that the methodology of extension of the SGTE data to temperatures below 298.15 K is transferable to more complicated structures such as **V₂Zr rhombohedral** and **C15 Laves**

phase [XVII]. The phase equilibria with these phases at low temperatures were evaluated and corresponding phase diagram was constructed.

List of author's publications and the specification of author's contribution

International refereed journals and one chapter in monography are listed below. The papers I-IV, VI, VII, IX-XI, XIII, XIV, XVI, XVII present the research summarised in this thesis.

Scientific papers in journals

- [I] Houserová J., Friák M., Šob M., Vřešťál J.: *Ab Initio Calculations of Lattice Stability of Sigma-phase and Phase Diagram in the Cr-Fe System*. Computational Materials Science 25 (2002) 562-569. DOI: 10.1016/s0927-0256(02)00335-x
Author's contribution (ca. 40%): All ab initio calculations (including analysis and interpretation), related figures and tables, the preparation of manuscript. The motivation for the project, CALPHAD modelling and finalisation of the manuscript is due to prof. Vřešťál. The help with technical problems and consultations about run of DFT codes were provided by M. Friák. Discussions about DTF approaches and the critical reading of the manuscript is due to prof. Šob.
- [II] Houserová J., Vřešťál J., Friák M., Šob M.: *Phase Diagram Calculation in Co-Cr System Using Ab Initio Determined Lattice Instability of Sigma Phase*. CALPHAD 26 (2002) 513-522. DOI: 10.1016/s0364-5916(02)80004-9
Author's contribution (ca. 40%): All ab initio calculations (including analysis and interpretation), related figures and tables, the preparation of manuscript. The motivation for the project, CALPHAD modelling and finalisation of the manuscript is due to prof. Vřešťál. The help with technical problems and consultations about run of DFT codes were provided by M. Friák. Discussions about DTF approaches and the critical reading of the manuscript is due to prof. Šob.
- [III] Chvátalová K., Houserová J., Šob M., Vřešťál J.: *First-principles Calculations of Energetics of Sigma Phase Formation and Thermodynamic Modelling in Fe-Ni-Cr System*. Journal of Alloys and Compounds 378 (2004) 71-74. DOI: 10.1016/j.jallcom.2003.10.071
Author's contribution (ca. 30%): Choice of ab initio methods, part of ab initio calculations (including analysis and interpretation), related figures and tables, supervision of the student's (K. Chvátalová) calculations, the preparation of part of manuscript. Part of ab initio calculations (including analysis and interpretation), related figures and tables, the preparation of part of manuscript by K. Chvátalová. The motivation for the project and CALPHAD modelling is due to prof. Vřešťál.

Discussions about DTF approaches and the critical reading of the manuscript is due to prof. Šob.

- [IV] Houserová J., Vřešťál J., Šob M.: *Phase Diagram Calculations in the Co-Mo and Fe-Mo Systems Using First-principles Results for the Sigma Phase*. CALPHAD 29 (2005) 133-139. DOI: 10.1016/j.calphad.2005.06.002
 Author's contribution (ca. 60%): All ab initio calculations (including analysis and interpretation), figures and tables, the whole text, but corrected by co-authors. The motivation for the project and work on CALPHAD modelling was shared with prof. Vřešťál. Discussions and the critical reading of the manuscript is due to prof. Šob.
- [V] Vogtenhuber D., Houserová J., Wolf W., Podloucky R., Pfeiler W., Püschl W.: *Comparative Ab Initio Study of Point Defect Energies and Atom Migration Profiles in the L1(2)-ordered Intermetallic Compounds Ni₃Al, Ni₃Ga, Pt₃Ga, Pt₃In*. Diffusion in Materials: DIMAT 2004, PTS 1 and 2; Book Series: Defect and Diffusion Forum Series Vol. 237-240 (2005) 133-138.
 Author's contribution (ca. 15%): Part of ab initio calculations (including analysis and interpretation). Introduction into the problem by prof. R. Podloucky is gratefully acknowledged.
- [VI] Vřešťál J., J. Pinkas, Kroupa A., Houserová J., Scott A., Watson A.: *Assessment of the Thermodynamic Properties and Phase Diagram of the Bi-Pd System*. CALPHAD 30 (2006) 14-17. DOI: 10.1016/j.calphad.2005.12.001
 Author's contribution (ca. 20%): Ab initio calculations (including analysis and interpretation), the text concerning this part of study.
- [VII] Chvátalová K., Vřešťál J., Houserová J., Šob M.: *First-principles Calculations of Energetics of Sigma Phase Formation and Thermodynamic Modelling in the Cr-Fe-W System*. Material Science and Engineering A 462 (2007) 153-158. DOI: 10.1016/j.msea.2006.02.474
 Author's contribution (ca. 30%): Choice of ab initio methods, some of ab initio calculations, supervision of the student's (K. Chvátalová) calculations, the correction of part of manuscript.
- [VIII] Pavlů J., Vřešťál J., Šob M.: *Re-modeling of Laves Phases in the Cr-Nb and Cr-Ta Systems Using First-principles Results*. CALPHAD 33 (2009) 179-186. DOI: 10.1016/j.calphad.2008.04.006
 Author's contribution (ca. 45%): Shared work with prof. Vřešťál. Critical reading of the manuscript is due to prof. Šob.
- [IX] Pavlů J., Vřešťál J., Šob M.: *Stability of Laves Phases in the Cr-Zr System*. CALPHAD 33 (2009) 382-387. DOI: 10.1016/j.calphad.2008.11.003
 Author's contribution (ca. 45%): Shared work with prof. Vřešťál. Critical reading of the manuscript is due to prof. Šob.
- [X] Pavlů J., Vřešťál J., Šob M.: *Ab Initio Study of Formation Energy and Magnetism of Sigma Phase in Cr-Fe and Cr-Co Systems*. Intermetallics 18 (2010) 212-220. DOI: 10.1016/j.intermet.2009.07.018
 Author's contribution (ca. 90%): The motivation for the project, the choice of the

methods, all ab initio calculations (including analysis and interpretation), figures and tables, the whole manuscript text. Critical reading of the manuscript is due to prof. Šob and prof. Vřešťál.

- [XI] Pavlů J., Vřešťál J., Šob M.: *Thermodynamic Modeling of Laves phases in the Cr-Hf and Cr-Ti Systems: Reassessment Using First-principles Results*. CALPHAD 34 (2010) 215-221. DOI: 10.1016/j.calphad.2010.03.003
Author's contribution (ca. 45%): Shared work with prof. Vřešťál. Critical reading of the manuscript is due to prof. Šob.
- [XII] Pavlů J., Vřešťál J., Chen X.-Q., Rogl P.: *Thermodynamic Modeling of Laves Phases in the Ta-V System: Reassessment Using First-principles Results*. CALPHAD 35 (2011) 103-108. DOI: 10.1016/j.calphad.2010.12.002
Author's contribution (ca. 40%): Ab initio calculations (including analysis and interpretation), the text concerning this part of study.
- [XIII] Meschel S.V., Pavlů J., Nash P.: *The Thermochemical Behavior of Some Binary Shape Memory Alloys by High Temperature Direct Synthesis Calorimetry*. Journal of Alloys and Compounds 509 (2011) 5256-5262. DOI: 10.1016/j.jallcom.2011.01.152
Author's contribution (ca. 30%): Ab initio calculations (including analysis and interpretation), the text concerning this part of study.
- [XIV] Vřešťál J., Štrof J., Pavlů J.: *Extension of SGTE Data for Pure Elements to Zero Kelvin Temperature – A Case Study*. CALPHAD 37 (2012) 37-48. DOI: 10.1016/j.calphad.2012.01.003
Author's contribution (ca. 15%): Participation on thermodynamic modelling and on critical reading. The motivation for the project is due to prof. Vřešťál.
- [XV] Legut D., Pavlů J.: *Electronic Structure and Elasticity of Z-phases in Cr-Nb-V-N System*. Journal of Physics: Condensed Matter 24 (2012) 195502. DOI: 10.1088/0953-8984/24/19/195502
Author's contribution (ca. 20%): Thermodynamic analysis, cooperation on the preparation of manuscript, critical reading.
- [XVI] Pavlů J., Šob M.: *Ab Initio Study of C14 Laves Phases in Fe-based Systems*. Journal of Mining and Metallurgy, Section B: Metallurgy 48 (3) B (2012) 395-401. DOI: 10.2298/jmmb120704050p
Author's contribution (ca. 90%): The motivation for the project, the choice of the methods, all ab initio calculations (including analysis and interpretation), figures and tables, the whole manuscript text. Critical reading of the manuscript is due to prof. Šob.
- [XVII] Štrof J., Pavlů J., Wdowik U. D., Buršík J., Šob M., Vřešťál J.: *Laves Phases in the V-Zr System Below Room Temperature: Stability Analysis Using Ab Initio Results and Phase Diagram*. CALPHAD 44 (2014) 62-69. DOI: 10.1016/j.calphad.2013.08.003
Author's contribution (ca. 25%): Ab initio calculations (including analysis and interpretation), the text concerning this part of study, motivation for the phonon spectra calculations, cooperation on finalisation of manuscript.

- [XVIII] Vřešťál J., Houserová J., Šob M.: *Energetics and Phase Diagrams of Fe-Cr and Co-Cr Systems from First Principles*. Journal of Mining and Metallurgy 38 (3-4) B (2002) 205-211.

Author's contribution (ca. 40%): Ab initio calculations (including analysis and interpretation), the corresponding part of manuscript. The motivation for the project, CALPHAD modelling and finalisation of the manuscript is due to prof. Vřešťál. Discussions about DTF approaches and the critical reading of the manuscript is due to prof. Šob.

Summarizing paper of publications [I] and [II].

Chapter in monography

- [XIX] Šob M., Kroupa A., Pavlů J., Vřešťál J.: *Application of Ab Initio Electronic Structure Calculations in Construction of Phase Diagrams of Metallic Systems with Complex Phases*. Solid State Phenomena: Solid Phase Transformations II 150 (2009) 1-28. DOI: 10.4028/www.scientific.net/SSP.150.1

Author's contribution (ca. 20%): Ab initio calculations (including analysis and interpretation), the corresponding part of manuscript.

Survey paper on combination of ab initio and CALPHAD technique.

Bibliography

- [1] Parr R.G., Yang W.: *Density-Functional Theory of Atoms and Molecules*. Oxford University Press, New York, USA, 1989.
- [2] Martin R.M.: *Electronic Structure: Basic Theory and Practical Methods*. Cambridge University Press, Cambridge, England, 2004.
- [3] Taylor Ph.L., Heinonen O.: *A Quantum Approach to Condensed Matter Physics*. Cambridge University Press, Cambridge, England, 2002.
- [4] Turek I., Drchal V., Kudrnovský J., Šob M., Weinberger P.: *Electronic Structure of Disordered Alloys, Surfaces and Interfaces*. Kluwer Academic Publishers, Boston, USA, 1997.
- [5] Saunders N., Miodownik A.P.: *CALPHAD (A Comprehensive Guide)*. Elsevier, London, England, 1998.
- [6] Grimvall G., Magyari-Koepe B., Ozolins V. et al.: *Rev. Mod. Phys.* 84 (2012) 945.
- [7] Wolverton C.: *Acta Mater.* 50 (2002) 2187.
- [8] Abe T., Chen Y., Yamabe-Mitarai Y., Numakura H.: *CALPHAD* 32 (2008) 353.
- [9] Kissavos A., Shallcross S., Meded V., Kaufman L., Abrikosov I.A.: *CALPHAD* 29 (2005) 17.
- [10] Zhao X.S., Yuan G.H., Yao M.Y., Yue Q., Shen J.Y.: *CALPHAD* 36 (2012) 163.
- [11] Karki B.B., Ackland G.J., Crain J.: *J. Phys.: Condens. Matter* 9 (1997) 8579.
- [12] Neuhaus T., Likos C.N.: *J. Phys. Condens. Matter* 23 (2011) 234112.
- [13] Dinsdale A.T., *CALPHAD* 15 (1991) 317.
- [14] Akiba E., Iba H.: *Intermetallics* 6 (1998) 461.
- [15] Inoue K., Tachikawa K.: *Appl. Phys. Lett.* 18 (1971) 235.
- [16] Stein F., Palm M., Sauthof G.: *Intermetallics* 12 (2004) 713.
- [17] Bain E.C.: *Chem. and Met. Eng.* 28 (1923) 23.

- [18] Villars P., Calvert L.D.: *Pearson's Handbook of Crystallographic Data for Inter-metallic Phases*. ASM International, Materials Park, Ohio, USA, 1991.
- [19] Yakel H.L.: *Acta Crystallogr.* B39 (1983) 20.
- [20] Dickins G.J., Douglas A.M.B., Taylor W.H.: *Acta Crystallogr.* 9 (1956) 297.
- [21] Forsyth J.B., d'Alte da Viega L.M.: *Acta Crystallogr.* 16 (1963) 509.
- [22] Heino S., Knutson-Wedel E.M., Karsson B.: *Materials Science and Technology* 15 (1999) 101.
- [23] Lundin L., Hättestrand M., Andrén H.-O.: *Parsons 2000 Advanced Materials for 21st Century Turbines and Power Plants*. edited by Strang A. et al., The Institute of Materials, London, 2000, GB, p. 603.
- [24] Hohenberg P., Kohn W.: *Phys. Rev.* 136 (1964) B864.
- [25] Kohn W., Sham L.J.: *Phys. Rev.* 140 (1965) A1133.
- [26] Hedin L., Lundquist B.I.: *J. Phys. C: Solid St. Phys.* 4 (1971) 2064.
- [27] von Barth U., Hedin L.: *J. Phys. C: Solid St. Phys.* 5 (1972) 1629.
- [28] Janak J.F.: *Solid State Commun.* 25 (1978) 53.
- [29] Ceperley D.M., Alder B.J.: *Phys. Rev. Lett.* 45 (1980) 566.
- [30] Perdew J., Zunger A.: *Phys. Rev. B* 23 (1981) 5048.
- [31] Vosko S.H., Wilk L., Nusair M.: *Can. J. Phys.* 58 (1980) 1200.
- [32] Perdew J.P., Wang Y.: *Phys. Rev. B* 45 (1992) 13244.
- [33] Ziman J.M.: *Principles of the Theory of Solids*. Cambridge University Press, London, England, 1972.
- [34] Vainstein B.K., Fridkin V.M., Indenbom V.L.: *Structure of Crystals*. Springer-Verlag, Berlin-Heidelberg, Germany, 1995.
- [35] Yip S.: *Handbook of Materials Modeling*. Springer, Dordrecht-Berlin-Heidelberg-New York, USA, 2005.
- [36] Moriarty J.A., Benedict L.X., Glosli J.N., Hood R.Q., Orlikowski D.A., Patel M.V., Söderlind P., Streitz F.H., Tang M., Yang L.H.: *J. Mater. Res.* 21 (2006) 563.
- [37] Guo Z.X. (ed.): *Multiscale Materials Modelling: Fundamentals and Applications*. Woodhead Publishing Ltd., Cambridge, England, and CRC Press LLC, Boca Raton, USA, 2007.
- [38] Singh D.: *Planewaves, Pseudopotentials and the LAPW Method*. Kluwer, Boston, USA, 1994.

- [39] Andersen O.K.: Phys. Rev. B 12 (1975) 3060.
- [40] Skriver H.L.: *The LMTO Method*. Springer-Verlag, Berlin, Germany, 1984.
- [41] Krier G., Jepsen O., Burkhardt A., Andersen O.K.: *Computer code TB-LMTO-ASA version 4.6*. Max-Planck-Institut für Festkörperforschung, Stuttgart, Germany, 1994.
- [42] Perdew J.P., Chevary J.A., Vosko S.H., Jackson K.A., Pederson M.R., Singh D.J., Fiolhais C., Phys. Rev. B 46 (1992) 6671.
- [43] Havránková J., Vřešťál J., Wang L.G., Šob M.: Phys. Rev. B 63 (2001) 174104.
- [44] Andersen O.K., Methfessel M., Rodriguez C.O., Blöchl P., Polatoglou H.M.: In *Atomistic Simulation of Materials: Beyond Pair Potentials*. edited by Vitek V., Srolovitz D.J., Plenum, New York-London, 1989, p. 1.
- [45] Tank R.W., Arcangeli C., Krier G., Andersen O.K., Jepsen O.: In *Properties of Complex Inorganic Solids*. edited by Gonis A., Meike A., Turchi, P.E.A., Plenum, New York-London, 1997, p. 233.
- [46] Blaha P., Schwarz K., Luitz J.: *Computer code WIEN97*. Vienna University of Technology, Vienna, 1997; improved and updated Unix version of the original copyrighted WIEN code, which was published by Blaha P., Schwarz K., Sorantin P., Trickey S.B.: Comput. Phys. Commun. 59 (1990) 399.
- [47] Blaha P., Schwarz K., Madsen G., Kvasnicka D., Luitz J.: *WIEN2k, An Augmented Plane Wave + Local Orbitals Program for Calculating Crystal Properties*. Vienna University of Technology, Vienna, 2001.
- [48] Kresse G., Furthmüller J.: Comput. Mater. Sci. 6 (1996) 15.
- [49] Kresse G., Furthmüller J.: Phys. Rev. B 54 (1996) 11169.
- [50] Blöchl P.E.: Phys. Rev. B 50 (1994) 17953.
- [51] Kresse G., Joubert J.: Phys. Rev. B 59 (1999) 1758.
- [52] Perdew J.P., Burke K., Ernzerhof M.: Phys. Rev. Lett. 77 (1996) 3865.
- [53] Šob M.: In *Multiscale Materials Modelling: Fundamentals and Applications*. edited by Guo Z.X., Woodhead Publishing Ltd., Cambridge, England, and CRC Press LLC, Boca Raton, USA, 2007.
- [54] Moroni E.G., Jarlborg T.: Phys. Rev. B 47 (1993) 3255.
- [55] Polcarová M., Goodwod K., Bak-Misiuk J., Kadečková S., Bradler J.: Phys. Stat. Sol. (a) 106 (1988) 17.
- [56] Moroni E.G., Kresse G., Hafner J., Furthmüller J.: Phys. Rev. B 56 (1997) 15629.
- [57] Gale W.F., Totemeier T.C. (eds.): *Smithells Metals Reference Book*. Elsevier Butterworth-Heinemann, Oxford, GB, 2004.

- [58] Rezukhina T.N., Kashina T.A.: *The Journal of Chemical Thermodynamics* 8 (1976) 519.
- [59] Meschel S.V., Chen X.Q., Kleppa O.J., Nash P.: *CALPHAD* 33 (2009) 55.
- [60] Dench W.A.: *Trans. Faraday Soc.* 59 (1963) 1279.
- [61] Zubkov A.A., Mogutnov B.M., Shaposhnikov N.G.: *Dokl. Akad. Nauk SSSR* 311 (1990) 388; *Dokl. Phys. Chem.* 311 (1990) 239.
- [62] Bell H.B., Hajra J.P., Putland F.H., Spencer P.J.: *Met. Sci. Journal* 7 (1973) 185.
- [63] Downie D.B., Arlasan F.: *J. Chem. Thermodynamics* 15 (1983) 654.
- [64] Kittel C.: *Introduction to Solid State Physics*. John Wiley and Sons, New York, USA, 1976.
- [65] Buschow K.H.J. (ed.): *Handbook of Magnetic Materials*. Elsevier Sci. B.V, Amsterdam, the Netherlands, 2001.
- [66] Nath B., Metcalfe E., Hald J.: *Microstructural Development and Stability in New High Strength Steels for Thick Section Applications at up to 620°C*. In *Microstructural Development and Stability in High Cr Ferritic Power Plant Steels*. edited by Strang A., Gooch D.J., TSM, Cambridge, UK, 1997, 123.
- [67] Lukas H.L., Fries S.G., Sundman B.: *Computational Thermodynamics*. Cambridge University Press, Cambridge, UK, 2007.
- [68] Redlich O., Kister A.T.: *Indust. Eng. Chem.* 40 (1948) 345.
- [69] Allibert C., Bernard C., Effenberg G., Nüssler H.-D., Spencer P.J.: *CALPHAD* 5 (1981) 227.
- [70] Ansara I., Chart T.G., Fernandez Guillermet A., Hayes F.H., Kattner U.R., Pettifor D.G., Saunders N., Zang K.: *CALPHAD* 21 (1997) 171.
- [71] Hillert M.: *CALPHAD* 22 (1998) 127.
- [72] Anderson J.-O., Sundman B.: *CALPHAD* 11 (1987) 83.
- [73] Chen Q., Sundman B.: *J. Phase Equilib.* 22 (2001) 631.
- [74] Born M., Huang K.: *Dynamical Theory of Crystal Lattices*, Oxford University Press, Oxford, UK, 1954.
- [75] Gimvall G.: *Thermophysical Properties of Materials*, Elsevier Science, North-Holland, Amsterdam, the Netherlands, 1999.
- [76] Vřešťál J.: *Arch. Metall.* 46 (2001) 9.
- [77] Cook A.J., Jones F.W.: *J. Iron Steel Inst.* 148 (1943) 217 and 223.

- [78] Hillert M., Qiu C.: *Met. Trans.* 22A (1991) 2187.
- [79] Rees W.P., Burns B.D., Cook A.J.: *J. Iron Steel Inst.* 162 (1949) 325.
- [80] Sopoušek J., Kruml T.: *Scripta Materialia* 35 (1996) 689.
- [81] Hasebe M., Nishizawa T.: *Analysis and Synthesis of Phase Diagrams of the Fe-Cr-Ni, Fe-Cu-Mn and Fe-CuNi Systems*. In *Applications of Phase Diagrams in Metallurgy and Ceramics: Proceedings of a Workshop Held at the National Bureau of Standards*, Gaithersburgh, MD, 1997, p. 911.
- [82] Schultz J.W., Merrick H.F.: *Met. Trans.* 3 (1972) 2479.
- [83] Keiber H., Geibel C., Renker B., Rietschel H., Schmidt H., Wühl H., Stewart G.R.: *Phys. Rev. B* 30 (1984) 2542.
- [84] Geibel C., Goldacker W., Keiber H., Oestreich V., Rietschel H., Wühl H.: *Phys. Rev. B* 30 (1984) 6363.
- [85] Zhang X., Chen L., Ma M., Zhu Y., Zhang S., Liu R.: *J. Appl. Phys.* 109 (2011) 113523.
- [86] Smith J.F.: In *Binary Alloy Phase Diagrams*. edited by Massalski T.B., 2nd ed., vol. 3, ASM International, Materials Park, OH, 1990, p. 3528.
- [87] Williams J.T.: *Trans. AIME* 203 (1955) 345.
- [88] Rapp O., Benediktsson G.: *Phys. Lett. A* 74 (1979) 449.
- [89] Moncton D.E.: *Solid State Commun.* 13 (1973) 1779.
- [90] de Boer F.R., Boom R., Mattens W.C.M., Miedema A.R., Niessen A.K.: *Cohesion in Metals*. Transition Metal Alloys, Elsevier Sci. Publ., The Netherlands, 1988.



ELSEVIER

Computational Materials Science 25 (2002) 562–569

 COMPUTATIONAL
 MATERIALS
 SCIENCE

www.elsevier.com/locate/commatsci

Ab initio calculations of lattice stability of sigma-phase and phase diagram in the Cr–Fe system

Jana Houserová^{a,*}, Martin Friák^b, Mojmír Šob^b, Jan Vřešťál^a

^a Faculty of Science, Institute of Theoretical and Physical Chemistry, Masaryk University, Kotlářská 2, CZ-611 37 Brno, Czech Republic

^b Institute of Physics of Materials, Academy of Sciences of the Czech Republic, Žitkova 22, CZ-616 62 Brno, Czech Republic

Abstract

Total energy of pure metals in the sigma-phase structure and in the standard element reference (SER) structure were calculated by full-potential linear augmented plane waves method in the general gradient approximation at the equilibrium volume of all phases. Relaxation of lattice parameters of sigma-phase and SER structure were performed. The difference of total energy of sigma-phase and of standard element phase for pure constituents ($\Delta^0 E_i^{\sigma-SER}$) was used in a new two-sublattice model of sigma-phase, which was subsequently employed for calculation of phase diagram.

Entropy term of Gibbs energy of elements in sigma-phase structure and excess Gibbs energy of mixing of sigma-phase have still to be adjusted to the experimental phase equilibrium data. This procedure was tested on the Fe–Cr system.

© 2002 Elsevier Science B.V. All rights reserved.

1. Introduction

Phase equilibria calculations performed by calculations of phase diagrams (CALPHAD) method are based on the axiom that complete Gibbs energy vs. composition curves can be constructed for all the structures exhibited by the elements right across the whole alloy system. This involves the extrapolation of $G(x)$ curves of many phases into regions where they are either metastable or unstable and, in particular, the relative Gibbs energy for various crystal structures of the pure elements of the system must therefore be established [1]. Utilising the results from ab initio electronic

structure calculations may be very useful for describing thermodynamic properties of complicated phases in the systems exhibiting slow changes of Gibbs energy with temperature T and concentration x (molar fraction), such as in sigma-phase, μ -phase, Laves phase etc.

The sigma-phase was first described by Bain [2] in the Cr–Fe system in 1923. At present, Villars et al. [3] report on about 110 different intermetallic phases with sigma-phase structure. This structure (space group no. 136, P42/mnm) contains 30 atoms in the repeat cell distributed into five crystallographically inequivalent sublattices (2a, 4f, 8i, 8i' and 8j). This structure is very brittle and stable and its inconvenient properties cause very strong degradation of materials (crack nucleation sites). In practice, it also develops in heat affected zones of welded superaustenitic stainless steels [4]; it was

* Corresponding author. Tel.: +420-5-41129316.

E-mail address: houser@chemi.muni.cz (J. Houserová).

concluded there that it formed after longer ageing times in the temperature range of 500–1100 °C and that its composition was 55 wt.% of Fe, 22 wt.% of Cr, 11 wt.% of Mo and 5 wt.% of Ni. It is also known that high concentrations of Cr and Mo promote precipitation of sigma-phase. Therefore, it is very important to have more information about its region of stability.

The ab initio (first-principles) electronic structure calculations are able to reproduce the difference of total energy between the standard element reference (SER) structures and the sigma-phase. Calculated results may constitute a basis for a new approach to the determination of phase equilibria and to the prediction of phase diagrams containing more complicated phases. The procedure of choosing equilibrium volume (corresponding to the minimum on the energy–volume curve) as the state of reference overcome the uncertainty connected with the use of experimental atomic volume of sigma-phases for total energy calculation of pure components in sigma-phase, although this procedure was successfully employed in [5].

The aim of this paper is to test the approach mentioned above on the Cr–Fe system. A new model for sigma-phase description [6] using ab initio calculations results is employed and verified.

It turns out that for description of energetics of sigma-phase and for construction of phase diagram only structural energy differences $\Delta^0 E_i^{\sigma\text{-SER}}$ for pure constituents are needed. Therefore, no ab initio calculations for sigma-phase systems have to be performed.

2. Calculations

2.1. Calculations of phase diagrams

The CALPHAD in this paper is based on finding the minimum of the total Gibbs energy of the system at a constant pressure and temperature respecting the mass conservation law.

Such a calculation is often performed by the CALPHAD method [1]. This method uses the structural Gibbs energy difference (the difference between the Gibbs energy of the phase in question and the Gibbs energy of SER) for various struc-

tures of pure elements, as e.g. bcc, fcc, hcp, Laves phase, sigma-phase etc. These Gibbs energy differences are functions of pressure, temperature and volume.

The total Gibbs energy of the system is given by

$$G^{\text{tot}} = \sum_f w^f G^f, \quad (1)$$

i.e. it is equal to the sum of Gibbs energies of all phases (G^f) multiplied by their volume fraction (w^f). The Gibbs energy of a phase of certain composition is obtained by

$$G^f = \sum_i y_i^0 G_i^f + G^{\text{id}} + G^{\text{E}} + G^{\text{mag}} + \dots, \quad (2)$$

where y_i is lattice fraction of the component i (the sum of lattice fractions in each lattice (sublattice) is equal to 1), ${}^0G_i^f$ is the Gibbs energy of pure element in the phase f , the term G^{id} describes the Gibbs energy of ideal mixing, G^{E} is the excess Gibbs energy describing real mixing and G^{mag} is the magnetic contribution to the Gibbs energy. The Gibbs energy of a certain phase G^f is used as an input for phase diagram calculations. It is quite easy to obtain these Gibbs energies for less complicated structures, for example for the fcc or bcc structures, because they could be determined experimentally or by extrapolation to the pure components, and are summarised in various databases [7]. But it is not the case of the sigma-phase. At the beginning of sigma-phase studies, the Gibbs energy of bcc phase was used instead of Gibbs energy of sigma-phase. Later on, the estimations were done using extrapolation of experimental data [8]. Now, one often applies the model of a substitutional structure $(\text{B})_8(\text{A})_4(\text{A},\text{B})_{18}$ or $(\text{B})_{10}(\text{A})_4(\text{A},\text{B})_{16}$. Such modelling is performed using the assumption that the atoms are ordered in two or more sublattices [9–11]. The problem consists in the dilemma into which sublattice each element goes and, further, how to reduce number of sublattices in order to restrict the number of model parameters. For a binary A–B sigma-phase (A being an element of the VIth group of the periodical table or lower, B being an element of the VIIth group or higher), a guideline for reducing the number of parameters was proposed as follows [10]:

- (i) Combine all sublattices with the same coordination number (CN) and similar point symmetry into one.
- (ii) If more than one remain, combine the two with the highest CN into one.
- (iii) Arrange the reduced set of sublattices in the order of increasing CN.
- (iv) B elements will go preferentially into the first sublattice but it may dissolve some A.
- (v) The next sublattice will be preferentially filled with A but it may dissolve some B.
- (vi) If there is a third sublattice, it will be reserved for A.

In the Cr(A)–Fe(B) system the CN of sublattices are following [9]:

$$2a \text{ (CN = 12), } 4f \text{ (CN = 15), } 8i \text{ (CN = 12),} \\ 8i' \text{ (CN = 14) and } 8j \text{ (CN = 14).}$$

The first and third sublattice and the fourth and fifth sublattice are combined according to the point (i) in order to obtain this preliminary formula $16_{(8i'+8j)}:4_{(4f)}:10_{(2a+8i)}$. Then the sublattices are arranged in the order of increasing CN according to (iii) and are occupied by atoms in order to satisfy the points (iv)–(vi) getting 10(AB):16(AB):4(A). At the end of the procedure of reducing of model parameters it is assumed [9] that the occupation of the second sublattice by A atoms is negligible (10(B):16(AB):4(A)) and the sublattice with mixed occupation is moved to the end of formula.

Such a way, this procedure yields the formula $(B)_{10}(A)_4(A,B)_{16}$. The expression for Gibbs energy of sigma-phase having Fe atoms in the first sublattice and Cr atoms in the second and third sublattices is

$${}^0G_{\text{Fe:Cr:Cr}}^\sigma = 10{}^0G_{\text{Fe}}^{\text{hfcc}} + 4{}^0G_{\text{Cr}}^{\text{hbcc}} + 16{}^0G_{\text{Cr}}^{\text{hbcc}} + C_{\text{Cr}}^\sigma(T). \quad (3)$$

We can obtain a similar equation for the Gibbs energy of sigma-phase having Fe atoms in the first and the third sublattices and Cr atoms in the second sublattice:

$${}^0G_{\text{Fe:Cr:Fe}}^\sigma = 10{}^0G_{\text{Fe}}^{\text{hfcc}} + 4{}^0G_{\text{Cr}}^{\text{hbcc}} + 16{}^0G_{\text{Fe}}^{\text{hbcc}} + C_{\text{Fe}}^\sigma(T). \quad (4)$$

Here ${}^0G_i^f$ is Gibbs energy of pure component i (Cr or Fe) in phase f ; hbcc, hfcc are symbols of hypothetical paramagnetic (non-spin-polarised) bcc and fcc phases, and $C_i^\sigma(T)$ is a temperature-dependent adjustable parameter. This parameter is defined by

$$C_i^\sigma(T) = A_i + B_i T_i, \quad (5)$$

where A_i, B_i are constants that can be adjusted to the phase equilibrium data.

It is obvious from Eqs. (3) and (4) that it is not possible to describe the Gibbs energy of sigma-phase close to the pure elements regions using this model. The Gibbs energy of sigma-phase is described here as empirical combination of Gibbs energies of some absolutely different structures. The above mentioned procedure only enables us to estimate the lattice stability of metastable phase by means of known Gibbs energies of stable phases of pure constituents with the same CN. Using this approach, we are not able to express the Gibbs energy of pure constituents in sigma-phase structure, and Gibbs energy of sigma-phase has to be adjusted to phase equilibrium data. The physical background of this procedure is, therefore, questionable. Further, it is known from X-ray studies [12] that the mixing of the constituents takes place in all sublattices, which is not respected by the proposed approach.

Electronic structure calculations could bring a substantial improvement of that model. Namely, knowledge of a correct value of the total energy difference between the sigma-phase and the SER-phase of pure constituents from first principles enables us to build up the Gibbs energy of the sigma-phase of pure elements on a physically correct energetic basis, and only the entropy term must be adjusted to phase equilibrium data.

Using this idea and the knowledge that the sigma-phase does not behave like rigid stoichiometric phase (1 1), that means that the sublattices in sigma-phase are not occupied exclusively by one kind of atoms (mixing is possible), we have proposed a new physical (two-sublattice) model (1 1). This is a model of a solid solution, as e.g. fcc or bcc [1]. The label (1 1) for sigma-phase means that this solution phase contains two sublattices, each of

them having one lattice site (the one atom only could be placed here).

In this thermodynamic description the five sublattices found in the X-ray experiments are reduced to two. This is possible because the mixing occurs in all five sublattices as mentioned above. This reduction give us the possibility to describe the sigma-phase in the whole composition region. In this procedure the results of first-principles calculations have crucial importance yielding the correct energetic basis of the model.

The Gibbs energy of sigma-phase in binary system Cr–Fe of a certain composition in two-sublattice solution model may be expressed by

$$G_{\text{Cr,Fe}}^{\sigma} = y_{\text{Fe}} {}^0G_{\text{Fe}}^{\sigma} + y_{\text{Cr}} {}^0G_{\text{Cr}}^{\sigma} + G_{\text{Cr,Fe}}^{\text{id},\sigma} + G_{\text{Cr,Fe}}^{\text{E},\sigma} \quad (6)$$

where y is lattice fraction of a component and ${}^0G_i^{\sigma}$ is Gibbs energy of hypothetical sigma-phase that contains only one pure element. These energies are defined as

$${}^0G_i^{\sigma} = G_i^{\text{SER}} + \Delta^0 E_i^{\sigma\text{-SER}} - S_i^{\sigma} T, \quad (7)$$

where ${}^0G_i^{\text{SER}}$ is Gibbs energy of pure element in SER state, $\Delta^0 E_i^{\sigma\text{-SER}}$ expresses the total energy difference of hypothetical sigma-phase and standard state of a pure metal; this difference may be obtained from ab initio electronic structure calculations. Further, S_i^{σ} is the entropy term in the Gibbs energy. It is a constant adjustable to the experimental data. $G_{\text{Cr,Fe}}^{\text{id},\sigma}$ is the Gibbs energy of ideal mixing of metals in sigma-phase and may be expressed as

$$G_{\text{Cr,Fe}}^{\text{id},\sigma} = RT(y_{\text{Cr}} \ln y_{\text{Cr}} + y_{\text{Fe}} \ln y_{\text{Fe}}), \quad (8)$$

where R is the gas constant. $G_{\text{Cr,Fe}}^{\text{E},\sigma}$ is excess Gibbs energy describing real mixing in sigma-phase. We may write this energy as

$$G_{\text{Cr,Fe}}^{\text{E},\sigma} = y_{\text{Cr}} y_{\text{Fe}} [L^0(T) + L^1(T)(y_{\text{Cr}} - y_{\text{Fe}}) + L^2(T) \times (y_{\text{Cr}} - y_{\text{Fe}})^2], \quad (9)$$

$$L^0(T) = D + ET, \quad L^1(T) = F + JT$$

and $L^2(T) = K + LT, \quad (10)$

where $L^0(T)$, $L^1(T)$, $L^2(T)$ are interaction parameters and D , E , F , J , K , L are fitting parameters adjusted to the phase data.

On the basis of presented equations the new two-sublattice model (1 1):

- (i) is able to describe the Gibbs energy and enthalpy dependencies vs. composition in the whole concentration region,
- (ii) has a solid physical background,
- (iii) yields a very simple description of sigma-phase based on ab initio calculated $\Delta^0 E_i^{\sigma\text{-SER}}$ term for pure constituents.

This model is used in the present paper for CALPHAD of Cr–Fe system. The Gibbs energies of phases needed for construction of phase diagram (bcc, fcc, liquid) were taken from recent assessments of thermodynamic data [7,11,13] and calculations of phase equilibria were performed by means of THERMO-CALC programme [14].

2.2. Calculations of total energy difference ($\Delta^0 E_i^{\sigma\text{-SER}}$)

The structural energy differences between the SER structure and sigma-phase structure of pure constituents were calculated by means of the full-potential linearized augmented plane waves (FLAPW) method incorporated in the WIEN97 code [15] using the generalized gradient approximation [16] for the exchange-correlation term. In all cases, the minima of the total energy as a function of lattice parameters were found, as described in more detail below.

By extensive testing, we have found that the changes of positions of atoms in the repeat cell of sigma-phase (within the limits found in literature) do not have a great effect on the total energy (the maximum change in energy was $\Delta E = 2$ mRy/atom and, in average, we had $\Delta E = 0.5$ mRy/atom). Therefore, we were able to keep the internal parameters constant during the calculations. Using various sigma-phases containing Fe (e.g. Fe–Cr, Fe–Mo etc.) and employing their crystal structure for calculating the total energy of hypothetical Fe sigma-phase, we have chosen that structure (i.e. that set of internal parameters) which exhibited the lowest total energy [17]. The same procedure was applied for hypothetical Cr sigma-phase; the

lowest total energy was obtained for the structure given in [18].

In the case of sigma-phase, preliminary optimisation of unit cell volume and c/a ratio was performed using the LMTO-ASA method [19]. Then the optimisations of RMT (muffin-tin radius) and of number of k -points were done. The final FLAPW optimisation was done in the following way: at first the optimisation of volume at the constant c/a ratio was performed. The second step was the calculation of the dependence of the total energy vs. c/a ratio when the volume of the repeat cell (V_{\min} from the previous step) was kept constant. These two steps were repeated until the total energy converged to its minimum.

Concerning the SER-phase (ferromagnetic bcc Fe and antiferromagnetic bcc Cr), the preliminary optimisation by LMTO-ASA method was not performed and the RMT parameter was used the same as in the sigma-phase calculation. We have used 2 atoms in the unit cell and found the equilibrium lattice constants corresponding to the minimum of total energy as a function of volume.

Then the total energy difference per atom, $\Delta^0 E_i^{\sigma-\text{SER}} = {}^0 E_i^{\sigma} - {}^0 E_i^{\text{SER}}$, was calculated.

3. Results and discussion

The total energy of sigma-phase of Cr and Fe as a function of the cell volume in the last step of optimisation described above is shown in Fig. 1. The full symbols represent the crossing points with the previous optimisation curves of c/a ratio at constant volumes. Because the total energies at the crossing points differ less than $\varepsilon = 0.2$ mRy/atom, we could stop the optimisation at this level. It turns out that three optimisation steps are sufficient to obtain the equilibrium lattice parameters of sigma-phase with the accuracy needed. The calculated equilibrium values of lattice parameters and cell volumes are given in Table 1.

The volume dependence of total energy of ferromagnetic Fe and antiferromagnetic Cr in bcc structure is presented in Fig. 2 and the values of equilibrium lattice parameters are given in Table 2.

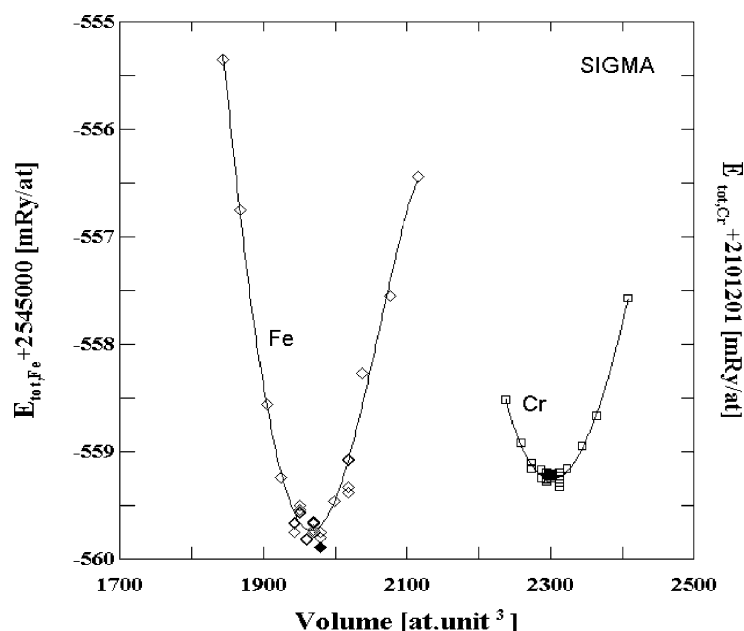


Fig. 1. Final FLAPW optimisation of the cell volume of sigma-phase (30 atoms) of pure Cr (\square) and Fe (\diamond) at constant c/a ratio ($c/a_{\text{Fe}} = 0.5174$, $c/a_{\text{Cr}} = 0.5237$). Full symbols represent the crossing points with previous optimisation of total energy vs. c/a ratio.

Table 1
Values of equilibrium FLAPW lattice parameters (calculated) and cell volumes (30 atoms) for hypothetical sigma-phase of end members in system Cr–Fe

Parameter	Cr	Fe
Volume (a.u. ³)	2301.38	1963.76
a (a.u.)	16.3792	15.5987
c (a.u.)	8.5783	8.0707

The deviation of the calculated equilibrium lattice constant from the experimental value is -0.43% for Cr and 0.27% for Fe.

The total energies of equilibrium hypothetical sigma-phase and the SER state of Fe and Cr as well as their differences are given in Table 3 together with the values obtained for the experimental volumes of Cr–Fe sigma-phase [5]. It turns out that in case of Cr, the volume optimisation has somewhat larger effect than in case of Fe.

Recently, we have attempted to apply the results of first-principles calculations to determine the phase diagram. In [6], the first-principles structural energy differences obtained on the basis of extrapolation of experimental volume of sigma-phase to the pure components [5] were used. For

Table 2
Values of experimental and equilibrium FLAPW lattice parameters for SER-phase of antiferromagnetic Cr and ferromagnetic Fe

Source	Cr (ab initio)	Cr [22]	Fe (ab initio)	Fe [22]
a (a.u.)	5.41653	5.44	5.41438	5.40

Table 3
Values of equilibrium total energies per atom for sigma-phase and SER-phase of Cr and Fe and their differences

Variable (Ry/atom)	Cr (ab initio)	Fe (ab initio)
Total energy per atom of σ -phase	-2101.7603	-2545.5597
Total energy per atom of SER	-2101.7832	-2545.5927
Total energy difference per atom (σ -SER)	0.0229	0.0330
Total energy difference per atom (σ -SER) [5]	0.0154	0.0309

the other phases, thermodynamic description of Cr–Fe system, based on high temperature vapour pressure measurements results published in [20], was adopted. In spite of approximations used,

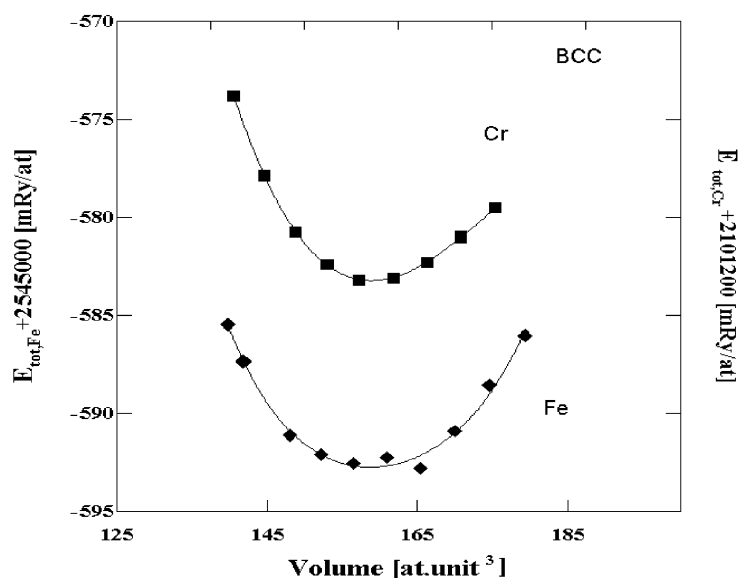


Fig. 2. The volume dependence of total energy of antiferromagnetic Cr and ferromagnetic Fe. The volume corresponds to two-atom unit cell.

calculated phase equilibria with sigma-phase were reproduced.

The procedure described in this work is based on the first-principles total energy calculations at equilibrium atomic volume and on reliably assessed low-temperature thermodynamic data [11,13]. It represents a new approach to the calculations of phase equilibria in systems containing the sigma-phase. The temperature dependence of excess Gibbs energy of sigma-phase (entropy term) has still to be adjusted to phase equilibrium data, following the traditional CALPHAD method. Comparison of phase diagrams with sigma-phase in Cr–Fe system calculated by three-sublattice model [11] and by new two-sublattice model is shown in Fig. 3. The values of adjustable parameters employed in the CALPHAD are given in Table 4.

The agreement of the phase diagram calculated by means of a new two-sublattice model employing equilibrium total energy values with experimentally determined phase equilibrium values [21] is better than for the case of three-sublattice model [11] or for the case of the two-sublattice model using the total energy values of pure constituents determined at the experimental atomic volume of the Cr–Fe sigma-phase [6].

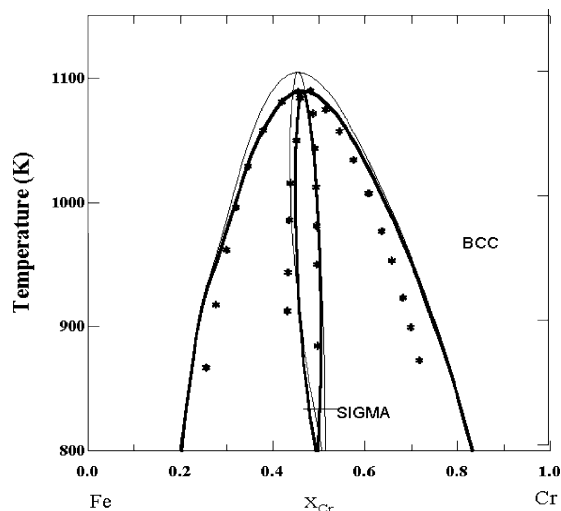


Fig. 3. Comparison of phase diagrams of Cr–Fe. Thick line: calculated by the new two-sublattice model (for data see Table 4), thin line: calculated by three-sublattice model (data from [11]), stars: experimental data [21].

Table 4
Values of parameters used in the Cr–Fe phase diagram calculation: parameters of description of σ -phase

Parameter	Cr	Fe
S^σ	+0.7	+0.7
L^0		-133 950
L^1		+31 000
L^2		-127 000

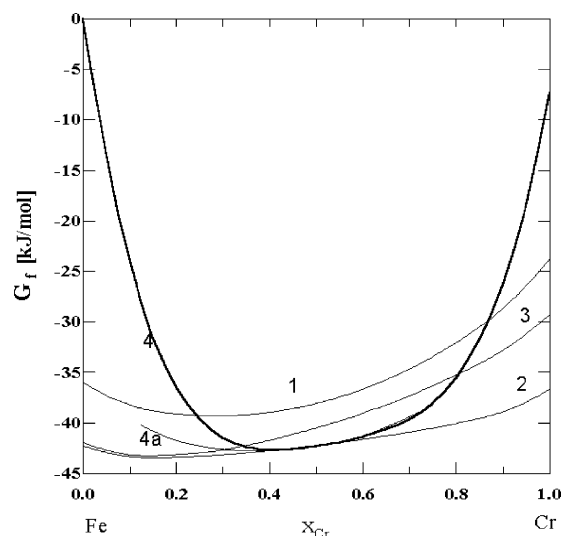


Fig. 4. Concentration dependence of Gibbs energy of phases at 1000 K in Cr–Fe system: (1) liquid phase, (2) bcc phase, (3) fcc phase, (4) sigma-phase (new two-sublattice model), (4a) sigma-phase (three sublattice model).

Composition dependencies of Gibbs energy (at 1000 K) and enthalpy calculated using new two-sublattice model are shown in Figs. 4 and 5. Here we also show the differences between the results obtained using the old (three-sublattices [11]) and new (two-sublattices [6]) model of description of sigma-phase. It may be seen that the new two-sublattice model yields the values of Gibbs energy and enthalpy of phases in the whole composition region; the old model gives these quantities only in a limited range of concentrations.

4. Conclusions

The results of ab initio calculations of total energy of sigma-phase and SER-phase of pure

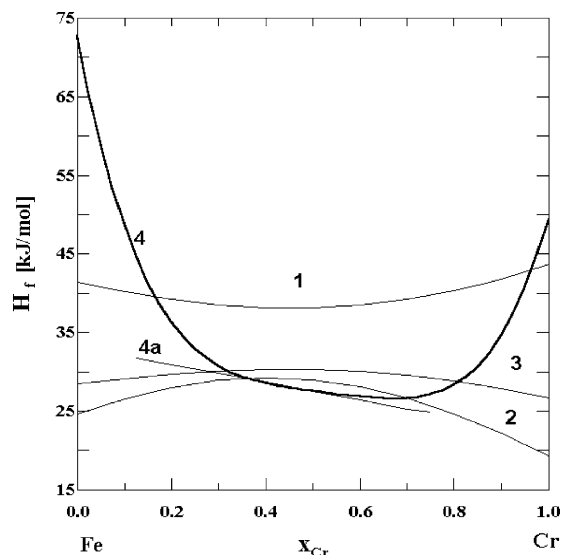


Fig. 5. Concentration dependence of enthalpy of phases in Cr–Fe system: (1) liquid phase, (2) bcc phase, (3) fcc phase, (4) sigma-phase (new two-sublattice model), (4a) sigma-phase (three-sublattice model).

constituents performed by FLAPW method were used in a new model of calculation of phase equilibria in systems containing the sigma-phase. The procedure was tested on the Cr–Fe system.

The phase diagram calculated using the new two-sublattice model [11] [6] yields better agreement with experimental data than that obtained by means of an older three-sublattice model [11].

The proposed procedure has a solid physical background and enables us to predict the stability region of sigma-phase in metallic materials.

Acknowledgements

This research was supported by the COST Action P3 (Simulation of physical phenomena in technological applications, Project nos. COST OC P3.90 and P3.10), by the Grant Agency of the Czech Republic (Project no. 106/99/1178) and by the Grant Agency of the Academy of Sciences of

the Czech Republic (Project no. A1010817). The use of computer facilities at the MetaCenter of Masaryk University, Brno, is acknowledged.

References

- [1] N. Saunders, P. Miodownik, *CALPHAD—A Comprehensive Guide*, Elsevier, London, 1998.
- [2] E.C. Bain, *Chem. Met. Eng.* 28 (1923) 23.
- [3] P. Villars, L.D. Calvert, *Pearson's Handbook of Crystallographic Data for Intermetallic Phases*, ASM International, Materials park, OH, 1991.
- [4] S. Heino, E.M. Knutson-Wedel, B. Karsson, *Mater. Sci. Technol.* 15 (1999) 101–108.
- [5] J. Havránková, J. Vřešťál, L.G. Wang, M. Šob, *Phys. Rev. B* 63 (2001) 174101.
- [6] J. Vřešťál, *Arch. Metall.* 46 (3) (2001) 9.
- [7] A.T. Dinsdale, *Calphad* 15 (1991) 317.
- [8] C. Allibert, C. Bernard, G. Effenberg, H.-D. Nüssler, P.J. Spencer, *Calphad* 5 (1981) 227.
- [9] I. Ansara, T.G. Chart, A. Fernandez Guillermet, F.H. Hayes, U.R. Kattner, D.G. Pettifor, N. Saunders, K. Zang, *Calphad* 21 (1997) 171.
- [10] M. Hillert, *Calphad* 22 (1998) 127.
- [11] J.-O. Anderson, B. Sundman, *Calphad* 11 (1987) 83.
- [12] S.H. Algie, E.O. Hall, *Acta Crystallographica* 20 (1966) 142, cited from Ref. [7].
- [13] B.-J. Lee, *Calphad* 17 (1993) 251.
- [14] B. Sundman, *THERMO-CALC*, version L, Royal Institute of Technology, Stockholm, 1997.
- [15] P. Blaha, K. Schwarz, J. Luitz, WIEN97, Vienna University of Technology, 1997; improved and updated Unix version of the original copyrighted WIEN code, which was published by P. Blaha, K. Schwarz, P. Sorantin, S.B. Trickey, *Comput. Phys. Commun.* 59 (1990) 399.
- [16] J.P. Perdew, J.A. Chevary, S.H. Vosko, K.A. Jackson, M.R. Pederson, D.J. Singh, C. Fiolhais, *Phys. Rev. B* 46 (1992) 6671.
- [17] H.Y. Yakel, *Acta Crystallographica B* 39 (1983) 20.
- [18] G.J. Dickins, Audrey, M.B. Douglas, W.H. Taylor, *Acta Crystallographica* 9 (1956) 297.
- [19] G. Krier, O. Jepsen, A. Burkhardt, O.K. Andersen, computer code TB-LMTO-ASA version 4.6, Max-Planck-Institut für Festkörperforschung, Stuttgart, 1994.
- [20] J. Vřešťál, J. Tomiska, P. Brož, *Ber. Bunsenges. Phys. Chem.* 98 (1994) 1601.
- [21] A.J. Cook, F.W. Jones, *J. Iron Steel Inst.*, London 148 (1943) 217, and 223.
- [22] E.G. Moroni, T. Jarlborg, *Phys. Rev. B* 47 (1993) 3255.



Pergamon

Calphad, Vol. 26, No. 4, pp. 513–522, 2002
 © 2003 Elsevier Science Ltd. All rights reserved
 0364-5916/02/\$ - see front matter

PII: S0364-5916(03)00003-8

Phase Diagram Calculation in Co-Cr System Using Ab Initio Determined Lattice Instability of Sigma Phase

Jana Houserová¹, Jan Věšál¹, Martin Friák² and Mojmír Šob²

¹Institute of Theoretical and Physical Chemistry, Faculty of Science, Masaryk University,
 Kotlářská 2, CZ-611 37 Brno, Czech Republic

²Institute of Physics of Materials, Academy of Sciences of the Czech Republic,
 Žitná 22, CZ-616 62 Brno, Czech Republic

*1: Corresponding author's e-mail: vrestal@chemi.muni.cz

(Received May 28, 2002)

Abstract. The calculations of phase equilibria in the Co-Cr system were performed using the CALPHAD method on the basis of a new two-sublattices model of sigma phase. This model enables us to utilise the results of ab initio calculations of total energy differences between the sigma phase structure and the Standard Element Reference (SER) structures of pure metal at the relaxed lattice parameters ($\Delta^0 E_{\text{SER}}^{\sigma}$). Total energies were calculated by Full-Potential Linear Augmented Plane Waves (FLAPW) method in the General Gradient Approximation (GGA). The entropy contribution to the Gibbs energy of the pure elements in the sigma phase structure, and the excess Gibbs energy of mixing of the sigma phase were adjusted to the experimental phase equilibrium data. © 2003 Elsevier Science Ltd. All rights reserved.

Introduction

The sigma phase was first observed by Bain [1] in Cr-Fe system in 1923. However, it obtained its name a little bit later. Since its discovery, more than 40 different sigma phases have been found in various binary systems of transition metals (e.g. Co-Cr, Fe-Mo, Ni-V) [2]. Many material engineers were interested in the prediction of regions of stability of the sigma phase because it has very disadvantageous properties. It is well known that the sigma phase is extremely brittle and therefore it increases the probability of the formation of crack nucleation sites. On the other hand, it is very stable from the thermodynamic point of view. Therefore, the knowledge of the regions of stability of sigma phase is very desirable in the Co-Cr system.

Experimental data on the sigma phase in the Co-Cr system were published in [3-10]. For the analysis of the region of stability of the sigma phase in the Co-Cr system by the CALPHAD method [11] it is necessary to know the dependence of the Gibbs energy on composition for all structures occurring in the system at all concentrations, even where these structures are metastable or unstable. The relative Gibbs energies of such hypothetical structures (that are unstable or metastable in some composition range) in the pure state are needed for this method.

This gap may be bridged by ab initio electronic-structure calculations of lattice stability in the case of complex non-stoichiometric phase such as sigma phase, μ phase, Laves phase etc. These calculations enable us to get some idea about the thermodynamic properties of those structures in such regions where the experimental data are unavailable (e.g. for the hypothetical sigma phase of the pure component). The only input for such calculations is the atomic numbers and concentrations of the constituents and the crystallographic data of the underlying structures. In the case of the hypothetical sigma phase for the pure elements, the uncertainty connected with the use of experimental lattice parameters of binary sigma phase is overcome by choosing the

equilibrium state of that phase, corresponding to the minimum of the total energy as a function of the lattice parameters. The total energy differences between the sigma phase and the SER structure of the pure constituents can be implemented into the new model of description of the sigma-phase [12].

The aim of this paper is to verify this approach in the case of the Co-Cr system.

Calculations

Calculation of Phase Diagrams

The behaviour of the system is defined by the minimum of the total Gibbs energy G^{tot} at given conditions of pressure and temperature. G^{tot} is equal to the sum of the Gibbs energies of all phases (G^f) multiplied by their volume fraction (w^f), i.e.

$$G^{\text{tot}} = \sum_f w^f G^f \quad (1)$$

The G^f is again a function of the thermodynamic conditions considered above, and it is defined as

$$G^f = \sum_i y_i {}^0G_i^f + G^{\text{id}} + G^{\text{E}} + G^{\text{mag}} + G^{\text{pres}}, \quad (2)$$

where y_i is the lattice fraction of the component i , ${}^0G_i^f$ is the Gibbs energy of a pure constituent i in the phase f , the term G^{id} describes the Gibbs energy of ideal mixing, G^{E} is the excess Gibbs energy describing real mixing, G^{mag} is the magnetic contribution and G^{pres} is the pressure contribution to the Gibbs energy. The ${}^0G_i^f$ constitute the main input information for phase diagram calculations based on the CALPHAD approach. These values are easily available for many structures of the pure elements, e.g. bcc, fcc, hcp, because they are usually quite well measurable. They are summarised in various databases, e.g. [13]. However, there is a problem in the case of the sigma phase because it is much more complicated, it is unstable for the pure constituents and its region of stability is too narrow for reasonable extrapolation. This experimentally unsolvable problem can be treated using ab initio calculations. The ab initio approach allows us to replace methods of construction of the Gibbs energy for the sigma phase that use the combination of Gibbs energies of bcc and fcc structures according to similarity in coordination number [14,15], or that estimate it using extrapolation of experimental data [16].

The model of a substitutional structure $(B)_8(A)_4(A,B)_{18}$ or $(B)_{10}(A)_4(A,B)_{16}$ is the one of the most widely used methods in recent time [14,15] but it has some disadvantages. The first step of description of the sigma phase in this model is the reduction of number of sublattices. It is known from X-ray experiments that the sigma phase (space group No. 136, $P4_2/mnm$) contains 30 atoms in the unit cell distributed into five crystallographically inequivalent sublattices (2a, 4f, 8i, 8i' and 8j) [17], too many for a reasonable CALPHAD description. Therefore, the number of sublattices should be reduced [14,15,18]. In [14], some general rules for such a reduction in the number of sublattices and for their occupation were formulated:

- (i) All sublattices with the same coordination number (CN) and similar point symmetry are combined into one.
- (ii) If more than one sublattice remains, combine the two with the highest CN into one.
- (iii) The reduced set of sublattices must be arranged in the order of increasing CN.
- (iv) B elements will go preferentially into the first sublattice but it may dissolve some A.
- (v) The next sublattice will be preferentially filled with A but it may dissolve some B.
- (vi) If there is a third sublattice, it will be reserved for A.

If A is an element of the VIth group of the Periodical Table or lower, and B is an element of the VIIth group or higher, then, in the case of a binary sigma phase, the CN of individual sublattices in Co(A)-Cr(B) are, by analogy to [18], as follows: 2a (CN=12), 4f (CN=15), 8i (CN=12), 8i' (CN=14) and 8j (CN=14). The first and third sublattice and the fourth and fifth sublattice are combined according to the point (i) above to obtain the preliminary formula $16(8i'+8j) 4(4f) 10(2a+8i)$. Then the sublattices are arranged in the order of increasing CN and are occupied by atoms in order to satisfy the points (iv) – (vi) getting $10(A,B):16(A,B):4(A)$. At the end of the procedure for reducing the number of model parameters, it is assumed [18] that the occupation of the second sublattice by A atoms is negligible, i.e. we have $10(B):16(A,B):4(A)$, and the sublattice with mixed occupation is moved to the end of the formula. So the resulting formula is $10(B) 4(A) 16(A,B)$ or, alternatively, $(B)_{10}(A)_4(A,B)_{16}$.

PHASE DIAGRAM CALCULATION IN Co-Cr SYSTEM

515

The Gibbs energy of the sigma phase depends on occupation of the third sublattice, where the mixing occurs, and therefore following two equations are useful:

$${}^0G_{\text{CoCrCr}}^{\sigma} = 10 {}^0G_{\text{Co}}^{\text{hfcc}} + 4 {}^0G_{\text{Cr}}^{\text{hbcc}} + 16 {}^0G_{\text{Cr}}^{\text{hbcc}} + C_{\text{Cr}}^{\sigma}(T). \quad (3)$$

$${}^0G_{\text{CoCrCo}}^{\sigma} = 10 {}^0G_{\text{Co}}^{\text{hfcc}} + 4 {}^0G_{\text{Cr}}^{\text{hbcc}} + 16 {}^0G_{\text{Co}}^{\text{hbcc}} + C_{\text{Co}}^{\sigma}(T). \quad (4)$$

where ${}^0G_i^f$ is the Gibbs energy of a pure constituent i (Cr or Co) in the phase f , ${}^{\text{hbcc}}, {}^{\text{hfcc}}$ are symbols of hypothetical paramagnetic (non-spin-polarised) bcc and fcc phases, and $C_i^{\sigma}(T)$ is a temperature-dependent adjustable parameter that is defined by

$$C_i^{\sigma}(T) = A_i + B_i T, \quad (5)$$

with A_i, B_i being the constants that can be adjusted to phase equilibrium data.

The problem of this model is that it does not capture the main idea of the CALPHAD method, i.e. it is not based on the lattice stability of the pure constituents. Therefore, it is not able to describe the thermodynamic properties of the system in the regions close to the pure constituents (the knowledge of the Gibbs energy in those regions is indispensable for computing ternary and higher-order systems). Nevertheless, the most serious objection from the physical point of the view is that the Gibbs energy of the sigma phase is described as an empirical combination of Gibbs energies of simple structures that are not related to the sigma phase.

Our new physical two-sublattices model describes the thermodynamic properties of the sigma phase in the whole composition range [12]. This is a model of solid solution, similar for example to the fcc or bcc one [11]. Here the sigma phase is described as a two-sublattices structure where each sublattice contains one atomic site per unit cell. The model is capable to use such a strong reduction in the number of sublattices (from five to two) because it is known from X-ray experiments [19] that the sigma phase behaves more or less like a solution, i.e. there is a mixing of atoms in all five sublattices, which was not respected by the previous model. Site occupancies of the binary sigma phases were critically reviewed by Ansara et al. [18]. Experimental evidence for fully preferentially occupied lattice sites was found in less than one half of studied systems. In particular, for Co-Cr system, Algie and Hall [19] reported mixing of atoms in all 5 inequivalent lattice sites.

Within the two-sublattices solution model, the Gibbs energy of the sigma phase in binary Co-Cr system is given by

$$G_{\text{CrCo}}^{\sigma} = y_{\text{Co}} {}^0G_{\text{Co}}^{\sigma} + y_{\text{Cr}} {}^0G_{\text{Cr}}^{\sigma} + G_{\text{CrCo}}^{\text{id},\sigma} + G_{\text{CrCo}}^{\text{E},\sigma}, \quad (6)$$

where y_i is the lattice fraction of a component i and ${}^0G_i^{\sigma}$ is the Gibbs energy of a hypothetical (unstable) sigma phase that contains only one pure constituent i . Such energies of pure sigma phases are defined as

$${}^0G_i^{\sigma} = G_i^{\text{SER}} + \Delta^0 E_i^{\sigma-\text{SER}} - S_i^{\sigma} T, \quad (7)$$

where ${}^0G_i^{\text{SER}}$ is the Gibbs energy of a pure constituent in the SER state and $\Delta^0 E_i^{\sigma-\text{SER}}$ denotes the total energy difference between hypothetical sigma phase and the standard state of that constituent. This total energy difference may be obtained from ab initio electronic-structure calculations. Further, S_i^{σ} is the entropy term in the Gibbs energy. It is a constant adjustable to the experimental data. $G_{\text{CrCo}}^{\text{id},\sigma}$ is the Gibbs energy of the ideal mixing of metals in the sigma phase and may be expressed as

$$G_{\text{CrCo}}^{\text{id},\sigma} = RT (y_{\text{Cr}} \ln y_{\text{Cr}} + y_{\text{Co}} \ln y_{\text{Co}}), \quad (8)$$

where R is the gas constant. $G_{\text{CrCo}}^{\text{E},\sigma}$ is the excess Gibbs energy describing real mixing in the sigma phase. It was expressed by frequently used Redlich-Kister equation

$$G_{\text{CrCo}}^{\text{E},\sigma} = y_{\text{Cr}} y_{\text{Co}} (L^0(T) + L^1(T) (y_{\text{Cr}} - y_{\text{Co}}) + L^2(T) (y_{\text{Cr}} - y_{\text{Co}})^2), \quad (9)$$

$$L^0(T) = D + ET, L^1(T) = F + JT \text{ and } L^2(T) = K + LT, \quad (10)$$

where $L^0(T), L^1(T), L^2(T)$ are interaction parameters and D, E, F, J, K, L are fitting parameters adjusted to the experimental phase equilibrium data.

Utilization of ab initio calculations in the determination of the $\Delta^0 E_i^{\sigma-\text{SER}}$ term constitutes a considerable improvement of the CALPHAD approach to the phase diagrams. It gives us the opportunity to determine the

Gibbs energy of the sigma phase for the pure constituents on a physically correct energy basis.

Let us note, however, that we are not able to incorporate the contribution from the zero-point motion. It is not excluded that, when evaluating the structural energy differences, this contribution may play quite an important role.

There is only one disadvantage in this model. We are not able to calculate the entropy of the system and, therefore, it is still adjusted to phase equilibrium data. This model was already successfully used in the case of Cr-Fe system [20] and the Co-Cr system is modelled in the present paper using existing assessments for remaining phases.

Calculation Of Total Energy Differences

The total energies of both structures (SER and sigma phase) at their equilibrium volumes were calculated within the Full-Potential Linearized Augmented Plane Waves (FLAPW) method incorporated in the WIEN97 code [21] using the Generalised Gradient Approximation (GGA) [22] for the exchange-correlation term.

At the beginning of our calculations, the internal parameters (i.e. the positions of all atoms in the unit cell) of the hypothetical sigma phase for pure cobalt were chosen. The total energies of the mentioned structure were calculated at constant lattice parameters [23] using various internal parameters of binary sigma-phases that contained cobalt (e.g. Co-Cr, Co-Mo etc.). We have chosen that set of internal parameters, which exhibited the lowest total energy [24]. The same procedure was applied for the choice of the internal parameters of a hypothetical Cr in the sigma phase structure. The lowest total energy of Cr sigma phase was found at the lattice parameters given in [25] and internal parameters given in [23].

In the following calculations, the internal parameters were kept constant because we have found that their optimisation does not have any significant influence on the total energy of the sigma phase. The changes in total energy caused by changing the internal parameters within the limits found in the literature did not exceed the value of 2 mRy/atom and, on average; they amounted to 0.5 mRy/atom.

Now, to estimate the equilibrium values of the lattice constants of the sigma-phase, we performed auxiliary calculations with the Linear Muffin-Tin Orbital method in the Atomic Sphere Approximation (LMTO-ASA) [26].

Then we continued the FLAPW calculations. The optimal RMT (muffin-tin radius) and number of k-points needed for the calculations were chosen. The RMT parameters used in this work are 1.97 a.u. in the case of cobalt and 2.1 a.u. in the case of chromium. Concerning the number of k-points in the irreducible zone found by preliminary optimisation, the used values are 42 in the case of cobalt and 36 in the case of chromium.

The process of optimisation of the lattice parameters is very simple. It is based on repeating two steps until the change in the total energy is small enough. These steps are the optimisation of the volume at constant c/a ratio (constant shape of unit cell) and optimisation of the c/a ratio at constant volume (V_{\min} from the previous step).

The calculations for the SER-phases (ferromagnetic hcp Co and antiferromagnetic bcc Cr) were not so time-consuming because the LMTO-ASA calculations had not been performed and the RMT parameters had been taken from the sigma phase calculations. The k-points convergence tests resulted in using 320 k-points for cobalt and 120 k-points for chromium in all following calculations. The optimisation of the unit cells with two atoms had the same theoretical basis as in the sigma phase calculations but the optimisation of the c/a ratio was not employed in the case of the cubic structure, and therefore the calculations of the bcc structure were finished already after the first optimisation step.

Results And Discussion

The calculated total energies for the pure constituents in both structures were used for evaluating the lattice stability of the sigma phase characterized by the total energy difference $\Delta^0 E_{\Gamma}^{\sigma-SER} = {}^0 E_{\Gamma}^{\sigma} - {}^0 E_{\Gamma}^{SER}$.

The profiles of the total energy as a function of volume in the case of both constituents in the sigma phase arrangement obtained from the last step of optimisation are shown in Fig. 1. The crossing points with previous optimisation curves are represented by full symbols. The difference in total energies obtained in the

PHASE DIAGRAM CALCULATION IN Co-Cr SYSTEM

517

last two steps was smaller than 0.2 mRy/at, and therefore we could stop the optimisation at this level. The lattice parameters of the unit cell corresponding to the minimum of total energy are listed in the Table 1.

Table 1. FLAPW calculated equilibrium volumes per atom (a.u.³) and lattice parameters (a.u.) of the thirty-atom unit cell of hypothetical sigma phase of end members Cr and Co.

Parameter	Cr	Co
Volume	76.7127	69.1070
<i>a</i>	16.3792	15.8602
<i>c</i>	8.5783	8.2419

The optimised total energy profiles for the SER structures (the first one for antiferromagnetic Cr in the bcc structure and the third one in the case of ferromagnetic Co in the hcp structure) are presented in Fig.2. The optimised lattice parameters together with the experimental ones are listed in Table 2.

Table 2. Values of experimental and FLAPW equilibrium lattice parameters (a.u.) for the SER phase of antiferromagnetic Cr and ferromagnetic Co.

Lattice parameter	Cr		Co	
	ab-initio	experiment [30]	ab-initio	experiment [2]
<i>a</i>	5.41653	5.44	4.62149	4.74
<i>c</i>	5.41653	5.44	7.40598	7.69

The deviation of the calculated equilibrium lattice constant from the experimental values is -0.43% for Cr and -2.41% for the *a* lattice parameter and -3.68% for the *c* lattice parameter in the case of Co. The calculated total energies for the optimised structures and their differences are summarised in Table 3.

Table 3. Ab initio calculated values of equilibrium total energies per atom (Ry/atom) for sigma phase and SER phase of Cr and Co and their differences.

Variable	Cr	Co
Total energy per atom of σ -phase	-2 101.7603	-2 786.8954
Total energy per atom of SER	-2 101.7832	-2 786.9190
Total energy difference per atom (σ -SER)	0.0229	0.0236

It is well known that the energy difference between the bcc and fcc structures and fcc and hcp structures of Cr and Co, predicted by first principles methods [27], are substantially larger than those estimated by the CALPHAD approach. So, it is not surprising that the energy differences between the bcc and sigma-phase Cr or hcp and sigma-phase Co are so large.

These total energy differences were used in the new two-sublattices model presented in [12] for phase diagram calculations. The temperature dependence of the excess Gibbs energy of the sigma phase (entropy term) had still to be adjusted to phase equilibrium data, following the traditional CALPHAD method.

The calculations of phase diagram and thermodynamic values were performed by means of the THERMO-CALC program [28]. The recent assessment [29] gave us the Gibbs energies of all phases (bcc, fcc, hcp, and liquid) that exist in the Co-Cr system using data for the pure constituents from [13]. The final calculated phase diagram is given in Fig.3 (full lines). The dashed lines represent the phase diagram calculated by the old model [29]. There is an important improvement in the position of the line that describes the equilibrium between the sigma phase, the paramagnetic hcp, and the ferromagnetic hcp phases at the Co-rich side. Our calculated position corresponds better to that reported in [30] which is approximately 610 K. The

phase diagram calculated using the new model is in good agreement with experimental data given in [3-10]. The values of the adjustable parameters used in this calculation are summarised in Table 4.

Table 4. Values of the adjustable parameters for the sigma phase (eqs. (7), (9), and (10)) used in the calculation of the phase diagram of Co-Cr. The values of E, J, and L in eq. (10) were set to zero.

PARAMETER	Cr	Co
S^σ	+ 0.7	+0.75
L^0	-115 950	
L^1	+ 10 800	
L^2	- 95 000	

The composition dependences of the Gibbs energy and the enthalpy were calculated for both models at 1200 K and they are shown in Figs. 4 and 5. We may see that the lines 5 and 5a obtained using the new two-sublattices model and the three-sublattices model, respectively, are quite different. Regrettably, available experimental values of enthalpy of formation provide no possibility to prefer one of them (see Fig. 5). It is worth noting that the description obtained from the old model is constrained to a limited range of concentrations while the two-sublattices model [12] provides these values in the whole range of composition.

Conclusions

The ab initio calculations of lattice stability for various structures performed by FLAPW method provide a possibility for improving phase diagram calculations. The results of ab initio calculations may be utilised in a new two-sublattices model [12] that yields a better agreement with experimental data than the old three-sublattices model [15]. In the present paper, the procedure was tested on the Co-Cr system.

Our approach has a solid physical background and enables us to predict the region of stability of the sigma phase in metallic materials.

Acknowledgements

This research was supported by the Grant Agency of the Czech Republic (Project No. 106/02/0877). The use of computer facilities at the MetaCenter of Masaryk University, Brno, is acknowledged.

References

1. E. C. Bain, *Chem. and Met. Eng.*, **28** (1923) 23.
2. P. Villars and L.D. Calvert, *Pearson's Handbook of Crystallographic Data for Intermetallic Phases*, ASM International, Materials Park, OH, 1991.
3. C.A. Allibert, C. Bernard, N. Valigant and M. Dombre, *J. Less-Common Met.*, **59** (1978) 221-228.
4. F. Wever and U. Hashimoto, *Mitt. Kaiser-Wilhelm-Inst. Eisenforsch.*, **11** (1929) 293-308.
5. Y. Matsungana, *Kinzoku-no-Kenkyu*, **8** (1931) 549-561.
6. A.G. Metcalfe, *Trans. AIME*, **197** (1953) 357-364.
7. A. Chiba, *Ph.D. thesis*, Tohoku Univ. Sendai, Japan, 1971.
8. Z. Jin, *Scand. J. Metall.*, **10** (1981) 279-287.
9. M. Hasebe, K. Oikawa and T. Nishizawa, *J. Jpn. Inst. Met.*, **46** (1982) 557-583.
10. J.W. Smits, S.B. Luitjens and F.J.A. den Broeder, *J. Appl. Phys.*, **55** (1984) 2260-2262.
11. N. Saunders and P. Miodownik, *CALPHAD – A Comprehensive Guide*, Elsevier, London, 1998.
12. J. V eš ál, *Archives of Metallurgy*, **46** (2001) 239-247.
13. A.T. Dinsdale, *Calphad*, **15** (1991) 317-425.

PHASE DIAGRAM CALCULATION IN Co-Cr SYSTEM

519

14. M. Hillert, *Calphad*, **22** (1998) 127-133.
15. J.-O. Anderson and B. Sundman, *Calphad*, **11** (1987) 83.
16. C. Allibert, C. Bernard, G. Effenberg, H.-D. Nüssler and P.J. Spencer, *Calphad*, **5** (1981) 227.
17. J.L.C. Daams, P. Villars and J.H.N. van Vucht, *Atlas of Crystal Structure Types for Intermetallic Phases*, vols. 1-4, ASM International, 1991.
18. I. Ansara, T.G. Chart, A. Fernandez Guillermet, F.H. Hayes, U.R. Kattner, D.G. Pettifor, N. Saunders and K. Zang, *Calphad*, **21** (1997) 171-218.
19. S.H. Algie and E.O. Hall, *Acta Crystallographica*, **20** (1966) 142.
20. J. Houserová, M. Friák, M. Šob and J. V eš ál, *Computational Materials Science*, in print.
21. P. Blaha, K. Schwarz and J. Luitz, *WIEN97*, Vienna University of Technology 1997 (improved and updated Unix version of the original copyrighted WIEN code, which was published by P. Blaha, K. Schwarz, P. Sorantin and S.B. Trickey in *Comput. Phys. Commun.* **59** (1990) 399).
22. J.P. Perdew, J.A. Chevary, S.H. Vosko, K.A. Jackson, M.R. Pederson, D.J. Singh and C. Fiolhais, *Phys. Rev. B*, **46** (1992) 6671.
23. G.J. Dickins, Audrey M.B. Douglas and W.H. Taylor, *Acta Crystallographica*, **9** (1956) 297.
24. J.B. Forsyth, and d'Alte da Viega, *Acta Crystallographica*, **16** (1963) 509-512.
25. H.L. Yakel, *Acta Crystallographica B*, **39** (1983) 20-28.
26. G. Krier, O. Jepsen, A. Burkhardt and O.K. Andersen, *Computer code TB-LMTO-ASA version 4.6*, Max-Planck-Institut für Festkörperforschung, Stuttgart, 1994.
27. H.L. Skriver, *Phys. Rev. B*, **31** (1985) 1909.
28. B. Sundman, *THERMO-CALC*, version L, Royal Institute of Technology, Stockholm, 1997.
29. A. Kusoffski and Bo Jansson, *Calphad*, **21** (1997) 321-333.
30. G.W. Qin, K. Okinawa, T. Ikeshoji, R. Kainuma and K. Ishida, *Journal of Magnetism and Magnetic Materials*, **234** (2001) L1-L5.
31. H.B. Bell, J.p. Hajra, F.H. Putland and P.J. Spencer, *Mat. Sci Journal*, **7** (1973) 185.
32. D.B. Downie and F. Arslan, *J. Chem. Thermodynamics*, **15** (1983) 654.
33. A.A. Zubkov, B.M. Mogutnov and N.O. Shaposhnikov, *Dokl. Akad. Nauk SSSR*, **31** (1990) 388. [*Dokl. Phys. Chem.*, **311**, (1990) 239.]

520

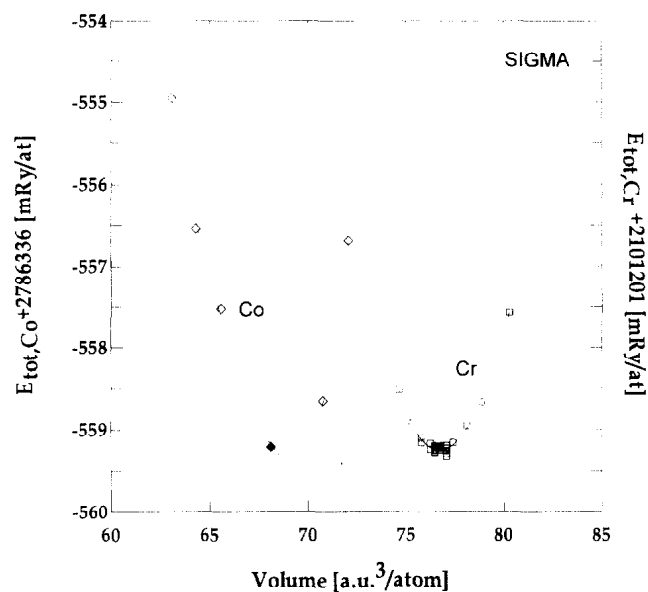
J. HOUSEROVÁ *et al.*

Fig. 1. Final FLAPW optimisation of the volume per atom of the sigma phase (30 atoms/cell) for pure Cr (squares) and Co (diamonds) at constant c/a ratio ($c/a_{\text{Co}} = 0.5237$ $c/a_{\text{Cr}} = 0.5197$, respectively). Full symbols represent the crossing points with previous optimisation profile of total energy (per atom) vs. c/a ratio.

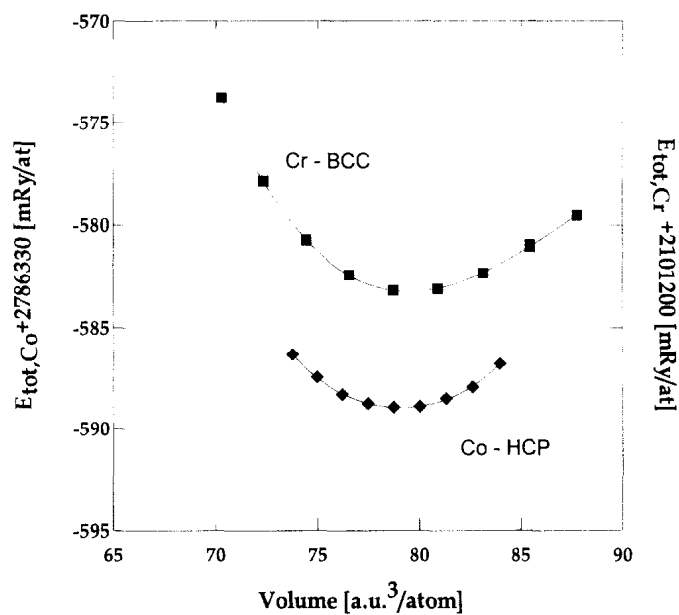


Fig. 2. The volume dependence of the total energy (per atom) of antiferromagnetic Cr and ferromagnetic Co.

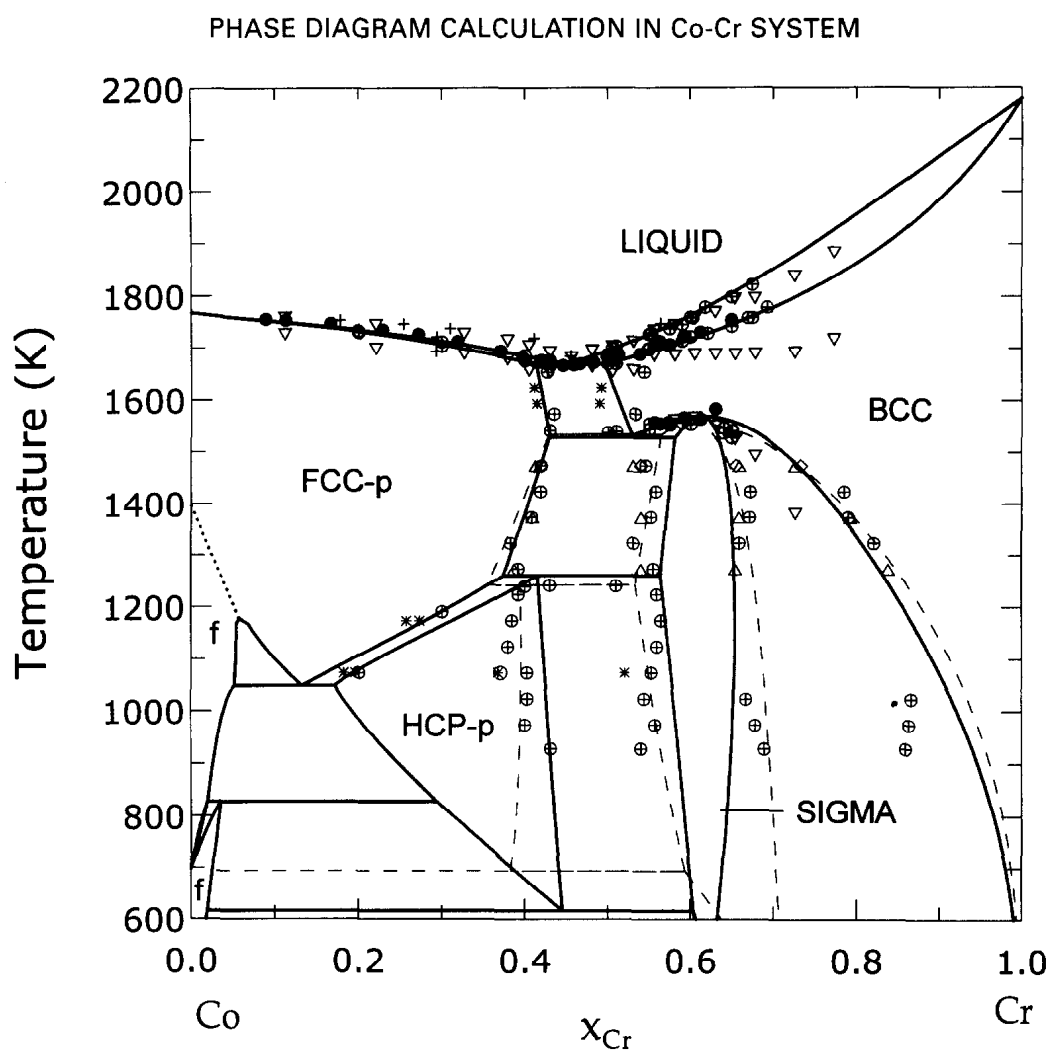


Fig. 3. Comparison of phase diagrams of Co-Cr. Full line: calculated by the new two-sublattices model (this work, for the adjustable parameters see Table 4), dashed line: calculated by the three-sublattices model [28], the experimental data: \oplus [3], ∇ [4], \bullet [5], $+$ [6], \diamond [7], \diamond [8], $*$ [9], \cdot [10]. The dotted line represents the concentration dependence of the Curie temperature [29], letter f denotes the ferromagnetic phase and p is the paramagnetic phase.

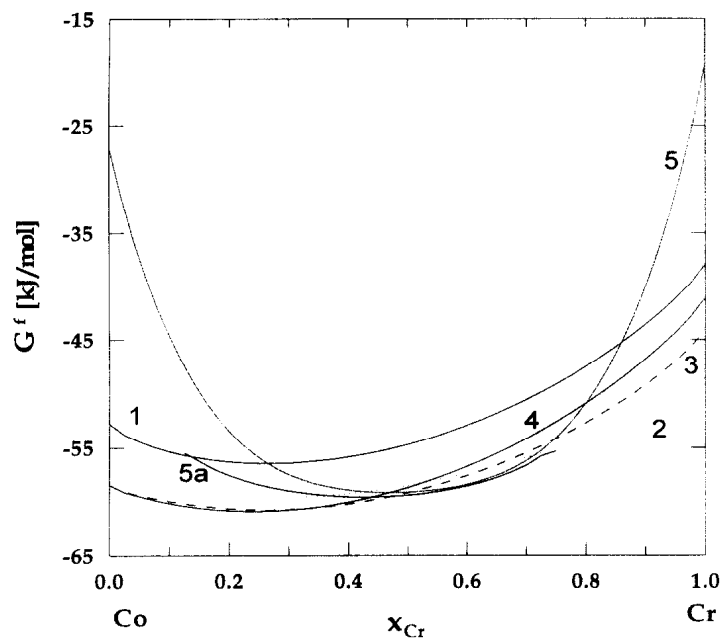


Fig. 4. Concentration dependence of the Gibbs energy for the Co-Cr system at 1200 K. 1: liquid phase, 2: bcc phase, 3: hcp phase, 4: fcc phase, 5: sigma phase (new two-sublattices model), 5a: sigma phase (three-sublattices model).

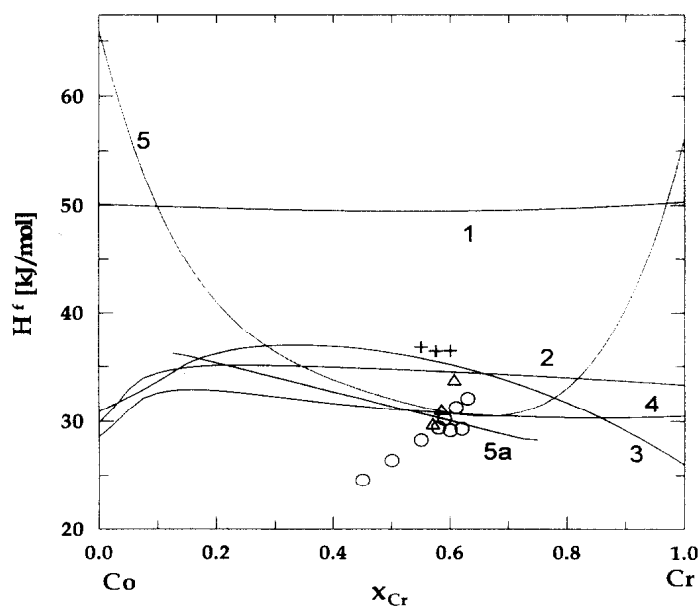


Fig. 5. Same as for Fig. 4 but for the concentration dependence of the enthalpy in the Co-Cr system at 1200 K. Available experimental data are denoted as + [31], Δ [32], O [33].



First-principles calculations of energetics of sigma phase formation and thermodynamic modelling in Fe–Ni–Cr system

K. Chvátalová^{a,*}, J. Houserová^b, M. Šob^b, J. Vřešťál^a

^a Faculty of Science, Institute of Physical Chemistry, Masaryk University, Kotlářská 2, 611 37 Brno, Czech Republic

^b Institute of Physics of Materials, Academy of Sciences of Czech Republic, Žitkova 22, 616 62 Brno, Czech Republic

Received 1 September 2003; accepted 14 October 2003

Abstract

A combination of full-potential linear augmented plane-wave (FLAPW) electronic structure method (for elemental constituents) with simpler linear muffin-tin orbital method in the atomic-sphere approximation (LMTO-ASA method, for mixtures) was employed for nickel systems (Ni–Fe and Ni–Cr) to calculate the energy of formation of sigma phase with respect to standard element reference (SER) structures of pure constituents. In all cases, the optimisation of the equilibrium volume of sigma phase and of the SER structures was performed.

Calculated energies of formation of sigma phase with respect to SER state of pure constituents in Ni–Cr and Ni–Fe systems were compared with the results of thermodynamic modelling. Phase diagram of ternary Fe–Ni–Cr system determined with the help of ab initio calculated sigma phase parameters in pure elements are in a good agreement with experimental data. Enthalpies of formation of sigma phase in Ni–Cr and in Fe–Ni systems obtained by thermodynamic modelling agree reasonably well with the energy of formation in these systems, calculated ab initio.

© 2004 Elsevier B.V. All rights reserved.

Keywords: Transition metals; Sigma phase; First-principles calculations

1. Introduction

The brittle sigma-phase (5 inequivalent lattice sites, 30 atoms per repeat cell, with large concentration range of stability, similarly as in solutions) was first described by Bain [1] in Fe–Cr system. Recently, Villars et al. [2] have reported 110 intermetallic phases with stable sigma-phase structure.

Energy of formation of sigma phase can be calculated ab initio for pure constituents and for alloys even in those systems where a stable sigma phase does not exist. In this case, experimental verification of calculated values is not possible. On the other hand, thermodynamic modelling in ternary systems containing sigma phase yields the optimised values of enthalpy of formation of sigma phase, which can be compared with calculated energies of formation. Therefore, the thermodynamic modelling of sigma phase in Fe–Ni and

Cr–Ni systems may be performed by CALPHAD (CALCulation of PHase Diagrams) method based on values of thermodynamic functions of phases where ab initio calculated energy differences for sigma- and standard element reference (SER) phases for pure constituents are used. The ternary system Fe–Ni–Cr, where the sigma phase is stable in the Fe–Cr basis with addition up to 15 wt.% Ni, enables us to perform this modelling as a boundary condition. Modelled phase diagrams in both binaries and also in ternary Fe–Ni–Cr system will be confronted with experimental data and the energies of formation of (hypothetical) sigma phases calculated ab initio in Ni–Cr and Fe–Ni systems will be compared with thermodynamically optimised values of enthalpy of formation.

2. The model of sigma-phase

Knowledge of the value of the total energy difference between the sigma phase and SER phase of end-members calculated from first-principles (we use the Full Potential

* Corresponding author. Tel.: +420-541-129-316;

fax: +420-541-211-214.

E-mail address: chvatalova@email.cz (K. Chvátalová).

Augmented Plane wave (FLAPW) method, the WIEN97 code [3]) makes it possible to determine the lattice stability of pure constituents (Gibbs energy differences) on physically correct energetic basis. Our model of sigma phase stems from the two-sublattice model, which is similar to a model of solid solution phase [4], and the structural energy differences $\Delta E_{tot,i}^{sigma-SER}$ between the sigma and SER phase of pure constituents are obtained from first-principles electronic structure calculations. The Gibbs energy of the sigma-phase may be then expressed by means of the following relations:

$$G_m^{sigma} = \sum_i x_i {}^oG_i^{sigma} - TS_m^{ideal} + G^E, \quad (1)$$

where

$${}^oG_i^{sigma} = {}^oG_i^{SER} + \Delta E_{tot,i}^{sigma-SER} - TS_i^{vib,sigma-SER} \quad (2)$$

$$S_m^{ideal} = -R \sum_i (x_i \ln x_i) \quad (3)$$

$$G^E = x_i x_j ({}^oL_{i,j}^{sigma} + {}^1L_{i,j}^{sigma} (x_i - x_j) + {}^2L_{i,j}^{sigma} (x_i - x_j)^2), \quad (4)$$

where L -parameters can be temperature dependent. The entropy term (Eq. (2)) and the excess term (Eq. (4)) have to be adjusted to phase equilibrium data.

3. Results and discussion

First-principles total energy calculations (FLAPW method was employed, the energies were optimised at relaxed equilibrium volume) yield the following structural energy differences between the sigma and SER phases at 0 K for Fe, Cr and Ni [3]:

$$\begin{aligned} \Delta E_{tot,Fe}^{sigma-SER} &= 43330 \text{ J mol}^{-1} = 33.0 \text{ mRy at}^{-1}, \\ \Delta E_{tot,Cr}^{sigma-SER} &= 30070 \text{ J mol}^{-1} = 22.9 \text{ mRy at}^{-1}, \\ \Delta E_{tot,Ni}^{sigma-SER} &= 31950 \text{ J mol}^{-1} = 24.3 \text{ mRy at}^{-1} \end{aligned}$$

(this work).

Total energies of the SER phases were calculated in the corresponding spin-polarized state (ferromagnetic Fe and Ni, antiferromagnetic Cr). The values of $\Delta S_i^{vib,sigma-SER}$ for Fe, Cr and Ni were adjusted to phase diagram data; they were found to be $0.7 \text{ J K}^{-1} \text{ mol}^{-1}$ in all three elements studied (for Fe and Cr, see also [3]).

The excess term G^E was expressed by Redlich–Kister polynomial (4), and the parameters L were also adjusted to phase equilibrium data. The resulting values (in J mol^{-1}) amount to ($L_{Cr:Fe}$ from [5]):

${}^oL_{Cr:Fe} = -133950$	${}^oL_{Cr:Ni} = -104000$	${}^oL_{Fe:Ni} = -7000$
${}^1L_{Cr:Fe} = 31000$	${}^1L_{Cr:Ni} = -14000$	${}^1L_{Fe:Ni} = -40000$
${}^2L_{Cr:Fe} = -127000$	${}^2L_{Cr:Ni} = 80000$	${}^2L_{Fe:Ni} = -50000$

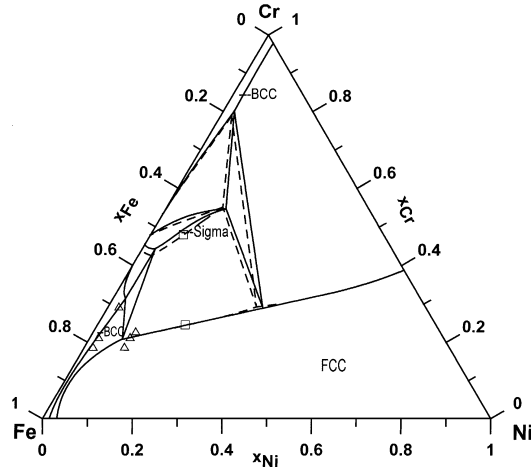


Fig. 1. Calculated phase diagram of Fe–Ni–Cr system at 1073 K according to the present model of sigma-phase (full lines), compared with the phase diagram calculated by the three-sublattice model [8] (dashed lines), using data from [9], and with experimental data: triangles for bcc/fcc from [10], squares for fcc/sigma from [11].

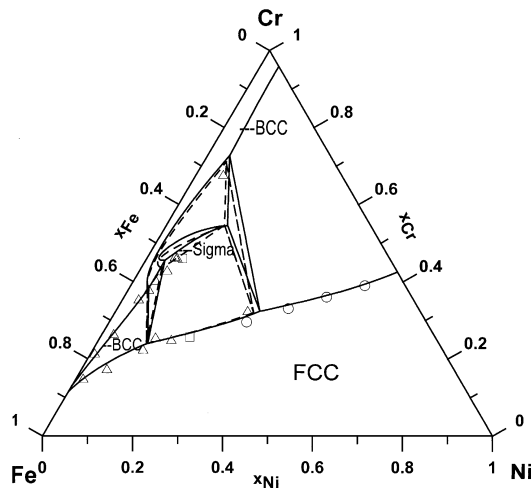


Fig. 2. Calculated phase diagram of Fe–Ni–Cr system at 1173 K according to the present model of sigma-phase (full lines), compared with the phase diagram calculated by the three sublattice model [8] (dashed lines), using data from [9] and with experimental data: triangles for bcc/fcc from [12], squares for FCC/sigma from [11], and circles for FCC from [13].

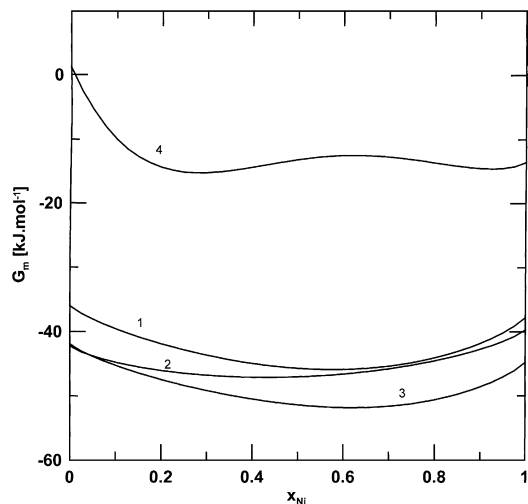


Fig. 3. Gibbs energy of phases in the Fe–Ni system at 1000 K: (1) liquid, (2) bcc, (3) fcc, (4) sigma, present model. Thermodynamic optimisation. No Gibbs energy of sigma phase according to [8,9].

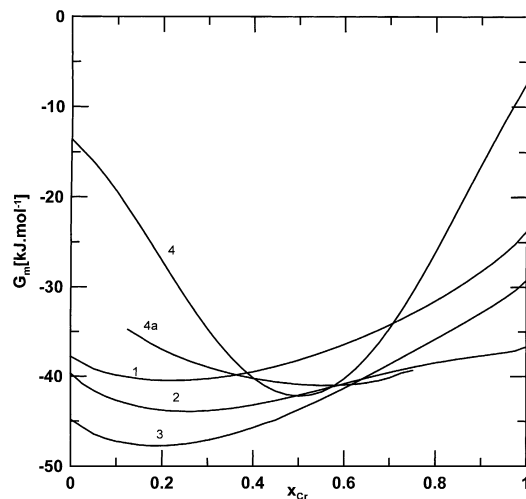


Fig. 5. Gibbs energy of phases in the Ni–Cr system at 1000 K: (1) liquid, (2) bcc, (3) fcc, (4) sigma, present model, (4a) sigma according to [8,9]. Thermodynamic optimisation.

Further, we performed first-principles calculations of total energies both of pure constituents and mixtures in the sigma-phase at 0 K by means of a simpler LMTO-ASA method [6]. In this way, we obtained the concentration dependence of the total energy E_{tot} of sigma-phase in various systems. Combining LMTO-ASA and FLAPW calculations, we obtained the energy of formation (Figs. 4 and 6). Detailed

description of this procedure may be found in [7], where we applied it for Fe–Cr and Co–Cr systems using unrelaxed volumes of the sigma phase.

As it follows from Figs. 1 and 2, the phase diagram calculation of Fe–Ni–Cr system at 1073 and 1173 K with the help of the sigma-phase description by means of the present model and ab initio results yields good agreement with ex-

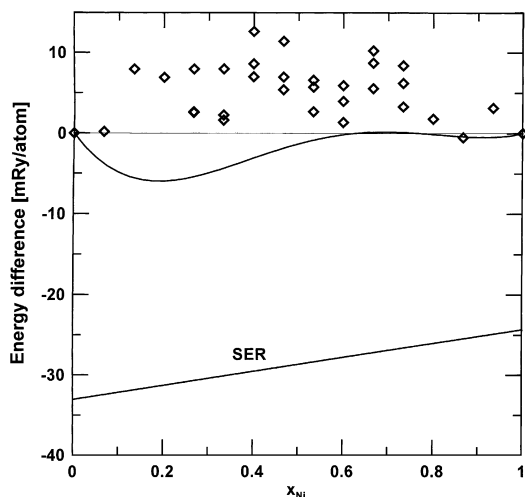


Fig. 4. Comparison of optimized enthalpy of formation (full line, thermodynamic calculations) and ab initio calculated energy of formation (diamonds, ab initio calculations) of sigma-phase in the Fe–Ni system with respect to energies of sigma phases of both constituents. The straight line denoted by SER shows the weighted average of total energies of SER states of pure constituents.

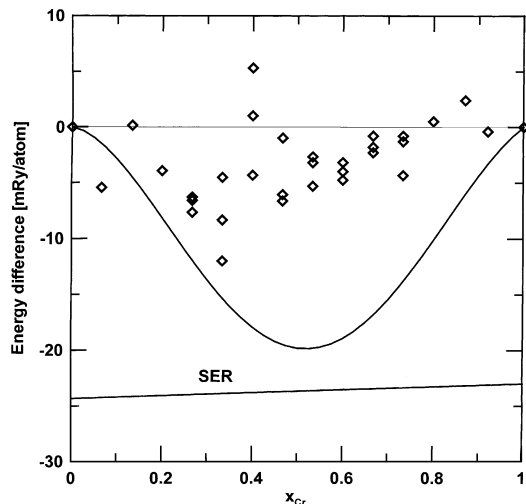


Fig. 6. Comparison of optimized enthalpy of formation (full line, thermodynamic calculations) and ab initio calculated energy of formation (diamonds, ab initio calculations) of sigma-phase in the Ni–Cr system with respect to energies of sigma phases of both constituents. The straight line denoted by SER shows the weighted average of total energies of SER states of pure constituents.

perimental data and also with calculations based on the three-sublattice model [8]. Optimised thermodynamic functions describing the Fe–Ni and Ni–Cr systems are shown in Figs. 3–6.

Figs. 3 and 5 display the Gibbs energies of various phases in Fe–Ni and Ni–Cr systems and Figs. 4 and 6 compare the optimised enthalpies of formation with the energies of formation with respect to energies of sigma phases of both constituents. The diamonds represent the values of energies of formation of binary sigma phases with various occupancies of sublattices [7]. Similarity in calculated energies of formation in Fe–Cr [5] and Ni–Cr systems is a strong support for the existence of sigma-phase in Ni–Cr system reported in [14] 30 years ago.

From the results presented in our article, it may be concluded that ab initio calculated energy differences between the sigma and SER structures for pure constituents can be successfully employed in the CALPHAD method.

Acknowledgements

This research was supported by the Grant Agency of the Czech Republic (Projects Nos. 106/02/0877 and 106/03/P002). First-principles electronic structure calculations were performed using the facilities of Metacentrum

of Masaryk University Brno and phase equilibria were determined by using Thermocalc software.

References

- [1] E.C. Bain, *Chem. Met. Eng.* 28 (1923) 23.
- [2] P. Villars, L.D. Calvert, *Pearson's Handbook of Crystallographic Data for Intermetallic Phases*, ASM International, Materials Park, Ohio, USA, 1991.
- [3] P. Blaha, K. Schwarz, L. Luitz, WIEN97, Vienna University of Technology, 1997.
- [4] J. Vřešťál, *Arch. Metall.* 46 (2001) 9.
- [5] J. Houserová, J. Vřešťál, M. Friák, M. Šob, *Comp. Mater. Sci.* 25 (2002) 562–569.
- [6] G. Krier, O. Jepsen, A. Burkhardt, O.J. Andersen, *Computer Code TB-LMTO-ASA*, ver. 4.6, Max-Planck-Institute für Festkörperforschung Stuttgart, 1994.
- [7] J. Havránková, J. Vřešťál, M. Friák, M. Šob, *Phys. Rev. B* 63 (2001) 174101.
- [8] O.J. Anderson, B. Sundman, *Calphad* 11 (1987) 83–92.
- [9] M. Hillert, C. Qiu, *Met. Trans.* 22A (1991) 2187–2198.
- [10] W.P. Rees, B.D. Burns, A.J. Cook, *J. Iron Steel Inst.* 162 (1949) 325.
- [11] J. Sopotšek, T. Kruml, *Scripta Materialia* 35 (1996) 689.
- [12] M. Hasebe, T. Nishizawa, in *Workshop NBS*. 1997. Gaithersburgh, MD, p. 911.
- [13] J.W. Schultz, H.F. Merrick, *Met. Trans.* 3 (1972) 2479.
- [14] N. Yukawa, M. Hida, T. Imura, M. Kawamura, Y. Miyuno, *Met. Trans.* 3 (1972) 887–8953.



ELSEVIER

Available online at www.sciencedirect.com

SCIENCE @ DIRECT®

Computer Coupling of Phase Diagrams and Thermochemistry 29 (2005) 133–139

www.elsevier.com/locate/calphad

Phase diagram calculations in the Co–Mo and Fe–Mo systems using first-principles results for the sigma phase

Jana Houserová^{a,*}, Jan Vřešťál^b, Mojmír Šob^{b,a}^a*Institute of Physics of Materials, Academy of Sciences of the Czech Republic, Žižkova 22, CZ-616 62 Brno, Czech Republic*^b*Department of Theoretical and Physical Chemistry, Faculty of Science, Masaryk University, Kotlářská 2, CZ-611 37 Brno, Czech Republic*

Received 16 February 2005; received in revised form 3 June 2005; accepted 8 June 2005

Available online 28 June 2005

Abstract

We calculate the phase diagrams of Co–Mo and Fe–Mo systems by means of a combination of ab initio electronic structure calculations and the CALPHAD approach. Ab initio calculations of the total energy differences between the sigma phase and standard element reference (SER) structures for pure constituents are accomplished by means of the full-potential linearized augmented plane wave (FLAPW) method in the generalized gradient approximation (GGA). During these calculations the structure relaxation is performed. The results obtained are employed as a part of the Gibbs energy describing the thermodynamics of the sigma phase. Subsequently, the thermodynamic data sets describing the sigma phases in the Co–Mo and Fe–Mo systems are optimized using the CALPHAD approach by employing both the experimental and thermodynamic data extended by ab initio calculations. Description of all other phases is taken from the literature. © 2005 Elsevier Ltd. All rights reserved.

Keywords: Ab initio calculation; Sigma phase; Phase diagram

1. Introduction

Molybdenum plays a controversial role in steel development. On one hand, it improves steel corrosion resistivity and, on the other hand, it increases the probability of formation of the unwelcome sigma phase. A reliable thermodynamic description of the Co–Mo and Fe–Mo systems is therefore needed to assess the regions of stability of various phases and may be used for further modelling of ternary systems containing Fe and Mo, which constitute a basis of some corrosion-resistant materials.

Information about phase equilibria and thermodynamic properties in the above-mentioned systems is of fundamental importance in the design of materials for applications under extreme conditions. The possibility of predicting phase equilibria provides a powerful tool for evaluating the properties and behaviour of materials. Such predictions can be performed by the CALPHAD (CALculation of PHase

Diagram) approach [1], which allows one to calculate the phase diagrams using thermodynamic functions of both pure constituents and all phases formed from these constituents.

The sigma phase is an intermetallic compound that can precipitate e.g. at grain boundaries as a secondary phase. It is extremely brittle and, therefore, it increases the probability of formation of crack nucleation sites. It also decreases the resistance of materials to various corrosive media. This phase can be found in many transition-metal systems (e.g. Fe–Cr, Co–Cr, Fe–Mo, Ni–V) [2]. It is well known that molybdenum stabilizes the sigma phase in iron-based alloys.

A full understanding of the behaviour of the sigma phase relies on the knowledge of the phase equilibria. This is primarily limited by a correct thermodynamic description of binary systems where the sigma phase can be treated using various models. The three-sublattice model [3–8] is one of the most frequently used ones.

The crystallographic structure of the sigma phase belongs to the space group No. 136 and is represented by 30 atoms in the unit cell. These atoms are accommodated in five inequivalent sublattices. The above-mentioned three-sublattice

* Corresponding author. Tel.: +420 532290 461; fax: +420 541218 657.
E-mail address: houserova@ipm.cz (J. Houserová).

model (which derives from the regular solution model [1] and the generalized multiple sublattice model [9]) is a substantial simplification of the sigma phase description, which is based on merging the sublattices with the same (or similar) coordination number to get a lower number of sublattices than found in the structural analysis. The Gibbs energy of the sigma phase modelled in this way is defined as a sum of the Gibbs energies of the bcc and fcc structures in the ratio given by simplified formula plus a correlation term, which is fitted to phase equilibrium and thermodynamic data. We have shown that another approach resulting in a two-sublattice model is sufficient [10–12]. This model describes the sigma phase as a solid solution with two sublattices (each having one site). In this case the Gibbs energy of the sigma phase is based on the Gibbs energies of the sigma phases of the pure constituents. The mixing of the elements involved occurs in the first sublattice and it is described by the sum of the Gibbs energies of the sigma phases of pure constituents weighted by their molar fractions. The second sublattice can be used for modelling interstitial phases and in the simplest cases, it is occupied by vacancies.

The assessment of stability of any structure (characterized by its energy of formation) is usually based on the standard element reference (SER) states, i.e. structures of the pure constituents that are stable at a temperature T of 298 K, and pressure p of 1 bar, such as hcp ferromagnetic Co, bcc ferromagnetic Fe and bcc non-magnetic Mo. This approach is very convenient because the thermodynamic functions describing these structures have been summarized in a published worldwide-accepted database [13] and verified in many thermodynamic assessments. Total energy differences between the sigma phase and the SER structure constitute a part of the Gibbs energy differences, and can be reliably calculated from first principles, e.g. by the full-potential linearized augmented plane waves (FLAPW) method [14] that provides high-precision solutions to Kohn–Sham equations as well as total energies for solid state structures.

The purpose of this work is to improve the thermodynamic modelling of the more complicated structures, such as the sigma phase, by employing the results of ab initio electronic structure calculations. We show that our model based on a combination of ab initio results and CALPHAD treatment provides a reliable approach for evaluating phase equilibria that involve such structures. The paper is organized as follows. After the introduction, we briefly characterize our thermodynamic model in Section 2. Section 3 describes the ab initio calculations of the total energy differences, which are used in Section 4 for predicting the phase diagrams. There we provide the values of the fitted parameters and discuss our results. Section 5 concludes the paper.

2. Thermodynamic model

Thermodynamic modelling allows one to describe arbitrary systems under various conditions (i.e. of pressure, temperature or composition) and enables us to predict the

behaviour of systems which are technologically important for the improvement of properties and manufacturing of current materials as well as for the development of new ones. In contrast to experiments, this treatment not only gives us an overview of the properties of actually existing structures but also is capable of characterizing metastable or even unstable configurations. The main variable used in such modelling is the molar Gibbs energy of the whole system G^{tot} , which is defined as the sum of molar Gibbs energies G^f of all included phases f multiplied by their molar fractions x^f :

$$G^{\text{tot}} = \sum_f x^f G^f, \quad (1)$$

where

$$G^f = \sum_i y_i {}^0G_i^f + G^{\text{id}} + G^E + G^{\text{mag}} + G^{\text{pres}}. \quad (2)$$

As shown in Eq. (2), the molar Gibbs energy G^f of phase f can be further divided in several terms, i.e. into the sum ($\sum_i y_i {}^0G_i^f$) of molar Gibbs energies ${}^0G_i^f$ of pure constituents i in the phase f multiplied by molar fractions y_i of the corresponding element in a given structure, terms describing ideal (G^{id}) and non-ideal (G^E) mixing and, when needed, some special terms such as the magnetic (G^{mag}) or pressure (G^{pres}) contribution. The last two terms are omitted in the case of the sigma phase in our work because we are modelling a solid metallic structure that is not very much influenced by pressure in the low-pressure region and this structure is supposed to be non-magnetic over the whole composition interval. We cannot exclude the possibility that the sigma phases of pure constituents could prefer some magnetic ordering. But the choice of the non-magnetic sigma phase as the reference state for the Gibbs energy in construction of the phase diagram could be justified by the fact that no magnetic sigma phase has been found in any system. Further, employing this non-magnetic reference state does not significantly influence thermodynamic modelling of the sigma phase in regions where this structure is stable. The terms describing mixing are evaluated using relatively simple formulas as follows:

$$G_{i,j}^{\text{id}} = RT(y_i \ln y_i + y_j \ln y_j), \quad (3)$$

$$G_{i,j}^E = y_i y_j (L^0(T) + L^1(T)(y_i - y_j) + L^2(T)(y_i - y_j)^2), \quad (4)$$

where L^0 , L^1 and L^2 are the expansion coefficients of the Redlich–Kister polynomial [15] and T stands for temperature.

The molar Gibbs energies of the pure components in more complicated phases are obtained in some cases with substantial difficulty, in contrast to the Gibbs energies of simple structures, such as bcc, fcc, hcp, which are summarized in various databases, e.g., Ref. [13]. Structures such as the Laves or sigma phase do not exist in the pure elemental state and therefore their Gibbs energies are experimentally inaccessible. In these situations ab initio

Table 1
FLAPW equilibrium and experimental lattice parameters of the SER structures

Structure	This work			Experiment			Ref.
	a (a.u.)	c/a	V_{at} (a.u. ³)	a (a.u.)	c/a	V_{at} (a.u. ³)	
FM hcp Co	4.7211	1.6194	73.7888	4.7357	1.6237	74.6722	[2]
FM bcc Fe	5.4144	1	79.3626	5.40	1	78.7320	[18]
				5.4160		79.4339	[19]
NM bcc Mo	5.9714	1	106.4619	5.9434	1	104.9723	[2]

FM stands for ferromagnetic and NM for non-magnetic states; V_{at} denotes the volume per atom.

methods can help us to get deeper insight into the thermodynamics of such structures.

The Gibbs energy of the sigma phase of the pure constituents can be written as

$$\begin{aligned} {}^0G_i^{\text{sigma}} &= {}^0G_i^{\text{SER}} + \Delta^0 G_i^{\text{sigma-SER}} \\ &= {}^0G_i^{\text{SER}} + \Delta^0 H_i^{\text{sigma-SER}} - \Delta^0 S_i^{\text{sigma-SER}} T, \end{aligned} \quad (5)$$

where H is enthalpy and S entropy.

The enthalpy of the sigma phase expressed with respect to the SER state, $\Delta^0 H_i^{\text{sigma-SER}}$, can be replaced by the ab initio calculated total energy difference between the sigma phase and the SER state, $\Delta^0 E_i^{\text{sigma-SER}}$, under the assumption that these two differences are equal. This is exactly fulfilled at zero temperature. We also suppose that $\Delta^0 H_i^{\text{sigma-SER}}$ and $\Delta^0 E_i^{\text{sigma-SER}}$ do not vary significantly with increasing temperature. This assumption may be verified on the basis of a combination of

- the Kirchoff equation ($\Delta H(T_1) = \Delta H(T_0) + \int_{T_0}^{T_1} \Delta C_p dT$, where $\Delta H(T_0)$ and $\Delta H(T_1)$ are the reaction enthalpies at T_0 and T_1 , respectively, and the difference between the heat capacities at constant pressure is $\Delta C_p = C_p^{\text{products}} - C_p^{\text{reactants}}$) and
- the Neumann-Kopp rule ($C_p(A_n B_m) = nC_p(A) + mC_p(B)$), which is reasonably valid for metallic systems.

This combination results in $\Delta C_p = C_p^{\text{products}} - C_p^{\text{reactants}} = C_p(A_n B_m) - nC_p(A) + mC_p(B) = 0$ and, subsequently, $\Delta H(T_1) = \Delta H(T_0) + \int_{T_0}^{T_1} 0 dT = \Delta H(T_0)$.

Therefore, we can write

$$\begin{aligned} {}^0G_i^{\text{sigma}} &= {}^0G_i^{\text{SER}} + \Delta^0 G_i^{\text{sigma-SER}} \\ &\cong {}^0G_i^{\text{SER}} + \Delta^0 E_i^{\text{sigma-SER}} - \Delta^0 S_i^{\text{sigma-SER}} T. \end{aligned} \quad (6)$$

The entropy term $\Delta^0 S_i^{\text{sigma-SER}}$ may be adjusted to experimental data (see Section 4). Expression (6) can then be employed in phase diagram calculations according to Eq. (2).

This procedure has been successfully used for the calculation of phase diagrams in other systems containing the sigma phase, such as Fe–Cr [11] and Co–Cr [12]. In this paper the Co–Mo and Fe–Mo systems are presented as further examples.

3. Ab initio calculations of total energies

We used the FLAPW method [14] incorporated into the WIEN97 code [16] to calculate the total energy differences between the sigma phase and the SER structure similarly to our previous studies [11,12]. The exchange–correlation energy was evaluated in the generalized gradient approximation (GGA) [17]. We used constant muffin-tin radii (RMT parameters) during all our calculations (1.97 a.u. for Co, 1.96 a.u. for Fe and 2.30 a.u. for Mo). The optimum numbers of k -points in the irreducible part of the Brillouin zone providing a sufficient convergence of the total energies of the SER states were found to be 288 for Co and 120 for Fe and Mo.

We decided to relax all structures to get reliable reference states for evaluating the energy differences. The relaxation is based on the alternating optimization of the volume and c/a ratio. In the case of the cubic structures only volume relaxation is sufficient to get the lowest-energy state. The resulting optimum lattice parameters for the SER states are listed in Table 1.

The same approach was applied to equilibrium calculations for the sigma phase. Since the sigma phase of the pure constituents does not exist we have used the structure parameters from the binary phases. For this purpose, we have utilized the lattice parameters a and c from such binary sigma phases that involve elements with similar atomic radii to the element chosen, i.e. for Co from the Co–Cr sigma phase [20], for Fe from the Fe–Cr sigma phase [21] and for Mo from the Mo–Mn sigma phase [22]. There are some other parameters besides lattice ones describing the structure of the sigma phase—so-called internal parameters, which describe the positions of atoms within the unit cell. We have examined their values from various binary sigma phases (e.g. the internal parameters for Cr–Fe, Fe–Mo etc. in the case of Fe) and, employing the linear muffin-tin orbital method in the atomic sphere approximation (LMTO-ASA) [23–25] within the GGA [17], we looked for those values that provided the lowest energies. These were acquired using the internal structure parameters of Fe–Cr [21] for Fe and of Co–Mo [26] for Co and Mo. The values of the internal structure parameters obtained in this way were kept constant in all subsequent calculations.

Afterwards we employed the FLAPW method again for the optimization of lattice parameters a and c in the same

136

J. Houserová et al. / Computer Coupling of Phase Diagrams and Thermochemistry 29 (2005) 133–139

way as was described for the SER structures. Performing convergence tests, we have found that 42 k -points in the irreducible part of the Brillouin zone were sufficient for all three constituents. As the sigma phases existing in nature are not spin-polarized, the calculations for pure constituents were also performed for a non-spin-polarized state. The resulting lattice parameters are summarized in Table 2. It may be shown that the differences in atomic volumes between the SER and sigma phase related to the equilibrium atomic volume of the SER state are comparable with the differences between the values obtained for the bcc, fcc, and hcp structures [27].

Table 2
FLAPW equilibrium lattice parameters of the sigma phase of pure constituents

Element in the sigma phase structure	This work		
	a (a.u.)	c/a	V_{at} (a.u. ³)
Co	15.8602	0.5197	69.1069
Fe	15.5987	0.5174	65.4586
Mo	18.1870	0.5241	105.1003

This procedure provided the total energies of the sigma phases of pure constituents at the equilibrium volumes and the justification for the statement that the sigma phase of pure constituents is stable with respect to the volume changes and tetragonal deformation. Unfortunately there is no absolute guarantee of the dynamic stability of this phase in the pure state. On the other hand, even if the sigma phase structure of the pure constituent were dynamically unstable, the total energy difference between this structure and SER phase at zero temperature has a well-defined value [28,29], which can be used as an effective value in the procedure of adjusting the thermodynamic parameters in the phase equilibrium data calculations. Hence we evaluated the total energy differences between the sigma phase and SER state (Table 3).

Table 3
Ab initio calculated total energy differences between the sigma and SER phases

Element		Co	Fe	Mo
ΔE_i^0 sigma-SER	(mRy atom ⁻¹)	45.58	33.03	17.77
	(kJ mol ⁻¹)	59.84	43.36	23.33

The present values for Co are somewhat different in comparison with those in [12] due to better approximations used in this work. The physical conclusions in paper [12] are not influenced by this difference.

4. Phase diagram calculations

The thermochemical basis of the CALPHAD method relies explicitly on the assumption that the composition of the equilibrium phase arises as a result of minimization of the Gibbs energy in a closed system at constant external conditions (temperature and pressure).

For modelling the sigma phase we employed the two-sublattice model [11,12] because it has a good physical background, it enables us to describe the sigma phase over the whole composition range and it should be able to provide a substantial improvement of the thermodynamic modelling of more complicated systems. The sigma phase is treated here as a solid solution (see Eq. (1)) and its Gibbs energy in the pure state is defined by Eq. (6) where the entropy term is adjusted to the experimental data. The L parameters describing the excess Gibbs energy G^E of non-ideal mixing in Eq. (4) are obtained in the same way. All these parameters (ΔS_i^0 sigma-SER and L) are listed in Tables 4 and 5.

Table 4
The adjusted entropy of the transition from the SER state to the sigma phase

Element	Co	Fe [11]	Mo
ΔS_i^0 sigma-SER (J K ⁻¹ mol ⁻¹)	0.75	0.70	0.75

Table 5
The adjusted L parameters describing the non-ideal mixing

Parameter/System	Co–Mo	Fe–Mo
L^0	$-171\,500 + 25.0 * T$	$-119\,000 + 5.1 * T$
L^1 (J mol ⁻¹)	35 000	-50 000
L^2	75 000	-108 400

The complete thermodynamic description of the sigma phase in the two-sublattice model is given in Appendix. The thermodynamic parameters for all other phases in Co–Mo and Fe–Mo systems, namely of the liquid, fcc, hcp, EPS, Mu, bcc, Laves phase and R phase, were taken from [6] and [30], respectively. The calculated phase diagrams are presented in Fig. 1.

It is obvious that our approach provides a very good description of the stability range of Co–Mo and Fe–Mo sigma phases with quality comparable to that of the earlier three-sublattice model ([6] and [30], respectively). Moreover, our model employs a transparent approach to the modelling of the sigma phase over the whole composition region that is based on ab initio calculations. It can be thought of as a reasonable starting point in approaching otherwise inaccessible regions of unstable sigma phases. In contrast, the three-sublattice model describes the sigma phase as a combination of the Gibbs energies of SER states, which has no relevance in the composition range close to the pure constituents. Therefore we expect the two-sublattice model to provide a better understanding when studying multicomponent systems. Our calculated phase equilibria also agree very well with the experimental phase equilibrium data [3,5,31–33] for both systems. It is not the purpose of this paper to study those regions of the phase diagram not containing the sigma phase because they cannot

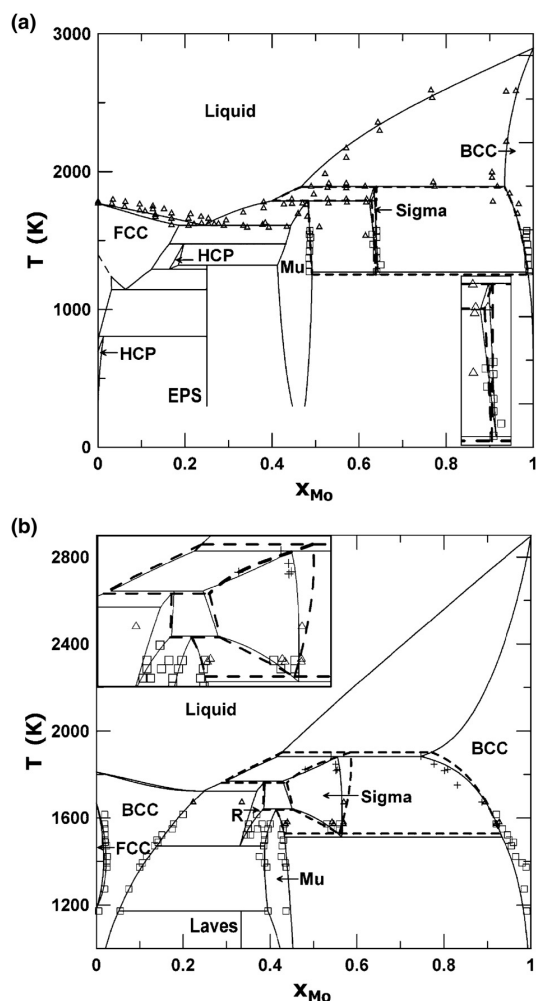


Fig. 1. Calculated phase diagrams of Co–Mo (a) and Fe–Mo (b). Thick dashed lines: the two-sublattice model (thermodynamic data are given in Tables 3–5), thin full lines: the three-sublattice model (thermodynamic data from [6] and [30]), experimental data according to [5] (Δ) and [31] (\square) for Co–Mo and [32] (Δ), [33] (\square) and [3] (+) for Fe–Mo. The dashed line in the left-hand part of the Co–Mo phase diagram divides the region of the fcc phase into the ferromagnetic (lower) and paramagnetic (upper) parts.

be influenced by changes in the sigma phase modelling and, therefore, the corresponding experimental data are not presented in Fig. 1.

The comparison between the Gibbs energy and enthalpy of the sigma phase calculated within both models and those for other phases (described using the data from [6,30]) is shown in Figs. 2 and 3. From these figures, we conclude that the two-sublattice model provides the proper composition dependence for both thermodynamic functions (i.e. G^f and H^f) over the whole composition range in contrast to the three-sublattice model (see lines 8 and 8a in those figures).

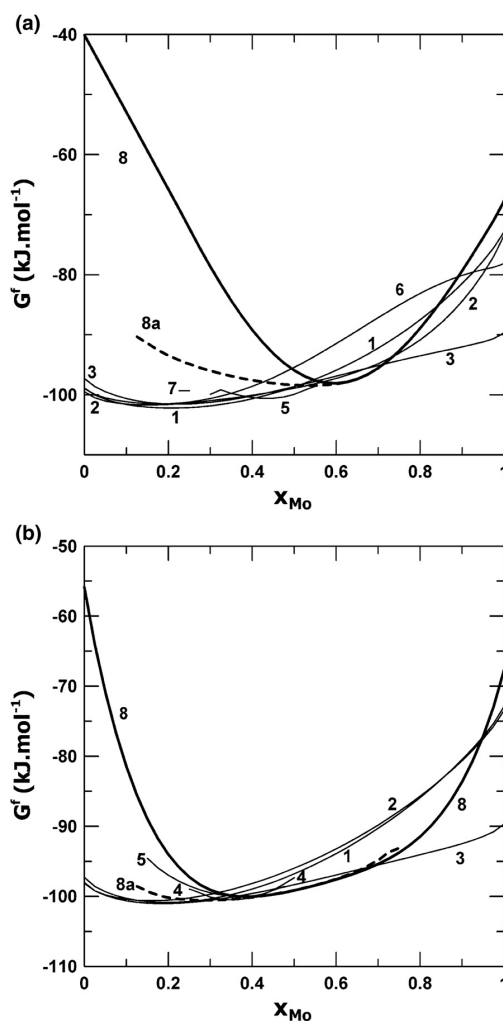


Fig. 2. Concentration dependence of the molar Gibbs energy G^f for various phases in the Co–Mo (a) and Fe–Mo (b) systems at 1700 K: 1—liquid, 2—fcc, 3—bcc, 4—R, 5—Mu, 6—hcp, 7—EPS, 8—sigma (two-sublattice model), 8a—sigma (three-sublattice model).

This is a great advantage of our method, which will enable us to extend the calculations to multicomponent systems.

5. Conclusions

Our approach provides a reasonable physical interpretation of the individual terms in the mathematical expression for the Gibbs energy difference between the sigma phase and SER state of the pure constituents. Total energy differences are reliably evaluated by the ab initio methods, and can be incorporated into the two-sublattice model [11,12] which consequently provides a transparent and effective way for constructing phase diagrams. This model can be used

138

J. Houserová et al. / Computer Coupling of Phase Diagrams and Thermochemistry 29 (2005) 133–139

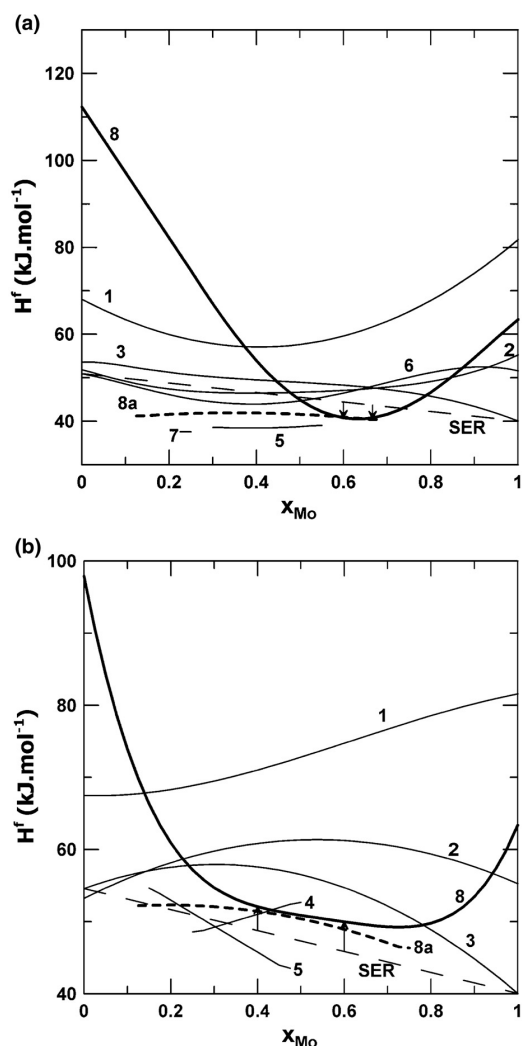


Fig. 3. Concentration dependence of the molar enthalpy H^f for various phases in the Co–Mo (a) and Fe–Mo (b) systems at 1700 K. The labelling of the lines is the same as in Fig. 2. The thin dashed straight line denoted as SER shows the weighted average of the molar enthalpy of the pure constituents in the SER states. The arrows indicate our predictions of molar enthalpies of formation of the alloy sigma phases with respect to the weighted average of molar enthalpies of SER states of pure constituents.

because the inequivalent lattices are not exclusively occupied by one component [7]. Recently, we have shown that the two-sublattice model can reproduce well the phase equilibria in a multicomponent system [34].

This paper illustrates the use of such model in the case of the Co–Mo and Fe–Mo binary systems. It was shown that the calculated equilibria involving the sigma phase agree well with the experimental data ([5,31] for Co–Mo and [3, 32,33] for Fe–Mo). Unlike the previously considered three-sublattice model, the two-sublattice model employed in this

study provides a description of the molar Gibbs energy G^f and the molar enthalpy H^f of the sigma phase over the whole composition range. Unfortunately, there are no experimental data which could prove or disprove our results concerning the enthalpy of the sigma phase in Mo-based systems. For the Cr-based systems, we have shown that the calculated enthalpies obtained from the two-sublattice model agree quite well with the experiments [12].

Acknowledgements

This research was supported by the Grant Agency of the Czech Republic (Projects Nos. 106/03/P002 and 106/02/0877), by Grant Agency of the Academy of Sciences of the Czech Republic (Project No. S2041105) and by the Research Projects AV0Z20410507 and MSM0021622410. The use of the computer facilities at the MetaCentre of the Masaryk University in Brno is acknowledged. Phase equilibria were calculated by means of the ThermoCalc code.

Appendix

Summary of sigma phase parameters:

For $298.15 < T < 6000$:

two sublattices, sites 1:1.

Constituents: Co, Mo, Fe:Va:

$${}^0G_{\text{Co:Va}}^{\text{sigma}} = {}^0G_{\text{Co}}^{\text{FM-hcp}} + 59\,840 - 0.75 * T.$$

$${}^0G_{\text{Fe:Va}}^{\text{sigma}} = {}^0G_{\text{Fe}}^{\text{FM-bcc}} + 43\,360 - 0.7 * T.$$

$${}^0G_{\text{Mo:Va}}^{\text{sigma}} = {}^0G_{\text{Mo}}^{\text{NM-bcc}} + 23\,300 - 0.75 * T.$$

$${}^0L_{\text{Co,Mo:Va}}^{\text{sigma}} = -171\,500 + 25 * T.$$

$${}^1L_{\text{Co,Mo:Va}}^{\text{sigma}} = +35\,000.$$

$${}^2L_{\text{Co,Mo:Va}}^{\text{sigma}} = +75\,000.$$

$${}^0L_{\text{Fe,Mo:Va}}^{\text{sigma}} = -119\,000 + 5.1 * T.$$

$${}^1L_{\text{Fe,Mo:Va}}^{\text{sigma}} = -50\,000.$$

$${}^2L_{\text{Fe,Mo:Va}}^{\text{sigma}} = -108\,400.$$

References

- [1] N. Saunders, A.P. Miodownik, CALPHAD (Calculation of Phase Diagrams): A Comprehensive Guide, in: Pergamon Materials Series, vol. 1, Elsevier Science Ltd, Oxford, UK, 1998.
- [2] P. Villars, L.D. Calvert, Pearson's Handbook of Crystallographic Data for Intermetallic Phases, ASM International, Materials Park, OH, USA, 1991.
- [3] A.F. Guillermet, CALPHAD 6 (1982) 127.
- [4] J.-O. Andersson, B. Sundman, CALPHAD 11 (1987) 83.
- [5] A.V. Davydov, U.R. Kattner, J. Phase Equilib. 20 (1999) 5.
- [6] A.V. Davydov, U.R. Kattner, J. Phase Equilib. 24 (2003) 209.
- [7] I. Ansara, T.G. Chart, A.F. Guillermet, F.H. Hayes, U.R. Kattner, D.G. Pettifor, N. Saunders, K. Zeng, CALPHAD 21 (1997) 171.
- [8] M. Hillert, CALPHAD 22 (1998) 127.
- [9] B. Sundman, J. Agren, J. Phys. Chem. Solids 42 (1981) 297.
- [10] J. Vřešťál, Arch. Metall. 46 (3) (2001) 9.

- [11] J. Houserová, M. Friák, M. Šob, J. Vřešťál, *Comput. Mater. Sci.* 25 (2002) 562.
- [12] J. Houserová, J. Vřešťál, M. Friák, M. Šob, *CALPHAD* 26 (2002) 513.
- [13] A.T. Dinsdale, *CALPHAD* 15 (1991) 317.
- [14] D. Singh, *Planewaves, Pseudopotentials and the LAPW Method*, Kluwer, Boston, 1994.
- [15] O. Redlich, A.T. Kister, *Ind. Eng. Chem.* 40 (1948) 345.
- [16] P. Blaha, K. Schwarz, J. Luitz, Computer code WIEN97, Vienna University of Technology, 1997 (improved and updated Unix version of the original copyrighted WIEN code, which was published by P. Blaha, K. Schwarz, P. Sorantin, S.B. Trickey, *Comput. Phys. Commun.* 59 (1990) 399).
- [17] J.P. Perdew, J.A. Chevary, S.H. Vosko, K.A. Jackson, M.R. Pederson, D.J. Singh, C. Fiolhais, *Phys. Rev. B* 46 (1992) 6671.
- [18] E.G. Moroni, T. Jarlborg, *Phys. Rev. B* 47 (1993) 3255.
- [19] M. Polcarova, K. Goodwod, J. Bak-Misiuk, S. Kadeckova, J. Bradler, *Phys. Status Solidi a* 106 (1988) 17.
- [20] G.J. Dickins, A.M.B. Douglas, W.H. Taylor, *Acta Crystallogr.* 9 (1956) 297.
- [21] H.L. Yakel, *Acta Crystallogr. B* 39 (1983) 20.
- [22] B.F. Decker, R.M. Waterstrat, J.S. Kasper, *J. Met., Trans. AIME* 6 (1954) 1406.
- [23] O.K. Andersen, *Phys. Rev. B* 12 (1975) 3060.
- [24] H.L. Skriver, *The LMTO Method*, Springer Verlag, Berlin, 1984.
- [25] G. Krier, O. Jepsen, A. Burkhardt, O.K. Andersen, Computer code TB-LMTO-ASA version 4.6, Max-Planck-Institut für Festkörperforschung, Stuttgart, 1994.
- [26] J.B. Forsyth, d'Alte da Viegas, *Acta Crystallogr.* 16 (1963) 509.
- [27] Y. Wang, S. Curtarolo, C. Jiang, R. Arroyave, T. Wang, G. Ceder, L.-Q. Chen, Z.-K. Liu, *CALPHAD* 28 (2004) 79.
- [28] G. Grimvall, *Ber. Bunsenges. Phys. Chem.* 102 (1998) 1083.
- [29] G. Grimvall, *CALPHAD and Alloy Thermodynamics*, TMS, Warrendale, PA, USA, 2002, p. 81.
- [30] J.-O. Andersson, *CALPHAD* 12 (1988) 9.
- [31] C.P. Heijwegen, G.D. Rieck, *J. Less-Common Met.* 34 (1974) 309.
- [32] P. Gustafson, *Z. Metallkde.* 79 (1988) 388.
- [33] C.P. Heijwegen, G.D. Rieck, *J. Less-Common Met.* 37 (1974) 115.
- [34] K. Chvátalová, J. Houserová, M. Šob, J. Vřešťál, *J. Alloys Compounds* 378 (2004) 71.

Available online at www.sciencedirect.com

SCIENCE @ DIRECT®

Computer Coupling of Phase Diagrams and Thermochemistry 30 (2006) 14–17

www.elsevier.com/locate/calphad

Assessment of the thermodynamic properties and phase diagram of the Bi–Pd system

J. Vřešťál^{a,*}, J. Pinkas^a, A. Watson^b, A. Scott^b, J. Houserová^c, A. Kroupa^c^a Masaryk University, Faculty of Science, Department of Physical Chemistry, Kottlářská 2, 611 37 Brno, Czech Republic^b University of Leeds, Institute for Materials Research, S.P.E.M.E., Leeds, UK^c Institute of Physics of Materials, Academy of Sciences of Czech Republic, Žitkova 22, 616 62 Brno, Czech RepublicReceived 11 October 2005; received in revised form 2 December 2005; accepted 2 December 2005
Available online 29 December 2005

Abstract

New experimental DTA, XRD, SEM, solution calorimetry and ab initio calculated results are used together with data from the literature to assess the thermodynamic parameters of the Bi–Pd system, necessary for calculation of the phase diagram by the CALPHAD method. Samples were prepared with compositions of 51 and 82 at.% Pd, and their homogeneity checked by SEM/EDX before being employed in DTA studies. High temperature solution calorimetry was used for the determination of the enthalpies of mixing of liquid Pd and Bi, in the range from 0 up to 50 at.% Pd at 1028 K. XRD determination of the structures of equilibrated samples after quenching to room temperature provided important information for the evaluation of structure. Ab initio electronic structure calculations provided information on the energetics of the intermetallic phases of the system. The calculated phase diagram was compared with new phase equilibrium data and with the data presented in the literature. © 2005 Elsevier Ltd. All rights reserved.

1. Introduction

The use of bismuth is not only important as a solvent of uranium in nuclear metallurgy, but also as a component in lead-free solder materials. In the study of the interaction of such solder materials with substrates, which often contain palladium, knowledge of the Bi–Pd phase diagram is of interest. Phase diagram studies have been carried out by Zhuravlev and Zhdanov [1], Zhuravlev [2] (without experimental details) and Brasier and Hume-Rothery [3]. The published liquidus data were confirmed by Schweitzer and Weeks [4] by the method of analysis after equilibrating annealing. The third paper of these [3] is a rich source of accurate phase equilibrium data, obtained by cooling curve analysis (2–3 °C/min, silica stirrer, argon atmosphere, recalibrated thermocouple, high purity metals), suitable for use in the assessment. New information on the solubility of bismuth in palladium at lower temperatures has been provided by Oberndorff [5], reporting no solubility of Bi in Pd at 200 °C and 215 °C following diffusion couple studies. For prediction of phase equilibria by

the CALPHAD (CALculation of PHase Diagram) method, the thermodynamic properties of the phases are required. Unfortunately, no thermodynamic information is available for this system.

Therefore, the aim of this work is to perform a thermodynamic assessment of the Bi–Pd system using new thermodynamic information gained by calorimetric experiments and first-principles calculations. Complementary SEM, DTA and XRD measurements have been performed to confirm the results.

2. Experimental

2.1. Calorimetry

A high temperature SETARAM HT1500 calorimeter was used for the measurement of the heat of dissolution of palladium in liquid bismuth at 1028 K by the drop technique; the apparatus has been described elsewhere [6]. Solid palladium (Alfa Aesar, 99.99%) was dropped from room temperature into a liquid bismuth (Alfa Aesar, 99.99%) bath held at 1028 K in an alumina crucible under a pure argon atmosphere. The heat flow from the reaction crucible to the reference crucible

* Corresponding author. Tel.: +420 549498134; fax: +420 541211214.
E-mail address: vrestal@chemi.muni.cz (J. Vřešťál).

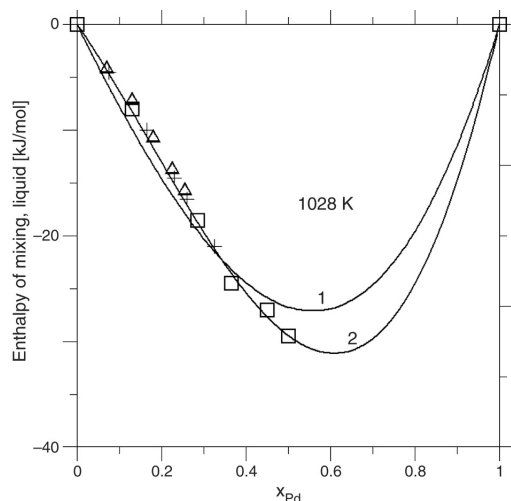


Fig. 1. Integral enthalpy of mixing of liquid Bi–Pd alloys (liquid standard state). Results of three independent runs. 1—Least squares fit of experimental results by a polynomial of second order. 2—Result of global optimization of calorimetric and phase equilibrium results, expressed by a polynomial of second order.

was recorded with respect to time via a thermopile. The total heat effect was then calculated by integration of the thermogram, the graphical representation of the output of the thermopile with respect to time. By subtracting appropriate amounts for the enthalpy of fusion and enthalpy increment of palladium ($H_{\text{Pd},1023} - H_{\text{Pd},298}$) the partial enthalpy of mixing can be calculated. By making successive palladium drops and summing the partial enthalpies, the integral enthalpy of mixing curve can be derived. The calorimeter was calibrated by dropping a bismuth sample immediately before the palladium drops and by dropping an alumina sample at the end of the run. The resulting integral enthalpies of mixing of Bi–Pd liquid alloys from three independent runs are shown in the Fig. 1, where the approximation of experiments to a smooth curve is also drawn. The value of the enthalpy of mixing at the composition $x_{\text{Pd}} = 0.5$ is determined to be $\Delta H_{\text{BiPd}}^M = -27 \text{ kJ mol}^{-1}$, approximating the concentration dependence of ΔH_{BiPd}^M by a quadratic polynomial. The reproducibility of calorimetric measurements can be estimated to be $\pm 1 \text{ kJ mol}^{-1}$ considering Fig. 1, where the results of three independent runs are displayed, and approximated by a polynomial of second order by the least squares method. On the other hand, global optimization of the calorimetric experiment with phase equilibrium data [1–4] expressed by a polynomial of second order for the thermodynamic parameters of the liquid phase, Fig. 1, lead to the small differences from the measured values of its enthalpy of mixing which may be regarded as acceptable.

2.2. DTA measurements of liquidus temperature

Liquidus temperatures were taken from the literature [1–4], but two samples of Bi–Pd alloys with $x_{\text{Pd}} = 0.51$ and with

$x_{\text{Pd}} = 0.82$ were prepared for verification of the published results.

A sample with $x_{\text{Pd}} = 0.51$ was prepared from the elements of the same purity as given above. Appropriate amounts of bismuth and palladium were melted together in an evacuated silica capsule, in a flame.

After solidification, the sample was annealed at $450 \text{ }^\circ\text{C}$ for 2 h followed by quenching into water. The homogeneity of the sample was checked by SEM, and two phases were found: an orthorhombic PdBi intermetallic and very small amount of a second phase, both of which were confirmed by XRD analysis (the Pd_5Bi_3 phase, which was expected considering the phase diagram, was not confirmed unambiguously, as its crystallographic structure is not reliably known).

Part of the sample was used in the determination of the melting temperature of the PdBi intermetallic compound by differential thermal analysis (DTA). The DTA was performed under an argon atmosphere, using a Derivatograph (MOM Budapest) instrument, employing a heating rate of $5 \text{ }^\circ\text{C/min}$ and alumina as the reference material. The melting temperature of PdBi was found to be $624 \text{ }^\circ\text{C}$ and the eutectic temperature on the palladium side was $578 \text{ }^\circ\text{C}$.

A similar procedure was followed for a sample with $x_{\text{Pd}} = 0.82$. SEM/EDS analysis of this sample revealed a two-phase structure with compositions 0.77 (Pd₃Bi) and 0.83 of palladium (FCC), respectively. This structure corresponds to that at the crystallization temperature and therefore represents a frozen equilibrium. Air cooling of the sample does not provide a slow enough cooling rate to give the true equilibrium at low temperature.

Corresponding DTA analysis revealed endothermic peaks at $939 \text{ }^\circ\text{C}$ and at $1081 \text{ }^\circ\text{C}$, which correspond to the peritectic temperature and to the temperature of full melting of the sample. These are in agreement with values in the literature [1–4] and were used in the optimization procedure.

3. Theoretical calculations

3.1. Ab initio calculated total energies of formation of PdBi₂ and PdBi

We have performed ab initio calculations of the total energies of PdBi (room temperature structure) and PdBi₂ (high temperature structure) intermetallics and of Bi and Pd in their experimentally observed structures (i.e., RHOMBOHEDRAL A7 Bi and FCC A1 Pd), which represent the standard element reference (SER) states.

The structural information for the PdBi and PdBi₂ intermetallics was taken from [7] and [8], respectively. Spin polarization was not included in our calculations as all phases studied are paramagnetic at ambient temperature. The FLAPW (Full Potential Augmented Plane Wave) method implemented in the WIEN 97 code [9] using the generalized gradient approximation (GGA) [10] for the exchange-correlation term was employed to evaluate the total energy difference between PdBi and the SER-phases at 0 K at equilibrium volume

16

J. Vřešťál et al. / Computer Coupling of Phase Diagrams and Thermochemistry 30 (2006) 14–17

(i.e., at the minima of the energy/volume curves). The calculated energy of formation of PdBi is:

$$\Delta E_f^{\text{PdBi}} = -34.13 \text{ kJ mol}^{-1} = -26.00 \text{ mRy at}^{-1}.$$

This result was checked using the pseudopotential Vienna Ab initio Simulation Package (VASP) code [11,12] by using the Projector Augmented Wave (PAW) pseudopotential for the Local Density Approximation (LDA). These calculations yielded results similar to the FLAPW case:

$$\Delta E_f^{\text{PdBi}} = -33.16 \text{ kJ mol}^{-1} = -25.26 \text{ mRy at}^{-1}.$$

For PdBi₂, the pseudopotential codes VASP and CASTEP [13] were employed, with the results (at equilibrium structure parameters):

$$\Delta E_f^{\text{PdBi}_2} = -23.17 \text{ kJ mol}^{-1} = -17.65 \text{ mRy at}^{-1} \text{ (VASP)}$$

$$\Delta E_f^{\text{PdBi}_2} = -27.0 \text{ kJ mol}^{-1} = -20.6 \text{ mRy at}^{-1} \text{ (CASTEP)}.$$

For thermodynamic considerations, the mean values $\Delta E_f^{\text{PdBi}} = -33.6 \text{ kJ mol}^{-1}$ and $\Delta E_f^{\text{PdBi}_2} = -25.1 \text{ kJ mol}^{-1}$ were used, because we cannot prefer any one of the computational methods over the rest.

The structure of the Pd₃Bi intermetallic compounds is very complex (Bi₄PbPd₁₅ structure type—16 atoms in the repeat cell with 6 inequivalent lattice sites) [14]. Ab initio calculations of total energy of this structure were not performed owing to this complexity.

3.2. Thermodynamic assessment

The main aim of this work is to derive a set of thermodynamic model parameters, describing the Gibbs energy of the phases in the system, which then can be used for phase diagram calculation by the CALPHAD method. This is based on finding the minimum total Gibbs energy of the closed system at constant temperature and pressure, yielding the composition and the amount of phases in equilibrium. The total molar Gibbs energy (G_{tot}) is equal to the sum of the molar Gibbs energies of all phases (G^f) multiplied by their molar fractions (x^f), i.e.,

$$G_{\text{tot}} = \sum_f x^f G^f. \quad (1)$$

G^f is defined as

$$G^f = \sum_i y_i^0 G_i^f + G^{\text{id}} + G^{\text{E}} + G^{\text{mag}} + \dots, \quad (2)$$

where y_i is the molar fraction of the component i in phase f , ${}^0G_i^f$ is the molar Gibbs energy of pure component in the phase f , the terms G^{id} and G^{E} stand for the molar Gibbs energy of ideal and excess mixing, and G^{mag} is the magnetic contribution to the Gibbs energy. The excess Gibbs energy G^{E} can be expressed as an empirical Redlich Kister polynomial [15]:

$$G_{ij}^{\text{E}} = y_i y_j ({}^0L_{i,j}^f + {}^1L_{i,j}^f (y_i - y_j) + {}^2L_{i,j}^f (y_i - y_j)^2), \quad (3)$$

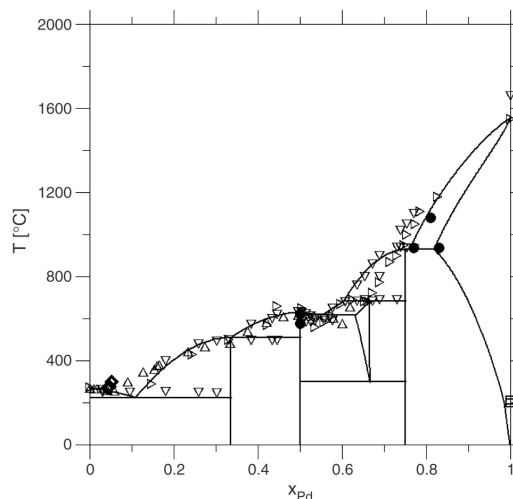


Fig. 2. Phase diagram of the Bi–Pd system calculated using thermodynamic parameters (see Appendix) determined in this work (solid lines) compared with experimental phase equilibrium data (\triangleright [1], ∇ [2], Δ [3], \diamond [4], \square [5], \bullet this work).

whereas G^{id} can be calculated according the theoretical relationship:

$$G^{\text{id}} = -RT \sum_i (y_i \ln y_i). \quad (4)$$

The Gibbs energies of phases, G^f , are used as an input for the phase diagram calculations.

To obtain parameters describing the Gibbs energies of the individual phases, various models for the excess Gibbs energy description are proposed. For the liquid phase, a simple subregular model was used (3), and for the solid phases, the sublattice model and compound energy formalism (CEF) [16] were applied. Thermo-calc software [17], and its module PARROT for optimization of model parameters by the least squares method, were employed to give the calculated phase boundaries and thermodynamic properties which gave the best fit with experimental data within their experimental uncertainties. The resulting values of these parameters are presented in the Appendix. The phase diagram calculated using these parameters is shown in the Fig. 2. The experimental data from the literature and those determined in the present work are also given. The homogeneity range of Pd₅Bi₃ is not described experimentally with any reliability; therefore, it is denoted in [3] by dotted lines. X-ray studies by Zhuravlev [18] suggested that the phase has a structure of the AsNi type, but data describing the mixing of the atoms are missing. Therefore, a simple two sublattice model was used (Bi,Pd:Va) and parameters were determined to best reproduce the dotted line region. Ab initio calculations were not performed.

4. Discussion

The value of the enthalpy of mixing in the liquid phase at the composition $x_{\text{Pd}} = 0.5$ determined by drop calorimetry

($\Delta H^M = -27 \text{ kJ mol}^{-1}$) is in fair agreement with value estimated by Miedema's model, $\Delta H^M = -21 \text{ kJ mol}^{-1}$, published in [19], and it was used as the fixed experimental thermodynamic quantity in this assessment. In the optimisation of the thermodynamic parameters, the values of the energy of formation of the PdBi and PdBi₂ intermetallics were not optimized. These values were used to check the reliability of the thermodynamic parameters resulting from the optimisation of the Bi–Pd system. Calculated values from first principles at 0 K represent a better choice for the temperature independent term than any constant value used in many cases previously. The optimisation of the temperature dependent parameters of the Gibbs energy of these compounds was used for tuning the assessment to the experimental phase equilibrium data.

Liquidus data published in the literature [1–4] are in mutual agreement, so all of these data were used in the assessment. Phase equilibrium data for Pd₅Bi₃ were taken from [3], similarly the data for the peritectic temperature of Pd₃Bi which were verified experimentally in this work. Data for the solubility of Bi in Pd at 200 °C and 215 °C, published in [5], complement the data set. It is evident from Fig. 2 that the phase diagram calculated using the parameters in the Appendix is in very good agreement with the experimentally determined phase equilibrium data.

5. Conclusions

The experimental thermodynamic enthalpies of mixing of liquid Bi and Pd measured by drop calorimetry, and ab initio calculated energies of formation of PdBi and PdBi₂ intermetallics were successfully used as a basis for a thermodynamic assessment of the phase diagram of the Bi–Pd system. New phase equilibrium data were determined by DTA, SEM and XRD methods, and were used together with phase equilibrium data from the literature in this thermodynamic assessment. Calculated thermodynamic parameters are presented that enable reliable calculation of the phase diagram of Bi–Pd system.

Acknowledgements

This research was supported by the Ministry of Education of Czech Republic (Projects Nos. OC 531.001, OC 531.002, AB0Z 20410507 and MSM 0021622410), EPSRC (UK) Platform Grant (GR/R95798) and COST Action 531 (STSM). First-principles electronic structure calculations were performed using the facilities of Metacentrum of Masaryk University Brno and phase equilibria were calculated by employing Thermo-calc software.

Appendix

Values of thermodynamic parameters for the Bi–Pd system (in Joules) for the temperature interval 298–4000 K (Eqs. (2) and (3)):

$${}^o G_{\text{Pd:Va}}^{\text{RHOMBO}} = \text{GHSERPD} + 4000$$

$${}^o L_{\text{Bi,Pd:Va}}^{\text{RHOMBO}} = -32000$$

$${}^o L_{\text{Bi,Pd:Va}}^{\text{FCC}} = -78000 + 1T;$$

$${}^o L_{\text{Bi,Pd}}^{\text{Liq}} = -107000 + 24T;$$

$${}^1 L_{\text{Bi,Pd}}^{\text{Liq}} = 20000;$$

$${}^o G_{\text{Bi:Bi}}^{\text{PdBi}_2} = 0.334 * \text{GHSERPD} + 0.666 * \text{GHSE RBI} - 25100 + 2.5 * T;$$

$${}^o G_{\text{Bi:Bi}}^{\text{PdBi}} = 0.5 * \text{GHSERPD} + 0.5 * \text{GHSE RBI} - 33600 + 7.65 * T;$$

$${}^o G_{\text{Bi:Bi}}^{\text{Pd}_3\text{Bi}} = 0.75 * \text{GHSERPD} + 0.25 * \text{GHSE RBI} - 22300 + 0.4 * T;$$

$${}^o G_{\text{Bi:Va}}^{\text{Pd}_5\text{Bi}_3} = \text{GHSE RBI} + 31000;$$

$${}^o G_{\text{Pd:Va}}^{\text{Pd}_5\text{Bi}_3} = \text{GHSERPD} + 9000;$$

$${}^o L_{\text{Bi,Pd:Va}}^{\text{Pd}_5\text{Bi}_3} = -179000 + 27.3 * T;$$

$${}^1 L_{\text{Bi,Pd:Va}}^{\text{Pd}_5\text{Bi}_3} = 20000.$$

Symbols GHSE RBI and GHSERPD in the expression for Gibbs energy of the intermetallic phases represent the Gibbs energy of the SER state for Bi (RHOMBOHEDRAL A7) and Pd (FCC A1), respectively. They were taken from [20]. *L*-parameters are related to the Redlich–Kister polynomial (Eq. (3)), and *G*-parameters express Gibbs energy of phases (Eq. (2)). Elements occupying the same sublattice are separated by commas; different sublattices are separated by a colon.

References

- [1] N.N. Zhuravlev, G.S. Zhdanov, Zhur. Exper. i Teor. Fiz. 25 (1953) 485.
- [2] N.N. Zhuravlev, Zhur. Exper. i Teor. Fiz. 32 (1957) 1305.
- [3] J. Brasier, W. Hume-Rothery, J. Less-Common Met. 1 (1959) 157.
- [4] D.G. Schweitzer, J.R. Weeks, Trans. ASM 54 (1961) 185.
- [5] P. Oberndorff, Ph.D. Theses, TU Eindhoven, 2001.
- [6] A. Watson, F.H. Hayes, J. Alloys Compounds 220 (1995) 94.
- [7] Y.C. Bhatt, K. Schubert, J. Less-Common Met. 64 (1979) 17.
- [8] N.N. Zhuravlev, Soviet Phys.-JETP, translated from Zhur. Exper. i Teor. Fiz. 5 (1957) 1064.
- [9] P. Blaha, K. Schwarz, J. Luitz, WIEN97, Technical University of Vienna 1997—improved and updated Unix version of the original copyrighted Wien-code, published by P. Blaha, K. Schwarz, P. Sorantin, S.B. Trickey, Comput. Phys. Commun. 59 (1990) 399.
- [10] J.P. Perdew, J.A. Chevary, S.H. Vosko, K.A. Jackson, M.R. Pederson, D.J. Singh, C. Fiolhais, Phys. Rev. B 46 (1992) 6671.
- [11] G. Kresse, J. Furthmüller, Comput. Mater. Sci. 6 (1996) 15.
- [12] G. Kresse, J. Furthmüller, Phys. Rev. B 54 (1996) 11169.
- [13] M.D. Segall, P.L.D. Lindan, M.J. Probert, C.J. Pickard, P.J. Hasnip, S.J. Clark, M.C. Payne, J. Phys.: Condens. Mater. 14 (11) (2002) 2717.
- [14] K. Schubert, S. Bhan, T.K. Biswas, K. Frank, P.K. Panday, Naturwissenschaften 55 (1968) 542.
- [15] O. Redlich, A.T. Kister, Ind. Eng. Chem. (2) (1948) 345.
- [16] N. Saunders, P. Miodownik, CALPHAD-A Comprehensive Guide, Elsevier, London, 1998.
- [17] B. Sundman, Thermo-calc, version L, Royal Institute of Technology, Stockholm, 1997.
- [18] N.N. Zhuravlev, Soviet physics-crystallography, translated from Kristallografiya 3 (1958) 506.
- [19] A.K. Niesen, F.R. de Boer, R. Boom, P.F. de Chatel, W.C.M. Mattend, A.R. Miedema, CALPHAD 7 (1983) 401.
- [20] A.T. Dinsdale, CALPHAD 15 (1991) 317.



First-principles calculations of energetics of sigma phase formation and thermodynamic modelling in the Cr–Fe–W system

K. Chvátalová^{a,*}, J. Vřešťál^a, J. Houserová^b, M. Šob^{a,b}

^a Masaryk University, Faculty of Science, Department of Theoretical and Physical Chemistry, Kotlářská 2, CZ-611 37 Brno, Czech Republic

^b Institute of Physics of Materials, Academy of Sciences of the Czech Republic, Žitkova 22, CZ-616 62 Brno, Czech Republic

Received 30 August 2005; received in revised form 2 February 2006; accepted 2 February 2006

Abstract

Ab initio total energies of the alloy sigma phase in Cr–W and Fe–W systems were calculated by means of the linear muffin-tin orbital method in the atomic sphere approximation. Total energies of the pure constituents in the sigma phase and standard element reference (SER) states were evaluated using the full-potential linear augmented plane wave method. The combination of these results was used for the prediction of the energy of formation of the sigma phase with respect to both sigma phase of pure constituents and SER states at equilibrium structure parameters. We have also provided a novel physical approach to the thermodynamic modelling of the sigma phase and a reliable construction of the phase diagram of the Cr–Fe–W system, using ab initio calculated total energy differences in the calculation of phase diagram (CALPHAD) approach. © 2006 Elsevier B.V. All rights reserved.

Keywords: Thermodynamic modelling; CALPHAD approach; Sigma phase; First-principles calculations; Chromium; Iron; Tungsten

1. Introduction

The sigma phase (space group 136, $P42/mmm$) has a relatively complicated structure. It contains 30 atoms in the repeat cell, which are distributed among five crystallographically inequivalent sublattices (2a, 4f, 8i, 8i' and 8j). The sigma phase is very brittle and stable and its presence causes strong degradation of materials. Therefore, the reliable and accurate prediction of the regions of stability of this structure is desirable.

The full-potential electronic structure calculations can reliably determine the total energy difference between the standard element reference (SER) states and the sigma phase.

This enables us to model thermodynamic functions of the sigma phase not only in systems where it really exists but also even in systems, where it is not stable at all. The purpose of this work is to perform a thermodynamic modelling of the sigma phase in the Fe–W and Cr–W systems (where this structure is not stable at 1 bar at any temperature) and, using the calculation of phase diagram (CALPHAD) approach [1], to construct the phase diagram of the Cr–Fe–W system, which contains the sigma phase regions.

2. Thermodynamic modelling

Phase equilibrium calculations performed by the CALPHAD method [1] are based on finding the minimum of the total Gibbs energy of the system at constant pressure, temperature and composition.

The total molar Gibbs energy (G_{tot}) is equal to the sum of the molar Gibbs energies of all phases (G^f) multiplied by their molar fractions (x^f), i.e.

$$G_{\text{tot}} = \sum_f x^f G^f. \quad (1)$$

The G^f is defined as

$$G^f = \sum_i y_i {}^0G_i^f + G^{\text{id}} + G^{\text{E}} + G^{\text{mag}} + \dots, \quad (2)$$

where y_i is the molar fraction of the component i in phase f , ${}^0G_i^f$ is the molar Gibbs energy of pure constituent in the phase f , the terms G^{id} and G^{E} stand for the molar Gibbs energy of ideal and real mixing of components in the phase f and G^{mag} is the magnetic contribution to the Gibbs energy. The Gibbs energies G^f are used as input values for phase diagram calculations.

To overcome the difficulty caused by extrapolations of thermodynamic functions of the sigma phase from the concentra-

* Corresponding author. Tel.: +420 541 129 316; fax: +420 541 211 214.
E-mail address: chvatalova@email.cz (K. Chvátalová).

tion region of its real existence to regions close to the pure constituents, a three-sublattice model for the sigma phase was proposed by Anderson and Sundman [2]. This empirical model reduces five sigma phase sublattices to three and contains adjustable parameters in the expression for the Gibbs energy, which are determined by fitting to all available experimental data. This procedure was summarised in the guideline for reducing the number of sublattices in modelling of intermetallic phases by the compound energy formalism (CEF) [3]. One of the most significant shortcomings of the CEF is the restriction of the entropy of mixing to that of an ideal random mixture. This assumption is contained also in the paper of Pratt and Jones [4], who used a pair-wise interaction model for the description of the sigma phase. By the restriction to randomness, the short-range order (SRO) is ignored and a part of the contribution of SRO to Gibbs energy is hidden in the “excess term” after the adjustment of parameters to experimental data. A better description of SRO can be achieved by the cluster variation method (CVM) for configurational entropy and by the cluster expansion method (CEM) for the internal energy. The application of these approaches in the CALPHAD treatment is promising, but not commonly used yet [5].

Using the three-sublattice model, the Gibbs energy of the sigma phase is described as an empirical combination of Gibbs energies of some absolutely different structures, i.e. bcc, fcc, etc. In this way, we are not able to express the Gibbs energy of pure constituents in the sigma phase structure and the Gibbs energy of the sigma phase of the corresponding binary system has to be adjusted to phase equilibrium data. The physical background of this procedure is, therefore, questionable. Further, it is known from X-ray studies [6] that the mixing of the constituents takes place in all sublattices, which is not respected by the above mentioned approach.

2.1. Two-sublattice model of sigma phase

Recently, we have extended the application of ab initio calculations of the total energies of complex phases to calculations of phase diagrams [7–12]. Here, the energy differences between the SER and the sigma phase structure of pure constituents were calculated by the full-potential augmented plane wave (FLAPW) method using the WIEN 97 code [13]. This approach enables us to utilize full physical information about the sigma phase (based on X-ray results) for its thermodynamic description. Knowledge of the above mentioned total energy differences from the first-principles calculations allows us to define the Gibbs energy difference between the sigma phase and SER structures (lattice stability) on physically correct energetic basis with only the entropy term adjusted to phase equilibrium data.

Using this idea and the fact that the sigma phase does not behave like a strictly ordered structure (mixing is possible), we have employed a new physical two-sublattice [8] model for its thermodynamic modelling. The molar Gibbs energy of the sigma phase in this model is based on Eq. (2) and is defined as:

$$G^{\text{sigma}} = \sum_i y_i {}^0G_i^{\text{sigma}} - TS^{\text{id}} + G^{\text{E}}, \quad (3)$$

where

$${}^0G_i^{\text{sigma}} = {}^0G_i^{\text{SER}} + \Delta E_i^{\text{sigma-SER}} - T \Delta S_i^{\text{sigma-SER}}, \quad (4)$$

$$S^{\text{id}} = -R \sum_i y_i \ln y_i, \quad (5)$$

$$G^{\text{E}} = \sum_{i \neq j} G_{ij}^{\text{E}} + G_{\text{ter}}, \quad (6)$$

and

$$G_{ij}^{\text{E}} = y_i y_j ({}^0L_{i,j}^{\text{sigma}} + {}^1L_{i,j}^{\text{sigma}} (y_i - y_j) + {}^2L_{i,j}^{\text{sigma}} (y_i - y_j)^2). \quad (7)$$

Here R is the gas constant, T is the temperature and $\Delta E_i^{\text{sigma-SER}}$ denotes the total energy difference between the hypothetical sigma phase and the standard state of a given constituent. Further, S^{id} expresses the entropy of ideal mixing in the sigma phase. The parameters L can be temperature-dependent and ternary correction term G_{ter} is defined by:

$$G_{\text{ter}} = y_i y_j y_k (y_i {}^1L^{\text{sigma}} + y_j {}^2L^{\text{sigma}} + y_k {}^3L^{\text{sigma}}). \quad (8)$$

This procedure gives a physical meaning to parameters from the mathematical expression for the Gibbs energy difference between the sigma phase and SER states of pure constituents. So, the knowledge of $\Delta E_i^{\text{sigma-SER}}$ can substantially simplify the physical modelling of the thermodynamic properties of the sigma phase (and other relevant intermetallic phases) in the CALPHAD method. This idea is further illustrated in this work, where the calculations of the phase equilibrium in the Cr-Fe-W system are performed by means of the THERMO-CALC programme [14].

3. Results and discussion

We performed ab initio calculations of the total energy of Cr, Fe and W in their experimentally observed structure (i.e. bcc) and in the sigma phase structure using the FLAPW method implemented in the WIEN 97 code [13] at the equilibrium lattice parameters, i.e. at the volume corresponding to the minimum total energy. The exchange-correlation term was evaluated within the generalized gradient approximation (GGA) [15]. Subsequently, we evaluated the total energy differences between the sigma phase and SER state at 0 K for all studied elements as follows:

$$\Delta E_{\text{Cr}}^{\text{sigma-SER}} = 30.07 \text{ kJ mol}^{-1} = 22.9 \text{ mRy at}^{-1},$$

from ref. [7],

$$\Delta E_{\text{Fe}}^{\text{sigma-SER}} = 43.33 \text{ kJ mol}^{-1} = 33.0 \text{ mRy at}^{-1},$$

from ref. [7],

$$\Delta E_{\text{W}}^{\text{sigma-SER}} = 144.62 \text{ kJ mol}^{-1} = 110.1 \text{ mRy at}^{-1},$$

this work.

The magnetic ordering of the SER phases (ferromagnetic bcc Fe, antiferromagnetic bcc Cr and nonmagnetic bcc W) was taken into account. The $\Delta E_W^{\text{sigma-SER}}$ difference is very large (in comparison with, e.g. $\Delta E_{\text{Mo}}^{\text{sigma-SER}} = 17.77 \text{ mRy at}^{-1}$ [12]), which may be indication of a very high degree of unstability of the W sigma phase and this issue should be subject of further investigation.

The values of $\Delta^0 S_i^{\text{sigma-SER}}$ were adjusted only to phase equilibrium data, supposing the sigma phase structure to be metastable. In the case of an unstable structure, where entropy is not defined, the value of $\Delta^0 S_i^{\text{sigma-SER}}$ adjusted to experimental phase data could be regarded as an “effective” value. In general, the $\Delta^0 S_i^{\text{sigma-SER}}$ values (Eq. (4)) providing the phase diagram exhibiting the best agreement with experiments are obtained by optimisation of particular binary systems containing the sigma phase and, if necessary, by a re-optimization using the ternary phase equilibrium data. But in our case, the sigma phase is not stable either in Fe–W or in Cr–W system, so the value of $\Delta^0 S_W^{\text{sigma-SER}}$ could not be optimised to experimental binary data and it was set to the same value as for Cr and Fe taken from ref. [7].

Values used for $\Delta^0 S_i^{\text{sigma-SER}}$ (in $\text{J K}^{-1} \text{ mol}^{-1}$) are:

$$\Delta^0 S_{\text{Cr}}^{\text{sigma-SER}} = 0.7, \quad \text{from ref. [7],}$$

$$\Delta^0 S_{\text{Fe}}^{\text{sigma-SER}} = 0.7, \quad \text{from ref. [7],}$$

$$\Delta^0 S_{\text{W}}^{\text{sigma-SER}} = 0.7, \quad \text{this work.}$$

The last quantity needed for the evaluation of the ${}^0 G_i^{\text{sigma}}$ in Eq. (4) is ${}^0 G_i^{\text{SER}}$ term and its values for particular constituents were taken from ref. [16]. The G_{ij}^E was expressed by the Redlich–Kister polynomial, Eq. (7), taking into account the SRO.

Values of G^E in the binary systems Fe–W and Cr–W could be adjusted only to phase equilibrium in ternary Cr–Fe–W system by means of the ternary term defined by Eq. (8). Therefore, we set the starting values of L -parameters in the Fe–W sigma phase to such values that provided $G_{\text{Fe-W}}^{\text{sigma}}$ not too much higher than the values of Gibbs energy of other present phases. Further, we performed optimisation of L -parameters of the sigma phase for Fe–W and Cr–W (including ternary ones) with respect to ternary experimental phase equilibrium data [17].

Resulting values of L -parameters (in J mol^{-1}) are:

$$\begin{aligned} {}^0 L_{\text{Cr:Fe}} &= -133950 & {}^0 L_{\text{Cr:W}} &= 225661 - 335.883T + 0.06114T^2 \\ {}^1 L_{\text{Cr:Fe}} &= 31000 & {}^1 L_{\text{Cr:W}} &= -999061 + 1083.025T - 0.1964T^2 \\ {}^2 L_{\text{Cr:Fe}} &= -127000 & {}^2 L_{\text{Cr:W}} &= 0 \end{aligned}$$

$$\begin{aligned} {}^0 L_{\text{Fe:W}} &= -390770 + 16.146T + 0.0589T^2 & {}^0 L_{\text{Cr:Fe:W}} &= 986778 - 829.86T \\ {}^1 L_{\text{Fe:W}} &= 103470 - 10.135T - 0.012T^2 & {}^1 L_{\text{Cr:Fe:W}} &= 49184.5 - 44.595T \\ {}^2 L_{\text{Fe:W}} &= 63257 + 43.749T - 0.0091T^2 & {}^2 L_{\text{Cr:Fe:W}} &= 197355 - 172.03T, \end{aligned}$$

where $L_{\text{Cr:Fe}}$ were taken from ref. [7].

To be able to describe the unstability of the sigma phase in whole temperature region, the expression for L -parameters of the Cr–W and Fe–W system are quadratic in temperature.

The values of thermodynamic functions of other phases in Cr–Fe–W system were taken from ref. [17]. This paper also presents a lot of reliable experimental phase equilibrium data (obtained by diffusion couple technique and precisely evaluated by SEM–EDX method) describing phase equilibria in the studied system at six temperatures in range between 1173 and 1673 K. These experiments were applied in our thermodynamic modelling which used the two-sublattice model for the sigma phase. The same two-sublattice model was employed also for fcc and bcc phases (including magnetic contribution). For other intermetallic phases the proper models [17] were used.

The phase diagrams of the Cr–Fe–W system at 1173 and 1673 K, calculated using the two-sublattice model, are given in Fig. 1(a and b). They are in reasonable agreement with experimental data taken from ref. [17].

The composition dependencies of the Gibbs energies were calculated for Cr–W and Fe–W systems at 1473 K. They are shown in Fig. 2(a and b). We can see that lines 6 and 7 in Fig. 2(b) obtained using the two- and three-sublattice model [2], respectively, yield different description of metastability of the sigma phase in the Fe–W system, which cannot be resolved experimentally. It is also evident that the two-sublattice model yields the values of Gibbs energy of the sigma phase in the whole composition region, whereas the old three-sublattice model gives this quantity only in a limited range of concentrations.

In addition to our FLAPW results for pure constituents, we have also performed first-principles calculations of total energies of both pure elements and alloy sigma phase by means of the linear muffin-tin orbital method in the atomic sphere approximation (LMTO-ASA), using the code by Krier et al. [18]. In this way, we obtained the concentration dependence of the total energy E^{sigma} in Fe–W and Cr–W system. As the LMTO-ASA method does not provide reliable structural energy differences for structures of different symmetry, we applied the values of $\Delta E_i^{\text{sigma-SER}}$ calculated by means of the FLAPW method to obtain the energy of formation of the sigma phases with respect to SER states in the whole composition range (Fig. 3(a and b)). These results suggest that the sigma phase is unstable in the whole concentration range both in the Cr–W and Fe–W systems. Fig. 3(a and b) also displays the comparison of optimised enthalpy of

156

K. Chvátalová et al. / Materials Science and Engineering A 462 (2007) 153–158

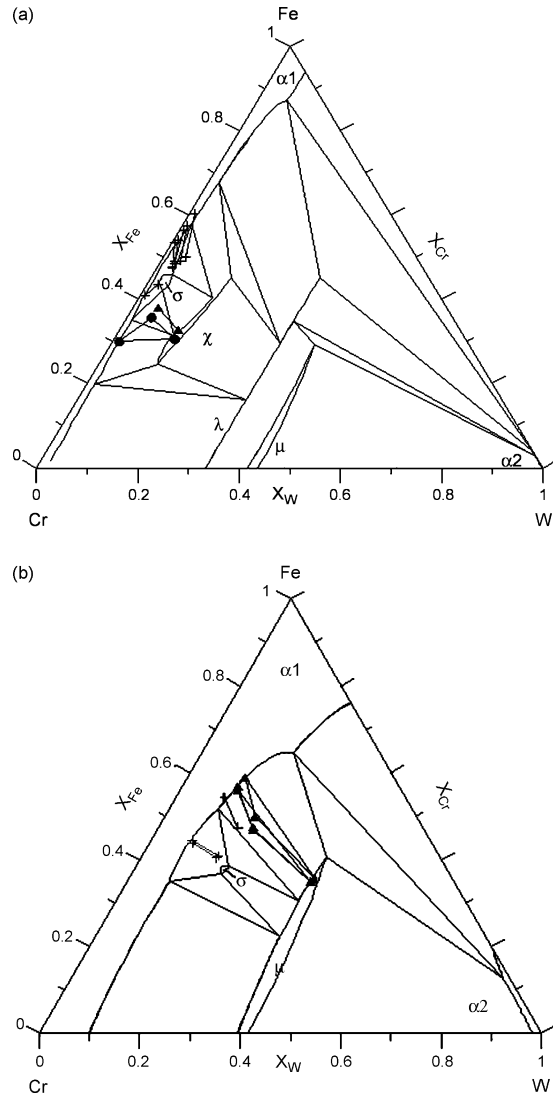


Fig. 1. (a) Calculated phase diagram of Fe–Cr–W system at 1173 K according to the two-sublattice model of sigma phase (full lines), compared with experimental equilibrium data with sigma phase from ref. [17]: crosses for equilibrium sigma/bcc, triangles for bcc/sigma/chi. The greek letters α_x , χ , λ , σ , μ are used to denote the bcc, chi, Laves, sigma and mu phases, respectively. (b) Calculated phase diagram of Fe–Cr–W system at 1673 K according to the two-sublattice model of sigma phase (full lines), compared with experimental equilibrium data with sigma phase from ref. [17]: crosses for equilibrium sigma/bcc, triangles for bcc/sigma/mu. The greek letters α_x , σ and μ are used to denote the bcc, sigma and mu phases, respectively.

formation from thermodynamic modelling and energy of formation from ab initio calculations. Thermodynamic modelling suggests energetic stabilization of sigma phase in Fe–W and partially in Cr–W system. These values are connected with enthalpy, modelled in Gibbs energy as “effective” value and cannot be exactly compared with ab initio calculations valid for 0 K.

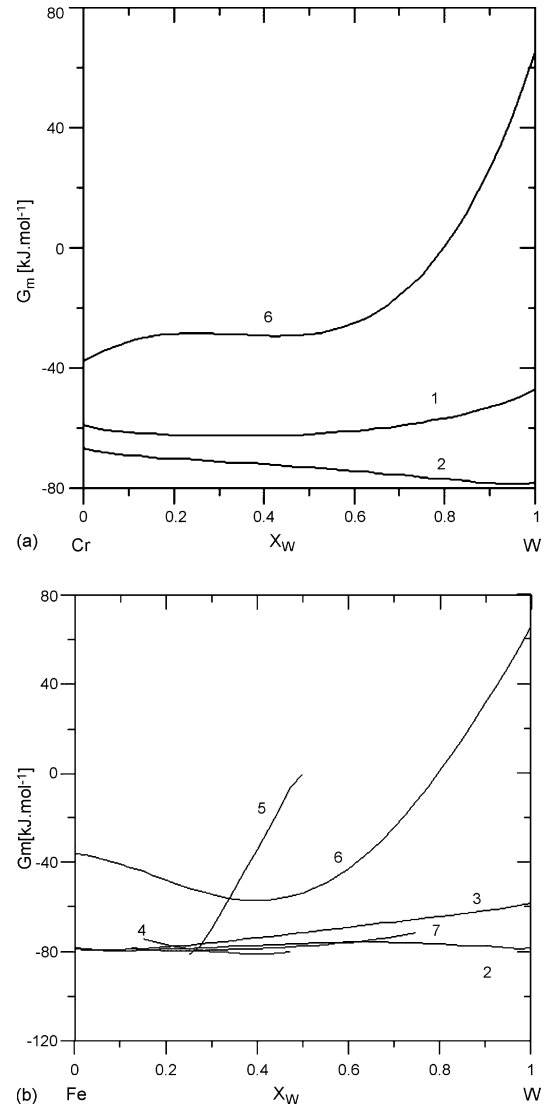


Fig. 2. (a) Concentration dependence of the Gibbs energy for phases in the Cr–W system at 1473 K. The notation of the lines: (1) L, (2) α , (6) σ (two-sublattice model). The letters L, α and σ are used to denote the liquid, bcc and sigma phases, respectively. (b) Concentration dependence of the Gibbs energy for phases in the Fe–W system at 1473 K. The notation of the lines: (2) α , (3) γ , (4) μ , (5) R, (6) σ (two-sublattice model), (7) σ (three-sublattice model) according to ref. [2]. The letters α , γ , μ , R and σ are used to denote the bcc, fcc, mu, R and sigma phases, respectively.

The sigma phase in Fe–Cr system is not stable above about 1100 K. However, as we can see by comparison of Fig. 1 (a and b), the addition of tungsten shifts the stability region of the sigma phase in the Cr–Fe–W system to higher temperature. The large value of $\Delta E_W^{\text{sigma-SER}}$ suggests that the sigma phase structure in pure W is not favourable and unstable. Therefore, thermody-

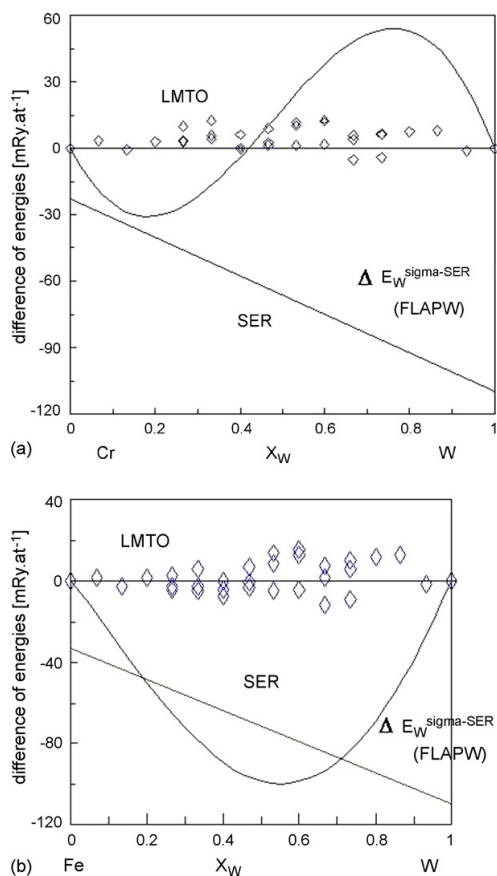


Fig. 3. (a) Comparison of optimized enthalpy of formation (full line, thermodynamic calculations) and the total energies of formation of sigma phase with various occupancies of sublattices (diamonds, ab initio calculations) with respect to energies of sigma phases of both constituents in the Cr–W system. The diamonds represent the total energies of all 32 possible occupations of sublattices calculated at equilibrium volumes. The lower line represents the total energy of linear combination of total energies of SER structures based on equilibrium lattice parameters. (b) Comparison of optimized enthalpy of formation (full line, thermodynamic calculations) and the total energies of formation of sigma phase with various occupancies of sublattices (diamonds, ab initio calculations) with respect to energies of sigma phases of both constituents in the Fe–W system. The diamonds represent the total energies of all 32 possible occupations of sublattices calculated at equilibrium volumes. The lower line represents the total energy of linear combination of total energies of SER structures based on equilibrium lattice parameters.

dynamic modelling with “effective” values of entropy and Gibbs energy of the sigma phase has to be performed. Due to the large value of $\Delta E_W^{\text{sigma-SER}}$ the thermodynamic modelling also cannot reproduce ternary phase diagram by only ternary interaction term without lowering energetic difference $\Delta E^{\text{sigma-SER}}$ in both Fe–W and Cr–W systems in the region of low W concentration (Fig. 3(a and b)). This large negative energetic term is compensated by the large negative entropy term yielding less negative Gibbs energy of the sigma phase (Fig. 2(a and b)).

4. Conclusions

It was found that the two-sublattice model of the sigma phase may be used for a reasonable description of phase equilibrium with this structure in the Fe–Cr–W system, although the sigma phase is not stable in two binary subsystems, i.e. in Fe–W and Cr–W. These good results were obtained in spite of the fact that the calculated value of $\Delta E_W^{\text{sigma-SER}} = 144.62 \text{ kJ mol}^{-1}$ is very large and should deserve further investigation. It may be an indication for a high degree of unstability of the sigma phase in both binary systems Fe–W and Cr–W. From the results presented in our article, it may be concluded that ab initio calculated energy differences between the sigma and SER structures for pure constituents could be successfully employed in the CALPHAD method.

Energy of formation of the sigma phase with respect to SER states obtained by combining the LMTO-ASA and FLAPW calculations is mainly positive and in agreement with supposed metastability of this phase in Fe–W and Cr–W binary systems.

Our first-principles calculations may be considered as the first step to determine the stability of various structures and to assess the formation of unwelcome phases devaluating the properties of materials.

Acknowledgements

This research was supported by the Grant Agency of the Czech Republic (Project Nos. 106/03/P002 and 106/03/1354), by the Grant Agency of the Academy of Science of the Czech Republic (Project No. S2041105) and by Research Projects AVOZ20410507 and MSM0021622410. First-principles electronic structure calculations were performed using the facilities of Metacentrum of Masaryk University Brno and phase equilibria were calculated by THERMO-CALC software.

References

- [1] P. Miodownik, N. Saunders, CALPHAD—A Comprehensive Guide, Elsevier, London, 1998.
- [2] J.O. Anderson, B. Sundman, Calphad 11 (1987) 83.
- [3] M. Hillert, Calphad 22 (1998) 127.
- [4] J.N. Pratt, I.P. Jones, Calphad 8 (1984) 75.
- [5] T. Mohri, Y. Chen, J. Alloys Compd. 23 (2004) 383.
- [6] S.H. Algie, E.O. Hall, Acta Crystallogr. 20 (1966) 142.
- [7] J. Houserová, J. Vřešťál, M. Friák, M. Šob, Comput. Mater. Sci. 25 (2002) 562.
- [8] J. Vřešťál, Arch. Metall. 46 (2001) 239.
- [9] J. Havránková, J. Vřešťál, M. Friák, M. Šob, Phys. Rev. B 63 (2001) 17410.
- [10] J. Houserová, J. Vřešťál, M. Friák, M. Šob, Calphad 26 (2002) 513.
- [11] K. Chvátalová, J. Vřešťál, J. Houserová, M. Šob, J. Alloys Compd. 378 (2004) 71.
- [12] J. Houserová, J. Vřešťál, M. Šob, Calphad 29 (2005) 133.
- [13] P. Blaha, K. Schwarz, J. Luitz, WIEN97, Technical University of Vienna 1997 – Improved and Updated Unix version of the Original Copyrighted Wien – code, published by P. Blaha, K. Schwarz, P. Sorantin, S. B. Trickey, Comput. Phys. Commun. 59 (1990) 399.

- [14] B. Sundman, THERMO-CALC, Version L, Royal Institute of Technology, Stockholm, 1997.
- [15] J.P. Perdew, J.A. Chevary, S.H. Vosko, K.A. Jackson, M.R. Pederson, D.J. Singh, C. Fiolhais, *Phys. Rev. B* 46 (1992) 6671.
- [16] A.T. Dinsdale, *Calphad* 15 (1991) 317.
- [17] P. Gustafson, *Metall. Trans.* 19A (1988) 2531.
- [18] G. Krier, O. Jepsen, A. Burkhardt, O.J. Andersen, Computer Code TB-LMTO-ASA, Version 4.6, Max-Planck-Institute für Festkörperforschung, Stuttgart, 1994.



Contents lists available at ScienceDirect

CALPHAD: Computer Coupling of Phase Diagrams and Thermochemistry

journal homepage: www.elsevier.com/locate/calphad

Stability of Laves phases in the Cr–Zr system

J. Pavlů, J. Vřešťál*, M. Šob

Department of Chemistry, Faculty of Science, Masaryk University, Kotlářská 2, CZ-611 37 Brno, Czech Republic
 Institute of Physics of Materials, Academy of Sciences of the Czech Republic, v.v.i., Žitkova 22, CZ-616 62 Brno, Czech Republic

ARTICLE INFO

Article history:

Received 8 July 2008
 Received in revised form
 18 November 2008
 Accepted 19 November 2008
 Available online 12 December 2008

Keywords:

Ab initio calculations
 Laves phases
 Chromium–zirconium system
 Phase diagram
 CALPHAD

ABSTRACT

The total energies of Laves phases with various occupations of inequivalent lattice sites in all three structural forms C14, C15 and C36 have been calculated *ab initio* by a pseudopotential VASP code with a complete relaxation of all structural parameters. The relative stability of Cr₂Zr polytypes is discussed. The calculated values were used in two-sublattice and three-sublattice models for the re-modeling of Gibbs energies of Laves phases and subsequently for the calculation of phase diagram of the Cr–Zr system by the CALPHAD method. A comparison of phase diagrams obtained by our model using first-principles results with previous treatments using an empirical approach as well as with experimental phase equilibrium data is presented. An application of the structural energy differences (lattice stabilities) calculated *ab initio* provides a similarly good description of the phase diagram of the Cr–Zr system as previous studies, but much fewer adjustable parameters are needed for a thermodynamic description of Laves phases.

© 2008 Elsevier Ltd. All rights reserved.

1. Introduction

Laves phases crystallize in cubic (MgCu₂, C15) or hexagonal (MgZn₂, C14 and MgNi₂, C36) type structures [1] which differ only by a different stacking of the same four-layered structural unit. These structures belong to the class of Frank–Kasper phases exhibiting topologically close-packed structures. Laves phases have become candidates for some functional as well as structural applications, e.g. hydrogen storage materials, such as X₂Zr (X = V, Mn, Ni), and materials with a high strength up to high temperatures [2]. Copper–chromium based alloys are also used for latter reasons [3], but at higher temperatures they suffer from intergranular cavitation. It has been found that the addition of magnesium or zirconium to copper–chromium alloys improves their mechanical properties at higher temperatures without impairing their good electrical and thermal conductivity [3]. It may be supposed that Cr₂Zr precipitates may be responsible for the enhancement of these technologically useful properties, which increases interest in Cr–Zr systems.

A rigorous approach for obtaining thermodynamic description of phases in Cr–Zr system was published in [4,5]. The thermodynamic assessment of data was carried out using the Wagner–Schottky model [4] and sublattice model [5] for Laves phases

including a thorough analysis of phase equilibrium data in the literature [6–12]. Unfortunately, no thermodynamic data were available at that time and are still lacking.

As a guide for thermodynamic assessment in [4,5], the empirical rules [13,14] could only be used.

In this work, we have calculated the differences of total energies between all three Laves phase structures (hexagonal C14, C36, and cubic C15) and Standard Element Reference (SER) structures of the constituents (antiferromagnetic BCC–Cr and nonmagnetic HCP–Zr) by *ab initio* method. These values represent the first available thermodynamic quantities, which encouraged us to re-assess the whole Cr–Zr system.

2. Ab initio calculations of total energies

Our electronic structure calculations were carried out within the Density Functional Theory (DFT). We have used the pseudopotential method [15] incorporated into the Vienna *Ab initio* Simulation Package (VASP) code [16,17] combined with the Projector Augmented Wave–Perdew–Burke–Ernzerhof (PAW–PBE) pseudopotential [18–20]. This method was applied to evaluate the total energies of all three Laves phase structures (C14, C15 and C36) and the SER structures. The cut-off energy restricting the number of plane waves in the basis set was 295 eV and 201 eV for Cr and Zr, respectively.

Spin polarization was included in BCC antiferromagnetic Cr. As to Laves phases, we performed a pilot study for hypothetical Cr₂Zr Laves phase with a C15 structure. It turns out that the

* Corresponding author at: Department of Chemistry, Faculty of Science, Masaryk University, Kotlářská 2, CZ-611 37 Brno, Czech Republic. Tel.: +420 549498134; fax: +420 541211214.

E-mail address: vrestal@chemi.muni.cz (J. Vřešťál).

Table 1

The calculated and experimental lattice parameters of the SER structures. The symbols a and c stand for lattice constants, V is the atomic volume and Δ shows the relative difference between the calculated and experimental atomic volume ($1 \text{ \AA} = 100 \text{ pm}$).

SER						
Structure		a (pm)	c (pm)	c/a	V/atom (10^7 pm^3)	Δ (%)
BCC Cr	Exp. [21]	287.87	287.87	1.0000	1.19281	
Antiferromagnetic	Relax.	285.48	285.48	1.0000	1.16327	-2.48
HCP Zr	Exp. [22]	323.18	514.83	1.5930	2.32835	
Nonmagnetic	Relax.	323.55	516.95	1.5977	2.34330	+0.64

Table 2

Optimized structural parameters of the C14, C15 and C36 Laves phases found in this work. The symbols a and c stand for lattice constants, x , y and z are the internal structural parameters, V is the atomic volume. The occupation of sublattices of various Laves phases in the Cr_2Zr configuration was as follows: C14: Cr(2a, 6h), Zr(4f), C15: Cr(16d), Zr(8a), C36: Cr(4f, 6g, 6h), Zr(4e, 4f). ($1 \text{ \AA} = 100 \text{ pm}$).

Structure	C14			C15			C15	
	a (pm)	c (pm)	V/atom (10^7 pm^3)	4f-z	6h-x	6h-y	a (pm)	V/atom (10^7 pm^3)
Exp. Cr_2Zr [21]	510.2	827.3	1.5542	0.057	0.829	0.658	720.0	1.5552
Calc. Cr_2Zr	508.7	807.4	1.5076	0.060	0.833	0.666	712.4	1.5062
Cr_2Cr	464.1	766.3	1.1912	0.046	0.829	0.658	658.0	1.1873
Cr_6Zr_6	636.3	636.7	1.8601	0.125	0.826	0.651	-	-
CrZr_2	647.9	674.3	2.0426	0.132	0.814	0.628	781.0	1.9847
$\text{Cr}_2\text{Zr}_{10}$	617.8	773.9	2.1319	0.071	0.833	0.667	-	-
Zr_2Zr	575.9	959.8	2.2970	0.060	0.825	0.649	824.9	2.3386
C36								
	a (pm)	c (pm)	V/atom (10^7 pm^3)	4e-z	4f-z	4f-z	6h-x	6h-y
Exp. Cr_2Zr [21]	510.0	1661.1	1.5592	0.094	0.844	0.125	0.167	0.334
Calc. Cr_2Zr	505.6	1633.9	1.5071	0.095	0.844	0.123	0.166	0.332
Cr_2Cr	465.1	1523.1	1.1889	0.100	0.849	0.124	0.162	0.325
Cr_6Zr_6	634.8	1281.4	1.8633	0.062	0.813	0.132	0.157	0.314
CrZr_2	646.5	1363.2	2.0557	0.058	0.809	0.129	0.144	0.288
$\text{Cr}_2\text{Zr}_{10}$	617.8	1544.5	2.1270	0.089	0.838	0.119	0.167	0.333
Zr_2Zr	577.1	1922.4	2.3106	0.096	0.846	0.133	0.155	0.311

spin polarized Cr_2Cr in the C15 structure is more stable than the nonmagnetic one by 31.2 meV/at (3.01 kJ mol^{-1} of atoms) which means that the magnetism of Laves phases should be considered at 0 K. However, at ambient temperatures, Laves phases in the Cr-Zr system are paramagnetic. Therefore, in the present paper, calculations of total energy differences for comparison of their relative stability were performed for nonmagnetic states only.

Preliminary calculations of Cr_2Cr , Cr_2Zr , Zr_2Cr , Zr_2Zr configurations of C14, C36 and C15 Laves phase structures needed for two-sublattice models $(A, B)_2(A, B)_1$ and also Cr_6Zr_6 and $\text{Cr}_2\text{Zr}_{10}$ configurations for C14 and C36 structures needed for three-sublattice model $(A, B)_4(A, B)_6A_2$ were accomplished. Calculations were carried out using the experimentally found lattice parameters for Cr_2Zr configurations published in [21] except for the C14 and C15 Laves phase of pure chromium, which was studied using the parameters of corresponding Cr_2Ta phases [21].

The structural parameters for the SER states of Zr were taken from [21] and of Cr from [22]. First, we performed convergence tests of total energies with respect to the number of k -points. The range of optimum values for the C14 Laves phases extends from a grid of $15 \times 15 \times 11$ points (pure Cr), $21 \times 21 \times 13$ points (Cr_6Zr_6), $21 \times 21 \times 15$ points (pure Zr), $23 \times 23 \times 15$ points ($\text{Cr}_2\text{Zr}_{10}$) and $25 \times 25 \times 19$ points (Cr_2Zr) towards $25 \times 25 \times 17$ points (CrZr_2). A similar interval was obtained for the C15 Laves phases which goes from a grid of $15 \times 15 \times 15$ points (pure Cr), $21 \times 21 \times 21$ points (pure Zr and CrZr_2) towards $23 \times 23 \times 23$ points (Cr_2Zr). A smaller range was obtained for the C36 Laves phases which spreads from a grid of $15 \times 15 \times 13$ points (pure Cr, and CrZr_2) and $17 \times 17 \times 13$ points (pure Zr) towards $19 \times 19 \times 13$ points (Cr_2Zr , Cr_6Zr_6 and $\text{Cr}_2\text{Zr}_{10}$). In the case of SER structures, we used a grid of $13 \times 13 \times 13$ and $21 \times 21 \times 15$ points for antiferromagnetic BCC Cr and nonmagnetic HCP Zr, respectively. Cr atoms with up and down spins were arranged as in B2 (CsCl) structure with a magnetic moment per atom equal to $1.0754 \mu_B$.

After these test calculations, each structure was fully relaxed which yielded the minimum total energy and the structural parameters of the corresponding equilibrium structure. To relax all configurations of Laves phases we have used a conjugate gradient algorithm. We calculated forces and stress tensors and relaxed positions of ions, cell shape and volume. After the relaxation procedure the static calculations were performed by tetrahedron method including Blöchl corrections [23]. The Cr and Zr SER structures were optimized using the quest for minima on the energy/volume or energy/volume and energy/(c/a) curves. The results obtained are summarized in the following text.

The calculated optimum lattice parameters for the SER structures are listed in Table 1, those for the cubic C15 structure and hexagonal C14 and C36 structures in Table 2.

Experimental and calculated structural parameters of Cr_2Zr in C14, C15 and C36 arrangement agree quite well. The calculated equilibrium atomic volume range from $96.7\% V_{\text{exp}}$ for C36 Cr_2Zr , to $96.8\% V_{\text{exp}}$ for C15 Cr_2Zr and $97.0\% V_{\text{exp}}$ for C14 Cr_2Zr ; here V_{exp} is the experimental atomic volume of respective structure of Cr_2Zr . For the sake of thermodynamic modeling, the total energies of the Cr_6Zr_6 and $\text{Cr}_2\text{Zr}_{10}$ occupations for C14 and C36 structure were calculated.

The total energy differences $\Delta^0 E^{L-\text{SER}}$ between the Laves phases of various types and SER states are then given in Table 3, where they are compared with the results of recent calculations [24–26].

It may be seen from Table 3 that the stability of Laves phase configurations of Cr_2Zr decreases in the sequence C15, C36 and C14. This is in agreement with the results of study [26], where the cutoff energy of 400 eV was chosen. The enthalpies of formation in [26] are in reasonable agreement with the results presented here. Recent experimental results of direct reaction calorimetry [27] suggest that one can estimate the standard enthalpy of formation of Cr_2Zr (presumably in the most stable C15 structure) to be about -3 kJ mol^{-1} of atoms. This value is

384

J. Pavlů et al. / CALPHAD: Computer Coupling of Phase Diagrams and Thermochemistry 33 (2009) 382–387

Table 3

Energy differences, $\Delta^0 E^{L-SER}$, between the total energy of Laves phases of various types and the weighted average of total energies of the SER states (BCC antiferromagnetic Cr, HCP nonmagnetic Zr) calculated in this work and compared with the values available in literature [24–26].

Composition		$\Delta^0 E^{L-SER}$ (kJ mol ⁻¹ of atoms)					
		Cr ₂ Cr	Cr ₂ Zr	Cr ₆ Zr ₆	CrZr ₂	Cr ₂ Zr ₁₀	Zr ₂ Zr
C14	This work	28.63	-1.22	44.46	66.73	15.21	20.51
	Refs. [24–26]	27.80 [24]	-3.0 [26]	-	-	-	19.70 [24,25]
C15	This work	27.29	-2.88	-	99.76	-	27.35
	Refs. [24–26]	26.40 [24]	-4.8 [26]	-	-	-	26.50 [24,25]
C36	This work	27.75	-2.14	46.25	71.18	15.04	22.80
	Ref. [26]	-	-4.0 [26]	-	-	-	-

only an estimate because the reaction in calorimeter was not fully complete. The value for standard enthalpy of formation determined in a similar Cr₂Hf system [27], which is about -5 kJ mol⁻¹ of atoms, supports this estimated value. Both of them are in a reasonable agreement with present calculated results (see Table 3).

The values of calculated structural energy differences for all other compositions are positive and about an order of magnitude higher than those of Cr₂Zr. This is a quantitative confirmation of the fact that the Laves phase structures are energetically very disadvantageous configurations for these compositions. Experimental evidence of existence of all three structure types of Laves phases in Cr₂Zr can be found in [11,12].

Ab initio calculated energy differences represent thermodynamic data which were used for the first time for thermodynamic assessment of phase diagram in the Cr–Zr system in this paper.

3. Thermodynamic modeling

A two-sublattice model (A, B)₂(A, B), where A = Cr and B = Zr, fits precisely to the C15 structure. Here two crystallographically different positions exist, namely 8a for Zr atoms and 16d for Cr atoms [28,29]. In the case of hexagonal structures the occupation of positions is different. It can be described within a three-sublattice approach. It turns out that the three-sublattice model (A, B)₄(A, B)₆A₂ corresponds perfectly to the C14 structure [28, 29]: Zr atoms go to the 4f positions and Cr atoms occupy the positions 2a and 6h but they can mix in 4f and in 6h positions. In the C36 configuration, the Zr atoms prefer the positions 4e and 4f and Cr atoms go to positions 4f, 6g, and 6h [21] and, therefore, in the three-sublattice model the 4e and 4f positions for Zr atoms and 6g and 6h positions for Cr atoms have to be merged. According to the crystallographic data [21], there is no mixing of atoms in the sublattices in the binary system studied. However, the mixing of atoms in sublattices in ternary Laves phases has already been investigated [30].

In the two-sublattice model, Gibbs energy of the reference state is:

$$G^{ref} = y_A^1 y_A^2 {}^0G_{A:A} + y_B^1 y_B^2 {}^0G_{B:A} + y_A^1 y_B^2 {}^0G_{A:B} + y_B^1 y_A^2 {}^0G_{B:B} \quad (1)$$

with lattice fractions of components A and B in sublattices 1 and 2 being, y_A^1, y_B^1, y_A^2 and y_B^2 . The Gibbs energies of “end-members” can be temperature dependent:

$${}^0G_{ij} = a_{ij} + b_{ij}T + c_{ij}T \ln(T). \quad (1a)$$

Here a_{ij}, b_{ij} and c_{ij} are constants determined from experiment or from optimization of the thermodynamic parameters.

From Gibbs energies of four “end-members”, only one, the ${}^0G_{A:B}$ can be experimentally determined in the Cr–Zr system (namely, that one for the Cr₂Zr composition).

Furthermore, the quantities ${}^0G_{A:A}$ and ${}^0G_{B:B}$ characterize, formally, the Gibbs energies of pure constituents in the Laves phase structures which may be given some reasonable positive value in CALPHAD modeling. In the present paper, the arbitrariness in

choosing the values of the Gibbs energy of these formal “end-members” is overcome by determining their total energies with the help of *ab initio* calculations. Thermodynamic descriptions of the other phases (liquid, HCP and BCC) were performed with the help of the subregular solution model.

The molar Gibbs energy of the whole system is defined as the sum of molar Gibbs energies of all included phases, G^f , multiplied by their molar fractions, x^f :

$$G^{tot} = \sum_f x^f G^f, \quad \text{where} \quad (2)$$

$$G^f = \sum_i y_i {}^0G_i^f + G^{id} + G^E + G^{mag} + G^{pres}. \quad (3)$$

The molar Gibbs energy of phase G^f contains the sum of molar Gibbs energies of pure constituents i in the phase f multiplied by their lattice fractions ($\sum y_i {}^0G_i^f$), the terms describing ideal (G^{id}) and nonideal (G^E) mixing and, when needed, some special terms such as magnetic (G^{mag}) or pressure (G^{pres}) contributions. For a binary system (A–B), the terms describing the mixing may be evaluated by relatively simple formulas as follows:

$$G^{id} = RT(y_A \ln y_A + y_B \ln y_B), \quad (4)$$

$$G^E = y_A y_B (L^0(T) + L^1(T)(y_A - y_B) + L^2(T)(y_A - y_B)^2 + \dots), \quad (5)$$

where L^0, L^1 and L^2 are the expansion coefficients of the Redlich–Kister polynomial [31] and T is temperature. Temperature dependence of L -parameters is again given by an equation of type (1a).

For the liquid phase, we use a standard model (A, B)₁, for the BCC phase we employ the usual (A, B)₁(Va)₃ model (Va denotes a vacancy), for the HCP phase we apply the (A, B)₁(Va)_{0.5} model and for Laves phases we use the (A, B)₂(A, B)₁ or (A, B)₄(A, B)₆A₂ models. Ideal mixing in two-sublattice model is then described by

$$G^{id} = RT[2(y_A^1 \ln y_A^1 + y_B^1 \ln y_B^1) + (y_A^2 \ln y_A^2 + y_B^2 \ln y_B^2)]. \quad (4a)$$

Here the superscripts are related to sublattices 1 and 2, where A and B atoms are mixed. In the case of two-sublattice model of Laves phase [28,29], the sum of molar Gibbs energies of pure constituents i in the phase f multiplied by their lattice fractions ($\sum y_i {}^0G_i^f$) is substituted by Eq. (1). The Gibbs energies of the “end-members” have to be calculated as mentioned below. The difference in Gibbs energies of the pure constituents in the phase f (L = Laves phase) and in the SER state (antiferromagnetic BCC Cr and nonmagnetic HCP Zr) is given by (for simplicity, the subscript i is omitted)

$$\Delta^0 G^{L-SER} = {}^0G^L - {}^0G^{SER} = \Delta^0 H^{L-SER} - T \Delta^0 S^{L-SER}, \quad (6)$$

where H is enthalpy and S entropy. The difference in enthalpies, $\Delta^0 H^{L-SER}$, is obtained as

$$\Delta^0 H^{L-SER} = \Delta^0 E^{L-SER} + \int \Delta C_p^{L-SER} dT, \quad (7)$$

Table 4
Optimized thermodynamic parameters for equilibrium phases (liquid, HCP and BCC) in the Cr–Zr system.

Phase	Parameter value (Eq. (5)) in J mol ⁻¹ of atoms
BCC	$L^0 = 32000$ $L^1 = 5000$
HCP	$L^0 = 25000$ $L^1 = -6500$
Liquid	$L^0 = -21050 + 12.61 * T$ $L^1 = -8700 + 6.30 * T$ $L^2 = -9000$

and vibrational contribution to the entropy can be expressed by

$$\Delta^0 S^{L-SER} = \int (\Delta C_p^{L-SER} / T) dT, \quad (8)$$

where C_p is the heat capacity at constant pressure.

At the equilibrium volume we may write $\Delta^0 H^{L-SER} = \Delta^0 E^{L-SER}$, i.e. the difference in enthalpies is equal to the total energy difference between the Laves phase and the SER state at $T = 0$ K, which we calculate *ab initio* in the present paper. These values may be successfully employed in the phase diagram calculations, as we show below.

Approximating the ΔC_p^{L-SER} by a simplest polynomial $\Delta C_p^{L-SER} = a + bT$, we obtain by integration in Eqs. (7), (8) and substitution into (6):

$$\Delta^0 G^{L-SER} = \Delta^0 E^{L-SER} + T(a - b - a \ln(T)) + (b/2)T^2. \quad (9)$$

For metallic systems and in not very extended temperature intervals, we may assume $b = 0$ and ignore the temperature dependence of $\ln(T)$. Then the coefficient at temperature T in Table 5 represents some average value of the product $\Delta C_p^{L-SER} \ln(T)$, adjusted to experimental data. It follows from the calculated phase diagrams (Section 4) that this approximation is quite reasonable.

4. Calculation of phase diagrams

The equilibrium phase composition arises as a result of minimization of Gibbs energy in a closed system at constant external conditions (temperature and pressure).

For modeling of the C15 Laves phases we employ the two-sublattice model (A, B)₂(A, B) [28,29]. We describe these

structures as the ordered solid solution phases (see Eq. (1)) with four “end-members”. Their Gibbs energy is modeled with the help of *ab initio* total energy differences, presented in Table 3. The C14 and C36 Laves phases are modeled by three-sublattice model (A, B)₄(A, B)₆A₂ as described above. In both cases, Gibbs energy is then obtained from Eq. (6) where the entropy term, containing also the vibration contribution to the enthalpy, is adjusted to the experimental data. The L -parameters describing the excess Gibbs energy G^E of non-ideal mixing in Eq. (5) are obtained in the same way. The thermodynamic parameters for all other phases (liquid, HCP and BCC) in Cr–Zr system are based on unary data from [32]. For the sake of completeness, they are presented in Table 4.

It may be seen from Table 4 that the enthalpy of mixing in liquid phase at component ratio 1:1 (-21.05 kJ mol⁻¹ of atoms) can be compared with the guess of Miedema [13] (-36 kJ mol⁻¹ of atoms) and also the ratio $\Delta H^M / \Delta S^E$ in liquid phase (1669 K) can be related to Tanaka’s recommendation (1064 K) [14]. Both values differ considerably from the value reported by [4,5], which is nearly an order of magnitude higher. Miedema’s estimate [13] and Tanaka’s recommendation [14] are based on statistical evaluation of corresponding experimental data and their reliability is usually better than $\pm 50\%$.

Numerical presentation of optimized thermodynamic parameters describing the Laves phases C14, C36 and C15 in the Cr–Zr system is given in Table 5. This optimization is, of course, not the standard CALPHAD optimization as the *ab initio* calculated values shown in boldface in Table 5 are kept fixed.

Let us note here that the values in Table 3 and in Table 5 are given in kJ or J per mol of atoms. It may be seen that the number of adjusted parameters is substantially lower (3 parameters for every Laves phase in this work) than in [4,5] (6 parameters for every Laves phase using Wagner–Schottky model and 8 parameters for every Laves phase when using sublattice model). It is evident that C36 and C14 structures are stabilized by entropy with highest entropy contribution for C14 structure.

The calculated parts of the phase diagram of Cr–Zr system are presented in Fig. 1(a)–(c), where they are compared with available experimental data.

Averaging of the literature data [8–11] used in Fig. 1 yields the values of invariant temperatures summarized in Table 6. Here we may see the differences between these invariant temperatures with those calculated by [4,5] and obtained in this work. It may be seen that root-mean-square deviation is slightly lower for our values in comparison with the values found in [4,5].

Table 5

Optimized thermodynamic parameters describing the Laves phases C14, C15 and C36 in Cr–Zr system. *Ab initio* calculated values shown in boldface were kept fixed during the CALPHAD optimization and, were taken from Table 3 (see text). Values of standard Gibbs energies were taken from [32].

Structure	Parameters G (Eq. (1)) and L (Eq. (5)) in J mol ⁻¹ of atoms
C14	$G(\text{Cr:Cr:Cr}) = \mathbf{28633} + \text{GHSERCR}$
	$G(\text{Cr:Zr:Cr}) = \mathbf{-1217.5} - 2.996 * T + 0.6667 * \text{GHSERCR} + 0.3333 * \text{GHSERZR}$
	$G(\text{Zr:Cr:Cr}) = \mathbf{44457} + 0.5 * \text{GHSERZR} + 0.5 * \text{GHSERCR}$
	$G(\text{Zr:Zr:Cr}) = \mathbf{15214} + 0.8333 * \text{GHSERZR} + 0.1667 * \text{GHSERCR}$
	$L(\text{Cr:Cr, Zr:Cr; 0}) = -17417$ $L(\text{Cr, Zr:Zr:Cr; 1}) = -5333$
C15	$G(\text{Cr:Cr}) = \mathbf{27292} + \text{GHSERCR}$
	$G(\text{Cr:Zr}) = \mathbf{-2875.0} - 2.177 * T + 0.6667 * \text{GHSERCR} + 0.3333 * \text{GHSERZR}$
	$G(\text{Zr:Cr}) = \mathbf{99760} + 0.6667 * \text{GHSERZR} + 0.3333 * \text{GHSERCR}$
	$G(\text{Zr:Zr}) = \mathbf{27351} + \text{GHSERZR}$
	$L(\text{Cr:Cr, Zr; 0}) = -14700$ $L(\text{Cr, Zr:Zr; 0}) = -7800$
C36	$G(\text{Cr:Cr:Cr}) = \mathbf{27752} + \text{GHSERCR}$
	$G(\text{Cr:Zr:Cr}) = \mathbf{-2140.7} - 2.528 * T + 0.6667 * \text{GHSERCR} + 0.3333 * \text{GHSERZR}$
	$G(\text{Zr:Cr:Cr}) = \mathbf{46254} + 0.5 * \text{GHSERZR} + 0.5 * \text{GHSERCR}$
	$G(\text{Zr:Zr:Cr}) = \mathbf{15043} + 0.8333 * \text{GHSERZR} + 0.1667 * \text{GHSERCR}$
	$L(\text{Cr:Cr, Zr:Cr; 0}) = -16108$ $L(\text{Cr, Zr:Zr:Cr; 0}) = -4867$

386

J. Pavlů et al. / CALPHAD: Computer Coupling of Phase Diagrams and Thermochemistry 33 (2009) 382–387

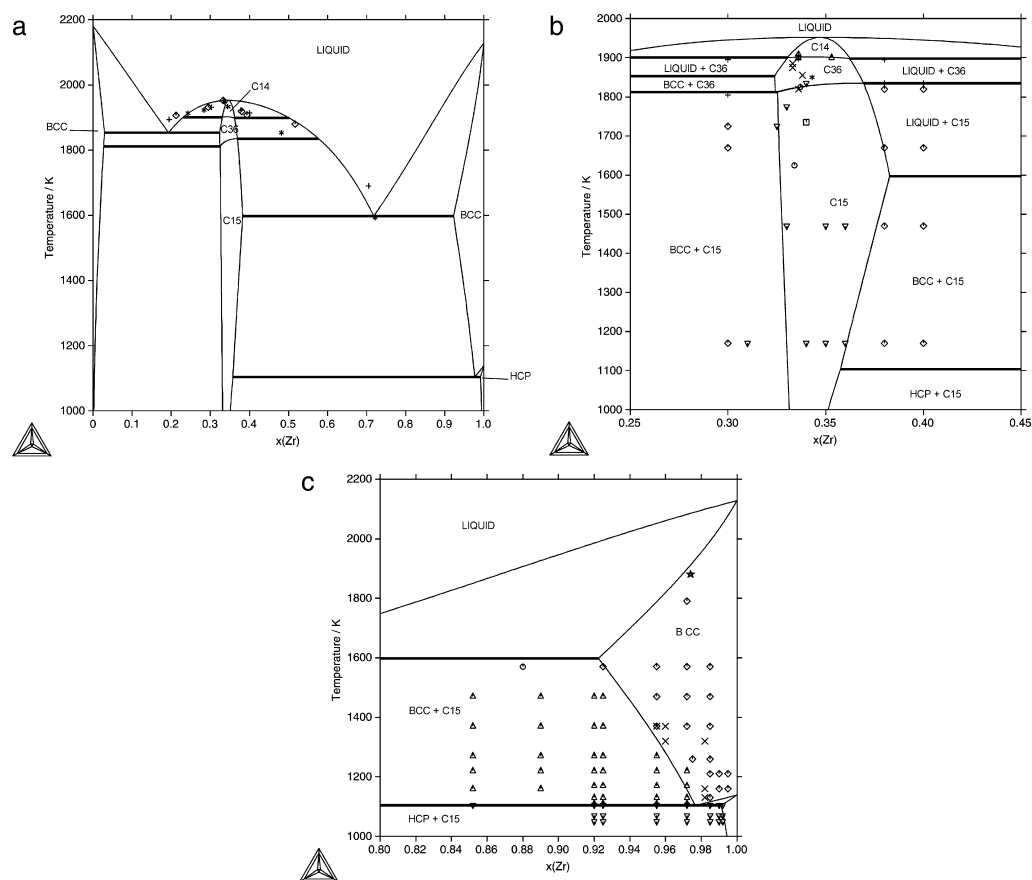


Fig. 1. Comparison of the phase diagram of Cr–Zr system calculated in this work with corresponding experimental data. (a) Phase diagram Cr–Zr. (b) Region of stability of Laves phases. (c) The Zr-rich region. Experimental points from various authors are: (a) Liquidus: ★ [8], ◇ [10], + [11]; (b) 3 phases: + [11], 2 phases: ◇ [11], C15: ○ [10], ▽ [11], □ [12], C36: × [11], ★ [12], C14: △ [10]; (c) Solidus: ★ [6], (BCC-Zr + C15): △ [6], ○ [7] (HCP-Zr + C15): ▽ [6] BCC-Zr: ◇ [6], × [9].

Table 6

Invariant temperatures and compositions based on literature data: [8–11] (temperatures), [9,11] (compositions), calculated in [4,5], and calculated in this work. (Index m means congruent melting, E eutectic, P peritectic and e eutectoid reactions.) The quantities x_{Zr} give the concentration of Zr in the phases denoted in the 2nd–4th columns.

Type	Phases			Experiment [8–11]				Calculated in [4,5]				Calculated-this work			
	(1)	(2)	(3)	T	$x_{Zr}(1)$	$x_{Zr}(2)$	$x_{Zr}(3)$	T	$x_{Zr}(1)$	$x_{Zr}(2)$	$x_{Zr}(3)$	T	$x_{Zr}(1)$	$x_{Zr}(2)$	$x_{Zr}(3)$
m	Liquid	C14	–	1948	0.336	0.336	–	1950	0.332	0.332	–	1952	0.346	0.346	–
P	Liquid	C36	C14	1895	0.45	0.35	0.35	1898	0.450	0.348	0.349	1898	0.502	0.362	0.363
P	Liquid	C36	C14	1895	0.20	0.32	0.32	1897	0.225	0.316	0.313	1901	0.231	0.331	0.330
E	Liquid	BCC	C36	1859	0.193	–	0.33	1864	0.172	0.011	0.310	1853	0.193	0.029	0.324
P	Liquid	C36	C15	1835	0.55	0.36	0.36	1833	0.570	0.355	0.355	1834	0.577	0.369	0.369
e	BCC	C36	C15	1805	–	0.32	0.32	1818	0.010	0.310	0.311	1812	0.027	0.324	0.325
E	Liquid	BCC	C15	1606	0.78	–	0.36	1605	0.763	0.916	0.378	1597	0.718	0.922	0.383
e	BCC	HCP	C15	1105	0.984	0.986	0.34	1110	0.982	0.995	0.360	1104	0.977	0.991	0.358

It is evident that our approach provides a very good description of the Cr–Zr Laves phase stability range. Our calculated phase equilibria agree also very well with the experimental phase equilibrium data of the Cr–Zr system.

From Fig. 1 it is also evident that the approach employing the total energy differences calculated *ab initio* in both the two-sublattice and three-sublattice model of Laves phases describes the phase diagrams (experimental points) in Cr–Zr system very well. The number of parameters needed for a satisfactory description of Laves phases in phase diagrams is substantially smaller in the case of employing the *ab initio* calculated parameters than in previous works of [4,5]. It seems that physically based energy

part of the Gibbs energy surface of Laves phases (i.e. that one obtained from *ab initio* calculations) does not require such a strong entropy correction. On the other hand, as it can be seen from Table 6, the optimized semiempirical parameters used in [4, 5] also provide a very good description of experimental phase data. Therefore, the standard CALPHAD optimization procedure can reproduce phase diagram satisfactorily even when some parameters describing Gibbs energy do not have any physical background. However, introducing physically based parameters is advantageous as it makes the optimization process predictable, simple, more effective and more reliable. In spite of the progress in modeling using *ab initio* values of energies of formation, any

experimental thermodynamic quantity, describing mixing in Cr–Zr system, is highly desirable.

5. Conclusions

It was shown that *ab initio* calculated structural energy differences fit well the two-sublattice model of C15 and three-sublattice model of C14 and C36 Laves phases. Moreover, we need a substantially smaller number of adjustable parameters necessary for thermodynamic description of Laves phases (Table 5) than in previous attempts in literature. Also, our results fulfil empirical rules for the liquid phase [13,14] much better than in previous assessments [4,5]. Present *ab initio* analysis of relative stability of Laves phase structures confirms the sequence of decreasing stability C15–C36–C14, and it can be fully utilized in the thermodynamic modeling of those phases.

Acknowledgements

This research was supported by the Grant Agency of the Czech Republic (Project no. 106/07/1078), Ministry of Education of Czech Republic (Project nos. OC164 and MSM0021622410) and Academy of Sciences of the Czech Republic (Project no. AV0Z20410507). The access to the computing facilities of the MetaCenter of the Masaryk University, Brno, provided under the Research Project MSM6383917201, is acknowledged. Phase equilibria were calculated by means of Thermocalc and MTDATA codes.

References

- [1] I. Ansara, T.G. Chart, A.F. Guillermet, F.H. Hayes, U.R. Kattner, D.G. Pettifor, N. Saunders, K. Zeng, CALPHAD 21 (1997) 171.
- [2] F. Stein, M. Palm, G. Sauthof, Intermetallics 12 (2004) 713.
- [3] M. Kanno, Z. Metallkd. 10 (1988) 687.
- [4] K. Zeng, M. Härmäläinen, R. Luoma, Z. Metallkd. 84 (1993) 23.
- [5] K. Zeng, M. Härmäläinen, K. Lilius, CALPHAD 17 (1993) 101.
- [6] R.F. Domagala, D.J. McPherson, M. Hansen, Trans. AIME 197 (1953) 279.
- [7] E. Gebhart, J. Rexer, G. Petzow, Z. Metallkd. 58 (1967) 534.
- [8] P.B. Budberg, S.P. Alisova, R.S. Musaev, Izv. Akad. Nauk SSSR Met. 3 (1968) 222.
- [9] W.M. Rumball, F.G. Elder, J. Less-Common Met. 19 (1969) 345.
- [10] V.N. Svechnikov, A. C. Spektor, Izv. AN SSSR, 4 (1971) 201.
- [11] V.V. Petkov, S.B. Prima, L.A. Tretyachenkov, Yu.A. Kocherzhinskij, Metallofiz. 46 (1973) 80.
- [12] V.V. Nemoshkalenko, A.P. Nesenyuk, V.P. Krivitskii, V.V. Petkov, L.I. Nikolaev, A.V. Polenur, B.P. Memko, A.P. Shpak, M.A. Mindlina, R.K. Ostafichuk, Metallofiz. 52 (1974) 54.
- [13] F.R. de Boer, R. Boom, A.R. Miedema, Physica 113B (1982) 18.
- [14] T. Tanaka, N.A. Gokcen, Z. Morita, Z. Metallkd. 81 (1990) 49.
- [15] D. Singh, Planewaves, Pseudopotentials and the LAPW Method, Kluwer, Boston, 1994.
- [16] G. Kresse, J. Furthmüller, Comput. Mater. Sci. 6 (1996).
- [17] G. Kresse, J. Furthmüller, Phys. Rev. B 54 (1996) 11169.
- [18] P.E. Blöchl, Phys. Rev. B 50 (1994) 17953.
- [19] G. Kresse, J. Joubert, Phys. Rev. B 59 (1999) 1758.
- [20] J.P. Perdew, K. Burke, M. Ernzerhof, Phys. Rev. Lett. 77 (1996) 3865.
- [21] P. Villars, L.D. Calvert, Pearson's Handbook of Crystallographic Data for Intermetallic Phases, ASM International, Materials Park, OH, USA, 1991.
- [22] E.G. Moroni, T. Jarlborg, Phys. Rev. B 47 (1993) 3255.
- [23] P.E. Blöchl, O. Jepsen, O.K. Andersen, Phys. Rev. B 49 (1994) 16223.
- [24] M.H.F. Sluiter, CALPHAD 30 (2006) 357.
- [25] Y. Wang, S. Curtarolo, C. Jiang, R. Arroyave, T. Wang, G. Ceder, L.-Q. Chen, Z.-K. Liu, CALPHAD 28 (2004) 79.
- [26] X.-Q. Chen, W. Wolf, R. Podloucky, P. Rogl, Phys. Rev. B 71 (2005) 174101.
- [27] S. Meschel, Private communication, 2008.
- [28] N. Saunders, A.P. Miodownik, CALPHAD – A Comprehensive Guide, Elsevier, Oxford, UK, 1998.
- [29] M. Hillert, L.-I. Steffansson, Acta Chem. Scand. 24 (1970) 3618.
- [30] X.-L. Yan, X.-Q. Chen, A. Grytsiv, P. Rogl, R. Podloucky, H. Schmidt, G. Giester, X.-Y. Ding, Intermetallics 16 (2008) 651.
- [31] O. Redlich, A.T. Kister, Indust. Eng. Chem. 40 (1948) 345.
- [32] A.T. Dinsdale, CALPHAD 15 (1991) 317.



Ab initio study of formation energy and magnetism of sigma phase in Cr–Fe and Cr–Co systems

J. Pavlů^{a,b,*}, J. Vřešťál^a, M. Šob^{a,b}

^a Department of Chemistry, Faculty of Science, Masaryk University, Kotlářská 2, CZ-611 37 Brno, Czech Republic

^b Institute of Physics of Materials, Academy of Sciences of the Czech Republic, Žitkova 22, CZ-616 62 Brno, Czech Republic

ARTICLE INFO

Article history:

Received 8 April 2009

Received in revised form

30 June 2009

Accepted 24 July 2009

Available online 15 August 2009

Pacs:

61.66.Dk

71.20.Be

82.60.Lf

Keywords:

A. Intermetallics

B. Magnetic properties

E. Ab initio calculations

ABSTRACT

First-principles electronic structure calculations of total energy differences between the sigma phase and Reference States (RS) of pure constituents in Cr–Fe and Cr–Co systems performed by various methods are presented and compared with enthalpies of formation measured by calorimetry. Both measurements and calculations provide positive values of enthalpy of formation with respect to the RS. Negative values can be obtained when the pure constituents in the sigma phase structure are taken as the RS. Total energy differences of all sigma phase configurations involved are calculated at equilibrium volumes, reproducing well the experimental energy of formation of the sigma phase. The magnetic configurations in Cr–Fe and Cr–Co are also investigated and the stabilizing effect of magnetic ordering in sigma phase at 0 K is demonstrated. It turns out that the magnetic moment depends on the type of the occupied sublattice and total composition of alloy.

© 2009 Elsevier Ltd. All rights reserved.

1. Introduction

In 1923, Bain [1] observed a new nonmagnetic (NM) phase in Cr–Fe system. It was named the sigma phase and, at present, about 50 binary transition-metal systems exhibiting this phase are known [2], e.g. Fe–Mo, Co–Mo, or Fe–V. Twenty years after the sigma phase detection Cook and Jones [3] described its crystallographic structure using X-rays. It has the space group No. 136 ($P4_2/mnm$) and its repeat cell contains thirty atoms accommodated in five crystallographically inequivalent sublattices (2a, 4f, 8i, 8i' and 8j) [4–6].

The sigma phase is very crucial in material science and technology because its properties are very disadvantageous. It is brittle and therefore it can cause a strong degradation of material (crack nucleation sites). In practice, it develops in heat affected zones of welded superaustenitic stainless steels [7] and it was concluded that it is formed after longer ageing times in the temperature range of 500–1100 °C. It is also known that high concentrations of Cr and Mo promote precipitation of this phase.

From the thermodynamic point of view, the sigma phase is very stable and its stability may be theoretically assessed using the Gibbs energy difference between the sigma phase and Reference States (RS). In our work, structures of pure constituents which are stable at Standard Ambient Temperature and Pressure (SATP) were taken as RS, i.e. ferromagnetic (FM) hcp Co, antiferromagnetic (AFM) bcc Cr and ferromagnetic bcc Fe. The Gibbs energy of formation of sigma phase (ΔG^f) is then given by

$$\Delta G^f = G^\sigma - G^{RS} = (H^\sigma - H^{RS}) - (S^\sigma - S^{RS})T,$$

where T is the thermodynamic temperature, S is the entropy, H is the enthalpy and the superscripts σ and RS associated with G , H and S refer to the sigma phase and the RS state, respectively.

Unfortunately, it is not possible to measure the values of Gibbs energies of formation of sigma phase directly. The only possibility to characterise the process of formation is the measurement of enthalpy of formation (ΔH^f) by calorimetry. If we want to compare the measured results with the ab initio values (calculated at temperature of 0 K), we may take advantage of the fact that, in metallic systems, the enthalpy of formation changes with temperature only very little because the temperature dependencies of the heat capacity of alloy sigma phase and RS structures are similar.

* Corresponding author. Department of Chemistry, Faculty of Science, Masaryk University, Kotlářská 2, CZ-611 37 Brno, Czech Republic.

E-mail addresses: houserova@ipm.cz (J. Pavlů), vrestal@chemi.muni.cz (J. Vřešťál), mojmir@ipm.cz (M. Šob).

Under such assumption we can extend the region of validity of the equation $\Delta H^f = \Delta E^f$, where ΔE^f is the ab initio calculated energy of formation of sigma phase, from $T = 0$ K to higher temperatures. Subsequently the value of ΔE^f can also be used to evaluate ΔG^f at finite temperatures. Here the entropy term, ΔS^f , is usually adjusted to the phase equilibrium data during the phase diagram calculations. Alternatively, the difference in vibrational entropy may be calculated with the help of the Debye approximation using phonon spectra and the difference in configurational entropy may be obtained by cluster variation method.

Let us note that vast majority of all measured values of enthalpy of formation reported by various authors [8–11] in Cr–Fe and Cr–Co systems as well as the calculated values [12,13] is positive. Therefore, from this point of view we could expect that the sigma phase is unstable with respect to the RS.

On the other hand, the obvious high stability of sigma phase is well known from experiments. Consequently, we can suppose that the configurational and vibrational entropies are responsible for this stability at higher temperatures.

In our previous paper [12], the calculations of energies of formation of sigma phase were performed at experimental lattice volumes of sigma phases, which is the first approximation only. The aim of this paper is to carry out these calculations on the physically more appropriate equilibrium volume basis. Furthermore, as Co, Cr and Fe in RS reveal high magnetic moments and the magnetism of the sigma phase in the Cr–Fe system at low temperatures was reported by both experimentalists [14,15] and theoreticians [16–19], we also analyse the stability of magnetic configurations. It transpires that magnetic ordering can influence the structure and stability of the sigma phase but, in agreement with Ref. [15], its importance depends on the composition of the alloy.

The paper is organized as follows: After introduction, Section 2 gives the details of our calculations. Section 3 contains the discussion of the results, and Section 4 summarizes our conclusions.

2. Calculations of total energies

To explain the experimentally determined heat of formation of the sigma phase, we have to know which combinations of occupancies of sublattices in the sigma phase structure are the most stable ones at a given concentration and, therefore, which total energies should be compared with the calorimetric data. For this purpose, we performed the first-principles electronic structure calculations of total energies for all possible 32 configurations occurring in the sigma phase structure of the systems studied. However, these configurations must be approached as some limiting situations as the experimental findings in literature suggest that there is no exclusive occupancy of any sublattice in sigma phases studied [20,21].

Total energies of Cr–Fe and Cr–Co compounds as well as of pure constituents in sigma phase structure were computed by means of the Linearised Muffin-Tin Orbital method in the Atomic Sphere Approximation (LMTO-ASA) [22] using the code by Krier et al. [23]. The exchange-correlation energy was evaluated within the Generalised Gradient Approximation (GGA) [24]. We have used the *s-p-d* basis with the *f* states incorporated by the down-folding procedure and with the combined-correction term included [22,23]. This is apparently the best performance the LMTO-ASA method may provide.

As the Cr–Fe and Cr–Co sigma phases existing at ambient conditions are not spin-polarised, the calculations for pure constituents were also performed for a non-spin-polarised state unless stated otherwise.

As it was mentioned above, the sigma phase contains five crystallographically inequivalent sublattices. The positions of most atoms within the unit cell are generally given in terms of three independent internal structure parameters *x*, *y*, *z* and generally, it would require an enormous amount of calculations to find the values of these parameters corresponding to the absolute minimum of total energy. Therefore, we have tried to find their most likely values in a different way.

For this purpose, in the case of the sigma phase of pure constituents we have picked up the lattice parameters *a* and *c* from such a binary sigma phase that involves elements with similar atomic radii as the element chosen (i.e. for Cr and Fe from the Cr–Fe sigma phase [4] and for Co from the Cr–Co sigma phase [5]). Then the total energies of sigma phases of the pure constituents were analysed with respect to the various sets of independent internal structure parameters of binary sigma phases that contained the studied element (e.g. sets of Cr–Fe, Fe–Mo etc. in the case of Fe). For subsequent calculations we have selected that set of independent internal structure parameters which exhibited the lowest total energy. The lowest energies for pure Co, Cr and Fe sigma phases were obtained using the internal structure parameters of Co–Mo [6], Co–Cr [5] and Cr–Fe [4] sigma phases, respectively (Table 1, columns 3–5).

By extensive testing we have verified that slight changes in the atomic positions in the repeat cell of the sigma phase (within the limits found in literature) do not have a very large effect on the total energy (the maximum change in energy was $\Delta E = 2$ mRy/atom and, in average, we obtained $\Delta E = 0.5$ mRy/atom). Therefore, we kept the above mentioned values of internal structure parameters *x*, *y* and *z* constant during our calculations unless stated otherwise.

After the determination of internal structure parameters, we optimised the lattice constants *a* and *c*. This was performed by alternating minimisation of total energy as a function of lattice parameter *a* at a constant *c/a* ratio and minimisation of total energy as a function of the *c/a* ratio at the constant parameter *a*_{min} from the previous optimisation. These two steps were repeated until the change of total energy was small enough (lower than 0.1 mRy/atom). In this way, the total energies of the hypothetical sigma phases of pure constituents at equilibrium volume and their lattice parameters (Table 2, columns 2–3) were obtained.

Using the alloy internal parameters given in Table 1 and LMTO equilibrium lattice constants as starting values, we performed similar structure optimisation employing the Full-Potential Linear Augmented Plane Wave (FLAPW) method [25] incorporated in the WIEN97 code [26] within the generalized gradient approximation

Table 1

Experimental (columns 3–5) and by VASP calculated (columns 6–8) equilibrium values of internal structure parameters of NM sigma phases.

Subl.	Param.	Cr–Fe ^a	Cr–Co ^b	Co–Mo ^c	Co	Cr	Fe
		Ref. [4]	Ref. [5]	Ref. [6]	this work – VASP		
4f	<i>x</i>	0.3986	0.3984	0.3973	0.4019	0.3982	0.4030
8i	<i>x</i>	0.4635	0.4627	0.4635	0.4613	0.4671	0.4572
	<i>y</i>	0.1312	0.1291	0.1283	0.1332	0.1285	0.1315
8i'	<i>x</i>	0.7399	0.7404	0.7450	0.7346	0.7434	0.7366
	<i>y</i>	0.0661	0.0654	0.0670	0.0669	0.0594	0.0660
8j	<i>x</i>	0.1827	0.1826	0.1820	0.1812	0.1877	0.1821
	<i>z</i>	0.2520	0.2500	0.2500	0.2507	0.2553	0.2503

The symbols x_{Cr} and x_{Co} below represent the molar fraction of Cr and Co, respectively. The exact atomic positions can be calculated from the parameters summarized in Table 2 using simple relations corresponding to the given sublattice and particular space group.

^a $x_{Cr} = 0.495$, $T = 923$ K.

^b $x_{Cr} = 0.564$.

^c $x_{Co} = 0.4$, $T = 1673$ K.

Table 2

Equilibrium lattice parameters and atomic volumes of NM sigma phase of pure constituents calculated by LMTO, WIEN97 and VASP codes. The parameters obtained by the WIEN97 code were subsequently used in the WIEN2k calculations.

Element	LMTO			WIEN97			VASP		
	a (au)	c/a	V_{at} (au ³)	a (au)	c/a	V_{at} (au ³)	a (au)	c/a	V_{at} (au ³)
Co	16.1116	0.5161	71.9496	15.8602	0.5197	69.1126	15.9252	0.5289	71.2044
Cr	16.6677	0.5216	80.5088	16.3792	0.5237	76.7078	16.5267	0.5214	78.4528
Fe	16.0465	0.5180	71.3427	15.5987	0.5174	65.4592	15.9325	0.5210	70.2374

(GGA) [24] for the exchange–correlation term. Optimisations of the Radius Muffin-Tin (RMT) parameters and number of k-points were done at the beginning of FLAPW calculations. The obtained values of RMT parameters used in all further FLAPW calculations are 1.97 au for Co, 2.10 au for Cr and 1.96 au for Fe. The convergence tests have shown that 600 k-points for Co and Fe and 400 k-points for Cr in the whole Brillouin zone are sufficient to obtain reliable total energies of sigma phases.

The only difference in the FLAPW optimisation compared to the LMTO one was that instead of the lattice parameter a the volume of unit cell was optimised or kept constant during this procedure. It was found that three optimisation steps were sufficient to reach the minimum of total energy and the lattice parameters corresponding to this minimum are listed in Table 2, columns 5–6.

To confirm the reliability of our process of relaxation, we also applied the pseudopotential method [25] incorporated in the Vienna Ab initio Simulation Package (VASP) code [27,28] combined with the Projector Augmented Wave–Perdew–Burke–Ernzerhof (PAW–PBE) pseudopotential [29–31]. The cut-off energy restricting the number of plane waves in the basis set was 21.7 Ry, 25.6 Ry and 25.6 Ry for Cr, Co and Fe, respectively. The convergence tests of total energies with respect to the number of k-points show that the range of optimum values for the sigma phase extends from a grid of $9 \times 9 \times 9$ points (Co and binary sigma phases) towards $9 \times 9 \times 11$ points (Fe) and $11 \times 11 \times 9$ points (Cr). After these test calculations, each structure of pure constituents was fully relaxed which yielded the minimum total energy and the corresponding equilibrium structural parameters (Table 1, columns 6–8, Table 2, columns 8–9).

The equilibrium data given in Table 1 reveal only very small scatter and the fully relaxed parameters describing the positions of atoms correspond well to those determined experimentally for alloy sigma phases. From the comparison of results shown in Table 2, we can see that the LMTO method provides the highest values of the lattice parameter a and atomic volume V_{at} , the intermediate values are found by the VASP code and finally the lowest numbers are obtained from the WIEN97 calculations. We can also conclude that the scatter of the results is reasonably small, in units of percent. From this point of view we can say that our procedure of relaxation used in LMTO and WIEN97 calculations (subsequent optimisation via separate parabolas) provides very good results in comparison with the full VASP relaxation.

Now, we can look for the minimum energies of all possible 32 configurations of alloy sigma phase. The alloy lattice constants a and c as well as the internal structure parameters x , y and z of various compositions were calculated according to the Vegard's law (linear change with composition). In the case of LMTO calculations, the c/a ratios of all 32 configurations were additionally optimised at the constant volume. In this way the total energies of alloy sigma phases were obtained and on the basis of these results, the energies of formation of sigma phase with respect to the weighted average of total energies of sigma phase of pure constituents were evaluated (Fig. 1).

Due to enormous time consumption, we performed the WIEN97 calculations only in the case of Cr–Fe system and for comparison

the VASP calculations of Cr–Fe and Cr–Co were carried out. In the FLAPW and VASP case the effect of magnetism was also considered, as it may be seen from Fig. 2. These magnetic calculations were performed to confirm the stabilising influence of the magnetism in the sigma phase at low temperatures and to study the magnetic moments of constituents in various sublattices. Further discussion is presented in Section 3.

To be able to compare our results with experimental data, the energies of formation must be determined with respect to the RS states of the pure constituents. However, the LMTO–ASA method does not provide reliable structural energy differences for structures of different symmetry, although the total energy differences calculated by this method for the same crystallographic structure are considered to be quite reliable [12,32,33]. Thus, we employed the FLAPW and pseudopotential method to establish the bridge between the LMTO energies of formation of sigma phase related to the weighted average of energies of sigma phases of pure constituents on one hand and the RS structures on the other hand.

The WIEN97 calculations of total energies of the pure constituents in the RS structures were accomplished using two atoms in the unit cell in the case of both bcc and hcp structure. The starting lattice parameters of these structures were found in literature [2]. In these calculations, the RMT parameters identical with those used for sigma phase were employed. The convergence tests have shown that 5000 k-points for hcp Co and 3500 k-points for bcc Fe and Cr in the whole Brillouin zone were sufficient to get reliable results. Then the lattice parameters corresponding to the minimum of total energy were found. In the case of hcp structure, the procedure of optimisation was the same as in the case of sigma phase; for the bcc structure, the minimum of total energy as a function of the single lattice parameter a was found. The lattice parameters corresponding to the minimum of total energy are listed in Table 3 together with the experimental values [2,34].

The calculations of total energies of the RS performed by the pseudopotential VASP code [27,28] were similar to the WIEN97 ones. The optimum numbers of k-points extend from a grid of $9 \times 9 \times 9$ points (Co,Fe) towards $13 \times 13 \times 13$ points (Cr). The calculated lattice parameters are also given in Table 3. We can see there that both VASP and WIEN97 calculations slightly underestimate the structural parameters in comparison with experiment except for the WIEN97 results of bcc Fe. The WIEN97 results are closer to the experiment and the scatter of deviations of calculated V_{at} goes from +0.80% V_{at}^{exp} for bcc Fe (WIEN97) to –2.48% V_{at}^{exp} for bcc Cr (VASP), which are small deviations, largely acceptable for present-day electronic structure calculations. If we compare the results obtained for RS and the sigma phase (Tables 2 and 3), we can conclude that the atomic volume increases in the sequence Fe sigma phase, Co sigma phase, hcp Co, Cr sigma phase, Fe bcc and bcc Cr, which is reproduced by both WIEN97 and VASP.

Let us note here that the WIEN97 results concerning the energetics of both sigma and RS phases were recalculated by the latest version of the FLAPW code (i.e. WIEN2k code [35]) using the same structural parameters, RMT and number of k-points as obtained in the WIEN97 calculations.

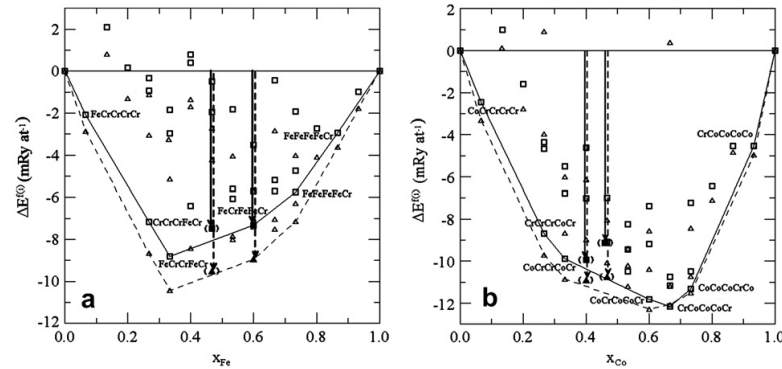


Fig. 1. Energies of formation of the nonmagnetic sigma phase with various occupancies of sublattices calculated by the LMTO-ASA method: (a) Cr–Fe, (b) Cr–Co. Hypothetical sigma phase structures of pure constituents are taken as reference states. The full (dashed) line and squares (triangles) correspond to the results from this work (from Ref. [12]). Arrows mark the energies of formation of the most stable configurations with respect to the sigma phases of pure constituents close to the border of the experimental region of existence of this structure. The occupation of the sublattices at the open squares is given in the order 2a, 4f, 8i, 8j', and 8j. For further discussion see Section 3.

Now the energy of formation of sigma phase at the compositions similar to the experimental ones with respect to the weighted average of the total energies of RS of pure constituents may be calculated. The corresponding formula is

$$\begin{aligned} \Delta E^f &= \{E^\sigma - [xE^{\sigma_1} + (1-x)E^{\sigma_2}]\}_{\text{LMTO}} + \{xE^{\sigma_1} + (1-x)E^{\sigma_2} \\ &\quad - [xE^{\text{RS}_1} + (1-x)E^{\text{RS}_2}]\}_{\text{FLAPW or VASP}} \\ &= \Delta E^{f(i)} + \Delta E^{f(ii)}. \end{aligned}$$

The subscripts 1 and 2 following the name of structure denote different pure constituents.

We can see that the ΔE^f consists of two parts: (i) the energy difference of alloy sigma phase with respect to weighted average of total energies of pure constituents in the sigma phase structure, both calculated by means of the LMTO, FLAPW (WIEN97) and pseudopotential (VASP) method (the LMTO method may be used here as the systems considered have the same type of structure), and (ii) the energy difference of weighted average of total energies of pure constituents in the sigma phase and RS (Table 4), both calculated by means of the FLAPW (WIEN2k) or pseudopotential (VASP) method (here a more reliable, but also more time consuming method had to be used as the structures involved have

different types of symmetry). Both energy differences (i) and (ii) may be considered as quite reliable, as the total energies used for their determination were obtained by the same method on equal footing.

If we apply the same method (FLAPW or VASP) for all calculations, the subscripts concerning the method used may be omitted and the formula is simplified to

$$\Delta E^f = E^\sigma - [xE^{\text{RS}_1} + (1-x)E^{\text{RS}_2}].$$

The results of these calculations are illustrated in Fig. 3 and the corresponding values of total energies are listed in Tables 4 and 5.

From Table 5, we can see that all methods provide slightly different values of the energy of formation of the sigma phase with respect to RS of pure constituents. The differences between our results might be caused by different level of relaxation included. Let us note that all values of total energies used in this paper correspond to the equilibrium lattice volumes. The choice of the equilibrium volumes for the reference states eliminates the uncertainties connected with the use of experimental volumes of binary sigma phases for total energy calculation of hypothetical (i.e. unstable) sigma phase structure of pure constituents as it was used in Ref. [12].

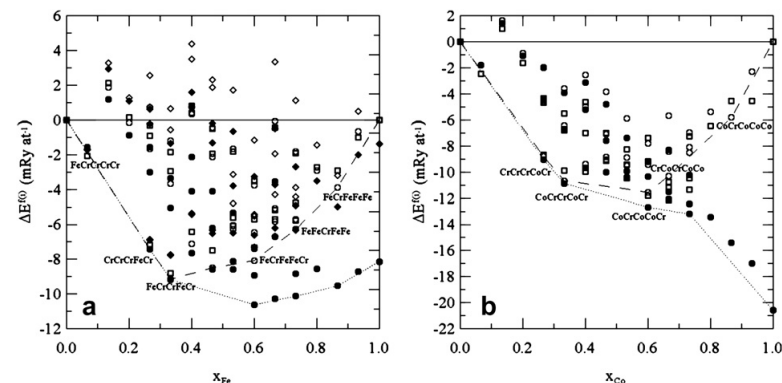


Fig. 2. Energies of formation of the sigma phase with various occupancies of sublattices calculated by the LMTO-ASA, WIEN97 and VASP codes: (a) Cr–Fe, (b) Cr–Co. Hypothetical sigma phase structures of pure constituents are taken as reference states. The squares correspond to the nonmagnetic LMTO results from this work. Open (full) diamonds show nonmagnetic (magnetic) results obtained by the WIEN97 code. The dashed (dotted) line and open (full) circles show nonmagnetic (magnetic) results obtained using the VASP code. The occupation of the sublattices at the open circles on the dashed line is given in the order 2a, 4f, 8i, 8j', and 8j.

Table 3

WIEN97 and VASP equilibrium lattice parameters of RS structures, compared with experiment. The WIEN97 parameters were also used in the WIEN2k calculations.

Element	WIEN97			VASP			Experiment			
	a(au)	c/a	V _{at} (au ³)	a(au)	c/a	V _{at} (au ³)	a(au)	c/a	V _{at} (au ³)	
Co (FM hcp)	4.7211	1.6194	73.7878	4.7084	1.6190	73.1758	4.7357	1.6237	74.6702	Ref.[2]
Cr (AFM bcc)	5.4165	1	79.4559	5.3947	1	78.5004	5.44	1	80.4946	Ref.[34]
Fe (FM bcc)	5.4144	1	79.3635	5.3589	1	76.9479	5.40	1	78.7320	Ref.[34]

3. Results and discussion

Fig. 1(a) and (b) display the LMTO total energies of formation of the sigma phases at various compositions. The open squares represent the total energies of all 32 possible occupations of sublattices in sigma phase structure calculated at equilibrium volumes. Let us note that for each studied Cr concentration belonging to the interval (0.267;0.733) we encounter three different configurations according to the occupation of sublattices 8i, 8i' and 8j. This corresponds to three different energies at each of these concentrations in Figs. 1–3 and in Table 6. These three configurations occurring at the same composition are called triplets in our article. The full squares in Fig. 1(a) and 1(b) correspond to the boundaries that approximately show the region of experimentally determined existence of sigma phase. The solid U-shaped line connects the points with the lowest energies and therefore the energy of formation may be related to this line. The descriptions of occupation of sublattices of the most stable configurations (lying on the line) are also given. The triangles represent the results of calculations based on experimental lattice parameters [12] and the dashed U-shaped line has the same meaning for calculations based on experimental parameters as the full one for the equilibrium results. The points in parentheses correspond to the states which are unstable with respect to line connecting the energies of the most stable configurations. The solid arrows show the energies of formation of sigma phase related to the weighted average of total energy of pure sigma phases calculated at equilibrium volume and the dashed ones correspond to the experimental lattice parameters [12].

The values of total energy of formation of alloy sigma phase calculated at equilibrium volume are somewhat smaller for both Cr–Fe and Cr–Co system in comparison with the results obtained at experimental volume and constant internal structure parameters [12]. The decrease in energy at the positions designated by full squares caused by LMTO relaxation is about 1.5–2 mRy/atom in the Cr–Fe system and 1 mRy/atom in the case of Cr–Co system. This effect could be expected because the calculations using the same experimental volume of an alloy sigma phase of certain composition in the whole interval of concentrations provide correct results only for the experimental compositions (no significant decrease in total energy) but they yield higher (non-equilibrium) values of total

energy for pure element phases and configurations close to them. Their energies fall down during the relaxation and cause a decrease of the total energy of formation related to the sigma phase of pure constituents.

From these figures and on the basis of our LMTO calculations, we can say that some atoms prefer to occupy certain sublattices, i.e. Fe and Co (in binary systems with Cr) prefer the sublattice 8i' and Cr the sublattices 8i and 8j. The same findings concerning the site preferences in Cr–Fe were reported by Korzhavyi [36] and were confirmed by experimental results [20]. This explains why for compositions $x_{Cr} > 0.5$ only one configuration in the triplet is favoured and the remaining two have higher and similar energies (the 8i' sublattice can be occupied by Fe or Co only once). On the other hand, in case of $x_{Cr} < 0.5$ two configurations are more stabilised and one of them exhibits a higher energy (the 8i' sublattice can be occupied by Fe or Co in two cases). These tendencies may be clearly seen from Table 6, where we present the total energies calculated by the VASP code.

Fig. 2(a) and (b) summarise all results of sigma phase calculations obtained in this study. It is obvious that all methods employed, i.e. LMTO-ASA, FLAPW (WIEN97, WIEN2k) and pseudopotentials (VASP) independently exhibit the same trends. In the case of nonmagnetic configurations (open symbols) the shapes of the U-curves are quite similar. This reveals that in Cr–Fe system the sigma phase of the highest stability lies close to the composition $x_{Fe} = 0.333$ (in the NM case) or at $x_{Fe} = 0.6$ (in the FM case). On the other hand, in the Cr–Co system the sigma phase of the highest stability lies close to the composition $x_{Co} = 0.6$ (in the NM case). For FM configurations at $x_{Co} \geq 0.667$ the trend of the U-curve is significantly changed, indicating a strong stabilisation of sigma phase by magnetic ordering. All methods employed also usually predict the same relative stability of configurations at the same composition. In general we can say that accommodation of Fe or Co atoms to sublattices 2a and 8i' has also a stabilising effect.

Furthermore the influence of the magnetic order is obvious here. The non-polarised states (WIEN97 and VASP) have higher energies than the polarised ones. Therefore, according to our WIEN97 and VASP calculations, the sigma phase in the Cr–Fe and Cr–Co system should be spin-polarised in most cases at zero temperature. Stabilisation effects of magnetic ordering were not found in the following configurations: CrCrCrCrCr (elemental Cr in the sigma phase structure), FeCrCrCrCr, CrCrCrFeCr and CrCrCoCrCr by VASP and CrCrCrCrCr with CrFeCrFeCr by WIEN97. However these configurations either contain too much Cr or their energies of NM and FM state are too close.

The magnetic order in sigma phases has already been found by experiments in Cr–Fe system [14,15]. Our stabilisation energies induced by magnetisation of the most stable configurations at given composition in Cr–Fe system are -2.36 kJ/mol at $x_{Cr} = 0.4$ in FeCrCrFeFe and -0.26 kJ/mol at $x_{Cr} = 0.533$ in FeFeCrFeCr (WIEN97) and -3.33 kJ/mol at $x_{Cr} = 0.4$ in CrFeFeFeCr and -0.11 kJ/mol at $x_{Cr} = 0.533$ in FeFeCrFeCr (VASP).

These values are in rough agreement with -6.36 kJ/mol published by A.L. Udovskii for the FeCrFeFeCr configuration ($x_{Cr} = 0.40$) [17]. However, the effect of magnetic ordering in some unstable configurations is even higher, e.g. for the FeFeFeCr configuration

Table 4

Energies of formation of NM sigma phases of pure constituents with respect to RS states.

Element	RS	$\Delta E^{\sigma-RS} = \Delta E^{(i)} (kJ/mol)$					
		WIEN2k ^a	WIEN2k ^b	VASP	Ref. [12]	Ref. [37]	Ref. [16]
Co	hcp	40.567	37.457	34.265	34.4	6.07 ^c	–
Cr	bcc	15.513	14.096	13.394	15.4	13.20	13.3
Fe	bcc	32.617	26.512	25.777	30.9	17.60	38.2

^a In WIEN2k calculations, the equilibrium lattice parameters obtained by WIEN97 were used.

^b In WIEN2k calculations, the equilibrium lattice parameters obtained by VASP code were used.

^c This value was obtained using the energy difference $E_{fcc}^{FM} - E_{hcp}^{FM} = 1.97$ kJ/mol [39], as the value of energy of formation of NM sigma phase in Co obtained in Ref. [37] was related to FM fcc Co.

Table 5
Energies of formation of sigma phase with respect to RS states, comparison with experiments.

System	x_{Cr}	ΔE^f (kJ/mol)					
		NM LMTO		VASP		Ref. [12]	Exp.
		+ WIEN2k	+ VASP	NM	FM		
Cr–Fe	0.400	16.16	11.21	10.23	6.89	20.28	7.7 ^a
	0.533	13.66	9.34	8.01	7.90	16.78	6.5 ^b
Cr–Co	0.533	15.22	11.15	11.50	9.98	17.56	9.37 ^c
	0.600	12.47	8.68	9.40	9.04	15.32	(–2.9; 5.1) ^d (2.64; 6.77) ^e

^a $x_{Cr} = 0.45$, Ref. [8].^b $x_{Cr} = 0.45$, Ref. [11].^c $x_{Cr} = 0.6$, Ref. [9].^d $x_{Cr} = 0.45–0.63$, Ref. [11].^e $x_{Cr} = 0.57–0.61$, Ref. [10].

at $x_{Cr} = 0.533$ the magnetic stabilisation energy amounts to -5.38 kJ/mol (VASP).

Similar stabilising effects were found in the Cr–Co system, where the configuration CoCoCrCoCr at $x_{Cr} = 0.533$ is stabilised by -1.52 kJ/mol and CrCoCrCoCr at $x_{Cr} = 0.6$ by -0.36 kJ/mol (VASP).

From analysis of total energies it follows that magnetism does not influence the order of configurations in triplets at given composition very much. However, it does change the shape of the U-curve. The region of the most stable configurations is shifted towards higher concentrations of iron or cobalt. The stability in the chromium rich part is not influenced by the magnetic effects.

The above mentioned stabilisation by magnetic effect is enhanced with increasing number of Fe (Co) atoms in the system and it can even reach values of -10.67 kJ/mol (VASP) for pure Fe sigma phase and -27.03 kJ/mol (VASP) for pure Co sigma phase. This may indicate that only the iron or cobalt atoms carry the magnetization. In both systems it was found that the stabilisation effect in triplets increases with average magnetic moment but the most stable configurations are not those with the highest average magnetic moment. On the contrary, they are usually the least stable ones (see Table 6).

Very significant results obtained by the ab initio analysis of magnetism in the studied systems deal with distribution of the magnetic moments in dependence on the kind and positions of atoms (Table 6). It turns out, for example, that elemental iron in the sigma phase structure exhibits quite different magnetic moments at different sublattices. At the 4f, 8i and 8j sublattices, the local magnetic moment of Fe atoms equals to $2.29 \mu_B/\text{atom}$, $2.00 \mu_B/\text{atom}$ and $1.87 \mu_B/\text{atom}$, respectively, the highest magnetic moment being at the sublattice 4f with the highest coordination number. Magnetic moments of iron in 8i' and 2a sublattices with the lowest coordination numbers are substantially lower: $1.22 \mu_B/\text{atom}$ and $1.10 \mu_B/\text{atom}$ (see the first line of Table 6).

In case of elemental Co, the magnetic moment decreases from $1.70 \mu_B/\text{atom}$, $1.67 \mu_B/\text{atom}$, $1.59 \mu_B/\text{atom}$ to $1.54 \mu_B/\text{atom}$, which corresponds to the sublattices 4f, (8i, 8j), 8i' and 2a, respectively. Again, the atomic magnetic moment decreases with decreasing coordination number. On the other hand, the sigma phase of elemental Cr is nonmagnetic because the magnetic moments found

Table 6

Magnetic moments per atom (VASP) at particular sublattices with corresponding energies of formation of the FM configuration ($\Delta E^{(i)}$) related to the energies of elemental NM sigma phases ($E^{\sigma_{1,NM}}$, $E^{\sigma_{2,NM}}$) as reference states. The numbers in parentheses give the coordination number of atom in the corresponding sublattice. Bold-face numbers mark the sublattices occupied by Cr. $\bar{\mu}$ denotes average magnetic moment per atom.

x_{Cr}	Cr–Fe							Cr–Co						
	Magnetic moment (μ_B/atom)					$\bar{\mu}$	$\Delta E^{(i)}$ (kJ/mol)	Magnetic moment (μ_B/atom)					$\bar{\mu}$	$\Delta E^{(i)}$ (kJ/mol)
	2a (12)	4f (15)	8i (14)	8i' (12)	8j (14)			2a (12)	4f (15)	8i (14)	8i' (12)	8j (14)		
0	1.10	2.29	2.00	1.22	1.87	1.75	-8.130	1.54	1.70	1.67	1.59	1.67	1.64	-20.587
0.067	-1.29	2.14	2.11	1.34	1.84	1.63	-8.721	-1.21	1.49	1.69	1.38	1.54	1.34	-16.993
0.133	0.47	-0.92	1.98	1.27	1.76	1.26	-9.527	1.11	-0.55	1.47	1.46	1.60	1.20	-15.378
0.2	-0.69	-0.68	1.99	1.14	1.72	1.17	-8.560	0.01	-0.33	1.52	1.27	1.49	1.09	-13.456
0.267	1.49	2.05	-0.83	0.82	1.78	0.85	-10.132	1.55	1.32	-0.10	0.95	1.36	0.86	-12.424
	0.94	2.04	1.75	-1.10	1.78	1.00	-8.847	0.57	1.44	0.86	-0.44	1.14	0.64	-10.224
	1.03	2.05	1.68	1.06	-0.61	0.92	-10.113	1.10	1.53	1.47	1.17	-0.28	0.90	-13.203
0.333	-0.84	1.93	-0.64	0.83	1.76	0.73	-10.277	-0.70	1.12	0.00	0.56	1.21	0.58	-11.497
	0.08	1.79	1.78	-0.88	1.75	0.96	-6.714	0.08	1.18	0.88	-0.22	1.11	0.63	-8.308
	-0.29	1.22	1.50	0.99	-0.16	0.76	-12.074							
0.4	0.88	0.30	-0.28	0.53	1.66	0.62	-8.930	1.20	0.41	-0.35	0.47	1.12	0.46	-10.340
	-0.19	-0.37	1.56	-0.74	1.66	0.61	-7.385	0.36	0.61	0.63	-0.16	1.17	0.54	-9.203
	0.87	-0.44	1.70	1.01	-0.37	0.63	-10.612	-0.06	-0.58	1.18	0.75	0.06	0.45	-12.674
0.467	-0.45	0.41	-0.30	0.51	1.63	0.52	-8.570	0.01	0.29	-0.30	-0.01	0.96	0.21	-9.940
	0.25	-0.10	1.65	-0.65	1.68	0.73	-5.312	0.10	0.43	0.71	-0.18	1.16	0.52	-7.398
	0.06	-0.22	1.69	0.94	-0.33	0.59	-8.105	0.43	-0.13	1.26	0.86	0.06	0.59	-10.405
0.533	0.56	2.06	1.52	-0.33	-0.13	0.60	-6.217	0.21	1.14	0.15	-0.01	-0.11	0.17	-7.592
	0.35	1.24	-0.16	-0.03	-0.07	0.12	-8.586	0.99	1.03	0.35	0.60	0.01	0.46	-10.018
	1.01	1.81	-0.13	-0.29	1.60	0.63	-4.114	0.67	1.14	-0.03	0.02	0.86	0.42	-4.799
0.6	0.03	1.95	1.52	-0.24	-0.10	0.58	-4.102	0.09	0.99	0.12	0.08	-0.02	0.18	-5.193
	-0.08	1.56	-0.20	0.25	-0.05	0.21	-7.645	-0.40	0.50	0.36	0.37	0.02	0.24	-9.678
	-0.25	1.64	-0.15	-0.11	1.56	0.55	-2.129	0.09	0.88	-0.01	0.04	0.85	0.36	-3.129
0.667	0.27	0.21	1.50	-0.39	-0.01	0.35	-5.049	0.45	0.59	0.20	0.05	-0.04	0.17	-6.722
	0.62	0.04	-0.03	0.17	-0.06	0.07	-9.173	0.04	-0.29	0.37	0.40	-0.02	0.17	-10.873
	0.07	0.27	-0.04	-0.19	1.53	0.39	-3.350	0.33	0.37	-0.04	0.01	0.93	0.31	-3.904
0.733	0.04	-0.06	1.44	-0.31	-0.05	0.28	-3.014	-0.03	0.22	0.24	-0.05	-0.02	0.08	-4.476
	0.01	0.00	0.00	-0.04	0.00	-0.01	-7.434	0.06	0.18	0.27	0.40	-0.01	0.21	-9.052
	-0.12	0.33	-0.08	-0.10	1.51	0.40	-1.566	-0.04	0.10	-0.06	0.02	0.60	0.16	-1.980
0.8	0.60	1.80	-0.11	0.16	-0.01	0.29	-0.872	0.45	1.04	0.00	0.08	0.01	0.19	-1.093
0.867	0.08	1.73	-0.11	0.18	0.05	0.27	1.200	0.22	0.83	0.01	0.08	0.00	0.15	1.413
0.933	0.00	0.00	0.00	0.00	0.00	0.00	-1.561	0.18	0.16	-0.03	0.10	0.03	0.06	-1.808
1	0.00	0.00	0.00	0.00	0.00	0.00	0.000	0.00	0.00	0.00	0.00	0.00	0.00	0.000

are very close to zero. However, it does not mean at all that the chromium atoms are nonmagnetic through the whole composition region. Their magnetic moment calculated by VASP reaches even $-1.21 \mu_B/\text{atom}$ ($-1.29 \mu_B/\text{atom}$) in CrCoCoCoCo (CrFeFeFeFe) – see the second line of Table 6. In binary sigma phases we can see that the atomic magnetic moments of all three constituents (i.e. Fe, Co, Cr) mostly decrease with increasing molar fraction of chromium. Similarly as in elemental Fe and Co, the highest values of magnetic moments are found at the 4f sublattice with the highest coordination number.

In Cr–Fe system, the Cr atoms exhibit very often antiferromagnetic behaviour with respect to Fe atoms, i.e., they have the opposite orientation of magnetic moments. This fact is fully manifested at 8i, 8i' and 8j sublattices with some exceptions for higher chromium concentrations. The antiparallel arrangement of magnetic moments is also found at the 2a and 4f sublattices, again with some exceptions. In sporadic cases the antiferromagnetic arrangement occurs at Fe atoms in the sublattice 2a for FeCrFeCrFe configuration and in 8i' for FeFeCrFeCr and CrCrCrFeCr.

In Cr–Co system Cr atoms also exhibit antiferromagnetic behaviour with respect to Co atoms. However, with increasing molar fraction of Cr atoms, we observe increasing amount of Cr atoms that behave in the ferromagnetic way with respect to Co atoms. In contrast to the Cr–Fe system the occurrence of this arrangement is not fully connected with particular sublattices, but it is most frequent at the 2a and 4f sublattices.

The WIEN97 (VASP) calculated average magnetic moment per atom of the most stable configurations in Cr–Fe extends from $0.26 \mu_B$ to $0.10 \mu_B$ ($0.63 \mu_B$ to $0.12 \mu_B$) for $x_{Cr} = 0.400$ – 0.533 . The corresponding values of the WIEN97 (VASP) calculated average magnetic moment per Fe atom of the most stable configurations in Cr–Fe extends from $0.65 \mu_B$ to $0.21 \mu_B$ ($1.30 \mu_B$ – $0.39 \mu_B$) for $x_{Cr} = 0.400$ – 0.533 , which is comparable with experiments. For example, Cieslak et al. [14] reported the average magnetic moment per Fe atom in the range of $0.287(3) \mu_B$ – $0.142(1) \mu_B$ for the composition range $x_{Cr} = 0.450$ – 0.496 , where the average Curie temperature T_C ranges from 38.9 K to 8.3 K. The magnetism of the sigma phase at low temperatures was also confirmed by Read et al. [38]. Furthermore Korzhavyi [36] claims that magnetic moments are vanishing on Fe atoms occupying icosahedral sites (sublattices 2a, 8i') and they are high, cca $2 \mu_B$, on Fe atoms occupying the sites with a high coordination numbers (sublattices 4f, 8i, 8j). Similar trends were confirmed

by our calculations. The magnetic moment of the Fe in icosahedral sites is significantly lower but not vanishing.

The VASP calculated average magnetic moment per atom for the most stable configurations in Cr–Co extends from $0.46 \mu_B$ to $0.24 \mu_B$ for $x_{Cr} = 0.533$ – 0.600 (see Table 6).

Fig. 3(a) and (b) demonstrate our approach to the calculations of the total energies of formation of sigma phase related to the total energies of RS structures. The triangles and squares have the same meaning as in Fig. 1(a) and (b) whereas the lower lines represent the linear combination of total energies of RS structures based on equilibrium lattice parameters (full line – WIEN2k results based on WIEN97 structure data, long-dashed line – VASP) or on the results calculated for the experimental lattice parameters [12] (dashed line). The zero of total energy is constituted by the weighted average of total energies of sigma phases of pure constituents similarly as in Fig. 1(a) and (b). The solid arrows show the energies of formation of sigma phase calculated at equilibrium lattice parameters and the dashed ones correspond to the experimental lattice parameters [12]. The lattice parameters corresponding to the minimum of total energies of RS are listed in Table 3.

Fig. 3(a) and (b) demonstrate that the total energy differences for the pure constituents ($\Delta E^{(ii)} = E^{\sigma-RS}$, Table 4) calculated by various methods are close. The results obtained are even quite close to the differences based on the experimental volumes. Let us note that for elemental Cr, our values of energy of formation agree very well with the previous calculations [12,16,37]. In case of Fe our calculated numbers are between the values calculated in Ref. [37] and Ref. [16]. Co sigma phase was not treated in Ref. [16] and the value from Ref. [37] is related to another reference state. Trying to get this value on equal footing, we arrived to 6.07 kJ/mol which is surprisingly low in comparison with other available values.

The equilibrium energies of formation of the sigma phase related to the weighted average of total energy of pure RS structures in the range of composition that corresponds to the experimental one (arrows in Fig. 3(a) and (b)) are summarised in Table 5 and in Fig. 4(a) and (b) together with the results of calculations performed at the experimental volumes [12] and the experimental values measured calorimetrically by various authors [8–11].

We can see that the energies of formation obtained by various methods reveal some scatter. Concerning the nonmagnetic arrangement, the values of the energies of formation of the sigma phase in the Cr–Fe system at both compositions decrease in series

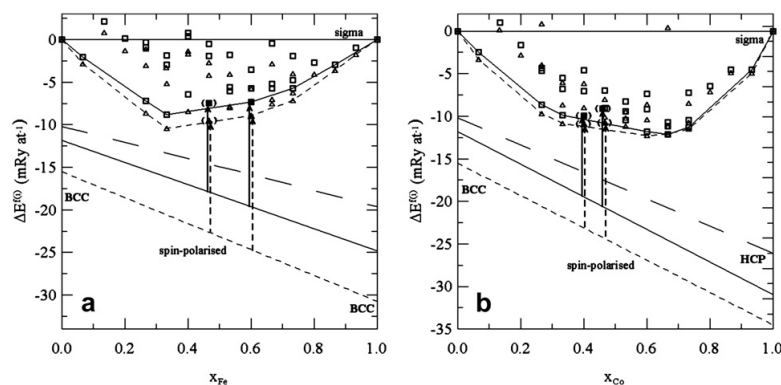


Fig. 3. Total energies of formation of sigma phase with respect to RS states: (a) Cr–Fe, (b) Cr–Co. The full (dashed) line and squares (triangles) correspond to the LMTO + WIEN2k (LMTO + WIEN97) results from this work (from Ref. [12]), based on the WIEN97 equilibrium (experimental) structure data. Long-dashed line shows the energy differences between the RS and the sigma phase of pure constituents calculated by the VASP code. The arrows mark the energies of formation of the most stable configurations with respect to the RS of pure constituents close to the border of the experimental region of existence of the sigma phase. Similar arrows for the VASP calculations can be also constructed but they were omitted for better clarity of the figure.

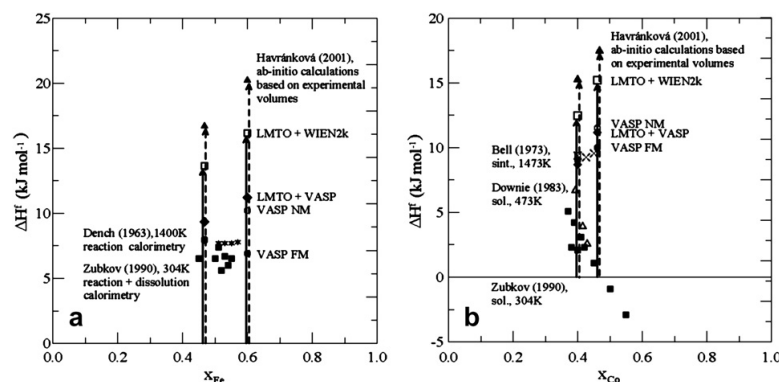


Fig. 4. Calculated energies of formation of sigma phase, compared with experimentally determined enthalpies of formation: (a) Cr–Fe, (b) Cr–Co. The RS structures correspond to the zero line. The full (dashed) arrows and open squares (full triangles) correspond to the LMTO + WIEN2k (LMTO + WIEN97) results from this work (from Ref. [12]), both based on the WIEN97 lattice parameters. Similar arrows for the VASP calculations and experiments were omitted for better clarity. Open and full circles and full diamonds describe the results of the NM VASP, FM VASP and LMTO + VASP analysis. Experiments done by Dench [8], Bell [9], Downie [10], and Zubkov [11] are marked by asterisks, crosses, open triangles and full squares, respectively.

LMTO + WIEN97 (based on experimental lattice parameters) [12], LMTO + WIEN2k, LMTO + VASP, and VASP. The same statement is valid also for the Cr–Co system except of the fact that the VASP numbers are above the LMTO + VASP ones. This tendency fully reflects the level of structure relaxation, i.e. the more relaxed sigma phase the lower energies of formation are obtained.

Furthermore the results provided by LMTO + VASP and VASP calculations correspond to the experimental data very well. From Fig. 4(a) and (b), we can see that inclusion of magnetic ordering improves the overall agreement with experiments. On the other hand, it is also necessary to take into account the reliability of the experimental data in these comparisons, and Fig. 4(b) shows that the scatter of measured values is indeed very large.

The accuracies given for the calorimetric measurements usually refer to their physical performance. Errors of chemical nature may often be much more serious (e.g. impurities, incomplete reactions, side reactions). So inspecting the results of Zubkov [11], whose results suggest decrease in heat of formation with Co concentration, the experimental error has to be assessed from results given in their Table 1, where the values of $-\Delta E_{\text{dissol}}$ for the sigma phase that contains more than 45 at% of Co were obtained by extrapolation of experimental data. It seems to be questionable to believe in decrease of heat of formation with Co composition on the basis of these results.

The comparison of heat of formation measured experimentally with the calculated values is performed under the assumption that $\Delta E(0\text{ K}) = \Delta H(T)$, which need not be valid exactly. Further we should take into account that $\Delta H(T)$ contains the PV term and vibrational $\int C_p dT$ term for both sigma and RS phase which are not included in $\Delta E(0\text{ K})$. It may elucidate the difference of calculated and measured energies of formation.

The difference between the experimental values of heat of formation in Cr–Co system for $\text{Co}_{0.4}\text{Cr}_{0.6}$ of Bell [9] (9.37 kJ/mol) and Zubkov [11] (2.1 kJ/mol) is more than 400%. So, the higher values of heat of formation calculated by the ab initio methods in comparison with the measured ones are not too bad in the case of Cr–Co system.

4. Conclusions

The new achievement of the present paper consists in calculations of total energies of sigma phase and RS at equilibrium volume. This removes the uncertainty connected with the use of lattice

parameters of experimentally found sigma phase for calculations of total energy of hypothetical configurations of pure constituents. Our study also provides the analysis of the influence of magnetism on the stability of the Cr–Fe and Cr–Co sigma phase.

The results of ab initio calculations of total energies of sigma and RS phases of pure constituents (obtained by FLAPW method) combined with total energies of sigma phases for different compositions and for pure elements calculated by LMTO-ASA and FLAPW method were employed to study the stability of sigma phase in Cr–Fe and Cr–Co systems. Furthermore the additional calculations performed by the pseudopotential code VASP and the analysis of the effect of magnetism were carried out. The influence of relaxation on lattice parameters of all structures was also included in this work. It turns out that the more structural relaxations are used the lower energies of formation are obtained. The lowest energies of formation were acquired by the VASP code with the full relaxation and the obtained energies are fully comparable with experimental data. The preferential occupation of the sublattices was analysed.

Inclusion of magnetic ordering in the Cr–Fe and Cr–Co sigma phase calculations causes the decrease of energy of formation and results in the shift of stability region towards the configurations with a higher concentration of iron or cobalt. We predict that Cr–Fe and Cr–Co sigma phases are magnetically ordered at 0 K, which corresponds to experimental findings. Our study reveals that the largest part of magnetization is carried by the iron or cobalt atoms and that the chromium atoms do not contribute to this effect very much although they induce a decrease of the total magnetic moment by their antiferromagnetic behaviour at some sublattices. The magnetic moments depend on the kind and position of the atom and agree satisfactorily with available experimental data. The influence of the sublattice on the magnetic moment is the same for both Fe and Co atoms and their magnetic moments decrease from the sublattices 4f, 8i, 8j, 8i' to 2a. The magnetic moment of Cr in the sigma phase structure is close to zero. However it increases with the increasing number of Fe or Co atoms.

Acknowledgments

This research was supported by the Ministry of Education of the Czech Republic (COST Project No. OC 164).

References

- [1] Bain EC. *Chem and Met Eng* 1923;28:23.
- [2] Villars P, Calvert LD. *Pearson's handbook of crystallographic data for intermetallic phases*. Materials Park (OH): ASM International; 1991.
- [3] Cook AJ, Jones FW. *J Iron Steel Inst* 1943;148:217. London;1943;148:223.
- [4] Yakel HL. *Acta Crystallogr* 1983;B39:20.
- [5] Dickins GJ, Douglas AMB, Taylor WH. *Acta Crystallogr* 1956;9:297.
- [6] Forsyth JB, d'Alte da Viegas. *Acta Crystallogr* 1963;16:509.
- [7] Heino S, Knutson-Wedel EM, Karlsson B. *Mater Sci Technol* 1999;15:101.
- [8] Dench WA. *Trans Faraday Soc* 1963;59:1279.
- [9] Bell HB, Hajra JP, Putland FH, Spencer PJ. *Met Sci Journal* 1973;7:185.
- [10] Downie DB, Arlasan F. *J Chem Thermodyn* 1983;15:654.
- [11] Zubkov AA, Mogutnov BM, Shaposhnikov NG. *Dokl Akad Nauk SSSR* 1990;311(2):388; *Dokl Phys Chem* 1990;311:239.
- [12] Havránková J, Vřešťál J, Wang LG, Šob M. *Phys Rev B* 2001;63:174104.
- [13] Sluiter MHE, Esfarjani K, Kawazoe Y. *Phys Rev Lett* 1995;75:3142.
- [14] Cieslak J, Reissner M, Steiner W, Dubiel SM. *J Magn Magn Mater* 2004;534:272.
- [15] Cieslak J, Reissner M, Steiner W, Dubiel SM. *Physica Status Solidi (A)* 2008;205:1794.
- [16] Korzhavii PA, Sundman B, Selleby M, Johansson B. *Mater Res Soc Symp Proc* 2005;842:54.10.1.
- [17] Udovskii AL. *SCTE2008 (16th International conference on solid compounds of transition elements in Dresden)* Abstract Book, 2008. Poster No.146-3, p. 139.
- [18] Kabliman EA, Mirzoev AA, Udovskii AL. *Fizika Metallov i Metallovedenie*, to be published.
- [19] Ackland GJ. *Phys Rev B* 2009;79:094202.
- [20] Joubert J-M. *Prog Mater Sci* 2008;53:528.
- [21] Ansara I, Chart TG, Fernández Guillermet A, Hayes FH, Kattner UR, Pettifor DG, et al. *Calphad* 1997;21:171.
- [22] Andersen OK. *Phys Rev B* 1975;12:3060; *Skriver HL. The LMTO method*. Berlin: Springer Verlag; 1984.
- Turek I, Drchal V, Kudrnovský J, Šob M, Weinberger P. *Electronic structure of disordered alloys, surfaces and interfaces*. Boston–London–Dordrecht: Kluwer; 1997.
- [23] Krier G, Jepsen O, Burkhardt A, Andersen OK. *Computer code TB-LMTO-ASA version 4.6*. Stuttgart: Max-Planck-Institut für Festkörperforschung; 1994.
- [24] Perdew JP, Chevary JA, Vosko SH, Jackson KA, Pederson MR, Singh DJ, et al. *Phys Rev B* 1992;46:6671.
- [25] Singh D. *Planewaves, pseudopotentials and the LAPW method*. Boston: Kluwer; 1994.
- [26] Blaha P, Schwarz K, Luitz J. *Computer code WIEN97*. Vienna: Vienna University of Technology; 1997; improved and updated Unix version of the original copyrighted WIEN code, which was published by Blaha P, Schwarz K, Sorantin P, Trickey SB. *Comput Phys Commun* 1990;59:399.
- [27] Kresse G, Furthmüller J. *Comput Mat Sci* 1996;6:15.
- [28] Kresse G, Furthmüller J. *Phys Rev B* 1996;54:11169.
- [29] Blöchl P. *Phys Rev B* 1994;50:17953.
- [30] Kresse G, Joubert J. *Phys Rev B* 1999;59:1758.
- [31] Perdew JP, Burke K, Ernzerhof M. *Phys Rev Lett* 1996;77:3865.
- [32] Andersen OK, Methfessel M, Rodriguez CO, Blöchl P, Polatoglou HM. In: Vitek V, Srolovitz DJ, editors. *Atomistic simulation of materials: beyond pair potentials*. New York–London: Plenum; 1989. p. 1.
- [33] Tank RW, Arcangeli C, Krier G, Andersen OK, Jepsen O. In: Gonis A, Meike A, Turchi PEA, editors. *Properties of complex inorganic solids*. New York–London: Plenum; 1997. p. 233.
- [34] Moroni EG, Jarlborg T. *Phys Rev B* 1993;47:3255.
- [35] Blaha P, Schwarz K, Madsen GKH, Kvasnicka D, Luitz J. *WIEN2k, An augmented plane wave plus local orbitals program for calculating crystal properties*. Vienna: Vienna University of Technology; 2001.
- [36] Korzhavii PA. *ADIS2006 (Ab initio description of iron and steel)*, February 19–24, 2006. Ringberg Castle, Germany. Invited talk: Theoretical design of hard materials.
- [37] Sluiter MHE. *Calphad* 2006;30:357.
- [38] Read DA, Thomas EH, Forsythe JB. *J Phys Chem Solids* 1968;29:1569.
- [39] Moroni EG, Kresse G, Hafner J, Furthmüller J. *Phys Rev B* 1997;56:15629.



Contents lists available at ScienceDirect

CALPHAD: Computer Coupling of Phase Diagrams and Thermochemistry

journal homepage: www.elsevier.com/locate/calphad

Thermodynamic modeling of Laves phases in the Cr–Hf and Cr–Ti systems: Reassessment using first-principles results

J. Pavlů*, J. Vřešťál, M. Šob

Department of Chemistry, Faculty of Science, Masaryk University, Brno, Czech Republic
 Institute of Physics of Materials, Academy of Sciences of the Czech Republic, Brno, Czech Republic

ARTICLE INFO

Article history:

Received 14 January 2010
 Received in revised form
 8 March 2010
 Accepted 9 March 2010
 Available online 30 March 2010

Keywords:

Ab initio calculations
 Laves phases
 Chromium–hafnium system
 Chromium–titanium system
 Phase diagrams

ABSTRACT

The Cr–Hf and Cr–Ti belong to interesting systems exhibiting the existence of all polytypes of Laves phases, i.e. lower-temperature cubic C15 and higher-temperature hexagonal C14 and C36, although in the Cr–Hf phase diagram only C14 and C15 phases occur. Comparison of total energies of these structures calculated from first principles with the total energy of the ideal mixture of elemental constituents reveals the relative stability of Laves phases in these systems. The effect of magnetic order in the Laves phases is also briefly discussed.

The calculated total energies of formation of all the three polytypes are employed in two- and three-sublattice models to revise the thermodynamic description of both the systems published recently. New remodeled Gibbs energies of Laves phases require less fitting parameters than those obtained in previous treatments and corresponding phase diagrams provide an excellent agreement with the experimental phase data found in the literature. The proposed procedure allows us to compare the optimised heat capacity differences with those determined experimentally or theoretically and to use them in phase diagram calculations.

© 2010 Elsevier Ltd. All rights reserved.

1. Introduction

The Laves phases consisting of chromium and an element from the IV group of the Periodic Table have been systematically investigated because they are part of structural materials at temperatures up to 1200 °C, e.g. Nb–silicide based in situ composites [1,2]. It has been widely accepted that Cr improves oxidation resistance and Hf enhances both oxidation resistance and strength of these materials. However, additions of new elements may introduce some detrimental phases to the composites which deteriorate the properties of the materials [3]. Therefore, reliable thermodynamic description of stability of phases in both Cr–Hf and Cr–Ti systems is needed for successful materials design.

The Cr–Hf and Cr–Ti systems have been critically reviewed by Yang et al. [3] and Zhuang et al. [4], respectively. Here the sublattice model [5,6] successfully described the thermodynamic behaviour and homogeneity ranges of solid solutions and different types of Cr₂Hf and Cr₂Ti Laves phases. In both systems, 6 equilibrium phases have been reported: liquid, HCP, BCC, C14, C15 and C36 Laves phases. In the Cr–Hf system, the Laves phase structure transforms as a function of temperature from the

lower-temperature cubic C15 polytype to the hexagonal C14 polytype at higher temperatures, avoiding C36 structure [7].

The Cr–Ti system was studied in more detail. It was found that the Laves phase structures transform with increasing temperature from the cubic C15 polytype to the hexagonal C36 polytype at intermediate temperatures and to the hexagonal C14 polytype at the highest temperatures. The C15–C36 transformation temperatures are reported to increase strongly with increasing Ti content from 804 °C at 33.5 at.% Ti to 1223 °C at 37.3 at.% Ti, whereas the transformation temperature from C36 to C14 seems to be nearly independent of composition at 1270 ± 1 °C. However, as described in detail in [4], there is contradicting information on the existence of C36 structure in the literature, connected with its metastability. C36 is an intermediate structure occurring in transformation from C14 to C15 during cooling and the transformation from C36 to C15 is very sluggish. Therefore, the phase diagram of Cr–Ti is still far from being well established. Existing experimental studies [4,8] conclude that the stoichiometric compositions are not incorporated in any of the phase fields of the Laves phases and show that all structures of Cr₂Ti are stable only with an excess of Ti atoms. During the last decade or so, structural energy differences (lattice stabilities) calculated from first principles have been employed in the construction of phase diagrams of systems containing complex phases (see e.g. [9–12]); a recent review may be found in [13,14].

In the present paper, the *ab initio* calculated total energies of formation of two polytypes in the Cr–Hf system and of all the

* Corresponding author at: Department of Chemistry, Faculty of Science, Masaryk University, Brno, Czech Republic. Tel.: +420 549493742; fax: +420 549491453.
 E-mail address: houserova@chemi.muni.cz (J. Pavlů).

three polytypes of Laves phases in the Cr–Ti system are successfully employed in the two- and three-sublattice models to revise the thermodynamic descriptions published in [3,4]. It turns out that total energies of individual phases from the *ab initio* calculations strongly reduce the number of fitting parameters needed in construction of phase diagrams in Cr–Ti and Cr–Hf systems and, in this way, bring more physics into CALPHAD method.

2. Thermodynamic modeling

Using thermodynamic modeling, behaviour of any system under various conditions (i.e. pressure, temperature or composition) can be described. This approach allows us to predict properties and behaviour of systems, which are technologically important for the improvement of current materials or for development of new ones. Contrary to experiments, this treatment provides not only the overview of properties of really existing structures but it is also capable to characterise metastable or even unstable configurations. The main quantity used in such modeling is the molar Gibbs energy of the whole system, which is defined as the sum of molar Gibbs energies of all included phases G^f multiplied by their molar fractions x^f :

$$G^{\text{tot}} = \sum_f x^f G^f, \quad (1)$$

where

$$G^f = \sum_i y_i^0 G_i^f + G^{\text{id}} + G^E + G^{\text{mag}} + G^{\text{pres}}. \quad (2)$$

The molar Gibbs energy of phase G^f contains the sum of molar Gibbs energies of pure constituents i in the phase f multiplied by their lattice fractions $\sum_i y_i^0 G_i^f$, the terms describing ideal (G^{id}) and non-ideal (G^E) mixing and, when needed, some special terms as magnetic (G^{mag}) or pressure (G^{pres}) contribution. For a binary system (A–B), the terms describing mixing may be evaluated by relatively simple formulas as follows:

$$G^{\text{id}} = RT(y_A \ln y_A + y_B \ln y_B) \quad (3)$$

$$G^E = y_A y_B (L^0(T) + L^1(T)(y_A - y_B) + L^2(T)(y_A - y_B)^2 + \dots) \quad (4)$$

where L^0 , L^1 and L^2 are the expansion coefficients of the Redlich–Kister polynomial [15] and T is temperature. Temperature dependence of L -parameters is given by an equation of type

$$L^i = a_j + b_j T + c_j T \ln T, \quad (5)$$

where a_j , b_j and c_j are constants. For liquid phase, we use a model (A, B)₁, for BCC and Laves phases, we employ the (A, B)₁(Va)₃ and (A, B)₂(A, B)₁ or (A, B)₄(A, B)₆A₂ models [5,6], respectively. Similar approach has already been used in systems Cr–Nb, Cr–Ta and Cr–Zr [11,12]. Ideal mixing in Laves phases is then described by expression

$$G^{\text{id}} = RT[(y_A^1 \ln y_A^1 + y_B^1 \ln y_B^1) + (y_A^2 \ln y_A^2 + y_B^2 \ln y_B^2)] \quad (6)$$

where the superscripts are related to sublattices 1 and 2.

In the case of two-sublattice model of Laves phase [5,6], the sum of molar Gibbs energies of pure constituents i in the phase f multiplied by their lattice fractions $\sum_i y_i^0 G_i^f$ is substituted by equation

$$G^{\text{ref}} = y_A^1 y_A^2 {}^0G_{A:A} + y_A^1 y_B^2 {}^0G_{A:B} + y_B^1 y_A^2 {}^0G_{B:A} + y_B^1 y_B^2 {}^0G_{B:B} \quad (7)$$

where Gibbs energies of all “end-members” (${}^0G_{i;j}$) have to be calculated, as mentioned above. For the sake of thermodynamic modeling with the help of the two-sublattice model, some of the experimentally found sublattices of Laves phases have to be merged, e.g. the 2a and 6h sublattice occupied by Cr atoms are joined to form one sublattice in thermodynamic model of the C14

phase. Similarly the 4e and 4f sublattices for X atoms (X = Hf, Ti) and 4f, 6g, and 6h sublattices for Cr atoms in C36 structure are also merged into two sublattices.

The difference in Gibbs energies of the pure constituents in the Laves (L) phase and in the Standard Element Reference (SER) state (i.e. antiferromagnetic (AFM) BCC Cr and nonmagnetic (NM) HCP Ti and Hf) is given by equation

$$\Delta^0 G^{L-\text{SER}} = {}^0G^L - {}^0G^{\text{SER}} = \Delta^0 H^{L-\text{SER}} - T \Delta^0 S^{L-\text{SER}}, \quad (8)$$

where H is enthalpy and S entropy.

At $T = 0$, we may write that $\Delta^0 H^{L-\text{SER}}(T = 0) = \Delta^0 E^{L-\text{SER}}(T = 0)$, i.e. the difference in enthalpies is equal to the difference of total energies, because the total energy at 0 K is calculated at equilibrium volume, where it holds $(\partial U / \partial V)_T = T(\partial p / \partial T)_V - p = 0$. The total energy differences have been calculated *ab initio* at equilibrium volume in the present paper. The difference in enthalpies, $\Delta^0 H^{L-\text{SER}}$ at finite temperature, is then obtained as (Kirchhoff law)

$$\Delta^0 H^{L-\text{SER}} = \Delta^0 E^{L-\text{SER}} + \int \Delta C_p^{L-\text{SER}} dT. \quad (9)$$

In the region without phase transformation, entropy can be expressed as

$$\Delta^0 S^{L-\text{SER}} = \int (\Delta C_p^{L-\text{SER}} / T) dT \quad (10)$$

which, substituted in Eq. (8), after integration (supposing $\Delta C_p^{L-\text{SER}} = \text{const.}$) yields

$$\Delta^0 G^{L-\text{SER}} = \Delta^0 E^{L-\text{SER}} + (\Delta C_p^{L-\text{SER}})T - (\Delta C_p^{L-\text{SER}})T \ln T. \quad (11)$$

This equation may be successfully employed in the phase diagram calculations. Usually, $\Delta^0 E^{L-\text{SER}}$ is calculated *ab initio*, $\Delta C_p^{L-\text{SER}}$ is optimised, as we show below. However, also the value of $\Delta C_p^{L-\text{SER}}$ may be taken from calculations (e.g. from phonon spectra) or from measurements (e.g. from the analysis of Einstein or Debye functions). In this way, we could further reduce the number of fitting parameters needed for description of phase diagrams.

3. *Ab initio* calculations of total energies

Our electronic structure calculations were performed within the Density Functional Theory (DFT). We have used the pseudopotential method [16] incorporated into the Vienna *Ab initio* Simulation Package (VASP) code [17,18] combined with the Projector Augmented Wave–Perdew–Burke–Ernzerhof (PAW–PBE) pseudopotential [19–21] (i.e. we have employed the generalised gradient approximation for the exchange–correlation energy), and calculated the total energies of all three Laves phase structures (C14, C15 and C36) as well as the total energy differences between the Laves phases and the SER structures. The cut-off energy restricting the number of plane waves in the basis set was 295 eV, 232 eV and 286 eV for Cr, Ti and Hf, respectively, for both pure constituents and the Laves phases. Spin polarisation was not included in our calculations, except when noted. Reason for this is the fact that all Laves phases found in the systems studied are paramagnetic at ambient temperatures. Nevertheless, calculations for spin-polarised Cr₂Cr Laves phase (C15) confirmed the influence of magnetism also on the stability of this structure at 0 K.

Preliminary calculations of A₂A, A₂B, B₂A, B₂B (A = Cr, B = Ti, Hf) configurations of C14, C15 and C36 Laves phase structures needed for two-sublattice model and also calculations of A₆B₆ and A₂B₁₀ configurations for C14 and C36 structures needed for three-sublattice model were accomplished using the experimentally found lattice parameters for Cr₂Ti and Cr₂Hf configurations published in [22] except for the C14 and C15 (C36) Laves phase of pure chromium, which was studied using the parameters

Table 1

Calculated and experimental lattice parameters of the SER structures. Symbols a and c stand for lattice constants, V_{at} is the atomic volume and Δ shows the relative difference between the calculated and experimental atomic volume.

SER						
Structure		a (pm)	c (pm)	c/a	V_{at} (10^7 pm 3)	Δ (%)
AFM BCC Cr	Exp. [23]	287.87	287.87	1.0000	1.19281	–2.48
	Relax.	285.48	285.48	1.0000	1.16327	
NM HCP Hf	Exp. [22]	323	512	1.5851	2.31300	–3.63
	Relax.	319.48	504.34	1.5787	2.22896	
NM HCP Ti	Exp. [22]	295.04	468.10	1.5866	1.76438	–2.97
	Relax.	292.39	462.49	1.5818	1.71204	

Table 2

Equilibrium structural parameters of the C14, C15 and C36 Laves phases found in this work. Symbols a and c stand for lattice constants, z , x and y are the internal structural parameters and V_{at} is the atomic volume.

Structure	C14						C15	
	a (pm)	c (pm)	V_{at} (10^7 pm 3)	4f-z	6h-x	6h-y	a (pm)	V_{at} (10^7 pm 3)
Exp. Cr $_2$ Hf [22]	505.6	821	1.51463	–	–	–	714	1.51664
Cr $_2$ Cr	464.09	766.32	1.19117	0.0464	0.8289	0.6578	658.04	1.18726
Cr $_2$ Hf	503.14	805.61	1.47179	0.0604	0.8315	0.6631	706.55	1.46966
Cr $_6$ Hf $_6$	626.68	634.46	1.79822	0.1223	0.8256	0.6513	–	–
CrHf $_2$	552.85	865.58	1.90930	0.0627	0.8253	0.6505	777.45	1.95797
Cr $_2$ Hf $_{10}$	602.11	783.44	2.04974	0.0702	0.8325	0.6650	–	–
Hf $_2$ Hf	569.53	950.50	2.22500	0.0540	0.8267	0.6535	815.72	2.26154
Structure	C36						C15	
	a (pm)	c (pm)	V_{at} (10^7 pm 3)	4e-z	4f-z	4f-z	6h-x	6h-y
Exp. Cr $_2$ Hf [22]	506.4	1647	1.52405	–	–	–	–	–
Cr $_2$ Cr	465.11	1523.11	1.18893	0.1003	0.8485	0.1236	0.1623	0.3247
Cr $_2$ Hf	500.90	1624.27	1.47056	0.0945	0.8439	0.1234	0.1647	0.3294
Cr $_6$ Hf $_6$	625.94	1275.76	1.80365	0.0638	0.8140	0.1323	0.1568	0.3137
CrHf $_2$	561.55	1771.11	2.01529	0.0600	0.8585	0.1266	0.1603	0.3207
Cr $_2$ Hf $_{10}$	601.38	1569.56	2.04832	0.0895	0.8394	0.1250	0.1652	0.3305
Hf $_2$ Hf	569.26	1915.81	2.24022	0.0999	0.8487	0.1302	0.1589	0.3177
Structure	C14						C15	
	a (pm)	c (pm)	V_{at} (10^7 pm 3)	4f-z	6h-x	6h-y	a (pm)	V_{at} (10^7 pm 3)
Exp. Cr $_2$ Ti [22]	493.22	800.53	1.40543	0.0625	0.833	0.666	6.9324	1.38816
Cr $_2$ Cr	464.09	766.32	1.19117	0.0464	0.8289	0.6578	658.04	1.18726
Cr $_2$ Ti	486.19	778.39	1.32789	0.0605	0.8299	0.6599	682.86	1.32676
Cr $_6$ Ti $_6$	569.68	631.96	1.48011	0.1111	0.8259	0.6518	–	–
CrTi $_2$	513.21	786.29	1.49463	0.0669	0.8237	0.6474	715.00	1.52301
Cr $_2$ Ti $_{10}$	563.73	706.72	1.62080	0.0754	0.8289	0.6579	–	–
Ti $_2$ Ti	517.22	894.65	1.72722	0.0523	0.8263	0.6527	749.63	1.75520
Structure	C36						C15	
	a (pm)	c (pm)	V_{at} (10^7 pm 3)	4e-z	4f-z	4f-z	6h-x	6h-y
Exp. Cr $_2$ Ti [22]	493.22	1601.10	1.40546	0.094	0.844	0.125	0.167	0.334
Cr $_2$ Cr	465.11	1523.11	1.18893	0.1003	0.8485	0.1236	0.1623	0.3247
Cr $_2$ Ti	484.27	1568.36	1.32720	0.0947	0.8437	0.1236	0.1633	0.3266
Cr $_6$ Ti $_6$	562.73	1290.70	1.47483	0.0729	0.8203	0.1286	0.1583	0.3167
CrTi $_2$	512.43	1587.44	1.50412	0.0908	0.8450	0.1288	0.1556	0.3112
Cr $_2$ Ti $_{10}$	563.17	1417.17	1.62188	0.0871	0.8374	0.1264	0.1615	0.3229
Ti $_2$ Ti	506.90	1882.28	1.74524	0.1004	0.8496	0.1276	0.1630	0.3259

of corresponding Cr $_2$ Ta (Cr $_2$ Zr) phases, also given in [22]. The structural parameters for the SER states of Ti and Hf were taken from [22] and of Cr from [23].

First, we performed convergence tests of total energies with respect to the number of k -points. The range of optimum values for the C14 Laves phases extends from a grid of $15 \times 15 \times 11$ points (Cr $_2$ Cr, Ti $_2$ Ti), $17 \times 17 \times 15$ points (Cr $_2$ Ti) and $19 \times 19 \times 13$ points (Cr $_6$ Ti $_6$ and Cr $_2$ Ti $_{10}$) towards $19 \times 19 \times 15$ points (CrHf $_2$), $21 \times 21 \times 15$ points (Cr $_2$ Hf, Cr $_2$ Hf $_{10}$), $21 \times 21 \times 17$ points (Hf $_2$ Hf, CrTi $_2$) and $23 \times 23 \times 15$ points (Cr $_6$ Hf $_6$). A similar interval was obtained for the C15 Laves phases which goes from a grid of $15 \times 15 \times 15$ points (Cr $_2$ Cr) and $19 \times 19 \times 19$ points (Cr $_2$ Ti) towards $21 \times 21 \times 21$ points (Hf $_2$ Hf, Cr $_2$ Hf, CrHf $_2$ and CrTi $_2$) and $23 \times 23 \times 23$ points (Ti $_2$ Ti). A smaller range was obtained for the C36 Laves phases which spreads from a grid of $15 \times 15 \times 13$ points (Cr $_2$ Cr) and $17 \times 17 \times 13$ points

(Hf $_2$ Hf, Cr $_2$ Hf, Cr $_2$ Ti, CrTi $_2$) towards $19 \times 19 \times 15$ points (Ti $_2$ Ti, Cr $_6$ Hf $_6$, CrHf $_2$, Cr $_2$ Hf $_{10}$, Cr $_6$ Ti $_6$ and Cr $_2$ Ti $_{10}$).

In the case of SER structures, we used a grid of $13 \times 13 \times 13$ points for AFM BCC Cr, of $19 \times 19 \times 15$ points for NM HCP Ti and of $21 \times 21 \times 13$ points for NM HCP Hf.

After these test calculations, each structure was fully relaxed which yielded the minimum total energy and the equilibrium structural parameters. The results obtained are summarised in the following subsections.

As the Cr SER structure and the C15 Laves phase are cubic, only volume relaxation is sufficient to get their lowest energy state. The calculated optimum lattice parameters for the SER structures are listed in Table 1 and those for the C14, C15 and C36 structures in Table 2.

Spin polarisation was included in AFM BCC Cr calculations. As for Laves phases, we performed a pilot study in [24] for

Table 3

Total energy differences, $\Delta^0 E^{L-SER}$, between the Laves phases of various types and the weighted average of the SER states (antiferromagnetic BCC Cr, nonmagnetic HCP Hf and Ti) calculated in this work, rounded, and compared with the calculated [25–28] and experimental [29] values available in literature. *Ab initio* results published in [25,26,28] were calculated using the generalised gradient approximation. All values are given in kJ/mol of atoms ($1 \text{ eV atom}^{-1} = 96.485 \text{ kJ mol}^{-1} \text{ atom}^{-1}$). The values marked by an asterisk (*) were obtained with the help of the energy difference $E_{FCC} - E_{HCP}$ from Ref. [26], as the value of energy of formation of Laves phase obtained in Ref. [25] was related to the FCC structure. (Let us note that in Ref. [25], nonmagnetic BCC structure is employed as the SER structure for Cr.)

Composition		$\Delta^0 E^{L-SER}$ (kJ mol ⁻¹ atom ⁻¹)					
		Cr ₂ Cr	Cr ₂ Hf	Cr ₆ Hf ₆	CrHf ₂	Cr ₂ Hf ₁₀	Hf ₂ Hf
C14	This work	28.63	-8.70	47.25	96.63	19.33	32.10
	Refs.	27.8 [25]	-9.9 [28]	-	-	-	30.92* [25]
C15	This work	27.29	-10.38	-	103.46	-	38.00
	Refs.		-13 [27]				
		26.4 [25]	-11.6 [28]	-	-	-	35.82* [25]
			-4.8 ± 4.3 [29]				
C36	This work	27.75	-9.68	49.77	97.02	19.57	34.14
	Ref.	-	-10.8 [28]	-	-	-	-
Composition		$\Delta^0 E^{L-SER}$ (kJ mol ⁻¹ atom ⁻¹)					
		Cr ₂ Cr	Cr ₂ Ti	Cr ₆ Ti ₆	CrTi ₂	Cr ₂ Ti ₁₀	Ti ₂ Ti
C14	This work	28.63	-8.47	35.46	51.39	12.59	27.20
	Refs.	27.8 [25]	-10.2 [28]	-	-	-	24.71* [25]
C15	This work	7.29	-10.16	-	57.27	-	32.26
	Refs.		-11 [27]				
		26.4 [25]	-12.0 [28]	-	-	-	25.81* [25]
C36	This work	27.75	-9.51	37.06	53.53	13.47	28.36
	Ref.	-	-11.0 [28]	-	-	-	-

hypothetical Cr₂Cr Laves phase with a C15 structure. It turns out that the spin polarised Cr₂Cr in the C15 structure is more stable than the nonmagnetic one by 31.2 meV/at ($3.01 \text{ kJ mol}^{-1} \text{ atom}^{-1}$) which means that the magnetism of Laves phases should be considered at 0 K. However, at ambient temperatures, Laves phases Cr₂Hf and Cr₂Ti are paramagnetic. Therefore, in the present paper, calculations of total energy differences for comparison of their relative stability were performed for nonmagnetic states only. It is a major approximation which appears to work reasonably well in this system.

Experimental and calculated structural parameters of all C14, C15 and C36 arrangements in Cr₂Hf structure agree quite well. The calculated equilibrium atomic volume ranges from 96.49% V_{exp} for C36 and 96.90% V_{exp} for C15 to 97.17% V_{exp} for C14, where V_{exp} is the experimental atomic volume. A little worse agreement was found for Cr₂Ti where calculated equilibrium atomic volume ranges from 94.43% V_{exp} for C36 and 94.48% V_{exp} for C14 to 95.58% V_{exp} for C15.

The total energy differences $\Delta^0 E^{L-SER}$ between the Laves phases and SER states are then given in Table 3, where they are compared with the results of other authors [25–29].

It is obvious that total energy of C36 structure of pure constituents lies between the values for C14 and C15 structures. However, for pure Cr occupation the stability of Laves phase structures increases from C14 over C36 to C15. This order is opposite to that found for pure Hf and Ti Laves phases where the stability increases from C15 over C36 to C14 configuration. This difference is supposed to be caused by different atomic size of elements studied.

The stability of particular Cr₂X binary Laves phase configuration decreases in the sequence C15, C36 and C14 which is the same as in the case of pure Cr. According to our calculations, the C15 structure should be the most stable configuration in both Cr₂Hf and Cr₂Ti system (Table 3). Stability of C14 and C36 structures at higher temperatures is facilitated by the effect of entropy.

As for CrHf₂ and CrTi₂ configurations, the absolute values of calculated structural energy differences are nearly an order of magnitude higher than those of Cr₂Hf and Cr₂Ti. This is a quantitative confirmation of the fact that the Laves phase structures CrHf₂ and CrTi₂ are energetically very disadvantageous configurations.

Experimental evidence of existence of all three structure types of Laves phases in Cr₂Hf and Cr₂Ti can be found in [22]. However in Cr–Hf system, only phase equilibria with C14 and C15 structures are reported [3,7]. Quantitative conclusions for improvement of phase diagrams in mentioned systems are not yet available.

4. Calculations of phase diagrams

The thermodynamic basis of the CALPHAD method relies explicitly on the assumption that the equilibrium phase composition arises as a result of minimisation of Gibbs energy in closed system at constant external conditions (temperature and pressure).

For modeling of C14 and C15 Laves phases in the Cr–Hf system we employ the two-sublattice model [5,6] as it was used in [3]. We describe these structures as the ordered solid solution phases (see Eq. (7)) with four “end-members”. Their Gibbs energy is modeled with the help of *ab initio* total energy differences, presented in Table 3, where the C36 structure data are included for possible future reference. The Gibbs energy of the Laves phases is obtained from Eq. (11) where the heat capacity term is adjusted to the experimental data. In addition the C14 Laves phase structure was modeled also using three-sublattice model inspired by crystallography.

For modeling of C15 Laves phases in the Cr–Ti system we employ the two-sublattice model [5,6], and for C14 and C36 structure the three-sublattice model, as it was used in [4]. Their Gibbs energy is modeled with the help of *ab initio* total energy differences, presented in Table 3. In addition, the modeling of C14 and C36 structure by using the two-sublattice model is performed for possible future use.

Results of this procedure are presented in Tables 4 and 5.

Let us note here that the values in Table 3 are given in kJ/mol of atoms, whereas the values given in Tables 4 and 5 are given in J/mol of compound (formula unit). That is why the quantities transferred from Table 3 to Tables 4 and 5 are 3000 times higher (in the case of two-sublattice model) or 12 000 times higher (in the case of three-sublattice model). Non-rounded values are given here.

Table 4

Optimised thermodynamic parameters describing the C14, C15 and C36 Laves phases in Cr–Hf system. *Ab initio* calculated values shown in boldface were taken from Table 3 and were kept fixed during the CALPHAD optimisation. Values of standard Gibbs energies are taken from [30].

Structure	Parameters G (Eq. (1)) and L (Eq. (5)) in J mol^{-1} of formula unit
C14 two-subl.	$G(\text{Cr:Cr}) = \mathbf{85\,900} + 3 * \text{GHSERCR}$ $G(\text{Cr:Hf}) = -\mathbf{26\,095} + 0.67 * T - 0.67 * T * \ln(T) + 2 * \text{GHSERCR} + \text{GHSERHF}$ $G(\text{Hf:Cr}) = \mathbf{289\,901} + 2 * \text{GHSERHF} + \text{GHSERCR}$ $G(\text{Hf:Hf}) = \mathbf{96\,312} + 3 * \text{GHSERHF}$ $L(\text{Cr, Hf:Hf; 0}) = -3500$
C14 three-subl.	$G(\text{Cr:Cr:Cr}) = \mathbf{343\,598} + 12 * \text{GHSERCR}$ $G(\text{Cr:Hf:Cr}) = -\mathbf{104\,379} + 2.67 * T - 2.67 * T * \ln(T) + 8 * \text{GHSERCR} + 4 * \text{GHSERHF}$ $G(\text{Cr:Cr:Hf}) = \mathbf{566\,979} + 6 * \text{GHSERHF} + 6 * \text{GHSERCR}$ $G(\text{Cr:Hf:Hf}) = \mathbf{231\,990} + 10 * \text{GHSERHF} + 2 * \text{GHSERCR}$ $L(\text{Cr:Hf:Cr, Hf; 0}) = -10\,000$
C15	$G(\text{Cr:Cr}) = \mathbf{81\,877} + 3 * \text{GHSERCR}$ $G(\text{Cr:Hf}) = -\mathbf{31\,130} + 0.17 * T - 0.17 * T * \ln(T) + 2 * \text{GHSERCR} + \text{GHSERHF}$ $G(\text{Hf:Cr}) = \mathbf{310\,380} + 2 * \text{GHSERHF} + \text{GHSERCR}$ $G(\text{Hf:Hf}) = \mathbf{114\,000} + 3 * \text{GHSERHF}$ $L(\text{Cr, Hf:Hf; 0}) = -24\,000$
C36 prediction	$G(\text{Cr:Cr:Cr}) = \mathbf{333\,020} + 12 * \text{GHSERCR}$ $G(\text{Cr:Hf:Cr}) = -\mathbf{116\,208} + 1.59 * T - 1.59 * T * \ln(T) + 8 * \text{GHSERCR} + 4 * \text{GHSERHF}$ $G(\text{Cr:Cr:Hf}) = \mathbf{597\,242} + 6 * \text{GHSERHF} + 6 * \text{GHSERCR}$ $G(\text{Cr:Hf:Hf}) = \mathbf{234\,827} + 10 * \text{GHSERHF} + 2 * \text{GHSERCR}$ $L(\text{Cr:Hf:Cr, Hf; 0}) = -15\,500$

Table 5

Optimised thermodynamic parameters describing the C14, C15 and C36 Laves phases in Cr–Ti system. *Ab initio* calculated values shown in boldface were taken from Table 3 and were kept fixed during the CALPHAD optimisation. Values of standard Gibbs energies are taken from [30].

Structure	Parameters G (Eq. (1)) and L (Eq. (5)) in J mol^{-1} of formula unit
C14 two-subl.	$G(\text{Cr:Cr}) = \mathbf{85\,900} + 3 * \text{GHSERCR}$ $G(\text{Cr:Ti}) = -\mathbf{25\,401} - 0.788 * T + 0.788 * T * \ln(T) + 2 * \text{GHSERCR} + \text{GHSERTI}$ $G(\text{Ti:Cr}) = \mathbf{154\,157} + \text{GHSERCR} + 2 * \text{GHSERTI}$ $G(\text{Ti:Ti}) = \mathbf{81\,592} + 3 * \text{GHSERTI}$ $L(\text{Cr, Ti:Ti; 0}) = -24\,000$
C14 three-subl.	$G(\text{Cr:Cr:Cr}) = \mathbf{343\,598} + 12 * \text{GHSERCR}$ $G(\text{Cr:Ti:Cr}) = -\mathbf{101\,605} - 3.157 * T + 3.157 * T * \ln(T) + 8 * \text{GHSERCR} + 4 * \text{GHSERTI}$ $G(\text{Cr:Cr:Ti}) = \mathbf{425\,552} + 6 * \text{GHSERTI} + 6 * \text{GHSERCR}$ $G(\text{Cr:Ti:Ti}) = \mathbf{151\,040} + 10 * \text{GHSERTI} + 2 * \text{GHSERCR}$ $L(\text{Cr:Ti:Cr, Ti; 0}) = -20\,000$
C15	$G(\text{Cr:Cr}) = \mathbf{81\,877} + 3 * \text{GHSERCR}$ $G(\text{Cr:Ti}) = -\mathbf{30\,486} - 1.414 * T + 1.414 * T * \ln(T) + 2 * \text{GHSERCR} + \text{GHSERTI}$ $G(\text{Ti:Cr}) = \mathbf{171\,806} + 2 * \text{GHSERTI} + \text{GHSERCR}$ $G(\text{Ti:Ti}) = \mathbf{96\,780} + 3 * \text{GHSERTI}$ $L(\text{Cr, Ti:Ti; 0}) = -57\,450$
C36 two-subl.	$G(\text{Cr:Cr}) = \mathbf{83\,255} + 3 * \text{GHSERCR}$ $G(\text{Cr:Ti}) = -\mathbf{28\,534} - 1.107 * T + 1.107 * T * \ln(T) + 2 * \text{GHSERCR} + \text{GHSERTI}$ $G(\text{Ti:Cr}) = \mathbf{160\,581} + \text{GHSERCR} + 2 * \text{GHSERTI}$ $G(\text{Ti:Ti}) = \mathbf{85\,066} + 3 * \text{GHSERTI}$ $L(\text{Cr, Ti:Ti; 0}) = -28\,000$
C36 three-subl.	$G(\text{Cr:Cr:Cr}) = \mathbf{333\,020} + 12 * \text{GHSERCR}$ $G(\text{Cr:Ti:Cr}) = -\mathbf{114\,139} - 4.435 * T + 4.435 * T * \ln(T) + 8 * \text{GHSERCR} + 4 * \text{GHSERTI}$ $G(\text{Cr:Cr:Ti}) = \mathbf{444\,725} + 6 * \text{GHSERCR} + 6 * \text{GHSERTI}$ $G(\text{Cr:Ti:Ti}) = \mathbf{161\,657} + 10 * \text{GHSERTI} + 2 * \text{GHSERCR}$ $L(\text{Cr:Ti:Cr, Ti; 0}) = -31\,000$

Table 6

Thermodynamic parameters for equilibrium phases (liquid, HCP and BCC) in the Cr–Hf and Cr–Ti system.

Phase	Parameter value (Eq. (4)) in J mol^{-1} per formula unit for Cr–Hf system [3]	Parameter value (Eq. (4)) in J mol^{-1} per formula unit for Cr–Ti system [4]
BCC	$L^0 = 42\,847.5 - 12 * T$ $L^1 = 12\,064$	$L^0 = 11\,824$ $L^1 = 5012$
HCP	$L^0 = 43\,774 + 0.64729 * T$ $L^1 = 15\,000$	$L^0 = 25\,500$
Liquid	$L^0 = -30\,000 + 8 * T$ – this work $L^1 = 3800$ – this work	$L^0 = -992$ $L^1 = 1811$

The L -parameters describing the excess Gibbs energy G^E of non-ideal mixing in Eqs. (4), (5) are obtained by fitting to the experimental data and are listed in Tables 4 and 5, too. The thermodynamic parameters for all other phases (liquid, BCC and HCP) in both systems were taken from [3,4] based on unary data

from [30]. For the sake of completeness, they are presented in Table 6.

For remodeling of liquid phase in Cr–Hf system, Miedema's guess of enthalpy of formation [27] and Tanaka's rule [31] for the enthalpy to entropy ratio in liquid phase were applied.

220

J. Pavlů et al. / CALPHAD: Computer Coupling of Phase Diagrams and Thermochemistry 34 (2010) 215–221

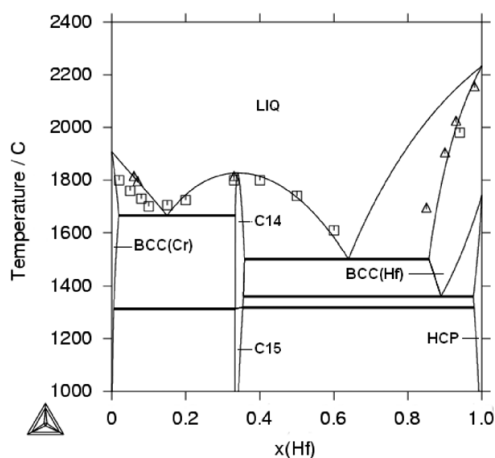


Fig. 1a. Phase diagram of the Cr–Hf system calculated in this work in comparison with experimental data. Here three- (two-)sublattice model for C14 (C15) phase was used. Parameters for BCC and HCP phases are from [3]. Experimental points were taken from Refs. [32] (squares) and [33] (triangles). Phase boundaries agree very well with [7].

The optimisation of parameters of Gibbs energies of Laves phases is, of course, not the standard CALPHAD optimisation as the *ab initio* calculated values shown in boldface in Tables 4 and 5 are kept fixed. Nevertheless this procedure gives us the possibility to employ values with clear physical meaning in our assessment.

The calculated phase diagrams of Cr–Hf and Cr–Ti system are presented in Figs. 1 and 2, where they are compared with existing experimental data. In spite of the above mentioned *ab initio* calculated intermediate lattice stability of C36 Laves phase in Cr–Hf system, the modeling of its thermodynamic properties could not be performed yet because of lack of experimental phase equilibrium data for the Cr–Hf system. The heat capacity and interaction parameters of C36 Laves phase in Cr–Hf system were calculated on the basis of the analogical values in Cr–Ti system for C14 and C36 structures, exploiting similarity of the electronic structure of Hf and Ti. The relative differences of the values of heat capacity and interaction parameter of those structures in both systems were retained.

From Figs. 1 and 2 it is evident that the use of total energy differences calculated *ab initio* into the two- or three-sublattice model of Laves phases describes the phase diagrams (experimental points) in both Cr–Hf and Cr–Ti systems very well.

Let us note that in the present treatment only two optimised parameters are needed for a complete thermodynamic description of any Laves phase: (1) the value of the ΔC_p^{L-SER} describing the temperature dependence of Gibbs energy of real Laves phases (Cr_2Hf , Cr_2Ti), connected with difference of heat capacity of Laves phases and SER states by Eqs. (9)–(11); it may be, in principle, calculated from Einstein or Debye functions or from phonon spectra, and (2) the value of the first *L*-coefficient of Redlich–Kister polynomial (Eq. (4)), which is obtained as a fitting parameter to experimental phase equilibrium data (here we neglect its temperature dependence as well as the higher-order terms). Its physical meaning is, in principle, connected with the binary interaction of atoms in the structure.

On the other hand, analyses employed in [3,4] require 4 and 6 fitting parameters, respectively, for each Laves phase. In addition to that, our approach provides a physical meaning to some coefficients in temperature dependence of Gibbs function connected with the differences in heat capacities (see Eq. (11)), which can further reduce the number of fitting parameters needed.

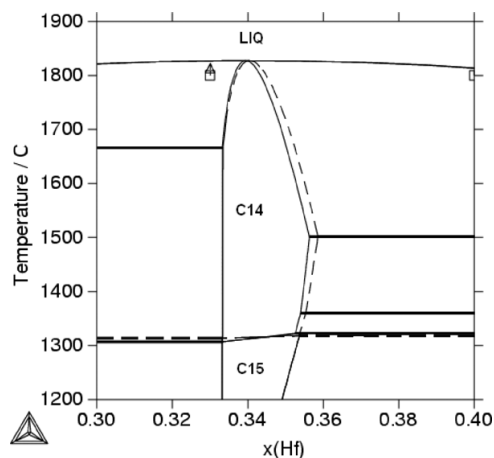


Fig. 1b. Detail of phase diagram of the Cr–Hf system. Three- (two-)sublattice model (marked by full (dashed) lines) for C14 phase is combined with two-sublattice model for C15 phase in both cases. Experimental points were taken from Refs. [32] (squares) and [33] (triangles).

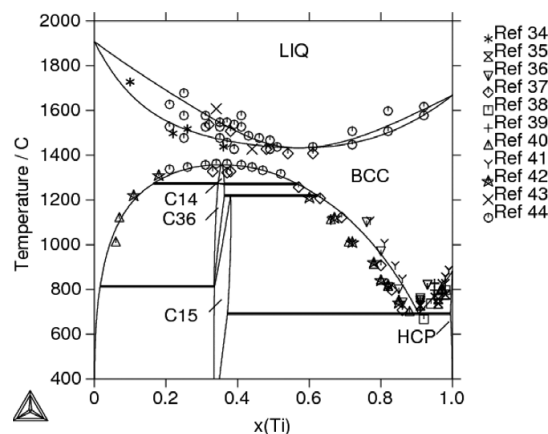


Fig. 2a. Phase diagram of the Cr–Ti system calculated in this work in comparison with existing experimental data [34–44]. Parameters for liquid, BCC and HCP phases are from [4]. Three-sublattice model was employed for C14 and C36 and two-sublattice model for C15 phase.

It seems that physically based energy part of Gibbs surface of Laves phases (i.e. that one obtained from *ab initio* calculations) does not require such a strong entropy correction in the present model. This situation is a little bit surprising, as the *ab initio* calculated parameters for Cr_2Cr , Hf_2Hf and Ti_2Ti energies of formation have more positive values than the guessed ones [3,4], which is, however, in agreement with [25].

We can see from Tables 4 and 5 that the stability of polytypes at 0 K is the highest for C15 structure and decreases in the sequence C15–C36–C14. On the other hand, as it may be expected, the vibrational entropy contribution (heat capacity contribution) increases in the same order when comparing the same models and values per atoms.

When comparing phase equilibria with Laves phases in Figs. 1b and 2b we can see that both our models (two- and three-sublattice) based on *ab initio* results provide a very good description of experimental phase data. Let us note, however, that the phase equilibria presented in [3,4] reproduce phase diagram satisfactorily as well,

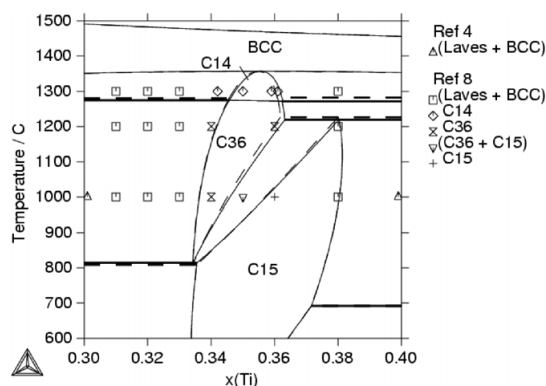


Fig. 2b. Detail of phase diagram of the Cr–Ti system. Three- (two-)sublattice model (marked by full (dashed) lines) for C14 and C36 phases is combined with two-sublattice model for C15 phase in both cases.

although some parameters describing Gibbs energy of Laves phases have no reasonable physical meaning. Introducing physically based parameters is advantageous as it makes the optimisation process simpler, more effective and more reliable for physically based extrapolations to higher order systems.

5. Conclusions

It was shown that *ab initio* calculated structural energy differences may be reliably applied in the two- and three-sublattice model of C14, C15 and C36 Laves phases and that even a smaller number of parameters for a thermodynamic description of Laves phases (Tables 4 and 5) is needed than in previous assessments.

Ab initio calculated energies of formation of Laves phases with respect to the SER (BCC, HCP) states correspond reasonably well to both experimental data where available and to previous theoretical results.

Our *ab initio* analysis of relative stability of Laves phase structures confirms the sequence of decreasing stability C15–C36–C14, but it cannot be fully utilised in thermodynamic modeling of these phases in Cr–Hf system because of lack of phase equilibrium data for C36 structure. However, it can be used in the future when more experimental data will be available. It may be expected that first-principles calculations of total energy differences of pure constituents in intermetallic and SER structures will represent a standard tool for modeling thermodynamics of intermetallic phases in near future. Furthermore, the proposed procedure also allows to compare the optimised heat capacity differences with those determined experimentally or theoretically and to use them in phase diagram calculations.

Acknowledgements

Financial support of the Grant Agency of the Czech Republic (Project Nos. 106/07/1078 and P108/10/1908), of Ministry of

Education of the Czech Republic (Project Nos. OC164 and MSM0021622410) and of Academy of Sciences of the Czech Republic (Project No. AV0Z20410507) is gratefully acknowledged. Phase equilibria were calculated by means of ThermoCalc code.

Appendix. Supplementary data

Supplementary data associated with this article can be found, in the online version, at doi:10.1016/j.calphad.2010.03.003.

References

- [1] B.P. Bewlay, M.R. Jackson, H.A. Lipsitt, *Metall. Mater. Trans. A* 27A (12) (1996) 3801.
- [2] P.R. Subramanian, M.G. Mendiratta, D.M. Dimiduk, M.A. Stucke, *Mater. Sci. Eng. A* 239–240 (1997) 1.
- [3] Y. Yang, J. Schoonover, B.P. Bewlay, D. Lewis, Y.A. Chang, *Intermetallics* 17 (2009) 305.
- [4] W. Zhuang, J. Shen, Y. Liu, L. Ling, S. Shang, Y. Du, J.C. Schuster, *Z. Metallkd.* 91 (2000) 121.
- [5] M. Hillert, L.I. Staffanson, *Acta Chem. Scand.* 24 (1970) 3618.
- [6] N. Saunders, A.P. Miodownik, *CALPHAD—A Comprehensive Guide*, Elsevier, Oxford, UK, 1998.
- [7] M. Venkatraman, J.P. Neumann, *Bull. Alloy Phase Diagrams* 7 (1986) 570.
- [8] K.C. Chen, S.M. Allen, J.D. Livingstone, *Mater. Res. Symp. Proc.* 364 (1995) 1401.
- [9] S.G. Fries, B. Sundman, *Phys. Rev. B* 66 (2002) 012203.
- [10] J. Houserová, J. Vřešťál, M. Šob, *CALPHAD* 29 (2005) 133.
- [11] J. Pavlů, J. Vřešťál, M. Šob, *CALPHAD* 33 (2009) 179.
- [12] J. Vřešťál, A. Kroupa, M. Šob, *Comp. Mater. Sci.* 38 (2006) 298.
- [13] M. Šob, A. Kroupa, J. Pavlů, J. Vřešťál, *Solid State Phenom.* 150 (2009) 1.
- [14] Z.-K. Liu, *J. Phase Equilib. Diffus.* 30 (2009) 517.
- [15] O. Redlich, A.T. Kister, *Ind. Eng. Chem.* 40 (1948) 345.
- [16] D. Singh, *Planewaves, Pseudopotentials and the LAPW Method*, Kluwer, Boston, 1994.
- [17] G. Kresse, J. Furthmüller, *Comput. Mater. Sci.* 6 (1996) 15.
- [18] G. Kresse, J. Furthmüller, *Phys. Rev. B* 54 (1996) 11169.
- [19] P. Blöchl, *Phys. Rev. B* 50 (1994) 17953.
- [20] G. Kresse, J. Joubert, *Phys. Rev. B* 59 (1999) 1758.
- [21] J.P. Perdew, K. Burke, M. Ernzerhof, *Phys. Rev. Lett.* 77 (1996) 3865.
- [22] P. Villars, L.D. Calvert, *Pearson's Handbook of Crystallographic Data for Intermetallic Phases*, ASM International, Materials Park, OH, USA, 1991.
- [23] E.G. Moroni, T. Jarlborg, *Phys. Rev. B* 47 (1993) 3255.
- [24] J. Pavlů, J. Vřešťál, M. Šob, *CALPHAD* 33 (2009) 382.
- [25] M.H.F. Sluiter, *CALPHAD* 30 (2006) 357.
- [26] Y. Wang, S. Curtarolo, C. Jiang, R. Arroyave, T. Wang, G. Ceder, L.-Q. Chen, Z.-K. Liu, *CALPHAD* 28 (2004) 79.
- [27] F.R. De Boer, R. Boom, A.R. Miedema, *Physica B* 113 (1982) 18.
- [28] X.Q. Chen, W. Wolf, R. Podlousky, P. Rogl, *Phys. Rev. B* 71 (2005) 174101-1-11.
- [29] S.V. Meschel, X.Q. Chen, O.J. Kleppa, P. Nash, *CALPHAD* 33 (2009) 55.
- [30] A.T. Dinsdale, *CALPHAD* 15 (1991) 317.
- [31] T. Tanaka, N.A. Gokcen, Z. Morita, *Z. Metallkd.* 81 (1990) 49.
- [32] O.N. Carlson, D.G. Alexander, *J. Less-Common Met.* 15 (1968) 361.
- [33] V.N. Svechnikov, A.K. Shurin, G.P. Dmitrijeva, *Prevrashchen Faz., AN Ukr. SSR*, 1965, p. 159.
- [34] M.K. McQuillan, *J. Inst. Met.* 80 (1951) 379.
- [35] F.B. Cuff, N.J. Grant, C.F. Floe, *Trans. AIME* 194 (1952) 848.
- [36] P. Duwez, J.L. Taylor, *Trans. AMS* 44 (1952) 495.
- [37] R.J. van Thyne, H.D. Kessler, M. Hansen, *Trans. AMS* 44 (1952) 974.
- [38] M.K. McQuillan, *J. Inst. Met.* 82 (1954) 433.
- [39] Yu.A. Bagarjatskij, G.I. Nosova, T.V. Tagunova, *Russ. J. Inorg. Chem.* 3 (1958) 330.
- [40] F. Ermanis, P.A. Farrar, H.M. Argolin, *Trans. AIME* 221 (1961) 904.
- [41] V.S. Mikheev, V.S. Alekashin, *Fiz. Met. Metall.* 14 (1962) 62.
- [42] P.A. Farrar, H. Margolin, *Trans. AIME* 227 (1963) 1342.
- [43] V.N. Svechnikov, M.Yu. Teslyuk, Yu.A. Kocherzhinskiy, V.V. Petkov, E.V. Dabizha, *Dopov. Akad. Nauk Ukr. SSR Ser. A* 32 (1970) 837.
- [44] S.A. Minayeva, P.B. Budberg, A.L. Gavze, *Russ. Metall.* 4 (1971) 205.



The thermochemical behavior of some binary shape memory alloys by high temperature direct synthesis calorimetry

S.V. Meschel^{a,b,*}, J. Pavlu^c, P. Nash^b

^a James Franck Institute, The University of Chicago, 5640 S. Ellis Avenue, Chicago, IL, 60637, USA

^b Illinois Institute of Technology, Thermal Processing Technology Center, 10W, 32nd Street, Chicago, IL, 60616, USA

^c Department of Chemistry, Masaryk University, Kotlarska 2, Brno, 61137, Czech Republic

ARTICLE INFO

Article history:

Received 18 November 2010

Received in revised form 19 January 2011

Accepted 20 January 2011

Available online 5 March 2011

Keywords:

Shape memory alloys

Enthalpy of formation

Calorimetry

ABSTRACT

The standard enthalpies of formation of some shape memory alloys have been measured by high temperature direct synthesis calorimetry at 1373 K. The following results (in kJ/mol of atoms) are reported: CoCr (-0.3 ± 2.9); CuMn (-3.7 ± 3.2); Cu₃Sn (-10.4 ± 3.1); Fe₂Tb (-5.5 ± 2.4); Fe₂Dy (-1.6 ± 2.9); Fe₁₇Tb₂ (-2.1 ± 3.1); Fe₁₇Dy₂ (-5.3 ± 1.7); FePd₃ (-16.0 ± 2.7); FePt (-23.0 ± 1.9); FePt₃ (-20.7 ± 2.3); NiMn (-24.9 ± 2.6); TiNi (-32.7 ± 1.0); TiPd (-60.3 ± 2.5). The results are compared with some earlier experimental values obtained by calorimetry and by EMF technique. They are also compared with predicted values on the basis of the semi empirical model of Miedema and co-workers and with ab initio calculations when available. We will also assess the available information regarding the structures of these alloys.

© 2011 Elsevier B.V. All rights reserved.

1. Introduction

W.J. Buehler and F.E. Wang, two crystal physicists observed in 1959 that NiTi alloy (Nitinol) has unique characteristics [1]. This alloy “remembers” its shape, and therefore such compounds are called shape memory alloys (SMA). Compounds in this group are held in the so called “parent” state, which is usually a cubic structure (Austenite) and heat treated to transform to another structure. When for example the NiTi wire cools below its transition temperature the atoms rearrange in another structure of lower symmetry, the Martensite phase. These are solid state transformations. The Martensite crystals are slightly flexible and can accommodate some degree of deformation. When the NiTi wire is warmed up the Martensite crystals revert to their undeformed, “parent” structure (Austenite). The earliest observations of this effect are credited to Olander in 1932 (Au–Cd), Greeninger and Mooradian (1938) (Cu–Zn) and later to Kurdjumov and Khandros (1949) and also to Chang and Read (1951) [2–5].

The shape memory phenomenon is associated with reversible martensitic transformations [6]. Such transformations may take place either by thermoelastic or by a non-thermoelastic process. When the material is heated up and the structure reverts to the original or “parent phase” it is called a thermoelastic process. How-

ever, there are exceptions, some of the Fe based alloys show a face centered cubic to hexagonal close pack martensitic transformation in a non-thermoelastic way [7,8].

In general, materials which allow structures to adapt to their environment are known as actuators [9]. They can change shape, hardness, position, frequency and other properties as a response to temperature, electricity or magnetism. The thermoelastic shape memory alloys (SMA) may respond to thermal stimuli, piezoelectric ceramics to electric stimuli (PZT = lead zirconate titanate) and magnetostrictive materials to changes of magnetic fields (Terfenol-D, Samfenol, Galfenol) [10]. While this definition is the most general one, we should keep it in mind that though SMA alloys are actuators not all actuators display shape memory phenomenon.

When a SMA recognizes only its “parent” state, it is undergoing a so called “one way” shape memory transition. If the sample undergoes specific “training” treatments, it is possible for the alloy to recognize both its “parent” shape and also its deformed state. The result is the fascinating so called two-way shape memory effect, which is much less well understood [11–14]. This is a unique effect in inanimate materials, however there are similar manifestations in the animal kingdom, for example in the training of homing pigeons.

The shape memory alloys are utilized in many areas of endeavor, including electrical engineering, machinery design, transportation, chemical engineering, space research and medicine. This indicates a great demand for these materials. To 1994 more than 15,000 patents were applied for utilization of SMA-s [13]. These include such diverse specific uses as pipe joints, eyeglass frames, orthodontic treatments, stents in bypass surgeries and many other ingenious applications.

* Corresponding author at: Illinois Institute of Technology, Thermal Processing Technology Center, 10W, 32nd Street, Chicago, IL, 60616, USA. Tel.: +1 773 684 7795; fax: +1 773 702 4180.

E-mail address: meschel@jfi.uchicago.edu (S.V. Meschel).

In both the experimental and the theoretical treatments of SMA-s the stability of the alloy is considered very important [15,16]. Since the enthalpies of formation are excellent indicators of the stability of alloys, we believe that understanding the thermochemical behavior of such compounds would be helpful to members of the scientific community who design new shape memory alloys with specific applications in mind [17,18]. We found the list of compounds where shape memory effect has been observed very helpful in identifying the more important shape memory alloys [13,19].

In some instances shape memory effects have been predicted for metallic systems where compound formation has not been reported. Some of the binary alloys which are reported to exhibit shape memory phenomena have only one reported crystal modification. It is questionable if the effect is due to thermoelastic SMA phenomenon if the alloys have no apparent “deformed” modification. We also noticed that in some studies compositions of binary alloys were proposed as exhibiting shape memory effect which are not stoichiometric. Therefore we assessed in the present communication the systems where shape memory effect was reported or predicted and surveyed their basic characteristics. Subsequently we prepared some stoichiometric compositions for detailed thermochemical study.

It is sometimes possible to find information regarding Gibbs' energies or estimate these quantities from phase diagrams, but enthalpies of formation are considerably more scarce. The entropy in these compounds is also a very significant quantity [16]. This quantity plays a crucial role in the transformation of the SMA from the Austenite to the Martensite phase. If the enthalpies of formation are available, it would be possible in principle to evaluate or at least estimate the entropies with existing or estimated Gibbs' energies.

Detailed knowledge of the specific heat could also be very important in understanding the Austenite–Martensite transition. One would anticipate a definite break or discontinuity in the relationship between the specific heat and the temperature at the transition point. Further study of the transition temperature could also advance our understanding of this fascinating process. Rane, Navrotsky and Rossetti studied the detailed thermodynamic behavior of one of the actuators, in a piezoelectric ceramics material (PZT) [10,20].

Therefore we decided to embark on a study of the thermochemical behavior of some SMA-s. In the current communication we are reporting standard enthalpies of formation for some binary SMA-s, namely FePd₃, FePt, FePt₃, Fe₂Tb, Fe₁₇Tb₂, Fe₂Dy, Fe₁₇Dy₂, NiMn, FeMn, CoCr, Cu₃Sn and CuMn. Even though the enthalpies of formation for NiTi, TiPd and several Pt alloys have already been measured by high temperature, direct synthesis calorimetry [21,22], we decided to remeasure the enthalpies of formation of NiTi and TiPd, because we felt that the information regarding their structures were not sufficient in the previous studies.

2. Experimental

The experiments were carried out at 1373 ± 2 K in a single unit differential calorimeter which has been described in an earlier communication by Kleppa and Topor [23] at the University of Chicago. The measurements in the current study were made at IIT. The changes in the equipment have been reported in an earlier communication [22]. All the experiments were performed under the protective atmosphere of Argon gas which was purified by passing it over titanium chips at 900 °C.

A boron nitride (BN) crucible was used to contain the samples.

All the metals were purchased from Johnson Matthey/Aesar (Ward Hill, MA, USA). The Tb and Dy samples were filed from solid ingots immediately prior to the experiments. For the alloys where we used Fe, Co, Ni or Cu, these were reduced prior to the calorimetric experiments at 600 °C under hydrogen gas flow to insure that we avoid surface oxidation of these metals. The two components were mixed in the appropriate molar ratio, compressed into small pellets of about 2 mm diameter and then dropped from room temperature into the calorimeter. In a subsequent set of experiments the reaction products were dropped into the calorimeter to measure

their heat contents. Between the two sets of experiments the samples were kept in a vacuum desiccator to prevent reaction with oxygen or moisture.

Calibration of the calorimeter was achieved by dropping weighed segments of high purity, 2 mm diameter Cu wire into the calorimeter at 1373 ± 2 K. The enthalpy of pure copper at 1373 K, 43.184 kJ/mol of atoms was obtained from Hultgren et al. [24]. The calibrations were reproducible to within ±2.0–2.5% precision.

The reacted samples were examined by X-ray powder diffraction analyses to assess their structure and to ascertain the absence of unreacted metals. In the course of the present study we attempted to prepare 19 binary alloys. Among these, 14 were found acceptable for fully quantitative measurements. We did not attempt to prepare compositions of binary alloys which were not indicated to exist in the phase diagram collection of Massalski et al. [25]. These are for example alloys in the Ti–Nb, U–Nb, In–Ti and Ti–V systems. We also did not include compounds which had no reported crystal structures either in the ASTM Powder diffraction file or in Pearson's collection of crystallographic data [26], as for example in Ti₃Ni₄, Fe_{81.6}Ga_{18.4}.

The physical characteristics and structures of the binary alloys we prepared are summarized in Table 1. In the second column we list the Chemical Abstracts (CAS) Registry Numbers (RN) of the compounds reported to display shape memory phenomenon. As CA currently indexes over 10 million compounds and alloys, if a compound has no RN assigned to it, it is unlikely to be appropriate for further measurements. In the third column we list the melting points of the compounds and alloys from the data available from the Massalski et al. [25] phase diagram collection. In the fourth column we list the Pearson symbols assigned to the structure of the compound available from the ASTM powder diffraction file and from Pearson's collection of crystallographic data [26]. In order to have a well defined shape memory alloy, both the parent structure and the structure after the transition should be well known. The fifth column designated as comments shows if the reaction was complete and the modification observed in the calorimetric measurements. We did not study the alloys in the systems Ag–Cd and Au–Cd, because the vapor pressure of Cd is such that direct synthesis calorimetry at 1100 °C is not possible. The compounds which we found to be ductile during the preparation could be quite suitable for preparing thin wires and coils.

To prepare the samples for XRD analyses we used an agate mortar and pestle. When this was not sufficient we used a hardened steel die and a hammer. In one case we needed to use a diamond wheel to cut the samples. The alloys we studied varied significantly in behavior, structure characteristics and physical properties. We will discuss some of the more important characteristics in the next section.

3. Discussion

3.1. Physical properties and structures

3.1.1. Unreacted alloys: RuTa, Ru₂Ta₃, Ti₄Mo₉

These are all listed as shape memory alloys, however we found that in our conditions they are unreacted. The XRD patterns clearly showed the presence of unreacted elements. In the XRD pattern of Ti₄Mo₉ we noticed the presence of approximately 20% reaction of the expected compound and two unidentified phases. The XRD equipment is sufficiently sensitive so that we could have observed solid solution formation had there been any.

3.1.2. Fe–Pd system

FePd was ductile and could not be powdered in preparation for XRD analysis. However, we performed an XRD analysis on a very thin pellet and a subsequent SEM study. Both samples show the presence of FePd and a substantial amount of unreacted Fe metal. FePd₃ was also ductile. However, the XRD pattern showed a single phase, a cubic structure. This is the only modification listed in both the ASTM powder diffraction file and Pearson's collection of crystallographic data [26].

3.1.3. Fe–Pt system

Our FePt sample could not be powdered, it yielded only small flakes. However, the XRD pattern showed that this compound is a single phase, a tetragonal structure. This is the only modification listed in the ASTM powder diffraction file and in Pearson's crystallographic data [26,27]. FePt₃ is ductile. We performed an XRD analysis on a very thin pellet and found an excellent match of the published cubic structure. Again, there is only one structure listed [26].

5258

 S.V. Meschel et al. / *Journal of Alloys and Compounds* 509 (2011) 5256–5262

Table 1
 Physical properties of some binary shape memory alloys.

Compound	RN	Melting point T (°C)	Structure Pearson symbol	Comment
NiTi	12035-60-8	1310(c)	cP2, mP4	tP2
Ni ₃ Ti	59328-60-8	1380(c)	hP16	
NiTi ₂	108503-16-8	984(p)	cF96	
Ti ₃ Ni ₄	105-884	–	–	
TiPd	12165-82-1	1400(c)	cP2, oP4	Both modif.
TiPd ₂	12333-98-1	960(c)	–	
TiPd ₃	12066-72-7	1530(c)	hP16	
Ti ₄ Mo ₉	–	–	–	XRD, SEM incomplete
TiNb	12384-42-8	–	–	
TiNb ₂	123188-71-6	–	–	
TiV	–	–	–	
TiV ₂	12067-84-4	–	–	
Ti ₂ V	–	–	–	
RuTa	–	1667(p)	oF*	XRD, SEM, unreacted
Ru ₂ Ta ₃	–	–	tP2	XRD, SEM unreacted
AgCd	12002-62-9	–	cP2, hP2, cI2, oC4	
Ag ₂ Cd	119187-00-7	–	–	
AgCd ₂	276691-61-3	–	–	
AuCd	12044-73-4	629 (c)	oP4, t*4, cP2 hP27, hP18	
InTl	–	–	–	
InTl ₂	–	–	–	
In ₂ Tl	–	–	–	
FePd	12022-86-5	790(p) 1304(ordering)	tP4	XRD, SEM Incomplete, ductile
FePd ₃	12310-93-9	820(p) 1304(ordering)	cP4	XRD, single phase ductile, cP4
FePt	12186-46-8	~1300(p)	tP4	XRD, single phase, tP4
FePt ₃	57679-16-0	~1350(p)	cP4	XRD, single phase Ductile, cP4
Fe ₃ Tb	–	1212(p)	hR12	XRD, mixed phase
Fe ₂ Tb	12023-38-0452	1187(p)	cF24, hR6	XRD, single phase Both modif.
Fe ₁₇ Tb ₂	12063-75-1	1312(p)	hR19, hP38	XRD, two hexag. modif.
Fe ₃ Dy	–	1305(c)	hR12	mixed phase
Fe ₂ Dy	12019-81-7	1270(p)	cF24, hR*	s.p., cF24
Fe ₁₇ Dy ₂	12060-29-6	1375(c)	hP38	two hexag. modif.
FeMn	12518-52-4	–(1246 °C, ordering)	cF4, cI2, t**	ductile, tetrag.
Fe ₃ Mn	12182-95-5	–	–	
Fe ₄ Mn	117443-48-8	–	hP2	
Fe ₃ Ga ₄	53237-41-5	906(p)	mc42, t*63	
Fe ₃ Ga	12063-30-8	–	hP8, hP2	
FeGa ₃	12062-72-5	824(p)	tP16	
CoCr	12052-27-6	~1283(c)	cI2, cP8	SEM, 90% 1:1
CoCr ₂	159201-78-2	–	–	
Co ₃ Cr	15381-39-4	–	hP8	
NiMn	12263-28-4	911(c)	cI2, tP2	tP2
Ni ₃ Mn	–	–	cP4	
CuMn	12272-98-9	–	cF4, t*4	Tetrag., ss
Cu ₃ Mn	104251-06-1	–	–	
CuGa ₂	68985-62-6	eutectic	tP3	
Cu ₁₁ Ga ₃₉	–	–	–	
Cu ₃ Sn	12019-61-3	676(c)	oC80, cF16, m**	oC80
Cu ₆ Sn ₅	12019-69-1	–	hP4, hR22	
Cu ₃ Si	12134-36-0	859(c)	hP72, hR*	
Cu ₃ Ge	12158-95-1	698(p)	oP8, cI2, hP8, mP4	mP4

3.1.4. Fe–Tb and Fe–Dy systems

In both systems the 3:1 compound did not form quantitatively at our conditions. We observed mixed phases where the 1:2 compound was predominant. In both systems the 2:1 compound formed quantitatively. In both 1:2 compounds two modifications are listed, a cubic and a hexagonal phase [26]. In TbFe₂ we observed both modifications. In our sample of Fe₁₇Tb₂ the XRD pattern of our sample clearly showed the presence of both the reported hexagonal modifications [26]. There were no indications of unreacted elements or secondary phases. Dy₂Fe₁₇ was very difficult to powder. We obtained the sample for the XRD analysis by placing it in a hardened stainless steel die and hammering it 300 times. The structure is a reasonably good match of the hP38 type hexagonal pattern. There were no unreacted elements or secondary phases

present. However, we noticed two unidentified lines in the pattern, which closely matched the hR19 type hexagonal pattern published for Tb₂Fe₁₇. This structure has not been published for Dy₂Fe₁₇ [26,28–30].

3.1.5. FeMn

This sample is ductile. The XRD performed on a very thin pellet did not match either the Fe or the Mn patterns. Subsequent SEM study showed that the large majority of the sample has a 1:1 composition with a minor component of 1:2 composition [31]. We will show the enthalpy of formation result as indicative.

3.1.6. CoCr

This sample did not melt, yielded light grey pellets. The samples are ductile and we could not crush them even in the hardened steel die. The XRD pattern of a very thin pellet did not match the tetragonal CoCr phase. The closest match was with the alpha-Co pattern. A subsequent SEM study showed that our sample was nearly 90% 1:1 composition. The study showed the presence of a few percent of two secondary phases. This alloy has gained considerable current significance by its use in hip joint arthroplasty [32].

3.1.7. NiMn

This sample melted, yielded a light grey bead. This alloy sample was very difficult to powder to prepare the XRD samples. We placed it in a hardened stainless steel die and hammered it several hundred times for powder preparation. There are two compounds reported in this system [25], however the XRD patterns are not listed in the ASTM powder diffraction file. We generated the pattern of the 1:1 composition from unit cell parameters and the atomic coordinates of the prototype structure [26]. The XRD pattern showed that we had no unreacted elements or any secondary phases. The experimental pattern closely matched the generated tp2 pattern. Heo et al. report this composition as a solid solution [33].

3.1.8. CuMn

This sample melted, and yielded a light grey bead. We could not powder it even in the hardened steel die. We cut the sample with a diamond wheel to prepare for heat content measurements. The XRD pattern showed solid solution formation. The pattern matched closely the tetragonal Mn pattern with significant shift toward the copper peaks [34]. Copper based shape memory alloys were reviewed by Tadaki [8,19].

3.1.9. Cu₃Sn

The samples melted, yielded a light grey bead. This sample could be powdered for XRD analysis. The XRD pattern clearly showed an excellent match of the published orthorhombic structure. There is no evidence for the presence of unreacted elements or secondary phases such as Cu₆Sn₅. We observed two extra peaks in the pattern which could possibly be attributed to the cubic modification. The pattern of the cubic modification is not listed in the ASTM powder diffraction file. Therefore we generated this pattern from available unit cell parameters and the appropriate atomic coordinates.

3.1.10. TiNi

This sample was a gold toned silvery alloy partially melted, which we could not crush. The sample for XRD analysis was filed from the bead. The XRD pattern showed complete reaction and the CsCl type cubic structure.

3.1.11. TiPd

This sample was partially melted, yielded a light grey alloy. Our sample could not be crushed to powder, we were only able to get chips for the XRD analyses.

The XRD pattern showed both the cubic and the orthorhombic modifications.

3.2. Standard enthalpies of formation

The standard enthalpies of formation of the shape memory alloys determined in this study were obtained as the difference of two sets of measurements. In the first set the following reaction takes place in the calorimeter:

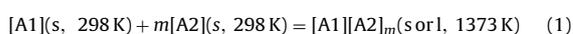


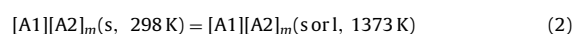
Table 2

Standard enthalpies of formation of some binary shape memory alloys. Data are in kJ/mol of atoms.

Compound	$\Delta H(1)$	$\Delta H(2)$	ΔH_f^o
FePd ₃	14.4 ± 1.1(5)	30.4 ± 2.5(5)	-16.0 ± 2.7
FePt	6.0 ± 1.5(5)	29.0 ± 1.1(5)	-23.0 ± 1.9
FePt ₃	9.0 ± 1.3(5)	28.7 ± 1.9(4)	-20.7 ± 2.3
Cu ₃ Sn	30.1 ± 2.5(6)	40.5 ± 1.8(4)	-10.4 ± 3.1
Fe ₂ Tb	25.1 ± 1.6(7)	30.6 ± 1.8(5)	-5.5 ± 2.4
Fe ₁₇ Tb ₂	28.9 ± 2.5(6)	31.0 ± 1.5(5)	-2.1 ± 3.1
DyFe ₂	28.6 ± 2.3(5)	30.2 ± 1.8(5)	-1.6 ± 2.9
Dy ₂ Fe ₁₇	24.0 ± 1.6(5)	29.3 ± 0.7(4)	-5.3 ± 1.7
NiMn	33.0 ± 1.9(4)	57.9 ± 1.8(5)	-24.9 ± 2.6
FeMn ^a	35.7 ± 2.7(6)	38.3 ± 1.6(5)	-2.6 ± 3.1
CoCr	34.3 ± 2.4(5)	34.6 ± 1.7(4)	-0.3 ± 2.9
CuMn	41.1 ± 1.3(5)	44.8 ± 2.9(4)	-3.7 ± 3.2
TiNi	-3.5 ± 0.4(5)	29.2 ± 0.9(5)	-32.7 ± 1.0
TiPd	-29.7 ± 1.8(5)	30.8 ± 1.6(5)	-60.3 ± 2.5

^a Indicative result.

Here m represents the molar ratio $[A1]/[A2]$, where A1 and A2 represent the elements in the binary shape memory alloys, while s denotes solid and l denotes liquid. The reacted pellets were reused in a subsequent set of measurements to determine their heat contents:



The standard enthalpy of formation is given by:

$$\Delta H_f^o = \Delta H(1) - \Delta H(2) \quad (3)$$

where $\Delta H(1)$ and $\Delta H(2)$ are the enthalpy changes per mole of atoms in the compounds associated with the reactions in Eqs. (1) and (2).

The experimental results are summarized in Table 2. The heat effects associated with the reactions in Eqs. (1) and (2) are given in kilojoules per mole of atoms as averages of about six consecutive measurements with the appropriate standard deviations. The fourth column shows the standard enthalpy of formation of the considered phases. The standard enthalpy of formation in that column also reflects the small contribution from the uncertainties in the calibrations. All the measurements were performed in BN crucibles.

We compared the experimental heat contents of the compounds we studied with the values calculated on the basis of the Neumann-Kopp rule from the heat contents of the elements as listed in Hultgren et al. [24] and found reasonable agreement for most compounds. The average experimental heat content for 14 compounds was 32.9 ± 5 as compared with 37.9 ± 3 kJ/mol of atoms for the calculated values. The experimental and calculated heat contents usually show better agreement when the component metals are all transition metals. We observed some notable deviations for the heat contents of Fe₂Tb, Fe₁₇Tb₂, FePt, Fe₂Dy, Fe₁₇Dy₂, FeMn and NiMn where the differences between the experimental and the calculated values are quite substantial. Since NiMn melted under our conditions, some of the difference may be accounted for by the heats of transformation and the heat of fusion.

In Table 3, we compare our results with experimental measurements from the published literature and with predicted values. Some of the enthalpies of formation of the shape memory alloys listed in Table 3 have been measured by Guo and Kleppa [21], by Topor and Kleppa [35] and by Gachon and Hertz [36]. It is noteworthy that our measurement for Cu₃Sn agrees well with the earlier measurement by Kleppa by tin solution calorimetry in 1957 [37]. We found reasonable agreement for the enthalpy of formation of Dy₂Fe₁₇ with Norgren et al. by solution calorimetry [38]. However our result is significantly different for DyFe₂. The authors refer to errors due to oxidation on p1373 of their study. Also, if we look at the enthalpies of formation of other Fe-LA systems by

5260

S.V. Meschel et al. / *Journal of Alloys and Compounds* 509 (2011) 5256–5262**Table 3**

Comparison of the standard enthalpies of formation of some binary shape memory alloys with literature and theoretical predictions. Data are in kJ/mol of atoms.

Compound	Current work	Literature	Method	Prediction Miedema et al. [41] ab initio	
NiTi	-32.7 ± 1.0	$-34(36)$ $-33.1 \pm 1.1(20)$	DSC DSC	-52	-33.1
TiNi ₃		$-43(36)$ $-42.2 \pm 1.2(20)$	DSC DSC	-37	
NiTi ₂		$-29(36)$	DSC	-40	
TiPd	-60.3 ± 2.5	$-51.6 \pm 6.4(20)$ $-53.3 \pm 1.8(20)$	DSC DSC	-97	
TiPd ₃		$-65.0 \pm 0.9(20)$	DSC	-62	
FePd ₃	-16.0 ± 2.7	-		-4	-10.0
FePt	-23.0 ± 1.9	$-25(\Delta G)$ (40)	EMF	-19	-23.1
FePt ₃	-20.7 ± 2.3	$-17(\Delta G)$ (40)	EMF	-11	-19.2
Cu ₃ Sn	-10.4 ± 3.1	$-9.1(37)$	SC	-5.4	
Fe ₂ Tb	-5.5 ± 2.4	-	DSC	-4.4	
Fe ₁₇ Tb ₂	-2.1 ± 3.1	$-3.3(39)$	EMF	-1.5	
Fe ₂ Dy	-1.6 ± 2.9	$-11.1(38)$	SC	-4.4	
Fe ₁₇ Dy ₂	-5.3 ± 1.7	$-1.9(38)$ $-4.6(39)$	SC EMF	-1.6	
NiMn	-24.9 ± 2.6	-	DSC	-12.3	
FeMn	-2.6 ± 3.1^a	-	DSC	+0.4	
CoCr	-0.3 ± 2.9	-	DSC	-6.7	
CuMn	-3.7 ± 3.2	-	DSC	+5.6	

DSC = Direct synthesis calorimetry.

SC = Solution calorimetry.

EMF = Electromotive force measurement.

^a Indicative result.

different methodologies, the enthalpy values appear to be small, between -1 and -5 kJ/mol of atoms. Therefore the reported value of -11.1 kJ/mol of atoms for DyFe₂ seems unusual. We also found good agreement for the enthalpy of formation of Fe₁₇Dy₂ with the measurements of Gozzi et al. [39]. We also found good agreement with the enthalpies of formation for NiTi measured by Gachon et al. by calorimetry [36] and for TiPd measured by Topor and Kleppa [35]. The results of Gozzi et al. and Hultgren et al. were measured by the EMF technique [39,40]. The fourth column indicates the method used in the cited results. The predicted values in the fifth column are from the semi empirical model of Miedema and co-workers [41].

We recently began comparing our results with predicted values by ab initio calculations. This is completely the work of Dr. Pavlu at Masaryk University, Czech Republic and all questions regarding the details of the calculations should be addressed to her. The energies of formation at 0 K temperature were evaluated using the Vienna's Ab initio Simulation Package (VASP), code working within the Density Functional Theory (DFT) [42,43]. This method utilizes the Projector Augmented Wave–Perdew–Burke–Ernzerhof (PAW–PBE) pseudopotentials [44–46]. The Generalized Gradient Approximation (GGA) program was used here to evaluate the exchange correlation energy. The preliminary calculations were accomplished using the experimentally found structural information published in Pearson's collection of crystallographic data and listed in Table 4 [26]. The FePd, FePd₃, FePt and FePt₃ structures considered here to be ferromagnetic (FM) whereas the NiTi intermetallics in both the cubic and in the monoclinic arrangement are treated as nonmagnetic (NM). The structural parameters for the standard element reference (SER) states: FM bcc Fe, NM fcc Pd and Pt, FM fcc Ni and NM hcp Ti were also cited from [26].

The cut off energy restricting the number of plane waves in the basis set was 348 eV, 326 eV, 299 eV, 350 eV and 232 eV for Fe, Pd, Pt, Ni and Ti respectively, both for pure constituents and constituents in the intermetallic compounds.

We first performed convergence tests of the total energies with respect to the number of k-points. The range of optimum

values extends from a grid of $23 \times 23 \times 17$ points for FePt, from $23 \times 23 \times 15$ for FePd, from $23 \times 23 \times 23$ points for FePd₃ and monoclinic NiTi, to $31 \times 31 \times 31$ points for FePt₃, and to $33 \times 33 \times 33$ points for cubic NiTi.

In the case of the SER structures we used a grid of $9 \times 9 \times 9$ points for FM bcc Fe and FM fcc Ni, of $19 \times 19 \times 15$ points for NM hcp Ti, of $37 \times 37 \times 37$ points for NM fcc Pd and of $41 \times 41 \times 41$ points for NM fcc Pt. After these calculations, each structure was fully relaxed, which yielded the minimum total energy and the equilibrium structural parameters at 0 K. As the Fe, Pd, Pt and Ni SER structures, FePd₃, FePt₃ and one of the NiTi modifications are cubic, only the volume relaxation is necessary to obtain their lowest energy state.

The results are summarized in Table 4. The agreement of calculated V/atom with experiments is very good as the deviations of calculated values from experiments (given in % of experimental value) lie in the interval of -5% (Pd) to $+9.5\%$ (Fe) for SER states and in the interval from -3.5% (FePd₃) to $+4.5\%$ (FePt) for intermetallic phases. The relatively high deviation for pure FM bcc Fe is given by the choice of experimental data. If this deviation is calculated with respect to the second experimental number given in Table 4 its value is only $+2.3\%$. The comparison of found and experimental magnetic moments (Table 4) in case of FM bcc Fe, FM fcc Ni, FM FePd, FM FePd₃ and FM FePt provides an excellent agreement. In the case of FePt₃ the antiferromagnetic (AFM) arrangement of the structures is reported [50]. Nevertheless the magnetic moments found in the literature agree very well with the calculated ones.

The above described approach can in principle evaluate the structural stabilities, precise heats of formation, electronic structural properties, chemical bonding, magnetic ordering and defect properties. However, it must be kept in mind that the data rigorously refer to 0 K. Therefore comparison with experimental data at 298 K may give rise to some discrepancies and the ab initio value should be recalculated. In general, the energy of formation of a binary intermetallic compound is obtained as a difference between its equilibrium total energy and the total energies of the

Table 4
Ab initio calculations.

A. Optimized structural parameters of the SER states found in this work and compared with experimental data.					
Structure	a (Å)	b (Å)	c (Å)	β	V/atom (Å ³)
FM bcc Fe Exp.	2.9315	a	a	90	12.5962
Exp. ^a	2.8576	a	a	90	11.6669
Calc.	2.8358	a	a	90	11.4023
FM fcc Ni Exp.	3.5236	a	a	90	11.0623
Exp. ^b	3.52	a	a	90	10.9036
Calc.	3.5227	a	a	90	10.9286
NM fcc Pd Exp.	3.890	a	a	90	14.7160
Calc.	3.9540	a	a	90	15.4538
NM fcc Pt Exp.	3.923	a	a	90	15.0937
Calc.	3.9772	a	a	90	15.7281
NM hcp Ti Exp.	2.9504	a	4.6810	120	17.6438
Calc.	2.9239	a	4.6249	120	17.1204

B. Optimized structural parameters of the intermetallic compounds found in this work and compared with experimental data. So-called internal parameters of phase describe the positions of atoms within the unit cell and symbols x, y, z denote the axes in the direction of which the position of atoms is defined.					
Structure	a (Å)	b (Å)	c (Å)	β	V/atom (Å ³)
FePd exp.	3.8552	a	3.7142	90	13.8006
Calc.	3.8360	a	3.7690	90	13.8649
FePd ₃ Exp.	3.8480	a	a	90	14.2444
Calc.	3.8919	a	a	90	14.7378
FePt Exp.	4.0001	a	3.6721	90	14.6891
Calc.	3.8619	a	3.7609	90	14.0230
FePt ₃ Exp.	3.8720	a	a	90	14.5126
Calc.	3.9122	a	a	90	14.9692
NiTi Exp.	3.0070	a	a	90	13.5947
Cubic Calc.	3.0047	a	a	90	13.5633
NiTi Exp.	4.6225	4.2105	2.8854	96.8000	13.9409
Monocl. Calc.	4.7812	4.0343	2.9147	102.2351	13.7361
Internal par.	2e – x Ni	2e – z Ni	2e – x Ti	2e – z Ti	
Exp.	0.8070	0.9475	0.2790	0.5274	
Calc.	0.8288	0.9362	0.2851	0.6147	

C. Optimized magnetic moments of the SER states and intermetallic compounds found in this work and compared with experimental data. μ Denotes average magnetic moment per atom.				
Structure	Ref.	μ_{Fe} (μ_{B})	$\mu_{\text{Ni/Pd/Pt}}$ (μ_{B})	Comment
FM bcc Fe	[47] This work	2.12 2.18		
FM fcc Ni	[48] This work		0.61 (Ni) 0.60 (Ni)	
FePd	[49] This work	2.85 2.96	0.35 (Pd) 0.36 (Pd)	
FePd ₃	[49] [49] This work	2.37(13) 3.10 3.30	0.51 (4) (Pd) 0.42 (Pd) 0.35 (Pd)	At 300 K
FePt	[50] This work	2.8 2.95	0.4 (Pt) 0.35 (Pt)	
FePt ₃	[50] [50] This work	3.3 – 3.26	– 0.38 (Pt) 0.38 (Pt)	AFM arr. FM arr.

D. Ab initio calculated total energy differences between the intermetallic compound and the weighted averages of total energies of the SER phases of pure constituents. All values are given in kJ/mol of atoms.	
Structure	$\Delta^0 E^{\text{intermet-SER}}$
FePd	–6.036
FePd ₃	–10.029
FePt	–23.095
FePt ₃	–19.232
NiTi (cubic)	–33.056
NiTi (monoclinic)	–37.057

Å = Angstrom.

1 Å = 0.1 nm.

^a Ref. [47].^b Ref. [48].

pure atomic constituents at the same conditions, both calculated ab initio at 0 K. Since in the ab initio calculations the energy per formula unit of the binary compound is evaluated at 0 K there is no entropy contribution. The enthalpy of formation at 0 K is therefore identical with the energy of formation at this temperature and can be calculated at 298 K using Kirchoff's law. Often the approximation of Neumann–Kopp's rule is used and the value of the energy of formation (at 0 K) is approximately compared with the value of the enthalpy of formation (at higher temperatures) without further calculation. The Gibbs' energy of formation is derived from the Gibbs' energy difference of the compound and the pure constituents. It follows that in the derivation of the formation Gibbs' energies it is necessary to know well the Gibbs' energies of the pure phases and include an entropy contribution. The fifth column in Table 3 and part D in Table 4. list the predicted values by ab initio calculations by Dr. Pavlu.

It is encouraging that most of the new predicted values compare quite well with the experimental measurements. Despite some exceptions where we noted discrepancies the agreement is far better than with the Miedema semi empirical model. However, we should keep it in mind that the ab initio calculations refer to 0 K and the experimental measurements to 298 K.

To illustrate the correlations between experimental and predicted values, we have reasonable agreement with the values predicted by the semi empirical model of Miedema and co-workers for 3 alloys from the total of 14 studied. By reasonable agreement our criteria was less than 20% difference between the experimental enthalpies and the predicted values. In comparison, we have reasonable agreement with the values predicted by the ab initio calculations in 3 alloys of the total of 4 for which calculations had been made using the same criteria.

4. Conclusions

- 1 Some aspects of the thermochemical behavior of 14 shape memory alloys are summarized.
- 2 The physical characteristics and the structures of the alloys studied are assessed. Several of the alloys in this study are ductile which is a relevant property in the application of shape memory alloys.
- 3 The standard enthalpies of formation have been measured by high temperature direct synthesis calorimetry.
- 4 The experimental enthalpies of formation were compared with previously determined enthalpies in the published literature and with calculated values from the semi empirical model of Miedema and co-workers and with the ab initio calculations in this work. We found that the ab initio calculations agree better with our experimental measurements.
- 5 The ab initio calculated equilibrium structural parameters and magnetic moments agree very well with those published in the literature. It was shown that the energies of formation corresponding to these equilibrium arrangements can significantly contribute to the analysis of the energetics of intermetallic phases in spite of the fact that they are calculated at 0 K.

Acknowledgements

This investigation has benefited from the MRSEC facilities at the University of Chicago and from the facilities in the Thermal Processing Center at IIT. This study was supported by NSF Grant # DMR 0964812 at IIT. Dr. Pavlu's theoretical work was supported by the Grant Agency of the Czech Republic, (Project No.

P108/10/1908), the Ministry of Education of the Czech Republic (Project No. MSM0021622410) and the Academy of Sciences of the Czech Republic (Project No. AV0Z20410507). We would like to express our appreciation to Dr. Ian Steele and to Dr. Joseph Pluth for help with the SEM and the XRD analyses.

References

- [1] G.B. Kauffman, I. Mayo, *Chem. Educator* 2 (1997).
- [2] A. Olander, *JACS* 56 (10) (1932) 3819–3833.
- [3] A.B. Greninger, V.G. Mooradian, *Trans. AIME* 128 (1938) 337–355.
- [4] G.V. Kurdjumov, L.G. Khandros, *Doklady Akad. Nauk SSSR* 66 (2) (1949) 211–221.
- [5] L.C. Chang, T.A. Read, *J. Met.* 189 (1951) 47–52.
- [6] K. Otsuka, T. Kakeshita (Eds.), *MRS Bulletin*, Febr, 2002.
- [7] J.H. Yang, H. Chen, C.M. Wayman, *Metall. Trans. A* 23A (1992) 2431–2437.
- [8] K. Otsuka, C.M. Wayman (Eds.), *Shape Memory Materials*, Cambridge University Press, 1998.
- [9] C.A. Rogers, *Sci. Am.* 273 (3) (1995).
- [10] M.V. Rane, A. Navrotsky, G.A. Rossetti Jr., *J. Solid State Chem.* 161 (2001) 402–409.
- [11] J.W. Xie, D. Fort, J.S. Abell, *J. Alloys Compd.* 366 (2004) 241–247.
- [12] R. Stalmans, J. Van Humbeck, L. Delaey, *Acta Metall. Mater.* 40 (1992) 2921–2931.
- [13] M. Fremond, S. Miyazaki, *Shape Memory Alloys*, Springer, NewYork, 1996, p. 108.
- [14] J. Perkins, D. Hodgson, in: T.W. Duerig, K.N. Melton, D. Stockel, C.M. Wayman (Eds.), *Engineering Aspects of Shape Memory Alloys*, Butterworth-Heinemann, London, 1990.
- [15] I. Muller, S. Seelecke, *Math. Comput. Model.* 34 (2001) 1307–1355.
- [16] I. Friedel, *J. Phys. Lett. (Paris)* 35 (1974) 59–63.
- [17] A.P. Jardine, *J. Mater. Sci.* 24 (1989) 2587–2593.
- [18] J.A. Shaw, Bi-chiau Chang, M.A. Iadicola, Y.M. Leroy, *Proceeding of the SPIE*, 2003, pp. 504976–504987.
- [19] T. Tadaki, K. Otsuka, K. Shimizu, *Ann. Rev. Mater. Sci.* 18 (1988) 25–45.
- [20] G.A. Rossetti Jr., A. Navrotsky, *J. Solid State Chem.* 144 (1999) 188–194.
- [21] Q. Guo, O.J. Kleppa, *J. Alloys Compd.* 321 (2001) 169–182.
- [22] S.V. Meschel, P. Nash, X.Q. Chen, *J. Alloys Compd.* 492 (2010) 105–115.
- [23] O.J. Kleppa, L. Topor, *Thermochim. Acta* 139 (1989) 291–297.
- [24] R. Hultgren, P.D. Desai, D.T. Hawkins, M. Gleiser, D.D. Wagman (Eds.), *Selected Values of the Thermodynamic Properties of the Elements*, ASM, Metals Park, OH, 1973.
- [25] T.B. Massalski, H. Okamoto, P.R. Subramanian, L. Kacprzak (Eds.), *Binary Alloy Phase Diagrams*, 2nd edition, ASM, Metals Park, OH, 1990.
- [26] P. Villars, C.D. Calvert (Eds.), *Pearson's Handbook of Crystallographic Data for Intermetallic Phase*, ASM, Metals Park, OH, 1985.
- [27] Yi-Qun Gao, Zhong-Min Wang, Sung H. Wang, *Materials Sci. Eng. A. Struct. Mater. A* 192–193 (1–2) (1995) 53–58.
- [28] K.N. Martin, P.A.J. de Groot, B.D. Rainford, K. Wang, G.J. Bowden, J.P. Zimmermann, H. Fangohr, *J. Phys. Condens. Matter* 18 (2006) 459–478.
- [29] K.H.J. Buschow, *J. Less Common Met.* 11 (1966) 204–208.
- [30] A.S. Van der Goot, K.H.J. Buschow, *J. Less Common Met.* 21 (1970) 151–157.
- [31] H. Schumann, *Naturwissenschaftliche Reihe* 37 (10) (1988) 47–50.
- [32] A.G. Cobb, T.P. Schmalzreid, *J. Eng. Med. Proc. I. Mech. Eng. Part H* 220 78 (2006) 385–398.
- [33] Y.-U. Heo, M. Kim, H.-C. Lee, *Acta Mater.* 56 (6) (2008) 1306–1314.
- [34] D.P. Oxley, R.S. Tebble, K.C. Williams, *J. Appl. Phys.* 34 (4) (1963) 1362–1364.
- [35] L. Topor, O.J. Kleppa, *Z. Metallkunde* 77 (1986) 633–636.
- [36] J.C. Gachon, J. Hertz, *CALPHAD* 7 (1983) 1–12.
- [37] O.J. Kleppa, *J. Phys. Chem.* 60 (1956) 852–858.
- [38] S. Norgren, F. Hodaj, P. Azay, C. Colinet, *Metall. Mater. Trans.* 29A (1998) 1367–1374.
- [39] D. Gozzi, M. Iervolino, A. Latini, *J. Chem. Eng. Data* 52 (2007) 2350–2358.
- [40] R. Hultgren, P.D. Desai, D.T. Hawkins, M. Gleiser, K.K. Kelley, *Selected Values of the Thermodynamic Properties of Binary Alloys*, ASM, Metals Park, OH, 1973.
- [41] F.R. deBoer, R. Boom, W.C.M. Mattens, A.R. Miedema, A.K. Niessen, *Cohesion in Metals. Transition Metal Alloys*, Elsevier Sci. Publ., The Netherlands, 1988.
- [42] G. Kresse, J. Furthmuller, *Comput. Mater. Sci* 6 (1) (1996) 15–50.
- [43] G. Kresse, J. Furthmuller, *Phys. Rev. B* 54 (16) (1996) 11169–11186.
- [44] P. Blochl, *Phys. Rev. B* 50 (24) (1994) 17953–17979.
- [45] G. Kresse, J. Joubert, *Phys. Rev. B* 59 (3) (1999) 1758–1775.
- [46] J.P. Perdew, K. Burke, M. Ernzerhof, *Phys. Rev. Lett.* 77 (18) (1996) 3865–3868.
- [47] E.G. Moroni, T. Jarlborg, *Phys. Rev. B* 47 (6) (1993) 3255–3267.
- [48] E.G. Moroni, G. Kresse, J. Hafner, J. Furthmuller, *Phys. Rev. B* 56 (24) (1997) 15629–15645.
- [49] H.P.J. Wijn (Ed.), *Magnetic Properties of Metals d-Elements, Alloys and Compounds*, Springer-Verlag, Berlin Heidelberg, Germany, 1991.
- [50] K.H.J. Buschow (Ed.), *Handbook of Magnetic Materials*, Elsevier Sci. B.V., Amsterdam, The Netherlands, 2001.



Contents lists available at SciVerse ScienceDirect

CALPHAD: Computer Coupling of Phase Diagrams and Thermochemistry

journal homepage: www.elsevier.com/locate/calphad



Extension of SGTE data for pure elements to zero Kelvin temperature—A case study

Jan Vřešťál^{a,c,*}, Jan Štrof^b, Jana Pavlů^{a,c}

^a Masaryk University, Central European Institute of Technology, CEITEC, Brno, Czech Republic

^b Masaryk University, Faculty of Science, Department of Chemistry, Brno, Czech Republic

^c Institute of Physics of Materials, Academy of Sciences of the Czech Republic, Brno, Czech Republic

ARTICLE INFO

Article history:

Received 3 October 2011

Received in revised form

14 January 2012

Accepted 14 January 2012

Available online 7 February 2012

Keywords:

Gibbs energy

Pure elements

Zero Kelvin

Einstein temperature

SGTE data

Heat capacity

ABSTRACT

A method for the extension of SGTE Gibbs energy expression for pure elements to zero Kelvin temperature is described. The method is based on the Einstein formula for the temperature dependence of heat capacity extended to give the temperature dependence of the Gibbs energy below the limiting temperature of validity of SGTE unary data (T_{lim}). The method maintains the SGTE unary data above the limiting temperature and forces the low temperature extension to have the same function value and the value of the first derivative at T_{lim} as the respective SGTE Gibbs energy polynomial. The extended heat capacity polynomials were also set to have the same function value and the value of the first derivative at T_{lim} .

© 2012 Elsevier Ltd. All rights reserved.

1. Introduction

The Gibbs energy data for the pure elements currently used in CALPHAD applications are represented by simple experimentally based polynomials [1], which are usually restricted at low temperatures to 298.15 K or to some other limiting temperature (T_{lim}).

For the modeling of phase transformations below this limit, it is necessary to extend the Gibbs energy polynomials for pure elements [1], to zero Kelvin temperature. Values of SGTE polynomials of Gibbs energy above T_{lim} should be left unchanged, because they are based on experiments and are widely used.

For the extension of Gibbs energy of pure elements below the limiting temperature, the Einstein and Debye model incorporates the vibrational contribution to the Gibbs energy, which is the prevailing contribution to it in the temperature region considered. In the present paper, the SGTE polynomials [1] are extended below T_{lim} using the Einstein formula for the temperature dependence of

the heat capacity, extended to give the temperature dependence of Gibbs energy. In this first step, magnetic and pressure contributions to the Gibbs energy and the temperature and concentration dependence of the Einstein and Debye temperature are not considered.

2. Thermodynamic model

According to [2], the heat capacity of the pure elements can be represented by

$$C_p = 3AR \left(\frac{T_E}{T} \right)^2 + aT + bT^4 + cT^2, \quad (1)$$

for nonmagnetic elements, where T is the temperature in K and $A = \frac{e^{T_E/T}}{(e^{T_E/T} - 1)^2}$ is introduced for simplification of further equations.

The first term in Eq. (1) represents the contribution of the harmonic lattice vibration, T_E is the Einstein temperature and R is the universal gas constant. The second term consists of contributions from electronic excitations and low-order anharmonic corrections (dilatational and explicitly anharmonic), and the parameter, a , can be related to a non-thermodynamic information, e.g., electron density of states at Fermi level. The third term is from the high-order anharmonic lattice vibrations, and it is seldom that one can find

* Correspondence to: Masaryk University, Central European Institute of Technology, CEITEC, 611 37 Brno, Czech Republic. Tel.: +420 549498134; fax: +420 541211214.

E-mail address: vrestal@chemi.muni.cz (J. Vřešťál).

38

J. Vřešťál et al. / CALPHAD: Computer Coupling of Phase Diagrams and Thermochemistry 37 (2012) 37–48

Table 1

Values of the Einstein temperature T_E for stable structures of elements recalculated from Debye temperatures from [6,7], where the values for T_C were taken from [9], values for γ from [10] and values for B were taken from [11]. Limiting temperatures T_{lim} were taken from [1], corresponding values of SGTE Gibbs energy at T_{lim} , $G(T_{lim})$, from [1], and values of parameters a , b , c and E_0 for extended Gibbs energy expression, Eq. (2), below limiting temperature T_{lim} are this work. Some values of T_E for unstable structures of elements are recalculated from T_D and added from literature [2] for Fe, from [6] for Ti, Zr and Hf, and from [8] for V. Temperatures are in Kelvin, energy in J mol^{-1} .

Element	T_E	T_{lim}	$G(T_{lim})$	E_0	a	b	c
Li-bcc_A2	264.88	200	-6260.44	-7962.63	0.0112590	2.37900E-09	-1.53294E-04
Na-bcc_A2	121.66	200	-10760.3	-8016.02	0.0257557	1.66252E-09	-1.50434E-04
K-bcc_A2	70.07	200	-13456.9	-7988.74	0.0194388	1.81586E-09	-1.17296E-04
Rb-bcc_A2	43.12	200	-15892.4	-8042.92	0.0120858	1.12973E-09	-4.12642E-05
Cs-bcc_A2	29.26	200	-17595.2	-8041.85	-0.0127130	-1.14058E-09	1.81210E-04
Be-hcp_A3	1108.8	298.15	-2832.42	-15659.3	0.00610649	-9.49706E-10	1.49314E-04
Mg-hcp_A3	308	298.15	-9740.85	-8833.11	0.0539769	8.10174E-10	-2.30295E-04
Ca-fcc_A1	177.1	298.15	-12399.4	-8060.32	0.0169877	5.21547E-11	-4.22890E-05
Sr-fcc_A1	113.2	298.15	-16605.1	-8186.46	0.0457474	7.33731E-10	-1.94534E-04
Ba-bcc_A2	84.7	298.15	-18634.3	-7911.40	0.0684640	2.92889E-09	-4.52605E-04
Sc-hcp_A3	277.2	298.15	-10328.9	-8706.90	0.0469648	5.81278E-10	-1.83312E-04
Y-hcp_A3	184.8	298.15	-13248.0	-8431.21	0.0482034	6.10041E-10	-1.89282E-04
La-DHCP	109.34	298.15	-16965.4	-8252.86	0.0446360	5.46438E-10	-1.70763E-04
Ti-hcp_A3	323.4	298.15	-9159.16	-8861.83	0.0441439	6.18793E-10	-1.74763E-04
Ti-bcc_A2	220.22	298.15	-4597.55	-1800.32	0.0210120	5.66515E-11	-5.16686E-05
Ti-fcc_A1	255.64	298.15	-3188.98	-2091.78	0.00378822	5.88120E-11	9.79921E-07
Zr-hcp_A3	224.07	130	-6587.28	-8313.16	0.0806209	1.31270E-08	-7.48881E-04
Zr-bcc_A2	147.07	298.15	-6719.72	-674.409	0.0328312	5.42043E-10	-1.48985E-04
Zr-fcc_A1	144.76	298.15	-4350.11	177.008	-0.0346112	-6.41923E-10	1.90319E-04
Hf-hcp_A3	194.04	298.15	-12987.4	-8421.33	0.0557452	8.33639E-10	-2.42998E-04
Hf-bcc_A2	126.28	298.15	-2998.58	4357.63	0.0386224	6.09732E-10	-1.73357E-04
Hf-fcc_A1	158.62	298.15	-3643.34	1905.99	0.0342399	4.98051E-10	-1.44210E-04
V-bcc_A2	292.6	298.15	-9209.85	-8475.16	0.0327470	5.26993E-10	-1.41840E-04
V-fcc_A1	306.46	298.15	-1202.99	-997.557	0.0255088	3.48182E-10	-9.96915E-05
V-hcp_A3	318.78	298.15	-4494.29	-4580.80	0.0258721	3.16351E-10	-9.62630E-05
Nb-bcc_A2	211.75	298.15	-10813.9	-7944.08	0.0196347	4.61047E-10	-1.01055E-04
Ta-bcc_A2	184.8	298.15	-12364.8	-8101.73	0.0295502	3.93215E-10	-1.21167E-04
Cr-bcc_A2	485.1	298.15	-7017.64	-9933.46	0.0488572	3.86670E-10	-1.60734E-04
Mo-bcc_A2	346.5	298.15	-8515.13	-8861.12	0.0428376	5.86744E-10	-1.78282E-04
W-bcc_A2	308	298.15	-9724.92	-8790.52	0.0562411	8.30265E-10	-2.47579E-04
Mn-bcc_A12	315.7	298.15	-9606.49	-8968.11	0.0477805	6.66697E-10	-1.79805E-04
Tc-hcp_A3	388.08	298.15	-9834.66	-9735.06	0.0942685	1.31947E-09	-4.00134E-04
Re-hcp_A3	331.1	298.15	-10890.3	-9466.06	0.0939376	1.23562E-09	-3.93606E-04
Fe-bcc_A2	308.77	298.15	-1841.40	22.9525	0.0963983	1.75273E-09	-4.61144E-04
Fe-fcc_A1	308.77	298.15	-2731.18	-1141.91	0.0822187	1.36384E-09	-3.70372E-04
Ru-hcp_a3	462	298.15	-8531.37	-10149.2	0.0826785	9.22441E-10	-3.20209E-04
Os-hcp_a3	385	298.15	-9730.18	-9711.29	0.0857969	9.43881E-10	-3.38392E-04
Co-hcp_a3	342.65	298.15	-2529.54	-1070.33	0.109565	1.73121E-09	-4.92418E-04
Rh-fcc_a1	369.6	298.15	-9408.34	-9434.27	0.0729270	9.59375E-10	-2.97118E-04
Ir-fcc_a1	323.4	298.15	-10585.9	-9287.76	0.0816946	1.01455E-09	-3.36578E-04
Ni-fcc_a1	346.5	298.15	-8006.62	-7481.20	0.0734882	9.20651E-10	-2.98323E-04
Pd-fcc_a1	210.98	298.15	-11277.0	-8108.69	0.0287734	5.98583E-10	-1.35483E-04
Pt-fcc_a1	184.8	298.15	-12412.2	-8152.49	0.0279310	3.31714E-10	-1.03994E-04
Cu-fcc_a1	264.11	298.15	-9883.67	-8342.85	0.0328876	5.34699E-10	-1.45771E-04
Ag-fcc_a1	173.25	298.15	-12686.2	-8035.52	0.0251270	3.03702E-10	-9.84096E-05
Au-fcc_a1	127.05	298.15	-14158.6	-7702.16	0.00399439	-3.03981E-11	-1.14985E-06
Zn-hcp_a3	251.79	298.15	-12411.9	-8961.08	0.0919485	1.47137E-09	-4.17994E-04
Cd-hcp_a3	160.93	298.15	-15444.1	-8609.56	0.0917643	1.67170E-09	-4.38435E-04
Hg-rhombo_a10	55.363	200	-16031.5	-10050.4	-0.0437813	-2.41620E-09	3.77809E-04
B-beta_rhombo_B	1216.6	298.15	-1759.08	-16255.1	0.0121461	-1.85030E-12	2.41989E-06
Al-fcc_a1	329.56	298.15	-8437.64	-8676.15	0.0306683	4.14808E-10	-1.20157E-04
Ga-orthorhombic	246.4	298.15	-12142.7	-8798.22	0.0844341	1.78765E-09	-4.13421E-04
In-tetragonal_a6	83.16	298.15	-17188.3	-7672.15	-0.00241309	-3.97574E-11	3.54384E-05
Tl-hcp_a3	60.445	200	-13331.4	-7440.98	0.00150820	1.89647E-09	-9.03568E-05
C-hex_a9(graphite)	1717.1	298.15	-1712.07	-13723.2	0.362613	6.03075E-09	-1.68581E-03
Si-diamond_a4	496.65	298.15	-5608.21	-9397.17	0.0344888	6.55998E-10	-1.72822E-04
Ge-diamond_a4	287.98	298.15	-9269.48	-8350.18	0.0393997	8.44279E-10	-2.04327E-04
Sn-bct_a5	154	100	-7403.69	-8217.96	0.165492	6.48251E-08	-2.13202E-03
Pb-fcc_a1	80.85	298.15	-19320.1	-8198.50	0.0533286	8.82599E-10	-2.34318E-04
As-rhombo_a7	217.1	298.15	-10640.8	-8008.48	0.0151794	1.87854E-10	-5.85733E-05
Sb-rhombo_a7	162.5	298.15	-13572.3	-8079.96	0.0420057	8.00203E-10	-2.01951E-04
Bi-rhombo_a7	91.63	298.15	-16915.5	-7725.07	0.0163926	2.86831E-10	-7.17683E-05

experimental information to validate the parameter, b . The reason for a choice of T^4 [2], rather than T^2 [3] in the third term, is that the former one gives a better fit to the high-temperature heat-capacity data for a wide spectrum of pure elements, and, most importantly, it results in reasonable values for the parameter, a , while a term in

T^2 does not [2]. In spite of that, the parameter c is added for smooth continuation of C_p through the T_{lim} (the term cT^2 having zero value at 0 K).

From the expression for C_p , Eq. (1), the Gibbs energy at 10^5 Pa relative to the standard element reference state can be evaluated

by Chen and Sundman [2]:

$$G(T) = E_0 + \frac{3}{2}RT_E + 3RT \ln(1 - e^{-T_E/T}) - \frac{a}{2}T^2 - \frac{b}{20}T^5 - \frac{c}{6}T^3 \quad (2)$$

where E_0 is the total energy of a nonmagnetic structure of an element at 0 K relative to the standard element reference state, and the second term is the energy of zero-point lattice vibrations [4,5].

The condition for smooth connecting of the extended $G(T)$ function below a contact temperature T_{lim} , (usually, but not always, 298.15 K) to the valid $G(T)$ function (SGTE) above this temperature is the equality of their function values and values of their first derivative at T_{lim} . This ensures fluent connecting also for $S = dG/dT$ and for $H = G + TS$. Similarly, the condition for a smooth connection of heat capacity $C_p(T)$ function below and above T_{lim} is the equality of their function values and values of their first derivative at contact temperature T_{lim} . Therefore, formulas for calculation of E_0 , a , b , and c parameters for the Gibbs energy of elements in a non-magnetic state below T_{lim} , Eq. (2), are based on the solution of the system of Eqs. (3)–(6):

$$G(T_{\text{lim}}) = E_0 + \frac{3}{2}RT_E + 3RT_{\text{lim}} \ln(1 - e^{-T_E/T_{\text{lim}}}) - \frac{a}{2}T_{\text{lim}}^2 - \frac{b}{20}T_{\text{lim}}^5 - \frac{c}{6}T_{\text{lim}}^3 \quad (3)$$

$$\frac{dG}{dT}(T_{\text{lim}}) = 3R \ln(1 - e^{-T_E/T_{\text{lim}}}) - 3BR \frac{T_E}{T_{\text{lim}}} - aT_{\text{lim}} - \frac{b}{4}T_{\text{lim}}^4 - \frac{c}{2}T_{\text{lim}}^2 \quad (4)$$

$$C_p(T_{\text{lim}}) = 3CR \left(\frac{T_E}{T_{\text{lim}}}\right)^2 + aT_{\text{lim}} + bT_{\text{lim}}^4 + cT_{\text{lim}}^2 \quad (5)$$

where the $B = \frac{e^{-T_E/T_{\text{lim}}}}{1 - e^{-T_E/T_{\text{lim}}}}$ and $C = \frac{e^{T_E/T_{\text{lim}}}}{(e^{T_E/T_{\text{lim}}} - 1)^2}$ are introduced for simplification of further equations.

Subsequently

$$\frac{dC_p}{dT}(T_{\text{lim}}) = DER + a + 4bT_{\text{lim}}^3 + 2cT_{\text{lim}}, \quad (6)$$

where the DER term stands for the derivative of the first term of Eq. (5) i.e.

$$DER = -6AR \frac{T_E^2}{T^3} - 3AR \frac{T_E^3}{T^4} + 6R \frac{T_E^3}{T^4} \frac{e^{2T_E/T}}{(e^{T_E/T} - 1)^3}.$$

Solution of the system of linear equations (3)–(6) in unknowns a , b , c and E_0 is trivial (e.g. sequential elimination of unknowns a and c from Eqs. (4) to (6)) and final expressions for unknowns a , b , c , and E_0 are as follows:

$$b = \frac{4}{3T_{\text{lim}}^4} \left[3R \ln(1 - e^{-T_E/T_{\text{lim}}}) - 3BR \frac{T_E}{T_{\text{lim}}} + \frac{9}{2}CR \left(\frac{T_E}{T_{\text{lim}}}\right)^2 - \frac{1}{2} \left(\frac{dC_p}{dT}(T_{\text{lim}})\right) T_{\text{lim}} - \frac{1}{2}DER T_{\text{lim}} - \frac{dG}{dT}(T_{\text{lim}}) - \frac{3}{2}C_p(T_{\text{lim}}) \right] \quad (7)$$

$$c = \frac{1}{T_{\text{lim}}^2} \left[-C_p(T_{\text{lim}}) + 3CR \left(\frac{T_E}{T_{\text{lim}}}\right)^2 + \left(\frac{dC_p}{dT}(T_{\text{lim}})\right) T_{\text{lim}} - DER T_{\text{lim}} - 3bT_{\text{lim}}^4 \right] \quad (8)$$

$$a = \frac{dC_p}{dT}(T_{\text{lim}}) - DER - 4bT_{\text{lim}}^3 - 2cT_{\text{lim}} \quad (9)$$

$$E_0 = G(T_{\text{lim}}) - \frac{3}{2}RT_E - 3RT_{\text{lim}} \ln(1 - e^{-T_E/T_{\text{lim}}}) + \frac{a}{2}T_{\text{lim}}^2 + \frac{b}{20}aT_{\text{lim}}^5 + \frac{c}{6}T_{\text{lim}}^3 \quad (10)$$

where T_{lim} is the mentioned contact temperature (usually, but not always, 298.15 K), for which the extension of unary data is connected to the SGTE unary data [1]. $G(T_{\text{lim}})$, $dG/dT(T_{\text{lim}})$, $C_p(T_{\text{lim}})$ and $dC_p/dT(T_{\text{lim}})$ represent function values and values of first derivative of respective SGTE polynomials at T_{lim} . T_E is the Einstein temperature. (Expressions $(1 - e^{-T_E/T_{\text{lim}}})$, $(1 - e^{-T_E/T_{\text{lim}}})$ and $\ln(1 - e^{-T_E/T_{\text{lim}}})$ can be evaluated in some softwares, e.g. Thermocalc, by using of FUNCTION statements in advance.)

3. A case study

The Einstein function used in Eq. (1), requires a value for the Einstein temperature. The Einstein temperature is related to the Debye temperature as $T_E \cong 0.777T_D$ [5]. The Debye temperature of interest is the low temperature limit of the Debye temperature, required for the purpose of extending the unary Gibbs energy data. This low temperature limit of Debye temperature for an ideal solid, $T_D(-3)$, can be obtained from either low temperature elastic constants (theoretically) or from heat capacity data (experimentally). $T_D(-3)$ means Debye temperature from the (-3) moment of phonon frequencies [6]. At temperatures $T \leq T_D$, anharmonic effects are still rather small, and therefore the low temperature limit of the Debye temperature describes well the behavior of the heat capacity of elements in the low temperature region.

The values of Debye temperature, $T_D(-3)$, were taken from the publications [6,7], for elements in their thermodynamically stable structures. Some values of T_D for unstable structures of elements are added from literature [2] for Fe, from [6] for Ti, Zr and Hf, and from [8] for V on the empirical basis described below. The Einstein temperatures T_E were obtained through use of the equation $T_E \cong 0.777T_D$ [5].

The values of parameters a , b , c and E_0 in Eq. (2), representing the extension of the Gibbs energy of SGTE data [1] to zero Kelvin for this case are given in Table 1. For dynamically unstable structures (e.g. V-hcp, Ti, Zr, Hf-bcc), it is impossible to calculate $T_D(-3)$. In this case the value of $T_D(0)$ can be calculated as the high temperature limit of T_D . The exact relation between $T_D(-3)$ and $T_D(0)$ cannot be found theoretically, but in [6] the empirical relation $T_D(-3) = T_D(0)/0.94$ was published for Ti, Zr, and Hf. Data found in this empirical way are also included in the Table 1.

An excel file for the calculation of parameters a , b , c , and E_0 is attached as supplementary material for future use when further Debye temperatures are available. Data in the form of G-HSER are added in Appendix together with the graphical pictures of extension of $G(T)$ and C_p curves to zero Kelvin temperature for all elements in Table 1. It is obvious, that the simple extrapolation of $G(T)$ values from [1] below the contact temperature T_{lim} fails close to zero Kelvin because of the term with negative exponent at T . Using the Einstein formula in the expression for $G(T)$ cures this problem and the smooth link to the SGTE data at the temperature T_{lim} makes it possible to use the existing SGTE data without change. For low values of Debye temperature, the continuation of C_p -curve in some cases (e.g. Ba, Cd, Pb, and in smaller extent in Sr, Zn, Sb, La, Co, Hf-bcc, Zr-bcc, Fe-bcc) exhibits extremum in continuation from SGTE values to the Einstein function values. Reason for it may be in anharmonicity contribution to C_p or more probably in the fact that some SGTE-data close to (but above) T_{lim} are not fully consistent with the low temperature information represented by the Debye temperature. Such a behavior may indicate that T_{lim} should be set to higher temperatures (in the case of Ba shift of T_{lim} to about 350 K cure this problem, Fig. 2b), but in some cases (Cd, Pb) the shift of T_{lim} to the melting temperature of the respective element is not enough for removing the extremum (Fig. 15b, Fig. 17b). Anyway, Gibbs energy continues fluently to zero Kelvin also in such cases.

4. Conclusion

Knowledge of the Debye (Einstein) temperature at low temperatures makes it possible to obtain a realistic extension of Gibbs energy function as the temperature falls towards 0 K. For the stable structures, the low temperature limit of the Debye temperature, $T_D(-3)$, can be calculated on the basis of elastic constants or experimentally by measurement of the heat capacity in the low temperature region. For dynamically unstable structures, the high temperature limit of Debye temperature $T_D(0)$ can be calculated. The relation between $T_D(0)$ and $T_D(-3)$ cannot be found theoretically, but an empirical relation can be validated and values of $T_D(-3)$ can be than used for the extension of SGTE unary data to zero Kelvin temperature [2,6,8].

Acknowledgement

Financial support of the grants GACR P108/10/1908, MSMT of MSM0021622410 and of the Project “CEITEC MU” (CZ.1.05/1.1.00/02.0068) from the European Regional Development Fund is gratefully acknowledged.

Appendix A

Table A.1 contains extended Gibbs energy data (Eq. (2)) in the form of G-HSER for elements listed in Table 1.

(In some softwares, the argument of logarithmic function should be calculated first).

Figs. 1–18 illustrate connection of $G(T)$ and $C_p(T)$ of extended functions with SGTE functions. Red color: extended functions, blue color: SGTE functions.

Table A.1

Li-BCC_A2 (0 < T < 200.00)	$-7962.63 + (3/2) (8.31451)(264.88) + 3(8.31451)T \ln(1 - \exp(-264.88/T)) - (0.0112590/2)T^2 - (-1.53294E - 04/6)T^3 - (2.37900E - 09/20)T^5$
Na-BCC_A2 (0 < T < 200.00)	$-8016.02 + (3/2) (8.31451) (121.66) + 3(8.31451)T \ln(1 - \exp(-121.66/T)) - (0.0257557/2)T^2 - (-1.50434E - 04/6)T^3 - (1.66252E - 09/20)T^5$
K-BCC_A2 (0 < T < 200.00)	$-7988.74 + (3/2) (8.31451) (70.07) + 3(8.31451)T \ln(1 - \exp(-70.07/T)) - (0.0194388/2)T^2 - (-1.17296E - 04/6)T^3 - (1.81586E - 09/20)T^5$
Rb-BCC_A2 (0 < T < 200.00)	$-8042.92 + (3/2) (8.31451) (43.12) + 3(8.31451)T \ln(1 - \exp(-43.12/T)) - (0.0120858/2)T^2 - (-4.12642E - 05/6)T^3 - (1.12973E - 09/20)T^5$
Cs-BCC_A2 (0 < T < 200.00)	$-8041.85 + (3/2) (8.31451) (29.26) + 3(8.31451)T \ln(1 - \exp(-29.26/T)) - (-0.0127130/2)T^2 - (1.81210E - 04/6)T^3 - (-1.14058E - 09/20)T^5$
Be-HCP_A3 (0 < T < 298.15)	$-15659.3 + (3/2) (8.31451) (1108.8) + 3(8.31451)T \ln(1 - \exp(-1108.8/T)) - (0.00610649/2)T^2 - (1.49314E - 04/6)T^3 - (-9.49706E - 10/20)T^5$
Mg-HCP_A3 (0 < T < 298.15)	$-8833.11 + (3/2) (8.31451) (308) + 3(8.31451)T \ln(1 - \exp(-308/T)) - (0.0539769/2)T^2 - (-2.30295E - 04/6)T^3 - (8.10174E - 10/20)T^5$
Ca-FCC_A1 (0 < T < 298.15)	$-8060.32 + (3/2) (8.31451) (177.1) + 3(8.31451)T \ln(1 - \exp(-177.1/T)) - (0.0169877/2)T^2 - (-4.22890E - 05/6)T^3 - (5.21547E - 11/20)T^5$
Sr-FCC_A1 (0 < T < 298.15)	$-8186.46 + (3/2) (8.31451) (113.2) + 3(8.31451)T \ln(1 - \exp(-113.2/T)) - (0.0457474/2)T^2 - (-1.94534E - 04/6)T^3 - (7.33730E - 10/20)T^5$
Ba-BCC_A2 (0 < T < 298.15)	$-7911.40 + (3/2) (8.31451) (84.7) + 3(8.31451)T \ln(1 - \exp(-84.7/T)) - (0.0684640/2)T^2 - (-4.52605E - 04/6)T^3 - (2.92889E - 09/20)T^5$
Sc-HCP_A3 (0 < T < 298.15)	$-8706.90 + (3/2) (8.31451) (277.2) + 3(8.31451)T \ln(1 - \exp(-277.2/T)) - (0.0469648/2)T^2 - (-1.83312E - 04/6)T^3 - (5.81278E - 10/20)T^5$
Y-HCP_A3 (0 < T < 298.15)	$-8431.21 + (3/2) (8.31451) (184.8) + 3(8.31451)T \ln(1 - \exp(-184.8/T)) - (0.0482034/2)T^2 - (-1.89282E - 04/6)T^3 - (6.10041E - 10/20)T^5$
La-DHCP (0 < T < 298.15)	$-8252.86 + (3/2) (8.31451) (109.34) + 3(8.31451)T \ln(1 - \exp(-109.34/T)) - (0.0446360/2)T^2 - (-1.70763E - 04/6)T^3 - (5.46438E - 10/20)T^5$
Ti-HCP_A3 (0 < T < 298.15)	$-8861.83 + (3/2) (8.31451) (323.4) + 3(8.31451)T \ln(1 - \exp(-323.4/T)) - (0.0441439/2)T^2 - (-1.74763E - 04/6)T^3 - (6.18793E - 10/20)T^5$
Ti-BCC_A2 (0 < T < 298.15)	$-1800.32 + (3/2) (8.31451) (220.22) + 3(8.31451)T \ln(1 - \exp(-220.22/T)) - (0.0210120/2)T^2 - (-5.16686E - 05/6)T^3 - (5.66515E - 11/20)T^5$
Ti-FCC_A1 (0 < T < 298.15)	$-2091.78 + (3/2) (8.31451) (255.64) + 3(8.31451)T \ln(1 - \exp(-255.64/T)) - (0.00378822/2)T^2 - (9.79921E - 07/6)T^3 - (5.88120E - 11/20)T^5$
Zr-HCP_A3 (0 < T < 130.00)	$-8313.16 + (3/2) (8.31451) (224.07) + 3(8.31451)T \ln(1 - \exp(-224.07/T)) - (0.0806209/2)T^2 - (-7.48881E - 04/6)T^3 - (1.31270E - 08/20)T^5$
Zr-BCC_A3 (0 < T < 298.15)	$-674.409 + (3/2) (8.31451) (147.07) + 3(8.31451)T \ln(1 - \exp(-147.07/T)) - (0.0328312/2)T^2 - (-1.48985E - 04/6)T^3 - (5.42043E - 10/20)T^5$
Zr-FCC_A1 (0 < T < 298.15)	$177.008 + (3/2) (8.31451) (144.76) + 3(8.31451)T \ln(1 - \exp(-144.76/T)) - (-0.0346112/2)T^2 - (1.90319E - 04/6)T^3 - (-6.41923E - 10/20)T^5$
Hf-HCP_A3 (0 < T < 298.15)	$-8421.33 + (3/2) (8.31451) (194.04) + 3(8.31451)T \ln(1 - \exp(-194.04/T)) - (0.0557452/2)T^2 - (-2.42998E - 04/6)T^3 - (8.33639E - 10/20)T^5$
Hf-BCC_A2 (0 < T < 298.15)	$4357.63 + (3/2) (8.31451) (126.28) + 3(8.31451)T \ln(1 - \exp(-126.28/T)) - (0.0386224/2)T^2 - (-1.73357E - 04/6)T^3 - (6.09732E - 10/20)T^5$
Hf-FCC_A1 (0 < T < 298.15)	$1905.99 + (3/2) (8.31451) (158.62) + 3(8.31451)T \ln(1 - \exp(-158.62/T)) - (0.0342399/2)T^2 - (-1.44210E - 04/6)T^3 - (4.98051E - 10/20)T^5$
V-BCC_A2 (0 < T < 298.15)	$-8475.16 + (3/2) (8.31451) (292.6) + 3(8.31451)T \ln(1 - \exp(-292.6/T)) - (0.0327470/2)T^2 - (-1.41840E - 04/6)T^3 - (5.26993E - 10/20)T^5$
V-FCC_A1 (0 < T < 298.15)	

(continued on next page)

Table A.1 (continued)

$-997.557 + (3/2) (8.31451) (306.46) + 3(8.31451)T \ln(1 - \exp(-306.46/T)) - (0.0255088/2)T^2 - (-9.96915E - 05/6)T^3 - (3.48182E - 10/20)T^5$
V-HCP_A3 (0 < T < 298.15)
$-4580.80 + (3/2) (8.31451) (318.78) + 3(8.31451)T \ln(1 - \exp(-318.78/T)) - (0.0258721/2)T^2 - (-9.62630E - 05/6)T^3 - (3.1635E - 10/20)T^5$
Nb-BCC_A2 (0 < T < 298.15)
$-7944.08 + (3/2) (8.31451) (211.75) + 3(8.31451)T \ln(1 - \exp(-211.75/T)) - (0.0196347/2)T^2 - (-1.01055E - 04/6)T^3 - (4.61047E - 10/20)T^5$
Ta-BCC_A2 (0 < T < 298.15)
$-8101.73 + (3/2) (8.31451) (184.8) + 3(8.31451)T \ln(1 - \exp(-184.8/T)) - (0.0295502/2)T^2 - (-1.21167E - 04/6)T^3 - (3.93215E - 10/20)T^5$
Cr-BCC_A2 (0 < T < 298.15)
$-9933.46 + (3/2) (8.31451) (485.1) + 3(8.31451)T \ln(1 - \exp(-485.1/T)) - (0.0488572/2)T^2 - (-1.60734E - 04/6)T^3 - (3.86670E - 10/20)T^5$
Mo-BCC_A2 (0 < T < 298.15)
$-8861.12 + (3/2) (8.31451) (346.5) + 3(8.31451)T \ln(1 - \exp(-346.5/T)) - (0.0428376/2)T^2 - (-1.78282E - 04/6)T^3 - (5.86744E - 10/20)T^5$
W-BCC_A2 (0 < T < 298.15)
$-8790.52 + (3/2) (8.31451) (308) + 3(8.31451)T \ln(1 - \exp(-308/T)) - (0.0562411/2)T^2 - (-2.47579E - 04/6)T^3 - (8.30265E - 10/20)T^5$
Mn-BCC_A12 (0 < T < 298.15)
$-8968.11 + (3/2) (8.31451) (315.7) + 3(8.31451)T \ln(1 - \exp(-315.7/T)) - (0.0477805/2)T^2 - (-1.79805E - 04/6)T^3 - (6.66697E - 10/20)T^5$
Tc-HCP_A3 (0 < T < 298.15)
$-9735.06 + (3/2) (8.31451) (388.08) + 3(8.31451)T \ln(1 - \exp(-388.08/T)) - (0.0942685/2)T^2 - (-4.00134E - 04/6)T^3 - (1.31947E - 09/20)T^5$
Re-HCP_A3 (0 < T < 298.15)
$-9466.06 + (3/2) (8.31451) (331.1) + 3(8.31451)T \ln(1 - \exp(-331.1/T)) - (0.0939376/2)T^2 - (-3.93606E - 04/6)T^3 - (1.23562E - 09/20)T^5$
Fe-BCC_A2 (0 < T < 298.15)
$22.9525 + (3/2) (8.31451) (308.77) + 3(8.31451)T \ln(1 - \exp(-308.77/T)) - (0.0963983/2)T^2 - (-4.61144E - 04/6)T^3 - (1.75273E - 09/20)T^5$
Fe-FCC_A1 (0 < T < 298.15)
$-1141.91 + (3/2) (8.31451) (308.77) + 3(8.31451)T \ln(1 - \exp(-308.77/T)) - (0.0822187/2)T^2 - (-3.70372E - 04/6)T^3 - (1.36384E - 09/20)T^5$
Ru-HCP_A3 (0 < T < 298.15)
$-10149.2 + (3/2) (8.31451) (462) + 3(8.31451)T \ln(1 - \exp(-462/T)) - (0.0826785/2)T^2 - (-3.20209E - 04/6)T^3 - (9.22441E - 10/20)T^5$
Os-HCP_A3 (0 < T < 298.15)
$-9711.29 + (3/2) (8.31451) (385) + 3(8.31451)T \ln(1 - \exp(-385/T)) - (0.0857969/2)T^2 - (-3.38392E - 04/6)T^3 - (9.43881E - 10/20)T^5$
Co-HCP_A3 (0 < T < 298.15)
$-1070.33 + (3/2) (8.31451) (342.65) + 3(8.31451)T \ln(1 - \exp(-342.65/T)) - (0.109565/2)T^2 - (-4.92418E - 04/6)T^3 - (1.73121E - 09/20)T^5$
Rh-FCC_A1 (0 < T < 298.15)
$-9434.27 + (3/2) (8.31451) (369.6) + 3(8.31451)T \ln(1 - \exp(-369.6/T)) - (0.0729270/2)T^2 - (-2.97118E - 04/6)T^3 - (9.59375E - 10/20)T^5$
Ir-FCC_A1 (0 < T < 298.15)
$-9287.76 + (3/2) (8.31451) (323.4) + 3(8.31451)T \ln(1 - \exp(-323.4/T)) - (0.0816946/2)T^2 - (-3.36578E - 04/6)T^3 - (1.01455E - 09/20)T^5$
Ni-FCC_A1 (0 < T < 298.15)
$-7481.20 + (3/2) (8.31451) (346.5) + 3(8.31451)T \ln(1 - \exp(-346.5/T)) - (0.0734882/2)T^2 - (-2.98323E - 04/6)T^3 - (9.20651E - 10/20)T^5$
Pd-FCC_A1 (0 < T < 298.15)
$-8108.69 + (3/2) (8.31451) (210.98) + 3(8.31451)T \ln(1 - \exp(-210.98/T)) - (0.0287734/2)T^2 - (-1.35483E - 04/6)T^3 - (5.98583E - 10/20)T^5$
Pt-FCC_A1 (0 < T < 298.15)
$-8152.49 + (3/2) (8.31451) (184.8) + 3(8.31451)T \ln(1 - \exp(-184.8/T)) - (0.0279310 / 2)T^2 - (-1.03994E - 04/6)T^3 - (3.31714E - 10/20)T^5$
Cu-FCC_A1 (0 < T < 298.15)
$-8342.85 + (3/2) (8.31451) (264.11) + 3(8.31451)T \ln(1 - \exp(-264.11/T)) - (0.0328876/2)T^2 - (-1.45771E - 04/6)T^3 - (5.34699E - 10/20)T^5$
Ag-FCC_A1 (0 < T < 298.15)
$-8035.52 + (3/2) (8.31451) (173.25) + 3(8.31451)T \ln(1 - \exp(-173.25/T)) - (0.0251270/2)T^2 - (-9.84096E - 05/6)T^3 - (3.03702E - 10/20)T^5$
Au-FCC_A1 (0 < T < 298.15)
$-7702.16 + (3/2) (8.31451) (127.05) + 3(8.31451)T \ln(1 - \exp(-127.05/T)) - (0.00399439/2)T^2 - (-1.14985E - 06/6)T^3 - (-3.03981E - 11/20)T^5$
Zn-HCP_A3 (0 < T < 298.15)
$-8961.08 + (3/2) (8.31451) (251.79) + 3(8.31451)T \ln(1 - \exp(-251.79/T)) - (0.0919485/2)T^2 - (-4.17994E - 04/6)T^3 - (1.47137E - 09/20)T^5$
Cd-HCP_A3 (0 < T < 298.15)
$-8609.56 + (3/2) (8.31451) (160.93) + 3(8.31451)T \ln(1 - \exp(-160.93/T)) - (0.0917643/2)T^2 - (-4.38435E - 04/6)T^3 - (1.67170E - 09/20)T^5$
Hg-RHOMBO_A10 (0 < T < 200)
$-10050.4 + (3/2) (8.31451) (55.363) + 3(8.31451)T \ln(1 - \exp(-55.363/T)) - (-0.0437813/2)T^2 - (3.77809E - 04/6)T^3 - (-2.41620E - 09/20)T^5$
B-BETA_RHOMBO_B (0 < T < 298.15)
$-16255.1 + (3/2) (8.31451) (1216.6) + 3(8.31451)T \ln(1 - \exp(-1216.6/T)) - (0.0121461/2)T^2 - (2.41989E - 06)T^3 - (-1.85030E - 12/20)T^5$
Al-FCC_A1 (0 < T < 298.15)
$-8676.15 + (3/2) (8.31451) (329.56) + 3(8.31451)T \ln(1 - \exp(-329.56/T)) - (0.0306683/2)T^2 - (-1.20157E - 04/6)T^3 - (4.14808E - 10/20)T^5$
Ga-ORTHORHOMBIC (0 < T < 298.15)
$-8798.22 + (3/2) (8.31451) (246.4) + 3(8.31451)T \ln(1 - \exp(-246.4/T)) - (0.0844341/2)T^2 - (-4.13421E - 04/6)T^3 - (1.78765E - 09/20)T^5$
In-TETRAGONAL_A6 (0 < T < 298.15)
$-7672.15 + (3/2) (8.31451) (83.16) + 3(8.31451)T \ln(1 - \exp(-83.16/T)) - (-0.00241390/2)T^2 - (3.54384E - 05/6)T^3 - (-3.97574E - 11/20)T^5$
Tl-HCP_A3 (0 < T < 200)
$-7440.98 + (3/2) (8.31451) (60.445) + 3(8.31451)T \ln(1 - \exp(-60.445/T)) - (0.00150820/2)T^2 - (-9.03568E - 05/6)T^3 - (1.89647E - 09/20)T^5$
C-HEXAGONAL_A9 (graphite) (0 < T < 298.15)
$-13723.16 + (3/2) (8.31451) (1717.1) + 3(8.31451)T \ln(1 - \exp(-1717.1/T)) - (0.362613/2)T^2 - (-1.68581E - 03/6)T^3 - (6.03075E - 09/20)T^5$
Si-DIAMOND_A4 (0 < T < 298.15)
$-9397.17 + (3/2) (8.31451) (496.65) + 3(8.31451)T \ln(1 - \exp(-496.65/T)) - (0.0344888/2)T^2 - (-1.72822E - 04/6)T^3 - (6.55998E - 10/20)T^5$

(continued on next page)

Table A.1 (continued)

Ge-DIAMOND_A4 ($0 < T < 298.15$)	$-8350.18 + (3/2)(8.31451)(287.98) + 3(8.31451)T \ln(1 - \exp(-287.98/T)) - (0.0393973/2)T^2 - (-2.04327E - 04/6)T^3 - (8.44279E - 10/20)T^5$
Sn-BCT_A5 ($0 < T < 100$)	$-8217.96 + (3/2)(8.31451)(154) + 3(8.31451)T \ln(1 - \exp(-154/T)) - (0.165492/2)T^2 - (-2.13202E - 03/6)T^3 - (6.48250E - 08/20)T^5$
Pb-FCC_A1 ($0 < T < 298.15$)	$-8198.50 + (3/2)(8.31451)(80.85) + 3(8.31451)T \ln(1 - \exp(-80.85/T)) - (0.0533286/2)T^2 - (-2.34318E - 04/6)T^3 - (8.82599E - 10/20)T^5$
As-RHOMBO_A7 ($0 < T < 298.15$)	$-8008.48 + (3/2)(8.31451)(217.1) + 3(8.31451)T \ln(1 - \exp(-217.1/T)) - (0.0151794/2)T^2 - (-5.85733E - 05/6)T^3 - (1.87854E - 10/20)T^5$
Sb-RHOMBO_A7 ($0 < T < 298.15$)	$-8079.96 + (3/2)(8.31451)(162.5) + 3(8.31451)T \ln(1 - \exp(-162.5/T)) - (0.0420057/2)T^2 - (-2.01951E - 04/6)T^3 - (8.00203E - 10/20)T^5$
Bi-RHOMBO_A7 ($0 < T < 298.15$)	$-7725.07 + (3/2)(8.31451)(91.63) + 3(8.31451)T \ln(1 - \exp(-91.63/T)) - (0.0163926/2)T^2 - (-7.17683E - 05/6)T^3 - (2.86831E - 10/20)T^5$

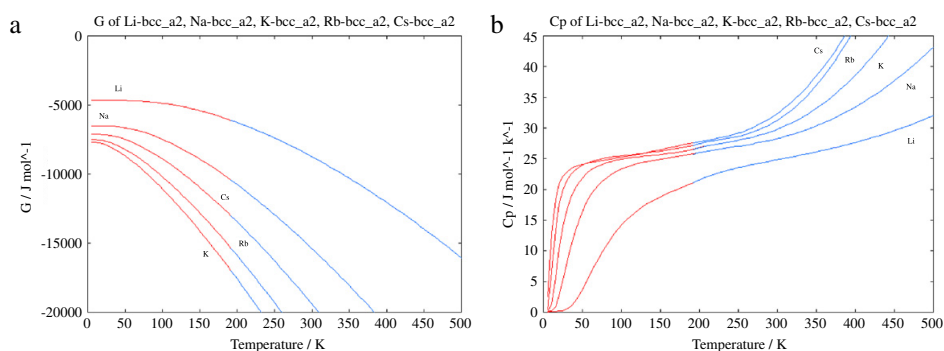


Fig. 1. Temperature dependence of Gibbs energy (a) and heat capacity (b) for extended and SGTE functions for elements Li, Na, K, Rb, Cs (Color online).

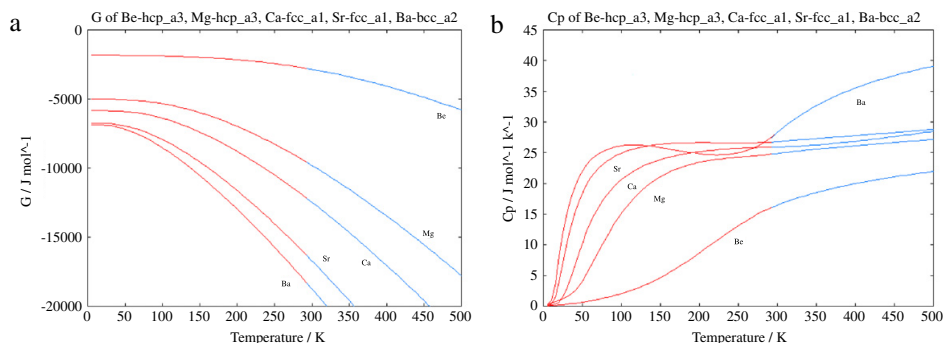


Fig. 2. Temperature dependence of Gibbs energy (a) and heat capacity (b) for extended and SGTE functions for elements Be, Mg, Ca, Sr, Ba (Color online).

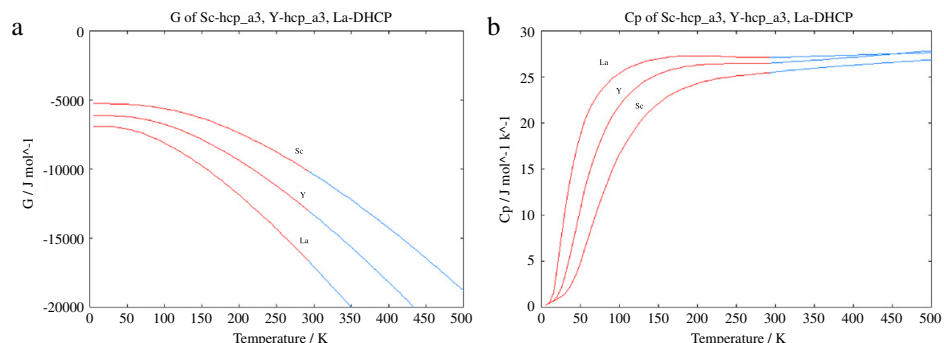


Fig. 3. Temperature dependence of Gibbs energy (a) and heat capacity (b) for extended and SGTE functions for elements La, Y, Sc (Color online).

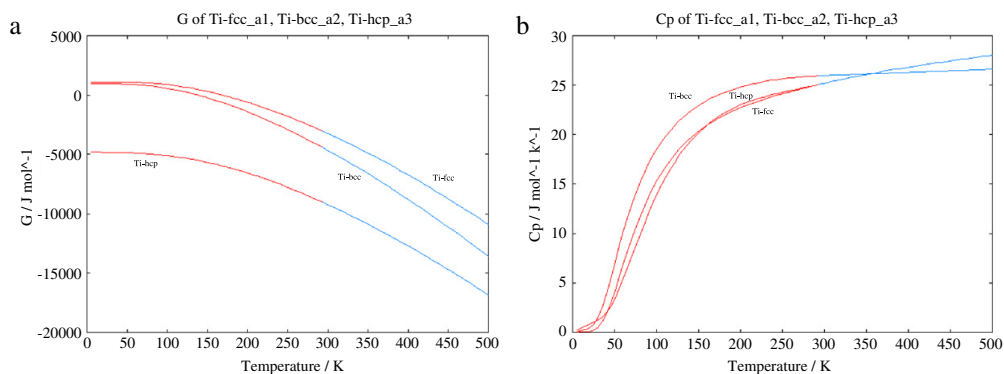


Fig. 4. Temperature dependence of Gibbs energy (a) and heat capacity (b) for extended and SGTE functions for element Ti in hcp, bcc and fcc structures (Color online).

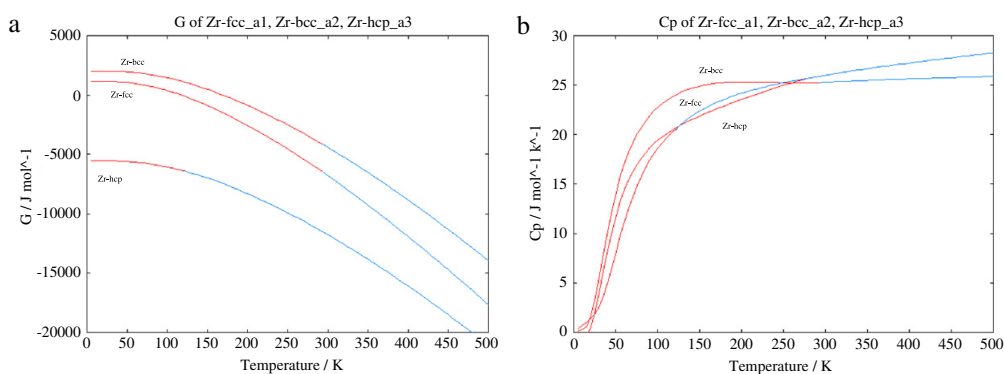


Fig. 5. Temperature dependence of Gibbs energy (a) and heat capacity (b) for extended and SGTE functions for element Zr in hcp, bcc and fcc structures (Color online).

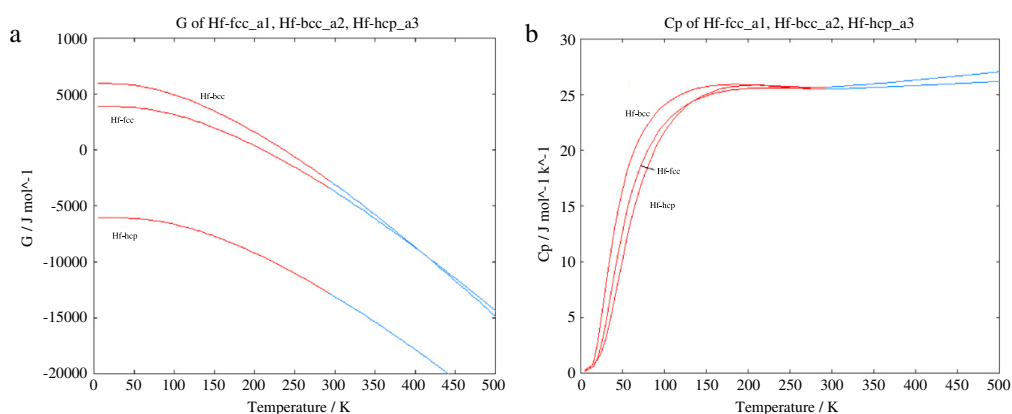


Fig. 6. Temperature dependence of Gibbs energy (a) and heat capacity (b) for extended and SGTE functions for element Hf in hcp, bcc and fcc structures (Color online).

44

J. Vřešťál et al. / CALPHAD: Computer Coupling of Phase Diagrams and Thermochemistry 37 (2012) 37–48

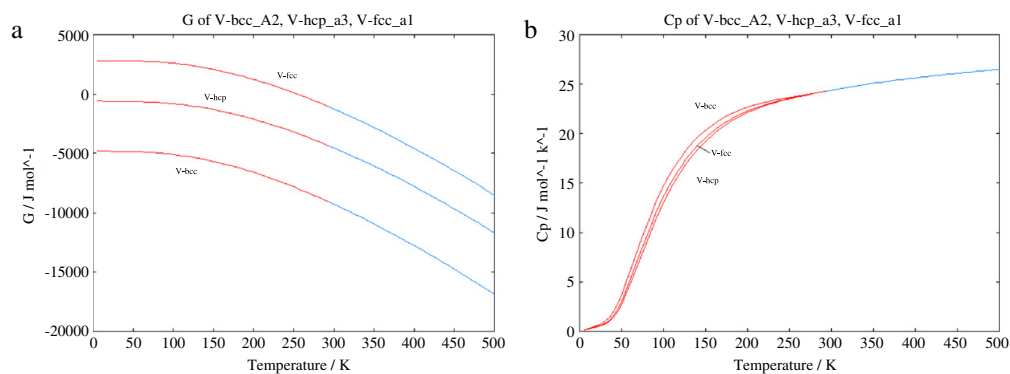


Fig. 7. Temperature dependence of Gibbs energy (a) and heat capacity (b) for extended and SGTE functions for element V in hcp, bcc and fcc structures (Color online).

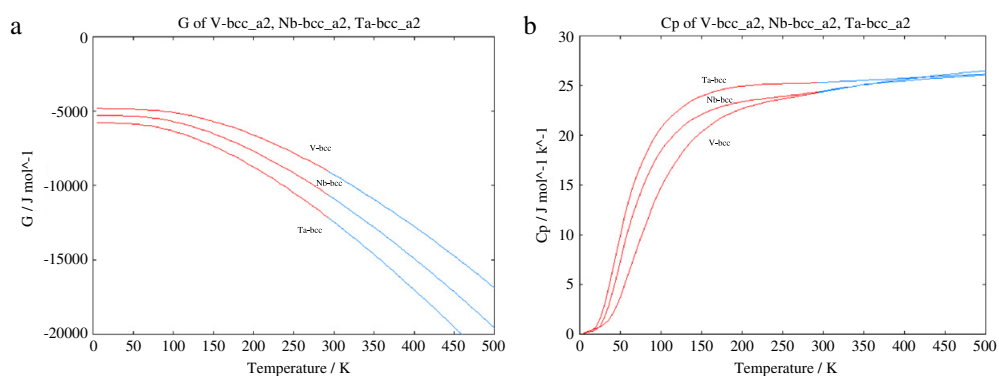


Fig. 8. Temperature dependence of Gibbs energy (a) and heat capacity (b) for extended and SGTE functions for elements V, Nb, Ta (Color online).

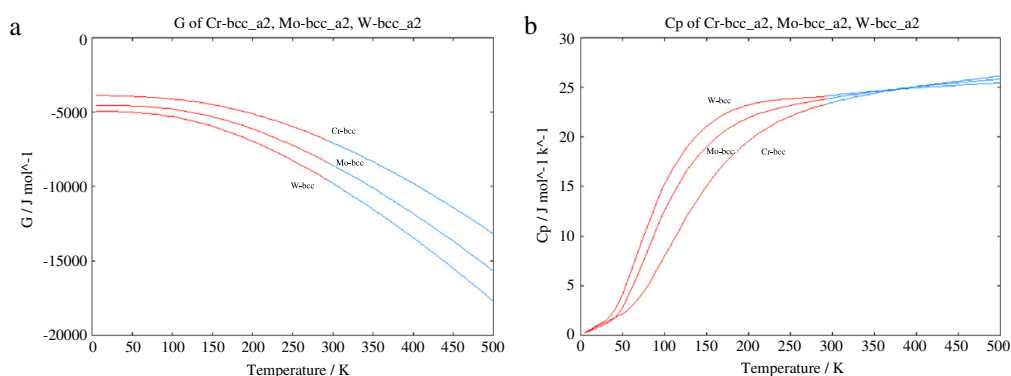


Fig. 9. Temperature dependence of Gibbs energy (a) and heat capacity (b) for extended and SGTE functions for elements Cr, Mo, W (Color online).

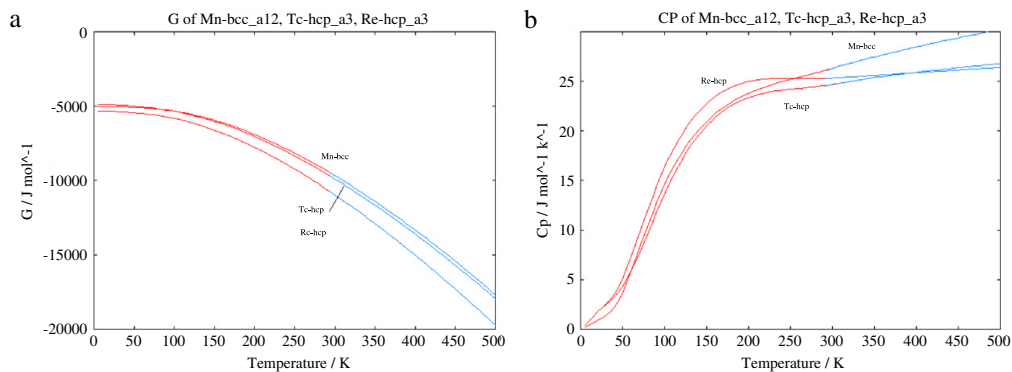


Fig. 10. Temperature dependence of Gibbs energy (a) and heat capacity (b) for extended and SGTE functions for elements Mn, Tc, Re (Color online).

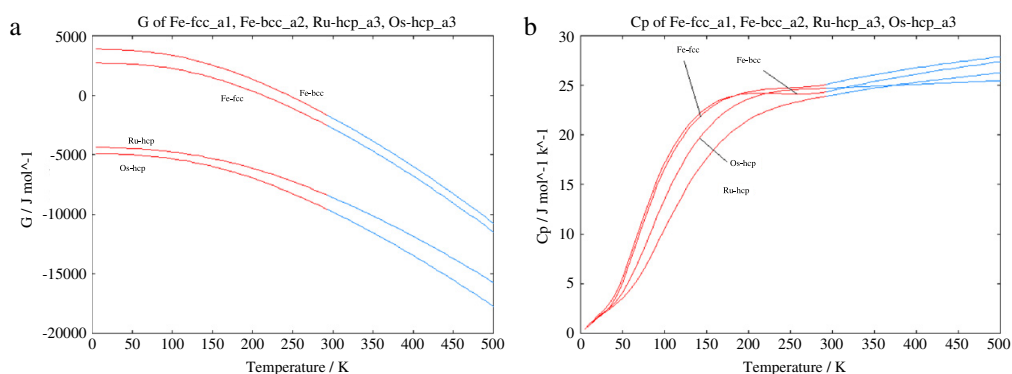


Fig. 11. Temperature dependence of Gibbs energy (a) and heat capacity (b) for extended and SGTE functions for elements Ru, Os, and Fe in bcc and fcc structures (Color online).

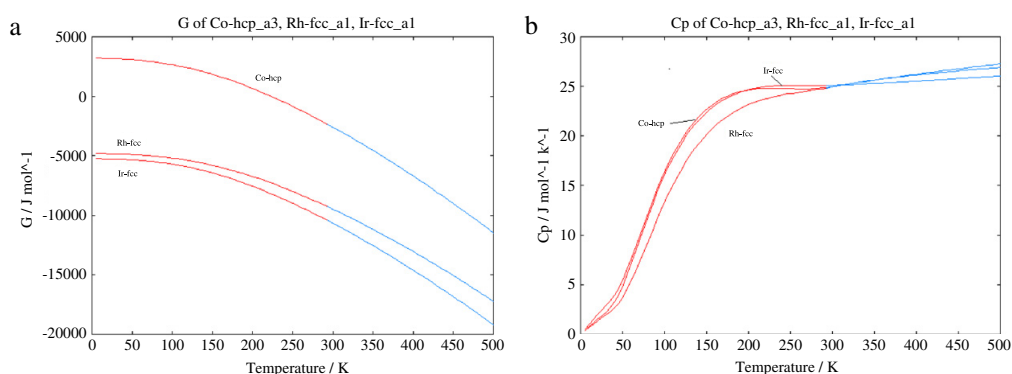


Fig. 12. Temperature dependence of Gibbs energy (a) and heat capacity (b) for extended and SGTE functions for elements Co, Ir, Rh (Color online).

46

J. Vřešťál et al. / CALPHAD: Computer Coupling of Phase Diagrams and Thermochemistry 37 (2012) 37–48

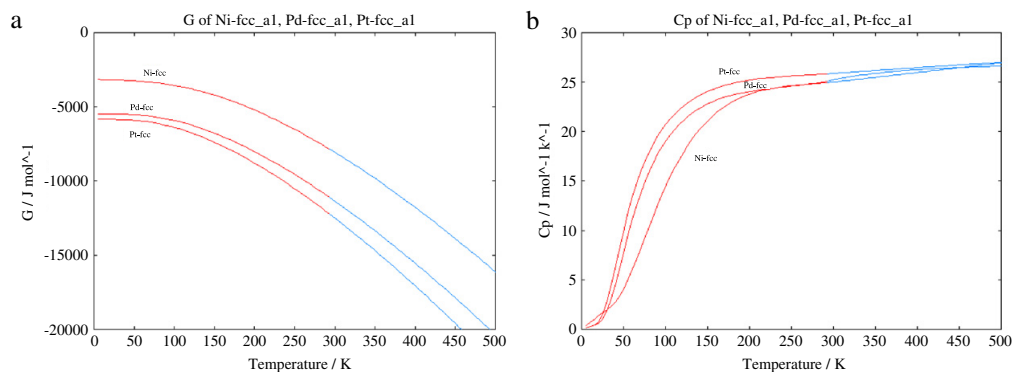


Fig. 13. Temperature dependence of Gibbs energy (a) and heat capacity (b) for extended and SGTE functions for elements Ni, Pd, Pt (Color online).

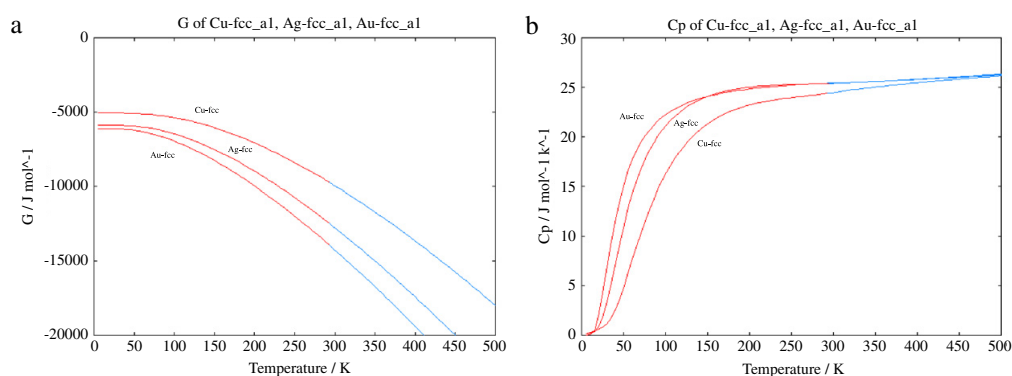


Fig. 14. Temperature dependence of Gibbs energy (a) and heat capacity (b) for extended and SGTE functions for elements Cu, Ag, Au (Color online).

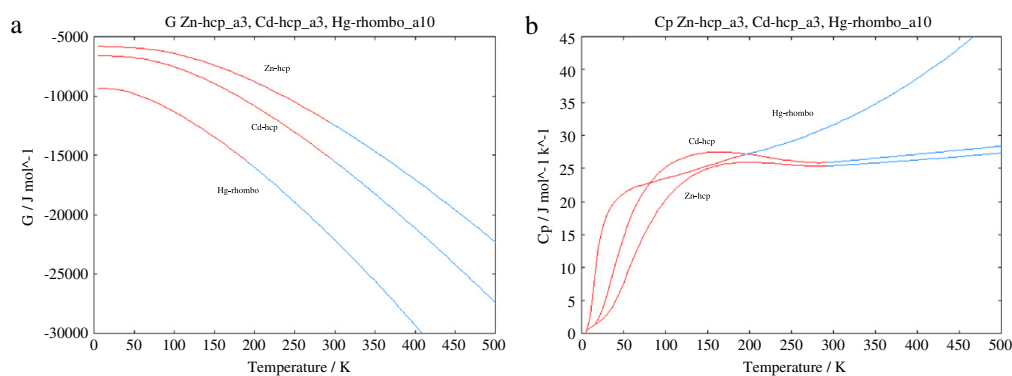


Fig. 15. Temperature dependence of Gibbs energy (a) and heat capacity (b) for extended and SGTE functions for elements Zn, Cd, Hg (Color online).

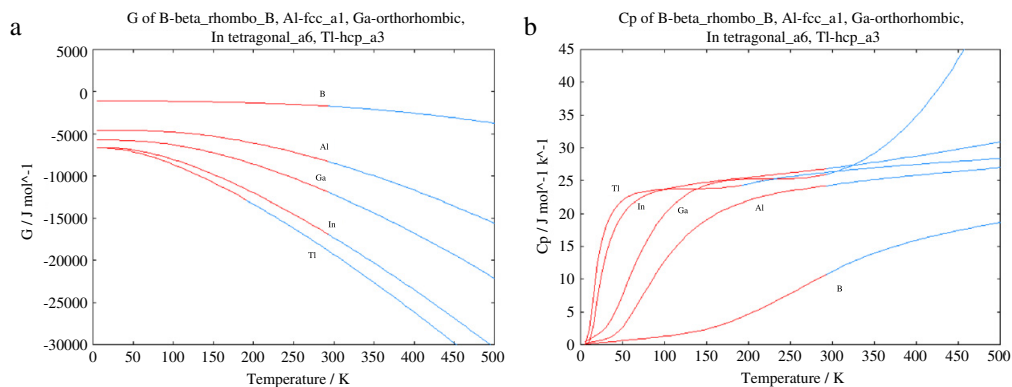


Fig. 16. Temperature dependence of Gibbs energy (a) and heat capacity (b) for extended and SGTE functions for elements B, Al, Ga, In, Tl (Color online).

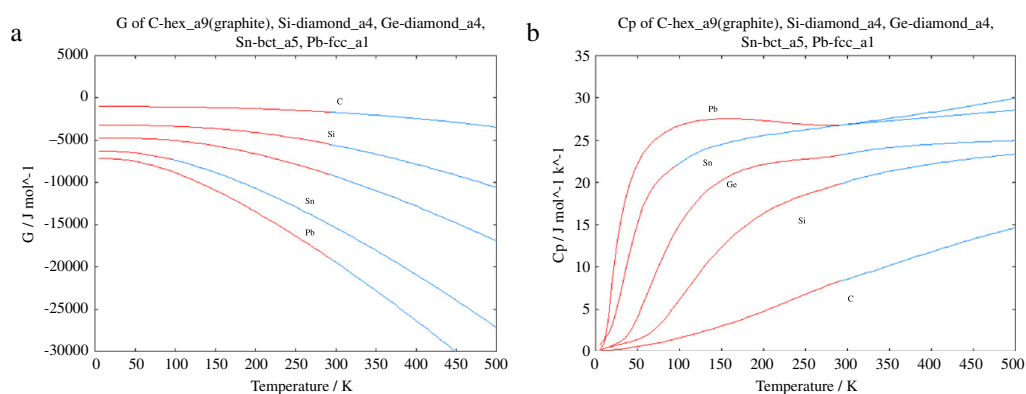


Fig. 17. Temperature dependence of Gibbs energy (a) and heat capacity (b) for extended and SGTE functions for elements C, Si, Ge, Sn, Pb (Color online).

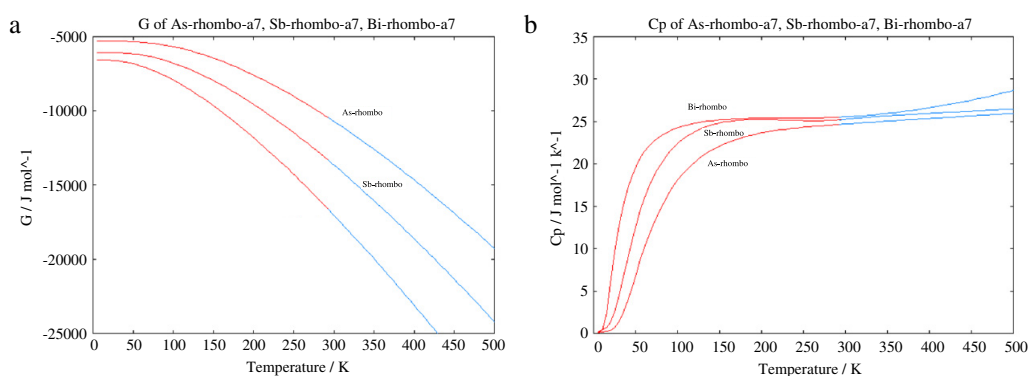


Fig. 18. Temperature dependence of Gibbs energy (a) and heat capacity (b) for extended and SGTE functions for elements As, Sb, Bi (Color online).

Appendix B. Supplementary data

Supplementary material related to this article can be found online at doi:[10.1016/j.calphad.2012.01.003](https://doi.org/10.1016/j.calphad.2012.01.003).

References

- [1] A.T. Dinsdale, CALPHAD 15 (1991) 317.
- [2] Q. Chen, B. Sundman, J. Phase Equilib. 22 (2001) 631.
- [3] M.W. Chase, I. Ansara, A. Dinsdale, G. Eriksson, G. Grimvall, L. Hoglund, H. Yokokawa, CALPHAD 19 (1995) 437.
- [4] M. Born, K. Huang, Dynamical Theory of Crystal Lattices, Oxford University Press, Oxford, UK, 1954.
- [5] G. Grimvall, Thermophysical Properties of Materials, Elsevier Science, North-Holland, Amsterdam, 1999.
- [6] Q. Chen, B. Sundman, Acta mater. 49 (2001) 947.
- [7] C. Kittel, Introduction to Solid State Physics, seventh ed. John Wiley and Sons, Inc, New York, 1996.
- [8] X. Li, Y. Xie, Y. Nie, H. Peng, Chinese Sci. Bull. 52 (22) (2007) 3041.
- [9] L. Fast, J.M. Wills, B. Johansson, O. Eriksson, Phys. Rev. B 51 (1995) 17431.
- [10] H.R. Schober, P.H. Dederichs, in: K.-H. Hellwege, J.L. Olsen (Eds.), Landolt–Bernstein Numerical Data and Functional Relationships In Science and Technology New Series, III/13a, Springer, Berlin, 1981.
- [11] G.V. Tsagareishvili, J. Less-Common. Met. 75 (1980) 141.

AB INITIO STUDY OF C14 LAVES PHASES IN Fe-BASED SYSTEMS

J. Pavlů^{a,b,*}, M. Šob^{a,b,c}

^a Central European Institute of Technology, CEITEC MU, Masaryk University, Brno, Czech Republic

^b Institute of Physics of Materials, Academy of Sciences of the Czech Republic, Brno, Czech Republic

^c Department of Chemistry, Faculty of Science, Masaryk University, Brno, Czech Republic

(Received 04 July 2012; accepted 30 September 2012)

Abstract

Structural properties and energetics of Fe-based C14 Laves phases at various compositions (i.e. Fe_2Fe , Fe_2X , X_2Fe , X_2X , where X stands for Si, Cr, Mo, W, Ta) were investigated using the pseudopotential VASP (Vienna Ab initio Simulation Package) code employing the PAW-PBE (Projector Augmented Wave - Perdew-Burke-Ernzerhof) pseudopotentials. Full relaxation was performed for all structures studied including the reference states of elemental constituents and the equilibrium structure parameters as well as bulk moduli were found. The structure parameters of experimentally found structures were very well reproduced by our calculations. It was also found that the lattice parameters and volumes of the unit cell decrease with increasing molar fraction of iron. Thermodynamic analysis shows that the Fe_2X configurations of Laves phases are more stable than the X_2Fe ones. Some of the X_2Fe configurations are even unstable with respect to the weighted average of the Laves phases of elemental constituents. Our calculations predict the stability of Fe_2Ta . On the other hand, Fe_2Mo and Fe_2W are slightly unstable (3.19 and 0.68 kJ.mol⁻¹, respectively) and hypothetical structures Fe_2Cr and Fe_2Si are found unstable as well.

Keywords: C14 Laves phases; Fe-based systems; Lattice stability; Ab-initio calculations

1. Introduction

C14 Laves phase represents a complex intermetallic structure, which can be found in many systems (e.g. Cr-Ta, Cr-Zr, Fe-Mo, Fe-W, Fe-Ta, Ta-V). If present it significantly influences material characteristics. The Fe-based systems are very important for the development of ferritic steels and Laves phases are considered to be promising strengthening phases under certain conditions. In binary systems, these phases can be usually found as stoichiometric but in higher systems they can exhibit some solubility of other elements (Si, Cr). For example, Si has been found to play an important role in the stability of this phase and, because of lack of experimental data concerning the influence of Si on Laves phase in simpler subsystems, a theoretical study of this effect is highly desirable.

In principle, basic properties of any phase are determined by its electronic structure. The purpose of this paper is to study, from first principles, the stability of C14 Laves phases in various binary systems consisting of Fe and some of the following elements: Si, Cr, Mo, Ta or W.

The paper is organised as follows: After the Introduction, we describe our ab initio calculations in Section 2. Section 3 presents the structural and

energetic analysis and discussion of the results. Section 4 concludes the paper.

2. Ab initio calculations

Our first-principles calculations were performed by the pseudopotential Vienna Ab initio Simulation Package (VASP) code [1,2] using the Projector Augmented Wave - Perdew-Burke-Ernzerhof (PAW-PBE) pseudopotential [3-5]. The exchange-correlation energy was evaluated within the Generalised Gradient Approximation [6]. Spin polarisation was not included in our calculations, except when noted. Reason for this is the fact that all Laves phases found in the above mentioned systems at ambient temperatures are paramagnetic. From the crystallographic point of view, the C14 Laves phase belongs to the hexagonal structures. It has 12 atoms in its unit cell and its symmetry is described by the space group No. 194 [7, 8].

Optimum calculation settings were achieved starting with the experimentally found lattice parameters. The structure parameters for the reference states (RS) (structures of elemental constituents, which are stable at Standard Ambient Temperature and Pressure (SATP), i.e. FM bcc Fe, NM diamond Si and NM bcc Mo, W and Ta) were taken from [8] and of AFM bcc Cr from [9] (Table 1). For Laves phases in Fe-(Cr,Mo,Si), Fe-Ta and Fe-W

* Corresponding author: houserova@chemi.muni.cz

systems the lattice parameters from Fe₂Mo, Fe₂Ta and Fe₂W [8] (Table 2), respectively, were implemented. Convergence tests of the total energies with respect to number of k-points have shown that the range of optimum values goes from a grid of 11x11x8 points (Fe₂Mo, W₂Fe and elemental Mo and W in C14 structure) towards 25x25x13 points (Fe₂W). In the case of RS, this range spreads from a grid of 9x9x9 points for FM bcc Fe and NM Si in diamond structure to 23x23x23 points for NM bcc Ta and W.

3. Results and discussion

3.1 Structure

Calculated structure parameters in comparison with experimental data are shown in Table 1 for RS structures of elemental constituents and in Table 2 for the C14 Laves phases studied. It may be seen that the theoretical results agree well with experimental values.

Table 1. Calculated and experimental lattice parameters of the RS structures (AFM stands for antiferromagnetic, FM for ferromagnetic and NM for nonmagnetic state, V_{at} denotes the volume per atom).

Structure	This work (relaxed)			Experiment		
	a (a.u.)	V_{at} (a.u. ³)	B_0 (Mbar)	a (a.u.)	V_{at} (a.u. ³)	Ref.
AFM bcc Cr	5.3947	78.5015	1.86	5.44	80.4946	[8]
FM bcc Fe	5.3589	76.9466	1.94	5.40 5.4160	78.7320 79.4339	[9] [10]
NM bcc Mo	5.9513	105.3921	2.71	59.4340	104.9723	[8]
NM diam. Si	10.3354	138.0030	0.90	102.6290	135.1209	[8]
NM bcc Ta	6.2531	122.2539	2.01	62.3970	121.4672	[8]
NM bcc W	5.9915	107.5396	3.15	59.8060	106.9582	[8]

Table 2. Calculated and experimental structure parameters and bulk moduli (B_0) of the C14 Laves phases in the Fe-X systems (X = Si, Cr, Mo, Ta, W).

Structure	a (a.u.)	c/a	V_{at} (a.u. ³)	$4f-z$	$6h-x$	B_0 (Mbar)
Fe ₂ Fe	8.5562	1.5976	72.2224	0.0804	0.8260	2.62
Fe ₂ Cr	8.6291	1.5938	73.9032	0.0775	0.8250	2.68
Cr ₂ Fe	8.7111	1.6095	76.7794	0.0621	0.8287	2.38
Cr ₂ Cr	8.7701	1.6512	80.3841	0.0464	0.8289	2.38
Fe ₂ Mo	8.8485	1.6146	80.7275	0.0695	0.8273	2.88
Fe ₂ Mo ^{exp} [8]	8.9668	1.6299	84.8053	0.063 ^a	0.83 ^a	- - -
Mo ₂ Fe	9.6076	1.5838	101.3668	0.0612	0.8280	2.11
Mo ₂ Mo	9.7465	1.6466	110.0248	0.0413	0.8298	2.42
Fe ₂ Si	8.6043	1.6601	76.3173	0.0714	0.8265	2.13
Si ₂ Fe	9.6519	1.3569	88.0536	0.0230	0.8214	1.43
Si ₂ Si	10.5905	1.2334	105.7317	0.0718	0.8158	0.89
Fe ₂ Ta	8.9710	1.6347	85.1753	0.0656	0.8293	2.68
Fe ₂ Ta ^{exp} [8]	9.1841	1.6284	91.0364	0.063 ^a	0.83 ^a	- - -
Ta ₂ Fe	10.0163	1.5921	115.4628	0.0329	0.8294	1.58
Ta ₂ Ta	10.3003	1.5922	125.5696	0.0623	0.8292	2
Fe ₂ W	8.8403	1.6219	80.8705	0.0686	0.8279	3.11
Fe ₂ W ^{exp} [8]	8.9522	1.6242	84.0975	0.063 ^a	0.83 ^a	- - -
W ₂ Fe	9.7322	1.5896	105.7456	0.0595	0.8291	2.26
W ₂ W	9.8110	1.6515	112.5596	0.0417	0.8301	2.82

^a As the corresponding experimental data were not found in [8], the values of C14 MgZn₂ Laves phase were used here.

The deviations in atomic volume are within the range from -3.1 to 2.1 % for RS (from Fe to Si) and from -3.8 to -6.4 % for Laves phases (from Fe_2W to Fe_2Ta). We have also found unambiguous trends in the geometry of Laves phase configurations (i.e. Fe_2Fe , Fe_2X , X_2Fe , X_2X) depending on the amount of Fe atoms in unit cell and on the size (or number of electrons) of X atom. These trends are demonstrated in Figure 1.

The most obvious tendency may be observed in behaviour of the lattice parameters (a , c) and atomic volumes (V_{at}) which increase with the concentration of X atoms involved except of the case of c parameter in Fe-Si system. This common trend results from the fact that Fe atoms are ones of the smallest particles studied in this work [11]. The differences in the size between the Fe and X atoms affect the distances between the individual lines in Figure 1(c) as here the effects of mutual interplay of a and c are “integrated” into the value of atomic volume. We can see there that the values of V_{at} of all structures increase in the series Fe-Cr, -Si, -Mo, -W and -Ta – individual curves in Figure 1(c) do not intersect. This tendency is similar to trends in empirical atomic radii [11] which give the order Si, W, Fe, Cr, Mo, Ta. What are the reasons for

disagreement in case of Si and W? The answer concerning W is simple. As we do not study separate atoms but bulk material our results should be compared rather with other experimental data e.g. covalent radii [12-16], metallic radii [12] or valence shell orbital radii [17]. These data show that V_{at} of W in bounded state moves toward higher values. The best agreement with our results was found in the case of the valence d-orbital radii in [17] (0.72 Fe, 0.86 Cr, 1.38 Mo, 1.47 W and 1.55 Ta (a.u.)), which increase exactly in the same order as our atomic volumes V_{at} . However it must be taken into account that there are several ways how to define radius for atoms. The further question is why such small atoms as Si provide a Laves phase with so relatively large V_{at} . In case of Si, although the atoms themselves are relatively small, covalent bonds can increase the average atomic volume quite a lot (cf. $V_{at} = 138 \text{ a.u.}^3$ in diamond structure). For metallic constituents, we may conclude that the effective atomic sizes (here valence d-orbital radii) play an important role in determining of the atomic volume of studied configurations.

We can also see that even the internal parameters describing positions of atoms in the unit cell depend

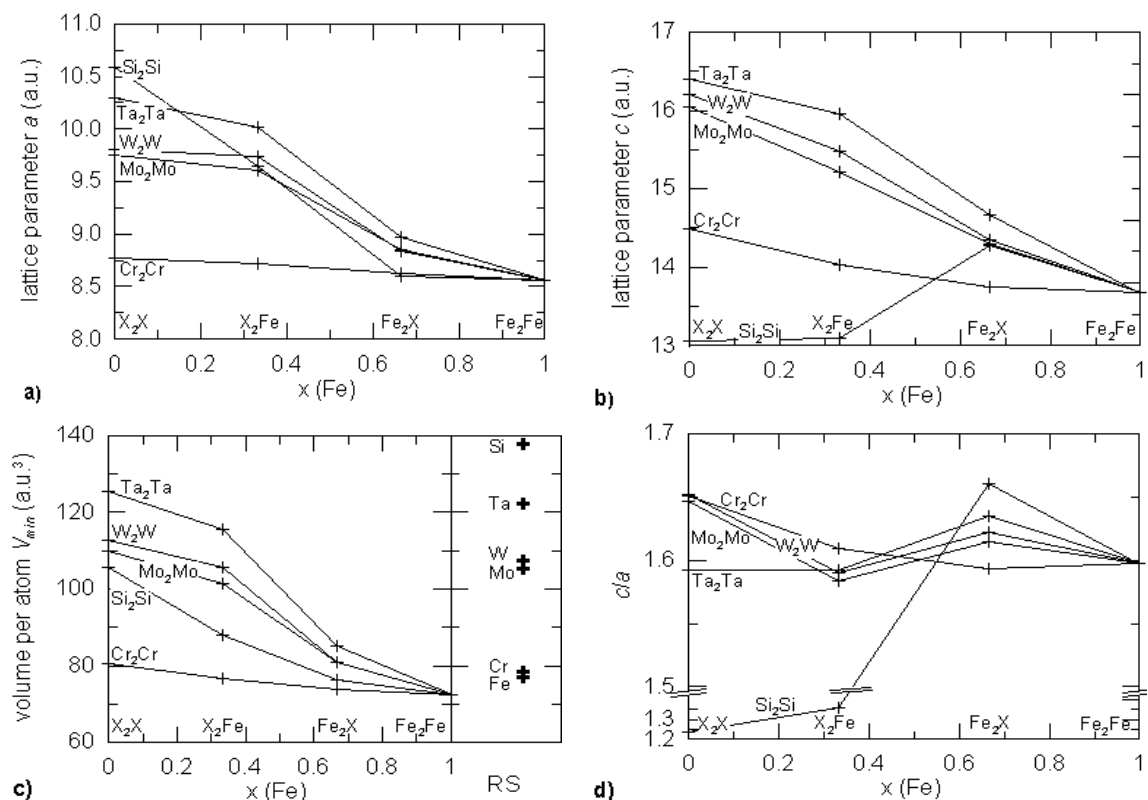


Figure 1. Concentration dependence of the a , c , V_{at} and c/a for C14 Laves phases in Fe-X systems ($X = \text{Si}, \text{Cr}, \text{Mo}, \text{Ta}, \text{W}$). The right-hand side of Fig. 1(c) shows the atomic volumes in the reference-state structures of elemental constituents. Numerical values are given in Table 2.

on the molar fraction of Fe in a regular way. (Fig. 2) The internal parameters $6h-x$ and $4f-z$ describe positions of atoms in $6h$ sublattice in direction of both x and y axes within the range of 0.8158-0.8301 and in $4f$ sublattice in the direction of the axis z in the interval 0.0230-0.0804, respectively. It is obvious that these parameters strongly depend on the composition of the structure. Except of Fe-Si system, the $6h-x$ parameter slightly increases with decreasing concentration of Fe atoms. The $4f-z$ parameter, on the other hand, reveals the opposite tendency in most cases. There are some exceptions from this trend in the Fe-Ta and Fe-Si system which may correspond to the irregularities in trends in c/a ratio (Fig.1(d)).

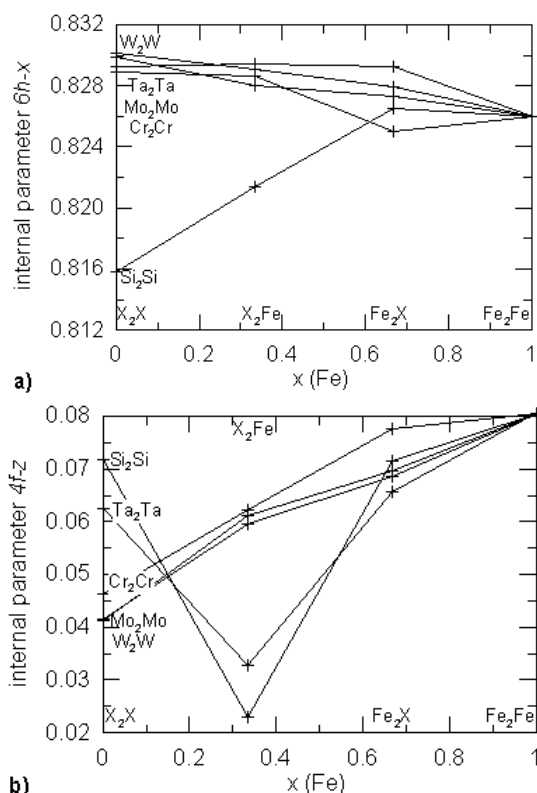


Figure 2. Concentration dependence of the $6h-x$ and $4f-z$ internal parameter for C14 Laves phases in the Fe-X systems ($X = Si, Cr, Mo, Ta, W$).

To study the distance in coordination spheres of atoms and kind of the Nearest Neighbours (NN), the values of the $6h-x$ and $4f-z$ parameters must be considered. In the case of sublattices in Laves phases studied, we found that the 1st NN atoms do not lie in the same distance from the central atom. They form some kind of shells whose widths are listed in Table 3.

The interplay of internal and lattice parameters can be seen in Figure 3 where the deviations from the trends observed earlier are not manifested and we get

Table 3. The average 1st NN distances (r) and the widths of the 1st NN shells (w) for C14 Laves phases in the Fe-X systems ($X = Si, Cr, Mo, Ta, W$).

Structure	r (a.u.)			w (a.u.)		
	$2a$	$4f$	$6h$	$2a$	$4f$	$6h$
No. of atoms in shell	12	16	12	12	16	12
Fe_2Fe	2.48	2.67	2.44	0.41	0.41	0.54
Fe_2Cr	2.50	2.68	2.46	0.41	0.36	0.52
Cr_2Fe	2.50	2.72	2.49	0.40	0.17	0.45
Cr_2Cr	2.53	2.76	2.54	0.34	0.50	0.54
Fe_2Mo	2.55	2.76	2.53	0.40	0.19	0.48
Mo_2Fe	2.75	2.98	2.73	0.46	0.22	0.50
Mo_2Mo	2.81	3.07	2.82	0.39	0.67	0.61
Fe_2Si	2.51	2.71	2.49	0.35	0.19	0.56
Si_2Fe	2.65	2.87	2.63	0.61	0.81	0.66
Si_2Si	2.88	3.05	2.82	0.78	0.92	0.61
Fe_2Ta	2.59	2.81	2.58	0.40	0.15	0.47
Ta_2Fe	2.85	3.12	2.87	0.44	0.84	0.63
Ta_2Ta	2.95	3.20	2.94	0.49	0.22	0.52
Fe_2W	2.55	2.76	2.53	0.40	0.18	0.49
W_2Fe	2.78	3.02	2.77	0.46	0.21	0.50
W_2W	2.83	3.09	2.84	0.39	0.70	0.60

smooth concentration dependencies of average 1st NN distances from central atom on composition.

We can draw the following conclusions concerning the 1st NN distances in various sublattices:

- In each configuration of C14 Laves phase, the 1st NN distance increases in series $6h$, $2a$ and $4f$ except for the Ta_2Fe , Mo_2Mo and W_2W where the $2a$ sublattice reveals slightly lower average 1st NN distance than the $6h$ sublattice.

- The $2a$ sublattice has the Coordination Number (CN) 12 and the 1st NN consist of six $6h$ and six $4f$ atoms in all Laves phase configurations studied. The average distances between the central atom and the 1st NN atom reveal smooth dependence on Fe composition, see Figure 3(a). The width of the 1st NN shell ranges from 0.34 a.u. for Cr_2Cr to 0.78 a.u. for Si_2Si configuration.

- The 1st NN coordination shell of the $6h$ sublattice (CN=12) consists of two $6h$, two $2a$, two $6h$, four $4f$ and two $4f$ atoms (in the order of increasing distances) and it reveals only tiny changes in its arrangement in the C14 Laves phases studied. There is only some rearrangement between the furthest six (4+2) $4f$ atoms found in the Fe-rich configurations. On the other hand, the X-rich configurations prefer to arrange these six $4f$ atoms in the opposite order, i.e. in subgroups of 2 and 4 atoms. Let us note that there are some anomalies in Si_2Fe and Si_2Si :

- In Si_2Fe the couple of $4f$ atoms substitutes the

first two $6h$ atoms in the shell i.e. the number of $4f/6h$ atoms is increased/lowered here by two. This fact can be a consequence of the significant decrease in $4f$ - z parameter which causes that the atoms of the $4f$ sublattice become to be the nearest surrounding of the $6h$ atoms.

- Si_2Si reveals, on the other hand, a shift of the first two $6h$ nearest atoms to the farthest position of the coordination sphere.

However, even in spite of these rearrangements in

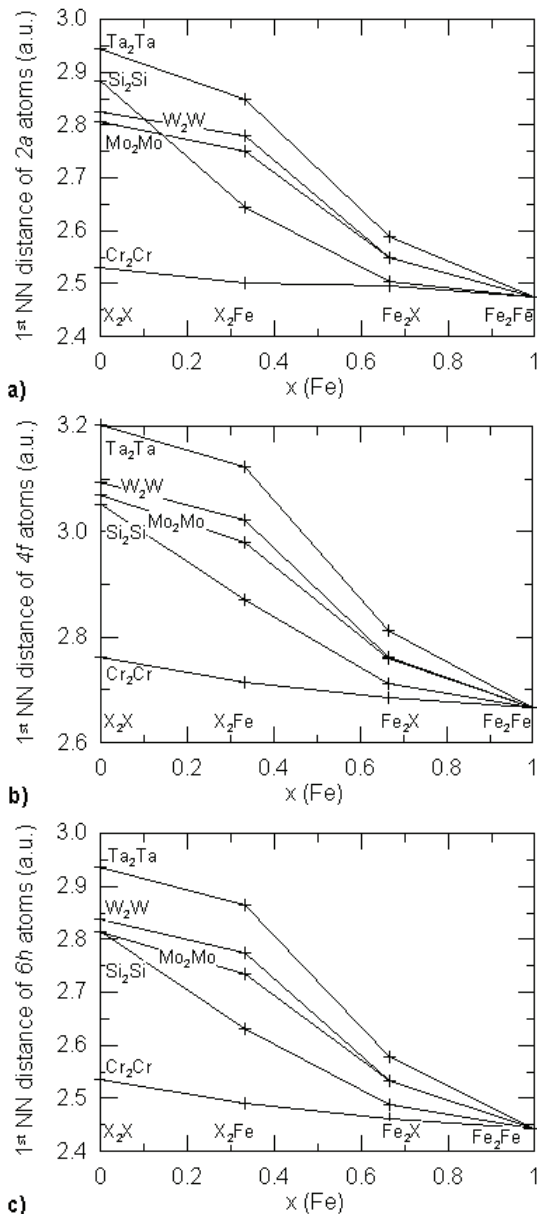


Figure 3. Concentration dependences of the average 1st NN distances for the $2a$, $4f$ and $6h$ sublattice for C14 Laves phases in the Fe-X systems ($X = \text{Si}, \text{Cr}, \text{Mo}, \text{Ta}, \text{W}$).

the 1st NN coordination shell of the $6h$ sublattice we can still see a smooth dependence of the average 1st NN distances on composition (Fig. 3(c)). The width of the 1st NN shell ranges from 0.45 a.u. for Cr_2Fe to 0.66 a.u. for Si_2Fe configuration.

• The $4f$ sublattice (CN=16) reveals many rearrangements of the order of three $2a$, six $6h$, three $6h$, three $4f$ and one $4f$ atom in the 1st NN coordination shell but there are no evident rules here. Again, the concentration dependences of the average NN distances are quite smooth.

Using ab initio methods, the values of bulk moduli of RS and Laves phases can be calculated and their values are listed in Tables 1 and 2. The composition dependence of bulk moduli is shown in Figure 4. It can be seen there that bulk moduli of Laves phases in all systems studied exhibit a strong composition dependence. The least influence of molar fraction of Fe can be found in Fe-Cr system which can be caused by similar size of atoms of these elements. Bulk moduli of both binary and pure constituent Laves phases also strongly depend on the kind of X component and their values decrease in the same order as in case of the RS, i.e. from W, Mo, Ta to Si, except for Fe-Cr system, which can be caused by magnetic ordering of Cr and Fe RS. The values of bulk moduli of pure element structures and of the Laves phases are very close in case of NM elements, i.e. bulk moduli of Mo, W, Si and Ta Laves phase are 89.3 %, 89.5 %, 98.9 % and 99.5 % of the RS value, respectively. On the other hand the bulk moduli of NM Cr and Fe Laves phase are much higher than those of magnetic RS (i.e. 128.0 % and 135.1 % of RS value, respectively).

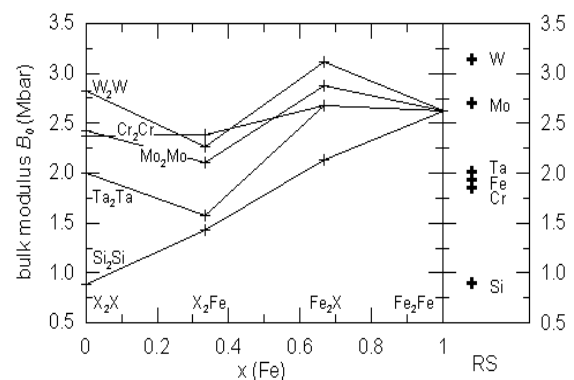


Figure 4. Concentration dependence of the bulk modulus for C14 Laves phases in the Fe-X systems ($X = \text{Si}, \text{Cr}, \text{Mo}, \text{Ta}, \text{W}$).

3.2 Energetics

Total energy of formation per atom may be obtained as

$$\Delta E_{\text{at}}^{\text{Laves-RS}} = E_{\text{at}}^{\text{Laves}} - (x_{\text{Fe}} E_{\text{at}}^{\text{RS}_{\text{Fe}}} + (1-x_{\text{Fe}}) E_{\text{at}}^{\text{RS}_X})$$

where E_{at} stands for total energy per atom and x_{Fe} denotes the molar fraction of Fe.

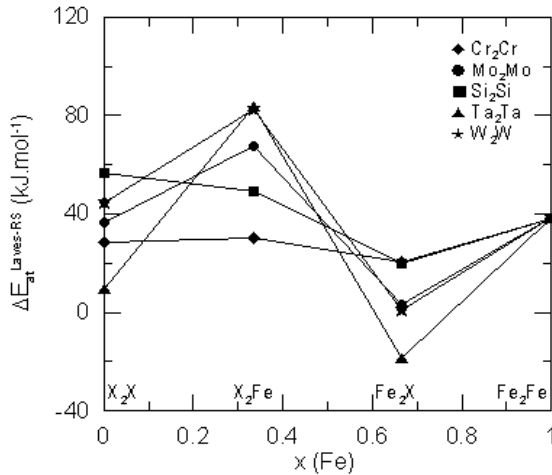


Figure 5. Concentration dependence of $\Delta E_{\text{at}}^{\text{Laves-RS}}$ for C14 Laves phases in the Fe-X systems ($X = \text{Si}, \text{Cr}, \text{Mo}, \text{Ta}, \text{W}$) (fully relaxed results).

All equilibrium total energy differences $\Delta E_{\text{at}}^{\text{Laves-RS}}$ are summarised in Table 4 and Fig. 5 which shows that the only stable configuration is the Fe_2Ta one. But there are two other structures Fe_2W and Fe_2Mo which are only slightly unstable in comparison with the remaining configurations. These three structures revealing the highest tendencies to stability are the only ones among the Fe-X systems studied which

have been experimentally found.

The comparison in Table 4 shows that our calculated data for C14 Laves phase of elemental constituents are in perfect agreement with ab initio calculated data published in [18]. The agreement with experimental data is worse. This is given by the fact that experiments are not performed at 0 K temperature.

4. Conclusions

The purpose of this work was to understand, with the help of ab initio electronic structure calculations, the relations between the electronic structure, size of the atoms and the thermodynamic as well as structural properties of the C14 Laves phases. We demonstrate that the structure parameters and heats of formations strongly depend on the molar fraction of Fe atoms and that the calculated equilibrium parameters correspond very well to the experimental values. Analysis of our results shows that both geometric and electronic factors are important for stabilization of the C14 Laves phase in the iron-based systems.

Our ab initio electronic structure calculations reveal that the C14 Laves phase is unstable at zero temperature in both Fe-Mo and Fe-W system which is in contradiction with experiments. However, the absolute value of the total energy of formation is very low. We suppose that the instability at higher temperatures is suppressed by the entropy effects. But, on the other hand, some other C14 Laves phases (e.g. Fe_2Ta) are stable even at low temperatures. We have found that the phase stability related to the reference state is significantly influenced by occupations of sublattices.

Table 4. Ab initio calculated total energies of formation $\Delta E_{\text{at}}^{\text{Laves-RS}}$ (kJ.mol^{-1}) of atoms) of various Laves phase configurations with respect to the weighted ratio of the RS compared with literature data.

Elem. X	Fe_2X		X_2Fe	X_2X	
	VASP	Exp.	VASP	VASP	Calc.
Cr	20.22	---	30.10	28.63	27.8 [18]
Mo	3.19	-14.1 [19]	67.38	36.60	36.5 [18]
Si	19.91	---	48.92	56.52	53.6 [18] ^a
Ta	-18.61	-6.3±1.9 [20] ^b	83.70	9.35	9.7 [18]
		-19.7 [21]			
		-19.25±2.79 [22]			
		-19.27 [23]			
W	0.68	-7.61±3.14 [24]	82.60	44.40	43.8 [18]
Fe	---	---	---	38.27	31.1 [18]

^a This value was obtained using the energy difference $E^{\text{bcc}} - E^{\text{diamond}} = 0.53 \text{ eV} = 51.1 \text{ kJ/mol}$ [25], as the value of energy of formation of Laves phase in Si obtained in Ref. [18] was related to bcc Si.

^b The sample showed significant amount of second phases in X-ray diffraction analyses [20].

Acknowledgements

Financial support of the Grant Agency of the Czech Republic (Project No. P108/10/1908) and of the Project "CEITEC - Central European Institute of Technology" (CZ.1.05/1.1.00/02.0068) from the European Regional Development Fund are gratefully acknowledged. This research was also supported by the Academy of Sciences of the Czech Republic (Project No. RVO:68081723). The access to computing and storage facilities owned by parties and projects contributing to the National Grid Infrastructure MetaCentrum, provided under the programme "Projects of Large Infrastructure for Research, Development, and Innovations" (LM2010005) is appreciated.

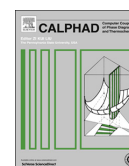
References

- [1] G. Kresse, J. Furthmüller, *Comput. Mater. Sci.* 6 (1996) 15.
- [2] G. Kresse, J. Furthmüller, *Phys. Rev. B* 54 (1996) 11169.
- [3] P. E. Blöchl, *Phys. Rev. B* 50 (1994) 17953.
- [4] G. Kresse, J. Joubert, *Phys. Rev. B* 59 (1999) 1758.
- [5] J. P. Perdew, K. Burke, M. Ernzerhof, *Phys. Rev. Lett.* 77 (1996) 3865.
- [6] J. P. Perdew, J. A. Chevary, S. H. Vosko, K. A. Jackson, M. R. Pederson, D. J. Singh, C. Fiolhais, *Phys. Rev. B* 46 (1992) 6671.
- [7] J. L. C. Daams, P. Villars, J. H. N. van Vucht, *Atlas of crystal structure types*, ASM International, Materials Park, Ohio, USA, 1991.
- [8] P. Villars, L. D. Calvert, *Pearson's Handbook of Crystallographic Data for Intermetallic Phases*, ASM International, Materials Park, Ohio, USA, 1991.
- [9] E. G. Moroni, T. Jarlborg, *Phys. Rev. B* 47 (1993) 3255.
- [10] M. Polcarová, K. Godwod, J. Bak-Misiuk, S. Kadečková, J. Bradler, *Phys. Stat. Sol. (a)* 106 (1988) 17.
- [11] J. C. Slater, *J. Chem. Phys.* 41 (1964) 3199.
- [12] R. T. Sanderson, *Chemical periodicity*, Reinhold, New York, USA, 1962.
- [13] L. E. Sutton (Ed.), *Table of interatomic distances and configuration in molecules and ions*, Supplement 1956-1959, Special publication No. 18, Chemical Society, London, UK, 1965.
- [14] J. E. Huheey, E. A. Keiter, R. L. Keiter, *Inorganic chemistry: Principles of structure and reactivity*, 4th Edition, HarperCollins, New York, USA, 1993.
- [15] W. W. Porterfield, *Inorganic chemistry, a unified approach*, Addison Wesley Publishing Co., Reading, Massachusetts, USA, 1984.
- [16] A. M. James, M. P. Lord, *Macmillan's chemical and physical data*, Macmillan, London, UK, 1992.
- [17] J. B. Mann, *Atomic structure calculations II. Hartree-Fock wave functions and radial expectation values: hydrogen to lawrencium*, LA-3691, Los Alamos Scientific Laboratory, USA, 1968.
- [18] M. H. F. Sluiter, *CALPHAD* 30 (2006) 357.
- [19] J. H. Zhu, C. T. Liu, L. M. Pike, P. K. Liaw, *Intermetallics* 10 (2002) 579.
- [20] S. V. Meschel, O. J. Kleppa, *Journal of Alloys and Compounds* 415 (2006) 143.
- [21] A. Miedema, R. Boom, F. De Boer, *Journal of the Less Common Metals* 41 (1975) 283.
- [22] Y. I. Gerassimov, V. I. Lavrentev, O. von Goldbeck, D. T. Livey, R. Ferro, A. L. Drago, *Tantalum: Physico-chemical properties of its compounds and alloys*, IAEA Review, Special Issue No. 3, IAEA, Vienna, 1972. In O. Kubaschewski and C.B. Alcock, *Metallurgical Thermochemistry*, 5th ed., Pergamon Press, Oxford 1979.
- [23] T. C. Totemeier, C. J. Smithells, *Smithells Metals Reference Book*, Elsevier Butterworth-Heinemann publications, Oxford, GB, 2004.
- [24] T. N. Rezukhina, T. A. Kashina, *The Journal of Chemical Thermodynamics* 8 (6) (1976) 519.
- [25] M. Y. Yin, M. L. Cohen, *Phys. Rev. B* 26 (1982) 5668.



Contents lists available at ScienceDirect

CALPHAD: Computer Coupling of Phase Diagrams and Thermochemistry

journal homepage: www.elsevier.com/locate/calphad

Laves phases in the V–Zr system below room temperature: Stability analysis using *ab initio* results and phase diagram

Jan Štrof^a, Jana Pavlů^{b,c,*}, Urszula D. Wdowik^d, Jiří Buršík^c, Mojmír Šob^{b,c,a}, Jan Vřešťál^{b,c}^a Department of Chemistry, Faculty of Science, Masaryk University, Brno, Czech Republic^b Central European Institute of Technology, CEITEC MU, Masaryk University, Brno, Czech Republic^c Institute of Physics of Materials, Academy of Sciences of the Czech Republic, Brno, Czech Republic^d Institute of Technology, Pedagogical University, Cracow, Poland

ARTICLE INFO

Available online 27 August 2013

Keywords:

Laves phases

V–Zr system

Ab initio calculations

Phase diagram

Zero Kelvin

ABSTRACT

V–Zr is a well known system where a phase transformation from rhombohedral V_2Zr structure to cubic C15 Laves phase occurs during heating at about 115 K. Here we provide a thermodynamic description of this phenomenon, supported by *ab initio* calculations. We utilize our new method of extension of the Scientific Group ThermoData Europe (SGTE) unary thermodynamic database to zero Kelvin and demonstrate that it may be applied also to complicated intermetallic phases. To keep our analysis on equal footing with previous results for higher temperatures, data regarding a recent thermodynamic assessment of the V–Zr system (valid for temperatures above 298.15 K) were reassessed. With the help of *ab initio* approach, we demonstrate that the ZrV_2 rhombohedral phase is not stable at 0 K and transforms to C15 Laves phase. The stability of C15 Laves phase is confirmed by analysis of elastic stability criteria and phonon spectra calculations.

© 2013 Elsevier Ltd. All rights reserved.

1. Introduction

Topologically close-packed intermetallic compounds such as Laves phases are promising candidates for high-temperature materials due to their interesting mechanical and corrosion resistance features [1] which can be influenced by their possible polymorphism and peculiar magnetic and electrical properties [2,3]. The solubility of hydrogen in Laves phases [4] and superconductivity [5] are also important properties of these compounds. Electronic structure, elastic properties and total energies of C15 Laves phases of V_2M type ($M=Zr, Hf, \text{ or } Ta$) were studied with the help of *ab initio* calculations in [6–8] and the relations between electronic structure, elastic moduli and stability were analyzed. It was found that the V_2Zr C15 Laves phase compound, which is cubic at room temperature, undergoes a structural transformation to a non-Laves rhombohedral phase at low temperatures [9–11]. The transformation temperature was determined to be 116.7 K by Moncton [11] and 110 K by Rapp [10], who also reported the corresponding latent heat of transformation as 31 J/mol. In general, it is very difficult to explore low-temperature phase diagrams describing such transformations both experimentally and theoretically and it is great challenge to

perform thermodynamic modeling in this region. It is the reason for doing this work.

The first step towards the low-temperature predictions of thermodynamic functions was done in works [12,13], where equations for Gibbs energy valid at low temperatures and necessary values of Debye temperatures for many elements are given. In our recent work [14], the expressions of Gibbs energies of 52 elements were extended to zero Kelvin on this basis and they may form the base for modeling of phase equilibria by the CALPHAD method at low temperatures.

Furthermore, one of the options how to model the Gibbs energy of any intermetallic phase at low temperatures is based on the extension of its Gibbs energy from high-temperature region towards zero Kelvin which also takes into account the value of its Debye temperature (T_D). A fundamental prerequisite for the success of this method is the existence of precise expression for the Gibbs energy of studied phase at high temperature *i.e.* above 298.15 K.

In the V–Zr system the data of phase equilibria above room temperature were determined in [15–17] and thermodynamic assessments were published for equilibria above room temperature by Servant [18] and Zhao et al. [19], where the description of Gibbs energy of V_2Zr C15 Laves phase was evaluated by the ATAT software [20,21].

In this work, we have taken the results of Zhao [19] as reliable and improved the description of C15 Laves phase and a hexagonal close-packed (HCP_A3) phase above room temperature. However,

* Corresponding author at: Central European Institute of Technology, CEITEC MU, Masaryk University, Kamenice 753/5, CZ-625 00 Brno, Czech Republic.
Tel.: +420 549493742; fax: +420 549492556.

E-mail addresses: houserova@chemi.muni.cz, houserova@ipm.cz (J. Pavlů).

Rapp [10], Moncton [11], Keiber [22] and Geibel [23] have found rhombohedral phase as stable phase below 113 K, which cannot be drawn in high-temperature phase diagram. Therefore, we have performed the extension of calculation of phase diagram down to zero Kelvin, using the description of unary data below room temperature [14] and the new extension of expression of Gibbs

energy of C15 Laves phase and rhombohedral phase to zero Kelvin compatible with Gibbs energy expressions above 298.15 K [19] and based on respective values of Debye temperatures [22–24].

In addition to that, our *ab initio* calculations of elastic constants and phonon spectra bring new findings concerning the stability and behavior of C15 and rhombohedral V_2Zr phase.

Table 1

Calculated and experimental lattice parameters and bulk moduli (B) of the SER states. Symbols a and c stand for lattice parameters, V_{at} is the atomic volume and Δ shows the relative difference between the calculated and experimental atomic volume and bulk modulus.

SER state	a (pm)	c/a	V_{at} (10^7 pm ³)	$\Delta\%$	B (GPa)	$\Delta\%$
NM BCC_A2 V						
Exp. [32]	303.09	1	1.392	–5.11	161.9 [33]	+16.46
This work	297.83	1	1.321		188.5	
NM HCP_A3 Zr						
Exp. [32]	323.18	1.593	1.164	+0.64	83.3 [33]	+17.22
This work	323.55	1.598	1.172		97.6	

Table 2

Equilibrium structural parameters and bulk moduli (B) of Laves phases and a non-Laves rhombohedral phase found in this work. Symbols a and c stand for lattice parameters and V_{at} is the atomic volume; Δ denotes the relative difference between the calculated and experimental atomic volume.

Structure	a (pm)	c/a	V_{at} (10^7 pm ³)	$\Delta\%$	B (GPa)
C14					
V_2V					
This work	493.22	1.5652	1.565	–	181.8
V_2Zr					
Exp. [32]	527.70	1.6386	2.007	–	–
This work	521.34	1.6032	1.893	–5.65	147.4
VZr_2					
This work	557.23	1.5929	2.297	–	91.6
Zr_2Zr					
This work	575.87	1.6667	2.652	–	88.6
C15					
V_2V					
This work	688.17	1	1.358	–	179.9
V_2Zr					
Exp. [32]	745.00	1	1.723	–	139 ^a
This work	732.90	1	1.640	–4.79	145.2
VZr_2					
This work	789.31	1	2.049	–	87.5
Zr_2Zr					
This work	824.88	1	2.339	–	85.3
C36					
V_2V					
This work	493.30	3.1324	1.567	–	181.1
V_2Zr					
This work	528.06	3.0890	1.895	–	146.9
VZr_2					
This work	558.41	3.1993	2.321	–	90.0
Zr_2Zr					
This work	577.14	3.3310	2.668	–	87.7
Rhombohedral phase (hexagonal coordinates)					
V_2V					
This work ^b	486.46	2.4518	1.358	–	180.6
V_2Zr					
Exp. [22]	535.61	2.3267	1.720	–	–
This work ^b	518.37	2.4480	1.641	–4.62	145.5
VZr_2					
This work	622.01	1.8027	2.087	–	81.0
Zr_2Zr					
This work	620.07	2.0429	2.343	–	85.8

^a Calculated value published in Ref. [24].

^b These values (written in rhombohedral coordinates) correspond to the C15 Laves phase arrangement and were obtained by the full structure relaxation.

2. *Ab initio* calculations of stability of V₂Zr phases

The energy of formation of chosen phase at 0 K can be obtained with the help of *ab initio* electronic-structure calculations, performed within the Density Functional Theory (DFT). We used the pseudopotential method [25] incorporated into the Vienna *Ab initio* Simulation Package (VASP) code [26,27] combined with the Projector Augmented Wave–Perdew–Burke–Ernzerhof (PAW–PBE) pseudopotential [28–30] (i.e. we employed the Generalized Gradient Approximation (GGA) for the exchange–correlation energy), and we calculated the total energies of the C15 V₂Zr Laves phase and a rhombohedral structure as well as the total energy of the Standard Element Reference (SER) states i.e. HCP_A3 Zr and BCC_A2 V, which are the phases stable at pressure of 10⁵ Pa (1 bar) and temperature 298.15 K.

In general, Laves phases form the largest group of intermetallic compounds and crystallize in cubic (MgCu₂, C15), or hexagonal (MgZn₂, C14 and MgNi₂, C36) type structures which differ only by a different stacking of the same four-layered structural units [31]. Therefore an additional *ab initio* study of stability of C14, C15 and C36 structures was performed to obtain a sound physical background for possible future thermodynamic modeling.

The preliminary calculations of C14 and C15 V₂Zr Laves phase modifications and SER states of Zr and V were accomplished using

the corresponding experimentally found lattice parameters published in [32]. For the C36 V₂Zr Laves phase, we employed the data of the Cr₂Zr phase from [32] and for rhombohedral phase, the data from [22]. The cut-off energy restricting the number of plane waves in a basis set was 241 eV for HCP_A3 Zr, Laves phases and rhombohedral structures except for pure V structures (BCC_A2 and V₂V – rhombohedral and Laves phase modifications) where the value of 201 eV was used.

The convergence tests of total energies with respect to the number of *k*-points were also performed. In the case of SER states with 2 atoms in the unit cell, we used a grid of 19 × 19 × 19 points for nonmagnetic (NM) BCC_A2 V and of 21 × 21 × 15 points for NM HCP_A3 Zr. The optimum values obtained for the C14 Laves phases are 15 × 15 × 13 (V₂V), 21 × 21 × 13 (V₂Zr), 21 × 21 × 15 (Zr₂Zr) and 21 × 21 × 17 (VZr₂) *k*-points, for the C15 Laves phases 13 × 13 × 13 (V₂V), 19 × 19 × 19 (V₂Zr, VZr₂) and 21 × 21 × 21 (Zr₂Zr) *k*-points and for the C36 Laves phases 13 × 13 × 13 (V₂V), 17 × 17 × 13 (Zr₂Zr, V₂Zr) and 19 × 19 × 13 (VZr₂) *k*-points. The optima 15 × 15 × 13 (V₂V, V₂Zr, VZr₂) and 17 × 17 × 13 (Zr₂Zr) *k*-points were found in case of rhombohedral phase described using the hexagonal lattice parameters.

The spin polarization was not included in our calculations. The reason for this is the fact that all Laves phases found in the systems studied are paramagnetic at ambient temperatures and V₂V and V₂Zr C15 Laves phase were found NM from *ab initio* calculations.

After the test calculations, each structure was fully relaxed yielding the minimum total energy and the equilibrium structural parameters. As the SER state of vanadium and the C15 Laves phases are cubic, only a volume relaxation is sufficient to get their lowest energy state. The calculated optimum lattice parameters and bulk moduli (*B*) for SER states, C14, C15 and C36 Laves phases and the non-Laves rhombohedral structure are listed in Tables 1 and 2.

Experimental and calculated structural parameters of SER states and V₂Zr configurations in C15 and C14 Laves phase agree quite well. Concerning the rhombohedral phase, the situation is more complicated. Here, the analyses of Nearest Neighbors (NN) distances and primitive cells were performed and the results obtained were compared with C15 Laves phase equilibrium data. It was found that the V₂V and V₂Zr configuration of rhombohedral phase transforms to the C15 Laves phase during the relaxation which is confirmed by the identity of their primitive cells. Furthermore, the corresponding total energy differences $\Delta^0 E^{L-SER}$ between the rhombohedral (C15 Laves) phase and SER states given in Table 3 are almost identical.

The same statement is also valid for their bulk moduli *B* listed in Table 2. On the other hand, the VZr₂ and Zr₂Zr configurations

Table 3

Total energy differences $\Delta^0 E^{L-SER}$ between the Laves phases of various types and the weighted average of the SER states (NM BCC_A2 V and NM HCP_A3 Zr) calculated in this work and compared with values available in literature [34,35]. The *ab initio* results published in [34,35] were obtained using the GGA. The energy of the energetically most favorable V₂Zr structure is denoted as boldface. All values are given in kJ/mol of atoms (1 eV/atom = 96.485 kJ/mol of atoms).

Composition	V ₂ V	V ₂ Zr	VZr ₂	Zr ₂ Zr
C14				
This work	9.81	3.32	68.53	20.51
C15				
This work	11.23	5.07	77.85	27.35
Ref.	11.0 [34]	–	–	26.50 [34,35]
C36				
This work	10.42	4.03	71.95	22.80
Rhombohedral phase				
This work	11.22 ^a	5.07 ^a	65.23	24.68

^a These values correspond to the C15 Laves phase arrangement and were obtained by the full structure relaxation. The total energy difference between this relaxed structure and C15 Laves phase in V₂V (V₂Zr) configuration is –0.0109 (–0.0015) kJ/mol of atoms.

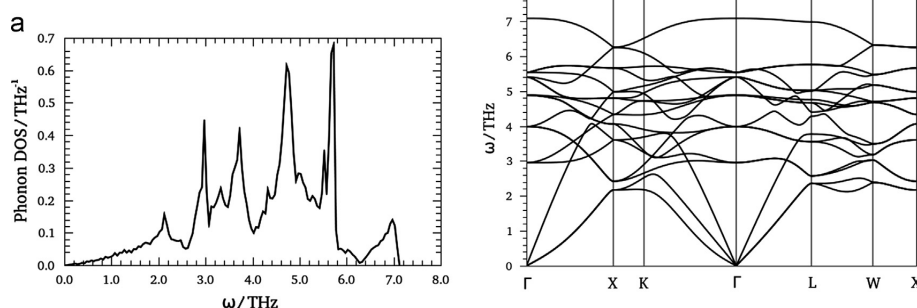


Fig. 1. Density of states of phonons (a) and dispersion relations of phonons (b) in V₂Zr C15 Laves phase, calculated by Phonon software [36].

Table 4
Calculated C_{11} , C_{12} and C_{44} elastic constants and phonon/sound velocities in C15 V_2Zr Laves phase. ρ is the mass density and subscripts T and L represent the transversal and longitudinal modes, respectively.

Source of data	C_{11} (GPa)	C_{12} (GPa)	C_{44} (GPa)	$\rho V_{T(110)}^2 = (C_{11} + C_{12} + 2C_{44})/2$	$\rho V_{L(110)}^2 = (C_{11} + C_{12} + 4C_{44})/3$	$\rho V_{T(111)}^2 = (C_{11} - C_{12} + 2C_{44})/2$	$\rho V_{L(111)}^2 = (C_{11} - C_{12} + 4C_{44})/3$	$\rho V_{T(100)}^2 = C_{11}$	$\rho V_{L(100)}^2 = C_{44}$
[24]	155.2	131	7.6	150.7	149.2	12.1	10.6	155.2	7.6
This work ^a	162.33	136.62	6.60	156.08	154.00	12.85	10.77	162.33	6.60
This work ^b	139.91	114.98	6.26	114.98	106.75	31.23	23.04	139.91	6.26

^a Values evaluated by calculating the total energy as a function of the shears.

^b Values based on the phonon spectra analysis.

Table 5

Reassessed L -parameters of C15 Laves phase and HCP_A3 phase.

Phase	T (K)	Parameter (J mol ⁻¹ per formula unit)	This work	Ref. [19]
HCP_A3	298–3000	${}^0L_{V,Zr}$	41,000 + 1.0T	1,180,172.2 + 10.096698T
		${}^1L_{V,Zr}$	8000 + 2.5T	1,137,938.4 + 25.73129T
V_2Zr _C15	298–2000	${}^0L_{V,VZr}$	60,000	–1998.517 + 40.88416T
		${}^1L_{V,VZr}$	–	2478.3464 + 5.0971524T
		${}^2L_{V,VZr}$	–	3388.8469 + 2.0837273T
		${}^0L_{V,Zr,Zr}$	25,000	19,133.339 – 31.652724T
		${}^1L_{V,Zr,Zr}$	–	9002.261 + 18.724243T
		${}^2L_{V,Zr,Zr}$	–	10,837.862 – 9.3671388T

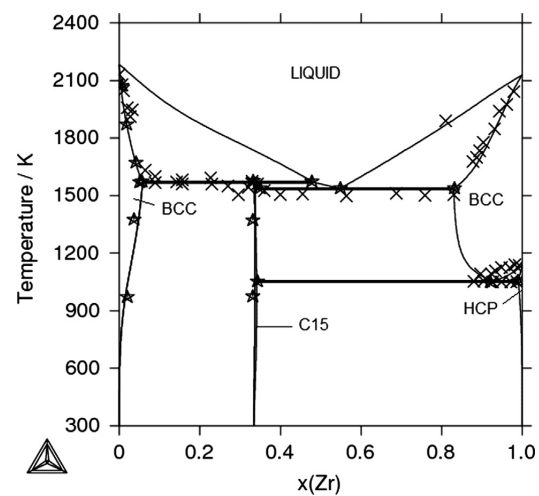


Fig. 2. Phase diagram of V–Zr system above 298.15 K calculated according to [19] (with HCP_A3 and C15 data reassessed), compared with experimental data: stars from [15], crosses from [16].

of rhombohedral phase do not converge to the C15 Laves phase arrangement during their structural relaxation. Even more, these structures become more stable than the C15 Laves phase.

The absolute values of energies of formation of VZr_2 configuration of C14, C15 and C36 Laves phase and rhombohedral structure are nearly 21, 15, 18 and 13 times higher, respectively, than those of V_2Zr configuration. This is a quantitative confirmation of the fact that the VZr_2 arrangement of the above mentioned structures is energetically very disadvantageous.

The stability of the C15 structure at higher temperatures is facilitated by the vibrational energy effect in spite of the positive value of energy of formation of C15 and non-Laves (rhombohedral) structure at 0 K.

3. Elastic constants and phonon spectra of V_2Zr C15 Laves phase

The phonon spectra of V_2Zr C15 Laves phase were calculated using the Phonon software [36]. The behavior of phonon density of states (DOS) is displayed in Fig. 1a together with the dispersion relations of phonons (Fig. 1b).

It may be seen that the V_2Zr in C15 Laves phase structure is dynamically stable at zero Kelvin which is in agreement with the findings published in [24] where the V_2Zr C15 structure is presented as mechanically stable according to the elastic stability

66

J. Štrof et al. / CALPHAD: Computer Coupling of Phase Diagrams and Thermochemistry 44 (2014) 62–69

criteria: $C_{11} > 0$; $C_{44} > 0$; $C_{11} > |C_{12}|$ and $(C_{11} + 2C_{12}) > 0$. To confirm this finding, the elastic constants of C15 Laves phase were calculated and are listed in Table 4.

From this table, we can see that the mechanical stability of the C15 phase predicted in [24] was confirmed by our results listed in last two lines. These results were obtained by calculating the total energy as a function of the shears [37,38] and are in very good agreement with data published in [24]. Furthermore, the elastic constants in cubic systems are related to the phonon and sound velocities as reported in [39]. Hence, our *ab initio* elastic constants were compared to those obtained from the least-square fits of the appropriate acoustic phonon slopes and applying density of ZrV_2 $\rho = 6518 \text{ kg m}^{-3}$ determined using the calculated lattice constant (see Table 2). Resulting values are given in the last line of Table 4. The C_{11} and C_{44} that are directly obtained from the slopes of the phonon branches differ from the respective elastic constants calculated in the *conventional* manner by about 14% and 5%, respectively. We note significant discrepancies between the slopes that involve combinations of the elastic constants. Therefore, the C_{12} appearing only in the combination of the elastic constants cannot be determined unambiguously. One has to note that estimates of the elastic constants appropriate for *zero-sound* propagation (long wave-length limit, i.e. $\mathbf{q} \rightarrow 0$ where \mathbf{q} denotes the wave-vector) are usually not as precise as those determined from deformation energy or stress-strain relationships and the discrepancies may reach several or more percent (see for example [40]).

4. Thermodynamic modeling and phase diagram above 298.15 K

In this temperature region, we adopted a recent assessment of thermodynamic parameters of V-Zr system [19] except for the overestimated number of parameters of C15 Laves phase which was reduced in our work. Subsequently, the corresponding parameters for HCP_A3 phase had to be also reoptimized. The obtained data are presented in Table 5 together with data published in [19].

It is obvious that lower values of ${}^0L_{V,Zr}$ and ${}^1L_{V,Zr}$ parameters of HCP_A3 phase are sufficient in our modeling. In addition to it, 1L and 2L parameters of C15 Laves phase are not needed in our approach. The same parameters as in [19] were used for a liquid and a body-centered cubic (BCC_A2) phase. The rhombohedral phase has not been modeled at this stage as it is not stable in this temperature region.

The calculated phase diagram is shown in Fig. 2. From Table 6, we can see that the differences in invariant temperatures calculated in [19] and in this work are very small.

The detail of the phase diagram in the region of BCC_A2/HCP_A3 transformation of Zr is presented in Fig. 3.

5. Thermodynamic modeling of V_2Zr phases below 298.15 K

The Compound Energy Formalism (CEF) [41,42] was also employed for thermodynamic modeling of the V-Zr system down

Table 6
Temperatures of invariant reactions in the V-Zr system.

Reaction	T (K) from [19]	T (K) [this work]
V-BCC_A2+liquid \rightarrow V ₂ Zr C15	1573	1569.1
Liquid \rightarrow V ₂ Zr C15 + Zr-BCC_A2	1538	1535.7
Zr-BCC_A2 \rightarrow V ₂ Zr C15 + Zr-HCP_A3	1050	1052.9

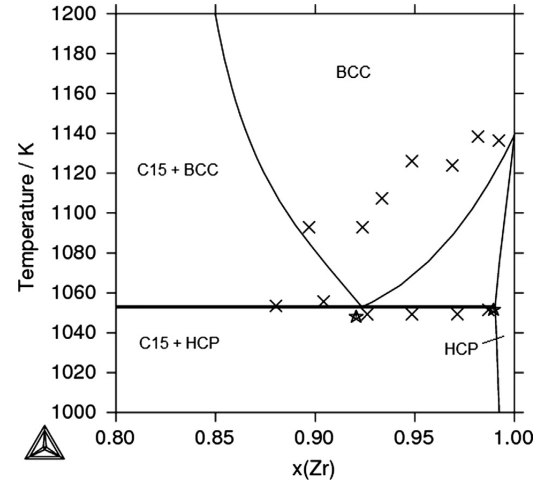


Fig. 3. Detail of the V-Zr phase diagram (Fig. 2) in the region of BCC_A2/HCP_A3 transformation of Zr. Stars from [15], crosses from [16].

to zero Kelvin. In this temperature region, the Gibbs energy of elemental constituents may be expressed with respect to SER state by equation [14]

$$G^0(T) = E_0 + \frac{3}{2}RT_E + 3RT \ln(1 - e^{-T_E/T}) - \frac{a}{2}T^2 - \frac{b}{20}T^5 - \frac{c}{6}T^3. \quad (1)$$

where T_E is the Einstein temperature and a , b and c are constants.

It is assumed that Gibbs energy of stoichiometric phases can be expressed also in the form of Eq. (1) and it is evaluated to reach a smooth connection at limiting temperature. Namely, the extended Gibbs energy of C15 Laves phase should have the same function value and the same values of the first and the second derivatives as the Gibbs energy polynomial for V₂Zr published in [19] at the limiting temperature (T_{lim}), which was chosen as 298.15 K. The resulting system of equations is based on general expressions for Gibbs energy valid for low temperatures published in [14] and was used as follows (parameter c in Eq. (1) is neglected):

$$\begin{aligned} G^{C15}(T_{lim}) &= E_0^{C15} + \frac{3}{2}RT_E^{C15} + 3RT_{lim} \ln(1 - e^{-T_E^{C15}/T_{lim}}) - \frac{a}{2}T_{lim}^2 - \frac{b}{20}T_{lim}^5 \\ &= 1135.53119 - 15.8195494T_{lim} + 1.34559042T \ln(T_{lim}) \end{aligned} \quad (2.1)$$

$$\begin{aligned} \frac{dG^{C15}(T_{lim})}{dT} &= 3R \ln(1 - e^{-T_E^{C15}/T_{lim}}) - 3R \frac{T_E^{C15}}{T_{lim}} \frac{e^{-T_E^{C15}/T_{lim}}}{(1 - e^{-T_E^{C15}/T_{lim}})} - aT_{lim} - \frac{b}{4}T_{lim}^4 \\ &= -14.47395898 + 1.34559042 \ln(T_{lim}) \end{aligned} \quad (2.2)$$

and

$$\begin{aligned} \frac{d^2G^{C15}(T_{lim})}{dT^2} &= -3R \frac{T_E^{C15}}{T_{lim}^2} \frac{e^{-T_E^{C15}/T_{lim}}}{(1 - e^{-T_E^{C15}/T_{lim}})^2} - a - bT_{lim}^3 \\ &= 1.34559042 \frac{1}{T_{lim}}. \end{aligned} \quad (2.3)$$

The Einstein temperature (T_E) can be calculated from the Debye temperature (T_D) according to the relation [43]

$$T_E = 0.77T_D. \quad (3)$$

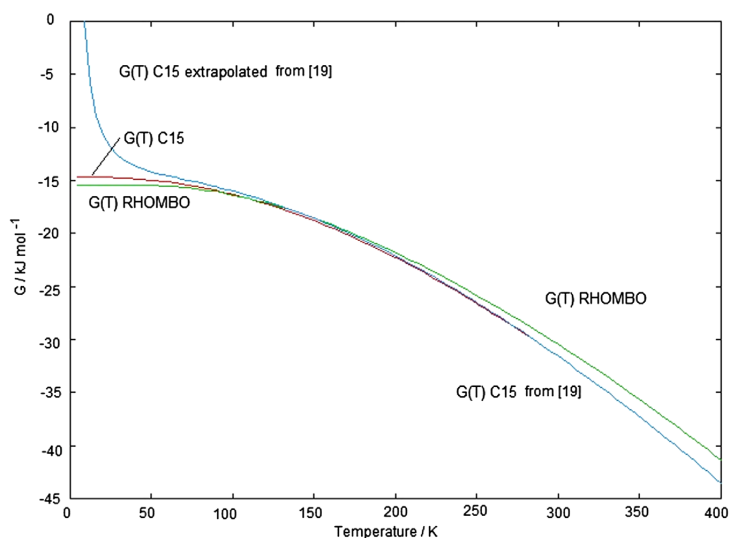


Fig. 4. Temperature dependence of the molar Gibbs energy of V_2Zr C15 Laves and of V_2Zr rhombohedral phase. Blue curve represents the Gibbs energy of the V_2Zr C15 Laves phase according to [19] including its extrapolation below 298.15 K performed in the present paper, the red/green curves show the extension of the Gibbs energy [14] of the V_2Zr C15 Laves phase/ V_2Zr rhombohedral phase based on our new model (this work) to zero Kelvin. Gibbs energy of V_2Zr rhombohedral phase above 298.15 is given by Eq. (6). (Our data of V_2Zr C15 Laves and rhombohedral phase are listed in Table 7. For elemental constituents, we employed SGTE data [44] above 298.15 K and data from [14] below 298.15 K.)

Table 7

The Gibbs energy data for V_2Zr C15 Laves and rhombohedral phase used for the calculation of Fig. 4.

V_2Zr C15 Laves phase ($0 < T < 298.15$)	$-2173.70 + 2062.8 + 24.94357 \ln(1 - \exp(-165.4T^{-1})) + 0.0597826T^2 - 6.3207 \times 10^{-11}T^5 + 2 \text{ GHSERV} + \text{GHSERZR}$
V_2Zr C15 Laves phase ($298.15 < T < 3000$) from Ref. [19]	$1135.53 - 15.8195T + 1.345590T \ln(T) + 2 \text{ GHSERV} + \text{GHSERZR}$
V_2Zr rhombohedral phase ($0 < T < 298.15$)	$-2173.70 + 1935.6 + 24.9427 \ln(1 - \exp(-155.2T^{-1})) + 0.075987T^2 + 2 \text{ GHSERV} + \text{GHSERZR}$
V_2Zr rhombohedral phase ($298.15 < T < 3000$)	$-1324.41 + 3.80309T + 2 \text{ GHSERV} + \text{GHSERZR}$

The value of Debye temperature of V_2Zr in C15 Laves phase structure was obtained by Zhang et al. [24] at zero pressure and zero Kelvin and amounts to $T_D = 214.8$ K, so that $T_E^{C15} = 165.4$ K.

The solution of the above mentioned system of equations by elimination method is

$$a = -0.119565 \text{ J mol}^{-1} \text{ K}^{-2},$$

$$b = 1.26414 \times 10^{-9} \text{ J mol}^{-1} \text{ K}^{-5},$$

$$E_0^{C15} = -2173.70 \text{ J mol}^{-1}.$$

For the Gibbs energy of V_2Zr rhombohedral phase the same approach is used and its Gibbs energy is defined as

$$G^{\text{RHOMBO}}(T_{\text{lim}}) = E_0^{\text{RHOMBO}} + \frac{3}{2}RT_E^{\text{RHOMBO}} + 3RT_{\text{lim}} \ln(1 - e^{-T_E^{\text{RHOMBO}}/T_{\text{lim}}}) - \frac{a}{2}T_{\text{lim}}^2 \quad (4)$$

and the parameter b was neglected in this expression. Furthermore, the value $E_0^{\text{RHOMBO}} = E_0^{C15}$ was used here because the *ab initio* calculated total energy difference between the relaxed rhombohedral structure and C15 Laves phase of -0.0015 kJ/mol of atoms (see Table 3) is negligible. In case of V_2Zr rhombohedral phase, Geibel et al. [23] published the value of $T_D = 203$ K and similar value, 200 K, was presented by Keiber et al. [22]. Therefore the average

value $T_D = 201.5$ K for the rhombohedral phase is accepted in present calculations.

The solution of system of thermodynamic equations results in:

$$a = -0.153448 \text{ J mol}^{-1} \text{ K}^{-2},$$

$$E_0^{\text{RHOMBO}} = E_0^{C15} = -2173.70 \text{ J mol}^{-1} \quad (\text{Table 3}),$$

which is calculated under the condition that $G^{\text{RHOMBO}}(T) = G^{C15}(T)$ at the transformation temperature of 113.3 K (average value of [10,11]).

The Gibbs energy for V_2Zr rhombohedral phase above 298.15 K is expressed simply as linear continuation of function

$$G^{\text{RHOMBO}}(T) = -2173.70 + \frac{3}{2}RT_E^{\text{RHOMBO}} + 3RT \ln(1 - e^{-T_E^{\text{RHOMBO}}/T}) - \frac{0.153448}{2}T^2 \quad (T < 298.15 \text{ K}) \quad (5)$$

which is valid below limiting temperature $T_{\text{lim}} = 298.15$ K. This linear continuation above T_{lim} is expressed as

$$G^{\text{RHOMBO}}(T) = -1324.41 + 3.80309T \quad (T > 298.15 \text{ K}) \quad (6)$$

Table 8

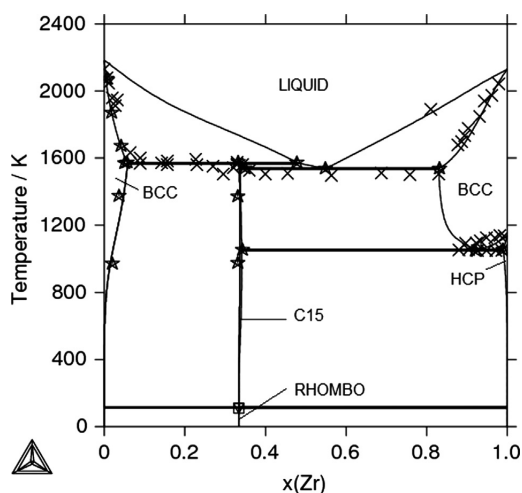
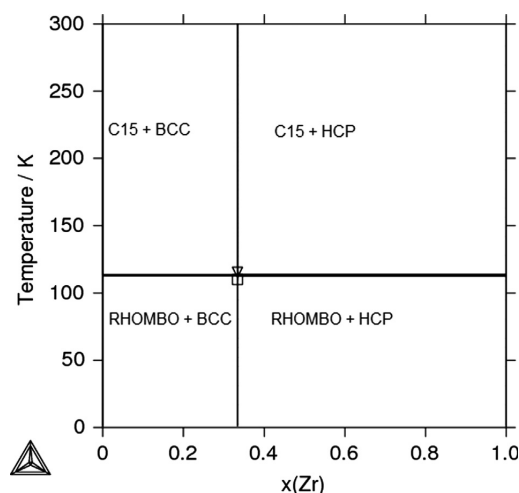
The zirconium Gibbs energy unary data extended to zero Kelvin in the form of GHSER in J/mol connected with corresponding SGTE data [14,44].

Zr HCP_A3 ($0 < T < 130$)	$-8313.16 + 2794.55 + 24.9435T \ln(1 - \exp(-224.07T^{-1})) - 0.0403104T^2 + 1.24814 \times 10^{-4}T^3 - 0.65635 \times 10^{-9}T^5$
Zr HCP_A3 ($130 < T < 2128$)	$-7827.595 + 125.6490T - 24.1618T \ln(T) - 0.00437791T^2 + 34.971T^{-1}$
Zr HCP_A3 ($2128 < T < 6000$)	$-26,085.92 + 262.7242T - 42.144T \ln(T) - 1.34289610^{31}T^{-9}$
Zr BCC_A2 ($0 < T < 298.15$)	$-674.409 + 1834.23 + 24.9435T \ln(1 - \exp(-147.07T^{-1})) - 0.0164156T^2 + 0.248308 \times 10^{-4}T^3 - 2.710215 \times 10^{-11}T^5$
Zr BCC_A2 ($298.15 < T < 2128$)	$-525.539 + 124.9457T - 25.6074T \ln(T) - 3.40084 \times 10^{-4}T^2 - 9.72897 \times 10^{-9}T^3 + 25.233T^{-1} - 7.614289 \times 10^{-11}T^4$
Zr BCC_A2 ($2128 < T < 4000$)	$4620.034 + 1.55998T + \text{GHSEZR} + 1.41035 \times 10^{32}T^{-9}; (\text{GHSEZR} = G(\text{ZR HCP_A3}))$

Table 9

Vanadium Gibbs energy unary data extended to zero Kelvin in the form of GHSER in J/mol connected with corresponding SGTE data [14,44].

V BCC_A2 ($0 < T < 298.15$)	$-8475.16 + 3649.24 + 24.9435T \ln(1 - \exp(-292.6T^{-1})) - 0.0163735T^2 + 0.23640 \times 10^{-4}T^3 - 2.63496 \times 10^{-11}T^5$
V BCC_A2 ($298.15 < T < 790$)	$-7930.430 + 133.346053T - 24.134T \ln(T) - 3.098 \times 10^{-3}T^2 + 1.2175 \times 10^{-7}T^3 + 69.460T^{-1}$
V BCC_A2 ($790 < T < 2183$)	$-7967.84 + 143.291T - 25.9T \ln(T) + 6.25 \times 10^{-5}T^2 - 6.8 \times 10^{-7}T^3$
V BCC_A2 ($2183 < T < 4000$)	$-41,689.8 + 321.1407T - 47.430T \ln(T) + 6.4439 \times 10^{31}T^{-9}$
V HCP_A3 ($0 < T < 298.15$)	$-4580.80 + 3975.75 + 24.9435T \ln(1 - \exp(-318.78T^{-1})) - 0.0129367T^2 + 1.60438 \times 10^{-5}T^3 - 1.58175 \times 10^{-11}T^5$
V HCP_A3 ($298.15 < T < 4000$)	$\text{GHSERV} + 4000 + 2.4T; (\text{GHSERV} = G(\text{V BCC_A2}))$


Fig. 5. The V–Zr phase diagram calculated in this work and compared with experimental data: stars [15], crosses [16], square [10] and triangle [11].

Fig. 6. The V–Zr phase diagram below 298.15 K calculated in this work and compared with experimental data: square [10], triangle [11].

The shape of molar Gibbs energy $G(T)$ functions for V_2Zr C15 Laves phase and for V_2Zr rhombohedral phase in the temperature region 0–400 K is illustrated in Fig. 4. We also show there the simple extrapolation of polynomial of molar Gibbs energy for V_2Zr C15 calculated in [19]. It may be seen that this extrapolation acquires unphysical values for temperatures lower than 50 K.

The values of a , b and E_0 parameters obtained in this section were successfully employed in the phase diagram calculations.

6. Calculation of phase diagram

The thermodynamic basis of the CALPHAD method relies explicitly on the assumption that the equilibrium phase composition arises as a result of a minimization of Gibbs energy in a closed system at constant external conditions (temperature and pressure) [42].

For the modeling of C15 Laves phase in the V–Zr system below T_{lim} , we employed the model of stoichiometric phase, where a continual extension of Gibbs energy from temperature region above $T_{\text{lim}}=298.15$ K (Section 5) was included. The V_2Zr rhombohedral phase was described below T_{lim} using analogous equation for Gibbs energy. The optimized thermodynamic parameters describing both V_2Zr C15 Laves phase and V_2Zr rhombohedral phase in the V–Zr system are summarized in Table 7 where $GHSERV=G(V \text{ BCC_A2})$ and $GHSERZR=G(Zr \text{ HCP_A3})$.

The thermodynamic L -parameters of both BCC_A2 and HCP_A3 phases for the temperatures below 298.15 K are kept equal to those published for temperatures above 298.15 K in [19] in Table 5 (Section 4). Their unary data were taken from [14]. For the sake of completeness, they are presented in Tables 8 (zirconium) and 9 (vanadium).

The phase diagram calculated by using these parameters is shown in Fig. 5 and its details below 298.15 K are in Fig. 6. It may be seen that a very good agreement of calculated phase diagram with available experimental data was obtained.

7. Conclusions

A thorough *ab initio* analysis of phases found in V–Zr system was performed at 0 K. *Ab initio* calculated values of Laves lattice parameters, bulk moduli and energies of formation of Laves phases with respect to the SER states, i.e. BCC_A2 for V and HCP_A3 for Zr, correspond reasonably well to both experimental data wherever available and previous theoretical results. It is shown from *ab initio* calculations that the ZrV_2 rhombohedral phase is not stable at 0 K and its structure transforms to C15 Laves phase arrangement. The stability of C15 phase was proved by analysis of elastic constants and phonon spectra calculations.

It was also shown that the methodology of calculation of unary data [14] at temperatures below 298.15 K is transferable to more complicated structures. The proposed procedure, using the Gibbs energy expression based on Debye temperature of modeled phases and on compatibility with SGTE unary data, extends CALPHAD-type modeling and enables us to calculate phase diagrams down to zero Kelvin. This may be important for modeling of phase equilibria in multicomponent systems in materials in extreme conditions.

Acknowledgments

Financial support of the Grant Agency of the Czech Republic (Project no. P108/10/1908) and of the Project “CEITEC – Central European Institute of Technology” (CZ.1.05/1.1.00/02.0068) from the European Regional Development Fund is gratefully acknowledged. This research was also supported by the Academy of Sciences of the Czech Republic (Project no. RVO: 68081723). The access to computing and storage facilities owned by parties and projects contributing to the National Grid Infrastructure MetaCentrum, provided under the program “Projects of Large Infrastructure for Research, Development, and Innovations” (LM2010005) is appreciated.

Authors are indebted to RNDr. Aleš Kroupa, CSc. for recalculating phase diagrams by the Thermo-Calc (version s) and to many

colleagues at CALPHAD XL (2011) and CALPHAD XLI (2012) conferences for fruitful discussions.

Appendix A. Supplementary material

Supplementary data associated with this article can be found in the online version at <http://dx.doi.org/10.1016/j.calphad.2013.08.003>.

References

- [1] A. von Keitz, G. Sauthoff, *Intermetallics* 10 (2002) 497.
- [2] X.Q. Chen, W. Wolf, R. Podlousky, P. Rogl, *Phys. Rev. B* 76 (2007) 014424.
- [3] B.M. Klein, W.E. Pickett, D.A. Papaconstantopoulos, L.L. Boyer, *Phys. Rev. B* 27 (1983) 6721.
- [4] E. Akiba, H. Iba, *Intermetallics* 6 (1998) 461.
- [5] K. Inoue, K. Tachikawa, *Appl. Phys. Lett.* 18 (1971) 235.
- [6] F. Chu, D.J. Thoma, T.E. Mitchell, C.L. Lin, M. Šob, *Philos. Mag. Part B* 77 (1998) 121.
- [7] F. Chu, M. Šob, R. Siegl, T.E. Mitchell, D.P. Pope, S.P. Chen, *Philos. Mag. Part B* 70 (1994) 881.
- [8] F. Chu, T.E. Mitchell, S.P. Chen, M. Šob, R. Siegl, D.P. Pope, *J. Phase Equilib.* 18 (1997) 536.
- [9] F. Stein, M. Palm, G. Sauthoff, *Intermetallics* 13 (2005) 1056.
- [10] O. Rapp, G. Benediktsson, *Phys. Lett. A* 74 (1979) 449.
- [11] D.E. Moncton, *Solid State Commun.* 13 (1973) 1779.
- [12] Q. Chen, B. Sundman, *J. Phase Equilib.* 22 (2001) 631.
- [13] Q. Chen, B. Sundman, *Acta Mater.* 49 (2001) 947.
- [14] J. Vřešťál, J. Štrof, J. Pavlů, *Calphad* 37 (2012) 37.
- [15] J.F. Smith, in: T.B. Massalski (Ed.), *Binary Alloy Phase Diagrams*, 2nd ed., vol. 3, ASM International, 1990, p. 3528.
- [16] J.T. Williams, *Trans. AIME* 203 (1955) 345.
- [17] W. Rostocker, A. Yamamoto, *Trans. ASM* 46 (1954) 345.
- [18] C. Servant, *J. Phase Equilib. Diff.* 26 (2005) 39.
- [19] X.-S. Zhao, G.-H. Yuan, M.-Y. Yao, Q. Yue, J.-Y. Shen, *Calphad* 36 (2012) 163.
- [20] A. van de Walle, M. Asta, G. Ceder, *Calphad* 26 (2002) 539.
- [21] A. van de Walle, *Calphad* 33 (2009) 266.
- [22] H. Keiber, C. Geibel, B. Renker, H. Rietschel, H. Schmidt, H. Wühl, G.R. Stewart, *Phys. Rev. B* 30 (1984) 2542.
- [23] C. Geibel, W. Goldacker, H. Keiber, V. Oestreich, H. Rietschel, H. Wühl, *Phys. Rev. B* 30 (1984) 6363.
- [24] X. Zhang, L. Chen, M. Ma, Y. Zhu, S. Zhang, R. Liu, *J. Appl. Phys.* 109 (2011) 113523.
- [25] D. Singh, *Planewaves, Pseudopotentials and the LAPW Method*, Kluwer, Boston, 1994.
- [26] G. Kresse, J. Furthmüller, *Comput. Mater. Sci.* 6 (1996) 15.
- [27] G. Kresse, J. Furthmüller, *Phys. Rev. B* 54 (1996) 11169.
- [28] P. Blöchl, *Phys. Rev. B* 50 (1994) 17953.
- [29] G. Kresse, J. Joubert, *Phys. Rev. B* 59 (1999) 1758.
- [30] J.P. Perdew, K. Burke, M. Ernzerhof, *Phys. Rev. Lett.* 77 (1996) 3865.
- [31] I. Ansara, T.G. Chart, A.F. Guillermet, F.H. Hayes, U.R. Kattner, D.G. Pettifor, N. Saunders, K. Zeng, *Calphad* 21 (1997) 171.
- [32] P. Villars, L.D. Calvert, *Pearson's Handbook of Crystallographic Data for Intermetallic Phases*, ASM International, Materials Park, OH, USA, 1991.
- [33] C. Kittel, *Introduction to Solid State Physics*, John Wiley and Sons, New York, USA, 1976.
- [34] M.H.F. Sluiter, *Calphad* 30 (2006) 357.
- [35] Y. Wang, S. Curtarolo, C. Jiang, R. Arroyave, T. Wang, G. Ceder, L.-Q. Chen, Z.-K. Liu, *Calphad* 28 (2004) 79.
- [36] K. Parlinski, Z. Q. Li and Y. Kawazoe, *Phys. Rev. Lett.* 78 (1997) 4063; K. Parlinski, Software PHONON, Cracow, Poland, 2011.
- [37] O. Eriksson, J.M. Wills, A.M. Boring, *Phys. Rev. B* 48 (1993) 5844.
- [38] B. Mayer, H. Anton, E. Bott, M. Methfessel, J. Sticht, J. Harris, P.C. Schmidt, *Intermetallics* 11 (2003) 23.
- [39] Y. Endoh, Y. Noda, *J. Phys. Soc. Jpn.* 46 (1979) 806.
- [40] P.T. Jochym, K. Parlinski, M. Sternik, *Eur. Phys. J. B* 10 (1999) 9.
- [41] M. Hillert, *J. Alloys Compd.* 320 (2001) 161.
- [42] H.L. Lukas, S.G. Fries, B. Sundman, *Computational Thermodynamics (The Calphad Method)*, Cambridge University Press, Cambridge, 2007.
- [43] G. Grimvall, *Thermophysical Properties of Materials*, Elsevier Science, North-Holland, Amsterdam, 1999.
- [44] A.T. Dinsdale, *Calphad* 15 (1991) 317.

